Dynamics of Long Term Fluvial Response in Postglacial Catchments of the Ladakh Batholith, Northwest Indian Himalaya

Daniel E. J. Hobley M.A.(cantab) MSci.

Thesis submitted for the degree of Doctor of Philosophy

University of Edinburgh

2010

ABSTRACT

Upland rivers control the large-scale topographic form of mountain belts, allow coupling of climate and tectonics at the earth's surface and are responsible for large scale redistribution of sediment from source areas to sinks. However, the details of how these rivers behave when perturbed by changes to their boundary conditions are not well understood. I have used a combination of fieldwork, remotely sensed data, mathematical analysis and computer modelling to investigate the response of channels to well constrained changes in the forcings upon them, focussing in particular on the effects of glacial remoulding of the catchments draining the south flank of the Ladakh batholith, northwest Indian Himalaya. The last glacial maximum for these catchments is atypically old (~100 ka), and this allows investigation of the response to glaciation on a timescale not usually available. The geomorphology of the catchments is divided into three distinct domains on the basis of the behaviour of the trunk stream – an upper domain where the channel neither aggrades above or incises into the valley form previously carved by glacial abrasion, a middle domain where the channel incises a gorge down into glacial sediments which mantle the valley floor, and a lower domain where the channel aggrades above this postglacial sediment surface. This landscape provides a framework in which to analyze the processes and timescales of fluvial response to glacial modification. The dimensions of the gorge and the known dates of glacial retreat record a time averaged peak river incision rate of approximately 0.5 mm/y; the timescale for the river long profile to recover to a smooth, concave up form must exceed 1 Ma. These values are comparable with those from similarly sized catchments that have been transiently perturbed by changing tectonics, but have never been quoted for a glacially forced basin-scale response.

I have also demonstrated that lowering of the upper reaches of the Ladakh channel long profiles by glacial processes can systematically and nonlinearly perturb the slope-area (concavity) scaling of the channel downstream of the resulting profile convexities, or knickzones. The concavity values are elevated significantly above the expected equilibrium values of 0.3-0.6, with the magnitude controlled by the

relative position of the knickzone within the catchment, and thus also by the degree of glacial modification of the fluvial system. This work also documents the existence of very similar trends in measured concavities downstream of long profile convexities in other transiently responding river systems in different tectonoclimatic settings, including those responding to changes in relative channel uplift. This previously unrecognised unity of response across a wide variety of different environments argues that such a trend is an intrinsic property of river response to perturbation. Importantly, it is consistent with the scaling expected from variation in incision efficiency driven by evolving sediment flux downstream of knickzones. The pervasive nature of this altered scaling, and its implications for fluvial erosion laws in perturbed settings, have significant consequences for efforts to interpret past changes in forcings acting on river systems from modern topography.

I follow this by examining in detail the channel hydraulics of the Ladakh streams as they incise in response to the glacial perturbation. I present a new framework under which the style of erosion of a natural channel can be characterized as either detachment- or transport-limited based upon comparison of the downstream distribution of shear stress with the resulting magnitude of incision. This framework also allows assessment of the importance of sediment flux driven effects in studied channels. This approach is then used to demonstrate that fluvial erosion and deposition in the Ladakh catchments is best modelled as a sediment flux dependent, thresholded, detachment-limited system. The exceptional quality of the incision record in this landscape enables an unprecedented calibration of the sediment flux function within this incision law for three different trunk streams. The resulting curves are not compatible with the theoretically-derived parabolic form of this relation, instead showing nonzero erosion rates at zero sediment flux, a rapid rise and peak at relative sediment fluxes of less than 0.5 and a quasi exponential decrease in erosional efficiency beyond this. The position of the erosional efficiency peak in relative sediment flux space and the magnitude of the curve are shown to be both variable between the catchments explored and also correlated with absolute sediment flux in the streams.

DECLARATION

This thesis has been composed by myself and represents my own work. I acknowledge my coauthors in chapters two to four, which are written in paper format, but I am first author on all of these and as such wrote the text, prepared all the diagrams and developed the intellectual arguments presented here. I also am solely responsible for writing the computer code employed in these works, with the exception of some scripts used to derive optimal model solutions in chapter four which were originally written by S. Mudd but later significantly modified by me. This work has not been submitted for any other degree or professional qualification.

Daniel Edward James Hobley

ACKNOWLEDGEMENTS

…And now I come to possibly the hardest bit of this thesis to write well – "the only bit that anyone ever reads in detail", as it was recently succinctly described to me – the acknowledgements section. I am so immensely grateful for all the support of everyone who has helped me out through the course of my PhD, and it feels like there are so many people who have! I would like to take this opportunity however to highlight a few of those who have really been amazing during the four and a half (!) years I've been in Edinburgh. I have successfully reached the end of writing up my PhD still really enjoying both my work and also living here, and for this I credit the people below entirely. I promise to try to be brief!

First of all I must extend all possible thanks to my main supervisor, Hugh Sinclair. Not only has he selflessly struggled through the worst excesses of my Byzantine prose style with a pair of metaphorical shears, but also he has really shown me how to get research done, and has always been ready to critique ideas or to guide my thinking. In the same breath I also need to thank Patience Cowie, my second supervisor and the perfect counterpoint to Hugh, and also my employer during my research sabbatical. In both roles I could not have wished for better guidance, criticism and support. I also owe an enormous debt of gratitude to Mikael Attal, Simon Mudd and especially Alex Whittaker, all of whom have taught me all manner of things useful both in this work and in wider academia, both technical and pastoral! Great thanks also must go to Tibor Dunai, Martin Hurst, Stewart Jamieson, Linda Kirstein, Mark Naylor and Rachel Walcott, all of whom have provided more advice and expertise of the highest calibre than I ever could have hoped for, and have made me really feel part of the Land Surface Dynamics research family. I also need to mention here both Elke Dengel of Sibiu and particularly Fida Hussein of Leh (and his many, many associates!), without whom I would probably have died many times over in the field, and who both gave freely of their time and local knowledge to make my fieldwork the best it could possibly have been.

I also need to thank the whole PhD community, particularly in the GI attic, both for academic support, but also for making my time here so uniformly enjoyable. Particular names I should mention include all of my various geo-housemates through the years – Alex Whittaker (again), Tim Ivanic, Rich Taylor, Tom Russon, Gillian McCay and Luke Ridley – who have all been awesome to live with. Great, great thanks also to my various long-suffering field assistants through the four months I haven't been in this country during my studies, Tim Ivanic, Martin Hurst, Ciaran Beggan and Jenny Rapp, who have all variously shed blood, sweat, tears and the products of other bodily functions on my account. The various occupants of the Tangerine Mansion – Caroline Graham, Louise Barron and Matt Untermann – also deserve special mention here: I say only GO TEAM!

Lastly and certainly not leastly, I want to thank my mum and dad, and also Jenny. Without these people and their constant support and love I would never have made it to where I am today, and it certainly wouldn't have been half as much fun trying to get here. Thank you so, so much.

CONTENTS

1. General Introduction **page**

1.1 Overview 1

1.2 Rationale 2

1.3 Motivation and Starting Point 4

1.4 Approach 7

1.5 Framework and Terminology 10

1.5.1 Pure detachment-limited channel dynamics 11
1.5.2 Pure transport-limited channel dynamics 13
1.5.3 Hybrid stream power models 16
1.5.4 Physical interpretations 18
1.5.5 List of parameters used 19

1.6 Thesis Outline 20

2. Processes, Rates, and Time Scales of Fluvial Response in an Ancient Postglacial Landscape of the Northwest Indian Himalaya

2.1 Introduction 23

2.2 Methodology 27

2.3 Field Area – Regional Setting 30

2.3.1 Geology 30
2.3.2 Topography 30
2.3.3 Climate 31
2.3.4 Geomorphology 31

2.4 Field Observations 33

2.4.1 Generalized catchment structure – Glacially modified valleys 36

2.4.1.1 Domain 1, upper reaches 36
2.4.1.2 Domain 2, middle reaches 39
2.4.1.3 Domain 3, lower reaches 42

2.4.2 Generalized catchment structure – Less glacially modified valleys 43

2.4.2.1 Hillslopes and valley floor 43

2.4.2.2 Channel and sediment load 44
2.4.2.3 Interpreted geomorphic structure 47
2.5 Remotely Sensed Data 48
2.6 Discussion 55
2.6.1 Causes of observed concavity trends *55*
2.6.2 Implications *58*
2.6.2.1 Direct control of downstream channel hydraulic scaling by upstream glacial modification 58
2.6.2.2 Rates and time scales of paraglacial recovery 59
2.7 Conclusions 63

3. River Scaling in Transient Landscapes

3.1 Introduction 65
3.2 Field Areas 67
3.2.1 South flank of the Ladakh Batholith, NW Indian Himalaya *67*
3.2.2 North flank of the Făgăraş Alps, Carpathians, Romania *69*
3.2.3 Red River region, Yunnan Province, China *70*
3.3 Methods 72
3.4 Results 73
3.5 Discussion 74
3.5.1 Causes of concavity scaling *74*
3.5.2 Reading uplift from topographic data *76*
3.6 Conclusions 77

4. Field Calibration of Sediment Flux Dependent River Incision

4.1 Introduction 79
4.2 Modelling Framework 81
4.2.1 Detachment-limited and transport-limited river incision *82*
4.2.2 A hybrid transport-limited model *87*
4.2.3 Discrimination between models *89*

4.3 Field Data 91

4.3.1 Field area *91*
4.3.2 Data collection methodology *94*
4.3.3 Gorge dimensions and shear stress *95*
4.3.4 Channel width and substrate grain size *97*

4.4 Channel Response Style 99

4.5 Incision Model 100

4.5.1 Approach *101*
4.5.1.1 Initial model setup 101
4.5.1.2 Sediment flux function 102
4.5.1.3 Sediment flux and capacity 102
4.5.1.4 Thresholds 104
4.5.1.5 Model output 105
4.5.1.6 Optimal solutions 106

4.5.2 Optimal results from the forward model *107*

4.6 Discussion 114

4.6.1 General form of the sediment flux function *114*

4.6.2 The K *parameter, absolute sediment flux and the Sobu curve* *115*

4.6.3 Tools and cover – If here, then everywhere? *116*

4.6.4 Implications *117*

4.6.4.1 Modelling channel erosion 117
4.6.4.2 Channel scaling 118
4.6.4.3 Reading past changes in boundary conditions from landscapes 119

4.7 Conclusions 120

5. Discussion and Synthesis

5.1 Overview and Synthesis 122

5.2 Importance, Impact and Implications 123

5.2.1 Postglacial landscapes as transient landscapes – Differences, but mainly similarities *123*

5.2.2 Transient landscapes, river scaling and the reading of tectonics from landscape *125*

5.2.3 Sediment flux and river incision *127*

5.2.4 Distinguishing incision models using field data *130*

5.3 Research Opportunities and Future Work 132

5.3.1 Landscape evolution in an ancient postglacial environment: Dynamics of the other domains *132*

5.3.2 The hybrid transport-limited erosion model *134*

5.3.3 Interaction of sediment flux and threshold *136*

5.3.4 Landscape and climate *137*

6. Conclusions 139

7. References 142

8. Appendices:

A - Methodology for Acquisition and Treatment of Raw Digital Elevation Model Data 158

A1. Ladakh 158
A2. Făgăraş 159
A3. Red River Region 159

B – Supporting Material for Chapter 2 161

B1. Long Profiles and Scaling Plots for All Analyzed Ladakh Catchments 161

B2. Field-DEM Slope Comparisons 161

B3. Variation of Scaling Metrics between Domains 162

C – Supporting Material for Chapter 4 192

Grain Size Distributions for Glacial Sediments 192

D – Raw Data from Ladakh 194

D1. Field Season 2006 – Basgo Valley 194
D2. Field Season 2006 – Leh Valley 195

D3. Field Season 2008 – Sobu Valley 196
D4. Field Season 2008 – Karu Valley 197

1. GENERAL INTRODUCTION

Dynamics of Long Term Fluvial Response in Postglacial Catchments of the Ladakh Batholith, Northwest Indian Himalaya

1.1 Overview

This thesis addresses the processes and styles of mountain river response to perturbation by glacial alteration of a landscape, and uses information gleaned in such a setting to improve our understanding of the long term evolution of rivers in upland environments. We use an integrated approach combining new field measurements, analysis of remotely sensed digital elevation models (DEM) and satellite imagery, modelling, and reinterpretation of existing theory. The work focuses primarily on a spectacular and hitherto poorly studied natural laboratory of catchments draining the Ladakh Range in the Northwest Indian Himalaya (Chapters 2 – 4) but also includes comparative observations made in contrasting study sites in the Făgăraş Alps of Romania and the Red River region, Yunnan Province, China (Chapter 3).

The central Chapters 2 – 4 of this manuscript are in the form of research papers either already or shortly to be submitted to journals, as noted at the start of each section. These discuss individual aspects of this study and can be read as self-contained units. These are followed in Chapter 5 by a synthesis of what we have shown in the course of this study *in toto* and a discussion of its implications for, and impact on, the wider study of fluvial geomorphology in upland landscapes, and then finally in Chapter 6 by conclusions.

We begin by presenting the wider rationale for the study of river evolution in landscapes, followed by a discussion of the prior state of the art regarding the research needs that this work addresses in particular. This section concludes with a detailed outline of the structure of this thesis.

1.2 Rationale

Rivers are one of the key elements of the Earth surface system. They are responsible for large scale redistribution of mass in the form of sediment across the Earth's surface, transferring material from source areas to basins, where it may be stored on a variety of time scales and later read as part of the stratigraphic record (Milliman and Meade, 1983; Milliman and Syvitski, 1992). In the same way that sediment is passed down a system creating a record of upstream processes, information about the base level of the network is also passed back upstream, making rivers vital links in the connectivity of terrestrial landscapes (Knighton, 1998; Rodriguez-Iturbe et al., 1992; Whipple and Tucker, 2002).

In highland areas, rivers are very often directly coupled to the surrounding hillslopes, which means that changes in the properties of the river channel can propagate directly into the surrounding nonfluvial environment (Burbank et al., 1996; Strahler, 1950). In this way, fluvial systems can be seen as the drivers of large scale topographic evolution in mountain belts (Burbank, 2002). Moreover, as high topography tends to form as a result of uplift driven by deeper Earth processes, mountain rivers also have the potential both to access and mobilize extremely large quantities of material brought to the surface by advection of rock. This allows a coupling of fluvial erosion to solid earth, geological processes and creates a feedback between climate, landscape and tectonics (Burbank, 2002; Burbank and Anderson, 2001; Montgomery and Stolar, 2006; Roe et al., 2008; Willett and Brandon, 2002; Zeitler et al., 2001).

However, hillslopes are not coupled directly to river channels in all mountain landscapes. Where glaciers develop in cold conditions at altitude, these may become the primary agents of flow in a landscape, with ice supplanting the erosive and transporting roles of water (Berger et al., 2008; Ehlers et al., 2006; Montgomery, 2002). Glaciers are delicate, however – they may only exist under a restricted range of climatic conditions, and are thought sometimes to be agents of their own downfall, restricting their own range by eroding their beds (Jamieson and Hulton, 2007; Kaplan

et al., 2009). The impact of glaciation on high topography can be intense but is highly localized, both in a temporal and spatial sense (Brocklehurst and Whipple, 2006; Hallet et al., 1996). If we wish to understand how glaciers may affect landscapes more widely, we must look to understand how they interact with the fluvial system which succeeds them – again both spatially and temporally. It will be these rivers that transfer glacially derived sediment downstream into longer-term basinal stores and propagate the signal created by disturbance of pre-existing fluvial systems into lower parts of the network (Church and Slaymaker, 1989; Harbor and Warburton, 1993; Herman and Braun, 2006). Moreover, on a global scale it is known that geologically synchronous rejuvenation of landscapes and associated filling of sedimentary basins has been enhanced over the last few millions of years, a signal thought to be driven by enhanced climate variability and intensification of glaciation (Ehlers et al., 2006; Molnar, 2004; Molnar and England, 1990; Zhang et al., 2001). An understanding of how rivers transiently respond to glacial growth, and indeed how they respond to changes in imposed climate more generally, is an underexplored but essential component of this story.

In addition to this, it has been widely noted that since rivers respond to environmental forcing in terms of climate, tectonics and substrate over which they flow, it ought to be possible to back-calculate aspects of these forcing variables from the form of channels (inter alia, Boulton and Whittaker, 2009; Cyr et al., 2009; Harkins et al., 2007; Kirby and Whipple, 2001; Kirby et al., 2003; Kobor and Roering, 2004; Snyder et al., 2000; Whittaker et al., 2008; Wobus et al., 2006b). This approach has been utilized extensively in landscapes which have experienced a tectonic change in boundary conditions, and has met with some success. Unfortunately, however, the reliability of many of these methods remains undemonstrated, since it is unusual to be able to constrain the (tectonic) boundary conditions tightly enough to prove that the conclusions drawn from a study are true. The best studies of this type tend to have used an exceptionally well constrained field site to investigate how well a prediction derived from channel data matches the known forcings, and have commonly been able to provide significant advances in our understanding of river dynamics by showing which assumptions in the river models

are robust, and which are not (e.g., Snyder et al., 2000; Valla et al., 2010; van der Beek and Bishop, 2003; Whittaker et al., 2008). However, approaches like this have been taken only rarely on landscapes responding to changing climate and, in particular, to glacial alteration of topography. In these settings, variation in hillslope-channel coupling driven by valley widening by ice, long profile alteration in the absence of active channel uplift and sharply increased sediment production around the landscape may all provide previously unexplored windows on the way in which channels adjust to externally imposed drivers.

1.3 Motivation and Starting Point

The starting central aim of this thesis was to use a landscape undergoing transient response to valley glaciation as a specific example of a perturbed landscape against which to test existing models and descriptions of channel dynamics. Many different models of long term channel evolution have been proposed in the literature (Anderson, 1994; Beaumont et al., 1992; Braun and Sambridge, 1997; Chatanantavet and Parker, 2009; Crave and Davy, 2001; Davy and Lague, 2009; Howard, 1994; Kooi and Beaumont, 1994; Sklar and Dietrich, 2004; Tucker and Bras, 1998; Turowski et al., 2007; Whipple and Tucker, 1999, 2002; Willgoose et al., 1991). There exists a wide range of modelling approaches, from very simplistic descriptions of how the flow may couple to the bed to full process-based analyses of the system, covering most intervening levels of model complexity (the details of these are introduced below in Chapter 1.5 and reviewed in depth in Chapter 4.2). However, it has been widely noted in the literature that these models do not lead to testable differences in landscapes which show the topographic characteristics of being in equilibrium with the forcings upon them (e.g., Howard, 1980; Tomkin et al., 2003; Tucker and Hancock, 2010; Tucker and Whipple, 2002; van der Beek and Bishop, 2003; Whipple, 2004; Willgoose et al., 1991).

The key testable differences do however emerge under transient conditions. Over the past five to ten years researchers have begun to use this realization to test some of the models against real data. Findings have tended to indicate that erosion models based around the channel expending energy on either detaching sediment from the bed or transporting clasts along in the flow can do a good job of describing real channel response, despite the simple treatment of channel processes which these models assume (Attal et al., 2008; Howard and Kerby, 1983; Valla et al., 2010; van der Beek and Bishop, 2003; Whipple et al., 2000b; Whittaker et al., 2008). However, these models allow for a large degree of "tuning" of internal parameters. Many authors have interpreted such tuning away from more physically preferable values to reflect the influence of factors such as channel width scaling, varying sediment supply or incision thresholds in the system (Finnegan et al., 2005; Sklar and Dietrich, 1998; Snyder et al., 2003b; Whipple, 2004; Whipple et al., 2000a; Whittaker et al., 2007a); physically realistic combinations of these effects provide nonunique response styles, however, making it hard to determine the exact role of each individual factor using a theoretical modelling approach (Snyder et al., 2003a, b). This difficulty applies both between different models (e.g., detachment versus transport limited erosion where sediment supply is considered important in both) and within each model (e.g., tradeoffs in the relative influences of sediment flux effects, thresholds and incision process efficiency within the detachment limited model).

A possible solution to this difficulty is to use very high quality field data where as many parameters as possible are constrained for the system, allowing independent characterization of each term which may be important in the incision process and eliminating the need for undirected tuning of the models. Theory suggests that the key landscape properties to be constrained should be:-

1) substrate variability,
2) climate (i.e., the probability distribution functions for rainfall rate and duration) ,
3) rate of tectonic uplift/base level change,

4) incision mechanism(s),
5) channel width,
6) incision threshold(s),
7) sediment flux.

Vitally, an understanding of the variability or otherwise of the above through both space and time is also required.

The role of sediment flux here is key. Even for a hypothetical field site where all other parameters were known and constant under steady state conditions, a transient response induced by a change through time in any one of these variables (for example, a step change in relative uplift rate) will necessarily also perturb the volume of sediment carried by the channel downstream; that is, the sediment flux response should always be apparent in a transient river network. This is not true of many of the other parameters listed above, which are more independent of each other (noting however the possible exception of channel width response; see, e.g., Whittaker et al. (2007a)). Moreover, in contrast to most of these other drivers of channel evolution, theoretical considerations and experimental study have both suggested that in an eroding landscape varying sediment flux should induce a strongly nonlinear effect on channel erosion – sediment can both act as tools to promote incision of the bed and as a cover to inhibit it (Cowie et al., 2008; Johnson and Whipple, in press; Johnson et al., 2009; Sklar and Dietrich, 1998, 2001, 2004; Turowski et al., 2007; Turowski and Rickenmann, 2009; Valla et al., 2010; Whittaker, 2007).

However, no study has yet been able to demonstrate convincingly the actual details of this sediment driven response in a real, natural channel. To a large part this is due to previous focus on tectonically forced landscapes, where problems related to variability of sediment flux shed from directly coupled threshold bedrock hillslopes into a channel and the manner in which the channel interacts with such material have thus far proven insurmountable. A transient postglacial landscape where loose, homogeneous sediment is abundant and the channel is decoupled from bedrock

hillslopes can provide an alternative and hitherto untried angle of attack on this problem.

The details of the models describing channel response are not just interesting in their own right. The form of the erosion laws also provides the theoretical underpinnings for attempts to read the record of past climate and tectonics affecting a landscape, as detailed in Section 1.2. The similarity of the predictions of most of the erosion laws under steady state conditions means that such approaches are robust where these forcings do not vary through time (e.g., Snyder et al., 2000), but over the past few years attempts have been made to extend these methods into landscapes responding transiently to changing boundary conditions (see Chapter 3). As detailed above, in these environments we remain significantly uncertain as to the relative importance of effects such as channel width scaling, thresholds and the role of sediment flux. All of these generally unmodelled complexities have the potential to create large amounts of systematic error in predictions which do not take them into account.

1.4 Approach

This work uses a carefully chosen postglacial field site to constrain the driving parameters of a transient landscape and to test them against the known river properties such as channel scaling and river dynamics through time. The key parameters in a well chosen glacial site (Fig. 1.1) which will make it distinct from a tectonically perturbed locality are:

1) predictable sediment loading on the channel through time, and known properties of this sediment entering the flow, based upon distribution of postglacial sediment in the surrounding landscape;
2) clearly preserved initial starting topography from which the channel evolves, left as an easily identifiable glacial surface;

3) strong variability of the extent of catchment alteration on a local, valley to valley scale, due to the previous extent of each individual valley glacier (in contrast, variability in tectonics tends to occur on a regional scale);
4) readily quantifiable alteration in the catchment based on the extent of glacial overprint on the pre-existing landscape;
5) lack of strong tectonic uplift or relative baselevel fall.

The field site discussed throughout this manuscript on the Ladakh Batholith fulfils these expectations. The work presented here first introduces this landscape and then establishes its structure and process geomorphology in order to demonstrate its appropriateness for a study of this kind. Subsequently, this natural laboratory has been used to answer four specific questions:

1) Do the characteristics of this landscape – for example the rates of response, time scales over which change occurs, and scaling relations of the channel – vary with extent of perturbation of the system?
2) Do the scaling metrics of the responding channels in this landscape match those seen in nonglacial but still transient environments? How well established are these values in the literature? Is there anything distinctively "glacial" about the landscape response in Ladakh?
3) Which erosion models can accurately reproduce the known past behaviour and present form of this landscape?
4) How important are sediment flux effects in controlling incision in this landscape, and thus perhaps more generally?

These questions are addressed in turn in the following chapters, as detailed in Section 1.6.

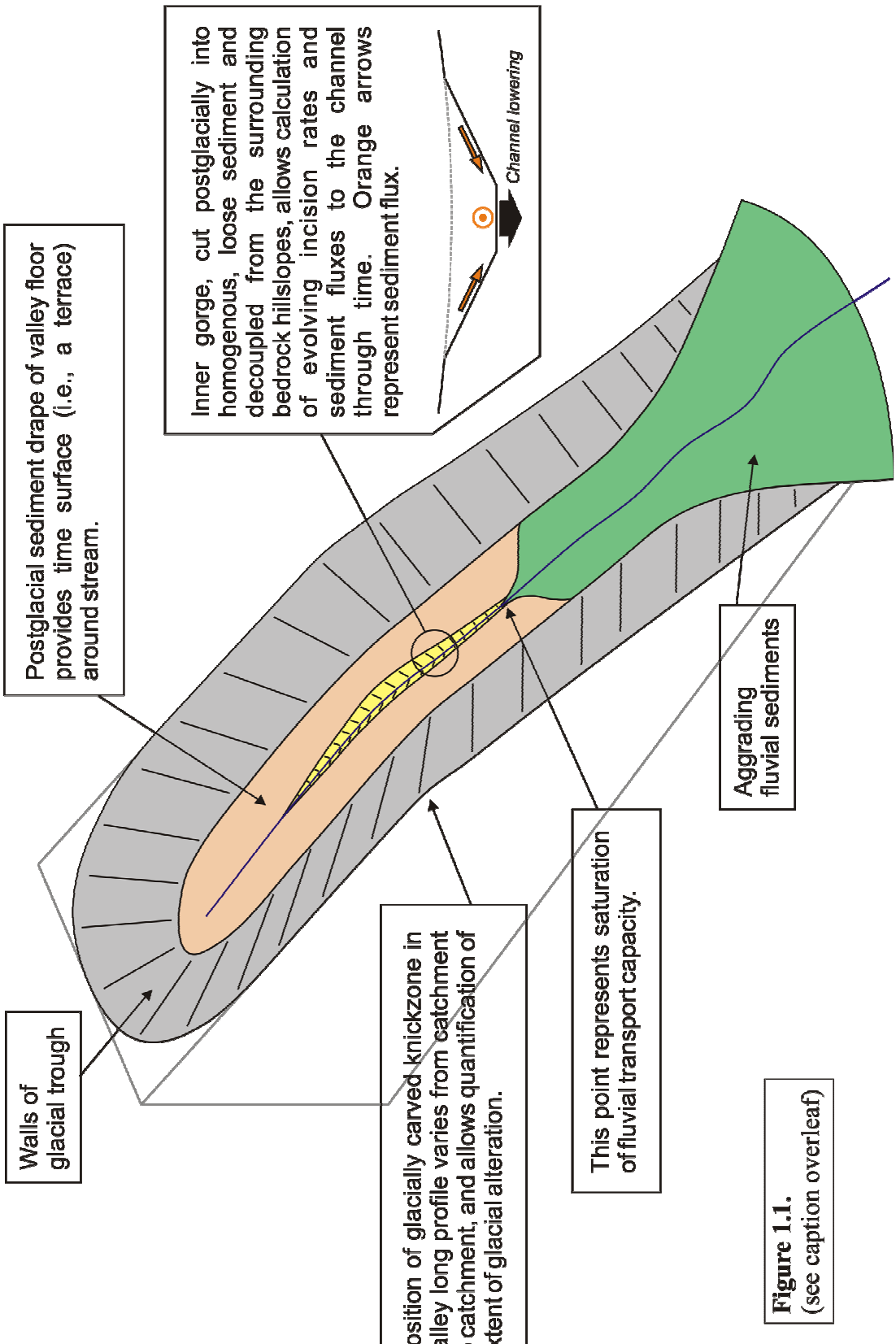

Figure 1.1.
(see caption overleaf)

Figure 1.1 (previous page). Landscape structure of an idealized glacially perturbed valley. The gradient of the upper reaches of the valley has been reduced by glacial erosion (c.f., Anderson et al., 2006; Brocklehurst and Whipple, 2006; MacGregor et al., 2000), creating a knickzone in the stream long profile. Features which would make such a catchment an ideal natural laboratory for studying transient landscape response are highlighted in the diagram.

1.5 Framework and Terminology

Much, though not all, of the analysis within this thesis is couched in terms of stream power. This treatment is simple, and does not attempt to physically model the processes occurring in the river channel. Instead, it is assumed that the geomorphic activity of the system is describable based on knowledge of its unit stream power (or equivalently of the shear stress it exerts on the bed), combined with scaling relations governing basin hydrology, conservation of mass and momentum in the channel, and hydraulic geometry. A brief overview of these types of models has already been given in Section 1.3 and details are emphasized within the body chapters of the thesis as appropriate, but in view of the importance of this framework to the thesis as a whole, a brief summary of how this basic idea is deployed within this work (and how this deployment differs somewhat from that used by other authors) is also presented here. This description loosely follows that presented by Whipple and Tucker (1999, 2002), and uncited statements within this section are drawn from those two works. A parameter definitions list is given at the end of this section, as Section 1.5.5.

1.5.1 Pure Detachment-Limited Channel Dynamics

There are two mutually exclusive ways of describing such a system mathematically. The first is to assume that the stream power (or shear stress, τ) describes the rate at which material can be removed from the bed: -

$$E = f(\tau) \quad \text{(shear stress)} \tag{1.1a}$$

$$E = f(\tau V) \quad \text{(unit stream power)} \tag{1.1b}$$

where E is incision rate and V is volume of flow. This function is typically a power function, but may also incorporate thresholds or other modifying elements. Note that this can only describe an incising system. This approach is termed "detachment-limited" since it assumes that the rate of response of the channel bed is limited by the rate at which material can be detached from the bed. If we then combine these two similar but distinct formulations of the detachment-limited model (assuming power laws and no thresholds for now) with expressions conserving mass (1.2) and momentum (1.3), and describing basin hydrology (1.4) we may simplify yet further: -

$$q_w = Vhw \tag{1.2}$$

$$\tau = \rho g h S = \rho C_f V^2 \tag{1.3}$$

$$q_w = k_q A^c \tag{1.4}$$

$$E = K' \left(\frac{A^c S}{w} \right)^{\frac{2}{3}a} \quad \text{(shear stress)} \tag{1.5a}$$

$$E = K'\left(\frac{A^c S}{w}\right)^a \quad \text{(unit stream power)}$$

(1.5b)

where q_w is water flux, h is flow depth, w is channel width, ρ is water density, g is gravitational acceleration, S is channel slope, C_f is a friction factor, A is upstream drainage area and other parameters are constants. If we also incorporate a (less reliable) relation for hydraulic geometry (c.f., Finnegan et al., 2005; Whittaker et al., 2007a),

$$w = k_w q_w^{\ b}$$

(1.6)

the equation simplifies yet further to

$$E = KA^m S^n$$

(1.7)

where

$$K = f(k_\tau, k_w, k_q, C_f, \rho, g, a, b), \quad m = \frac{2}{3}ac(1-b), \quad n = \frac{2}{3}a \quad \text{(shear stress)}$$

(1.8a)

$$K = f(k_\tau, k_w, k_q, \rho, g, a, b), \quad m = ac(1-b), \quad n = a \quad \text{(unit stream power)}$$

(1.8b)

Values for b and c are directly measurable for channels and well established in the literature; they typically around $0.4 \leq b \leq 0.6$ and $0.7 \leq c \leq 1$ respectively (Whipple and Tucker, 1999). In contrast, the value of a is not directly measurable from a channel, though it can be estimated for various pure and idealised erosion processes, e.g., plucking, abrasion, cavitation (Whipple et al., 2000a) – this difficulty is in part responsible for the ongoing ambiguity over whether the shear stress or unit stream power model is preferable. A value of $a = 1$ is often selected both on grounds of

parsimony and since it describes acceptably the process of plucking. However, we note that in both of these cases we may write from (1.8), independent of a,

$$\frac{m}{n} = c(1-b) \tag{1.9}$$

If a river is in topographic steady state, i.e., everywhere uplift (U) = erosion, and is in a constant uplift field then we may use equation (1.7) to show that

$$\ln S = \frac{1}{n}\ln\left(\frac{U}{K}\right) - \frac{m}{n}\ln A \tag{1.10}$$

In other words, (strictly only under the assumptions made above!) the gradient of a slope-area plot in logarithmic space for such a channel should be equal to $-m/n$. The value of m/n is termed the "intrinsic concavity", θ_I, while the value of the gradient derived from a slope area plot is known simply as the "concavity index", or simply "concavity", and is denoted θ. From the ranges for b and c presented above, we would expect $0.35 \leq \theta_I \leq 0.6$, and if we choose to make the constants in equations (1.4) and (1.6) dimensionless then we select $b = 0.5$, $c = 1$ and $\theta_I = 0.5$. Satisfyingly, in landscapes which have been argued to be at steady state and under uniform uplift, this ratio almost always sits within these ranges (e.g., Whipple, 2004). This provides support for the basic underlying assumptions for the stream power approach.

1.5.2 Pure Transport-Limited Channel Dynamics

Alternatively, it may be assumed that the stream power (or shear stress) describes the carrying capacity of the flow, q_c: -

$$q_c = f(\tau) \quad \text{(shear stress)} \tag{1.11a}$$

$$q_c = f(\tau V) \quad \text{(unit stream power)} \tag{1.11b}$$

Using very similar arguments to the detachment-limited case above, we may likewise write this relation as

$$q_c = K_t A^{m_t} S^{n_t} \tag{1.12}$$

where m_t and n_t are constants. The evolution of the bed is then in turn described by the downstream divergence of sediment flux, which is assumed to always be at capacity: -

$$\frac{dz}{dt} = U - \frac{1}{1-\lambda_p}\frac{d}{dx}\frac{1}{w}q_c \tag{1.13}$$

where z is bed elevation, t is time, λ_p is sediment porosity and x is downstream distance. This approach is termed "transport-limited" since it assumes that the rate limiting factor is the rate at which material can be transported away by the flow; in the simple form of the model the fact that the sediment flux is equal to the sediment transport capacity assumes that detaching material from the bed is of negligible difficulty. It is important to note in the context of this thesis that the transport-limited model may describe both incision and aggradation occurring on the bed, while the detachment-limited model may only describe incision.

The intrinsic concavity of the transport-limited end-member is derived similarly to that for the detachment-limited, and is calculated as $(m_t - 1)/n_t$ (Willgoose et al., 1991). m_t and n_t vary depending on which transport equation is

used to derive (1.12), but are often of similar magnitude, e.g., under the Einstein-Brown equation (if $c = 1$), $m_t = 1.8$, $n_t = 2.1$ (ibid.). Under these conditions note that again the predicted intrinsic concavity is around 0.5, as for the detachment-limited model. It is in fact possible to prove that under steady state these two intrinsic concavities (let us call them θ_{ID} and θ_{IT}) are almost identical (see Box 1.1).

1.5.3 Hybrid Stream Power Models

These two end member scenarios are mutually exclusive – it is not possible to internally consistently model both the (saturated) transport capacity and the erosion of the bed as functions of the same driving parameter. However, there is a middle ground between these end members, where erosion is sensitive both to the sediment carrying capacity of the channel and also to the shear stress it exerts on the bed. This is equivalent to saying that neither the difficulty of detaching a clast nor of transporting it away is negligible.

This model space can be envisioned graphically on a plot of relative efficiency of incision versus relative sediment flux (Fig. 1.2). Relative incision efficiency is a measure of the amount of incision occurring relative to total work done by the river – a value of 0 indicates no incision, a value of 1 indicates that the river does the maximum amount of incision it could for the total work done by the flow. Relative sediment flux describes the amount of sediment carried by the channel relative to its carrying capacity – a value of 0 corresponds to clearwater flow, a value of 1 corresponds to sediment saturation. Values >1 are physically forbidden in any given flow (hence dashed lines), but on the long term may be apparently exceeded if the transport capacity is calculated from the representative discharge (see Chapter 4). The parameter spaces where both the pure detachment-limited (red) and transport-limited (green) models operate are shown. The yellow space corresponds to the domain of hybrid incision models. Several of these from the literature are shown as black curves.

Box 1.1. A new proof for the stream power models.

For sediment transport we may always write as the most general case (Sinha and Parker, 1996):

$$q_c* = \alpha_q (\tau*)^p$$

where q_c* is dimensionless transport capacity, $\tau*$ is Shields stress (shear stress non-dimensionalized by dividing by grain size), and α_q and p are parameters which will be constant within a reference flow regime characterized by $\tau*_0$ and $q*_0$. This is a fuller statement of (1.11). We take the Meyer-Peter-Muller equation as an example, and may show by differentiation

$$\alpha_q = q*_0 \left(\tau*_0\right)^{-p}, \quad p = \frac{1.5}{\left(1-\frac{\tau_c}{\tau_0}\right)}.$$

Now we already know that we are modelling

$$q_c = K_t A^{m_t} S^{n_t} = K'_t \tau^{\chi}$$

and by direct comparison

$$\chi = p.$$

So using 1.2-1.5 again we can explicitly write (assuming shear stress version of stream power, but makes little difference)

$$\tau \propto A^{2c(1-b)/3} S^{2/3}$$

Now rolling all this together, along with $\theta_{IT} = (m_t\text{-}1)/n_t$, we find

$$m_t = \left(\frac{\tau_0}{\tau_0 - \tau_c}\right) c(1-b), \quad n_t = \frac{\tau_0}{\tau_0 - \tau_c}, \quad \theta_{IT} = c(1-b) + \left(\frac{\tau_c}{\tau_0} - 1\right)$$

$$\Rightarrow \quad \theta_{IT} = \theta_{ID} + \left(\frac{\tau_c}{\tau_0} - 1\right).$$

Now under uniform uplift and steady state conditions, τ (= τ_0) is a constant, incrementally greater than τ_c at all points in the transport-limited domain, as in fact is demanded by the assumptions of this model. Hence

$$\theta_{IT} \rightarrow \theta_{ID},$$

i.e., θ_{IT} is incrementally smaller than θ_{ID}. Hence the steady state concavities should be indistinguishable but transport-limited conditions should always develop downstream of their detachment-limited equivalents (c.f., Whipple and Tucker, 2002).

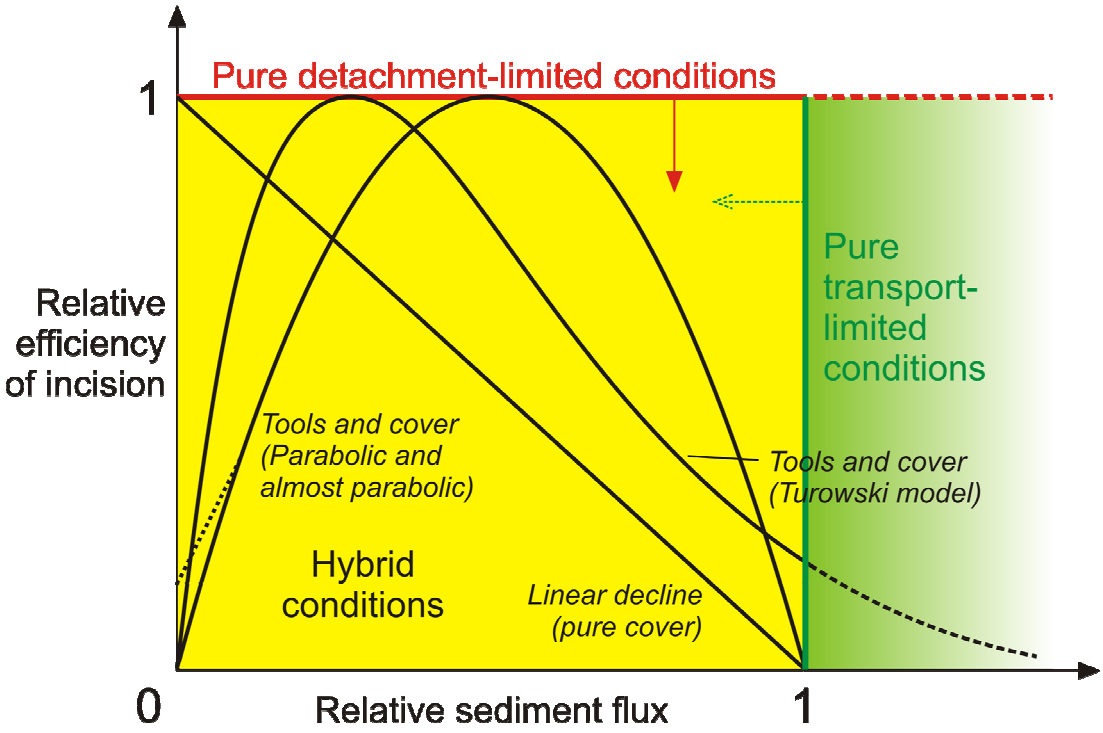

Figure 1.2. Model space for stream power-based incision laws. Full description is in text. Hybrid models shown are linear decline (Beaumont et al., 1992), and three versions of "tools and cover"-type models, parabolic (Sklar and Dietrich, 2004), almost parabolic (Gasparini et al., 2006), and Turowski and coworkers' (2007) dynamic cover model; all three are based upon detachment-limited-type assumptions (i.e., Equs. (1.1a,b)), though note the Turowski et al. formulation depends on relative sediment supply rather than flux. The figure emphasizes that the pure detachment- (red) and transport-limited (green) domains are orthogonal. Transport-limited conditions are not simply the "end-point" of a pure detachment-limited system, and all efficiencies of incision are possible in a sediment-saturated channel (depending on sediment flux divergence downstream, as opposed to its magnitude).

This plot brings out an important point however – when we describe the hybrid model domain, should we do it by extending the rules applying to the detachment-limited conditions downwards across the space (small solid red arrow), or by extending transport-limited conditions leftwards (dashed green arrow)? Existing hybrid incision models from within the stream power paradigm all use the former method, deploying to greater or lesser extents modified versions of equation

(1.7), typically modulated by a function which responds to relative sediment supply (Whipple, 2004): -

$$E = K_r K_c K_{\tau c} f(q_s, q_c) A^m S^n \tag{1.14}$$

where now we have parameters sensitive independently to lithology (K_r), climate (K_c), incision threshold ($K_{\tau c}$) and sediment flux ($f(q_s,q_c)$). However, to my knowledge there has been no published attempt to describe this hybrid domain through the transport-limited assumptions represented by equations (1.12) and (1.13). This idea is developed further in the early sections of Chapter 4.

1.5.4 Physical Interpretations

It is important to stress that in this work the terms "detachment-limited" and "transport-limited" are defined explicitly in terms of the mathematics describing the processes: in detachment-limited incision erosion proceeds as a function of a power law of shear stress or stream power, while in transport-limited incision it proceeds as a function of the downstream divergence of carrying capacity, and thus shear stress (see Chapter 4). I would argue this is the way of describing these terms least open to misinterpretation. However, this means that it is not always possible to accurately and intuitively predict which of these approaches to modelling incision will be most appropriate based only on qualitative field observations. In particular, any channel which is very sediment rich could reasonably be argued to be eroding in a transport-limited style, and equally, channels in substrates which are entirely loose sediment could still be eroding according to the detachment-limited laws. The only way to be sure of this distinction will be to either analyse quantitative measurements describing the channel (Section 4.2.3), or to examine their long-term topographic responses to changes in forcing parameters (c.f., Whipple and Tucker, 2002; see Sections 1.3 and 5.2).

1.5.5 List of Parameters and Constants Used In This Section

A Drainage area upstream	α Multiplier in generic sediment flux equation
C_f Coefficient of friction	θ Channel concavity (measured)
E Erosion rate	θ_I Intrinsic channel concavity
S Local slope of bed	θ_{ID}, θ_{IT} Intrinsic concavities (for detachment-, transport- limited channels)
U Uplift rate	
V Flow velocity	λ_p Sediment porosity
a Power law exponent for erosion process	ρ Density of water
	τ Shear stress
b Power law exponent for channel width	τ^* Shields stress
c Power law exponent for basin hydrology	χ Power law exponent for sediment transport capacity-shear stress relation
g Acceleration due to gravity	
h Flow depth	k,K Assorted constants. Those denoted prime (') are "dustbin" constants, and not preserved between equations.
m Power law exponent on drainage area	
n Power law exponent on slope	
p Power law exponent in generic sediment flux equation	
	Subscripts where otherwise not noted denote:
q Flux in channel	c "Threshold", or "capacity"
q^* Dimensionless flux in channel	r "Rock"
t Time	s "Sediment"
w Channel width	t "Transport-limited version"
x Downstream distance (horizontal)	w "Water"
z Channel elevation	

1.6 Thesis Outline

The body of this thesis consists of three paper-chapters, each of which can be read independently, but also contribute sequentially and holistically to a greater understanding of the dynamics of the transient landscape of the Ladakh region as a whole, and through that to a wider picture of the importance of sediment flux in evolving natural mountain river systems. An outline of the role of each chapter in addressing the big picture questions listed in Section 1.4 is provided below.

Chapter 2 presents a thorough and unique geomorphic description of the catchments draining the Ladakh batholith southwards into the Indus River, focussing in particular on their fluvial process geomorphology, coupled with a review of the existing literature describing the region. This forms a qualitative underpinning for much of the quantitative analysis of the channel system which follows, both in this and subsequent chapters. The chapter goes on to use the exceptional age of the local last glacial maximum (10^5 years) to explore the nature of the transient fluvial response of this postglacial landscape across time scales not usually observed. It is demonstrated that glacial modification of the upper reaches of a catchment can have a profound first-order influence on the hydraulic scaling of the downstream channel, perturbing the channel slope-area scaling systematically and nonlinearly away from the values expected under steady state. We also calculate both the incision rates (up to 1mm/y) and response time scales (> 10^6 years) during the postglacial recovery. The latter of these values is an order of magnitude slower than any glacial relaxation process previously reported. Both this rate and time scale are however consistent with values suggested for tectonically perturbed transient landscapes. This paper has been published in the *Geological Society of America Bulletin* this year (Hobley et al., 2010).

Chapter 3 explores an idea raised in Chapter 2, and tests whether the fluvial scaling perturbations driven by glacial modification on the Ladakh batholith are characteristic of all transient channels, regardless of the forcing mechanisms. Slope-

area (concavity) scaling in the Ladakh streams is contrasted with data taken from field sites with differing climatic and/or tectonic regimes in Romania and the south-eastern margin of the India-Asia collision. All three sites show systematically and predictably elevated concavity values downstream of long profile convexities. The trends in each of the datasets are very similar, demonstrating unity of response regardless of whether these convexities were formed by glacial or tectonic perturbation of the landscape. This altered scaling is consistent with the response expected if a nonlinear sediment flux term is included in the erosion laws describing the incision. This chapter concludes by discussing the consequences of this pervasive and previously unrecognized altered concavity scaling for attempts to read past tectonic forcing from the topographic form of transient channel long profiles. This paper is in review for *Geology*.

Chapter 4 looks specifically at the incising component of the Ladakh channels and uses it to address questions of how we should model such a system. A new framework is presented for understanding the predictions of detachment-limited and transport-limited formulations of erosion based around interaction of separate sediment flux dependent and shear stress dependent terms in each case. This framework is then used to demonstrate that incision into the coarse, loose, poorly sorted sediment of the thick postglacial surface in the Ladakh catchments is occurring in a detachment limited manner, but also incorporates an incision threshold and a nonlinear sediment flux effect. In the later sections of the chapter, a combination of analytical and numerical forward modelling is used to calibrate the forms of the sediment flux functions which are active in each of the analyzed catchments. The resulting functions comprise the best constrained examples in the literature and are unique in their description of the details of the interaction of the tools and cover effects in a real field setting. This paper is shortly to be submitted to the *Journal of Geophysical Research: Earth Surface*.

Finally, **Chapter 5** then goes on to synthesize key research findings from the preceding chapters and to discuss how this work fits into the wider context of the literature, bringing out the importance, impact and implications of these findings.

Outstanding questions raised by this work are then addressed, and possible future research directions based upon these are outlined. The thesis then concludes with a brief summary of the main research outcomes of this study.

2. PROCESSES, RATES, AND TIME SCALES OF FLUVIAL RESPONSE IN AN ANCIENT POSTGLACIAL LANDSCAPE OF THE NORTHWEST INDIAN HIMALAYA[1]

CHAPTER ABSTRACT

Both glacial and fluvial processes are key elements in molding landscapes in high mountain environments—glaciers are highly efficient erosional agents and producers of sediment but are restricted spatially, while rivers can transmit information about upstream changes through landscapes and flush this sediment out of mountain belts and into sedimentary basins. However, little research has focused on the manner in which these two agents of landscape change interact, especially on longer time scales. We analyze a suite of catchments draining the previously glaciated Ladakh batholith in the northwest Indian Himalaya, which preserve the oldest known moraine succession in this mountain chain. We describe and quantify the rates, processes, and time scales of postglacial recovery of the fluvial system across a previously unstudied time interval of 10^5–10^6 yr. We demonstrate that glacial modification of the upper reaches of a catchment can have profound first-order influence on the hydraulic scaling of the channel downstream, where increasing degree of glacial modification systematically and nonlinearly elevates the channel concavities of downstream reaches above the expected value range of 0.3–0.6. We also demonstrate that the response time of these systems as they recover must exceed 500 k.y., which is longer than any previously reported estimate for recovery times from glaciations, but is comparable with estimates from many tectonically perturbed landscapes.

2.1 Introduction

Fluvial dynamics are widely recognized as the primary control on the style and pace of landscape evolution in unglaciated upland areas. River networks transmit base-level change signals widely though landscapes by coupling to hillslopes (Burbank et al., 1996; Strahler, 1950), and they govern the routing of sediment from erosive areas to depositional basins (Milliman and Syvitski, 1992). Removal of rock

[1] A version of this paper has been published in *Geological Society of America Bulletin*:
Hobley, D.E.J., Sinclair, H.D., and Cowie, P.A., in press, Processes, rates, and time scales of fluvial response in an ancient postglacial landscape of the northwest Indian Himalaya: GSA Bulletin, v. 122, no. 9/10, p. 1569-1584, doi: 10.1130/B30048.1.

from upland areas also provides a direct isostatic feedback mechanism, whereby changes in the erosional capacity of the climate couple with rock uplift (Dahlen and Suppe, 1988; Molnar and England, 1990).

In mountain ranges where glaciers are developed, however, long-term erosional history is determined by the action of ice as well as water, and the boundary between the glacial and fluvial domains shifts in response to climate fluctuations (Berger et al., 2008; Hallet, 1990). Despite this, the nature and response of the fluvial system in previously glaciated settings have been underexplored, particularly across time scales exceeding a few thousand years. Moreover, although it is well recognized that transient landscapes hold great potential for understanding the mechanics of fluvial incision (e.g., Whipple, 2004), few researchers have attempted to use climatically induced transience to understand such processes, and instead studies have focused on tectonic forcing (e.g., Finnegan et al., 2005; Lavé and Avouac, 2001; Snyder et al., 2000, 2003a; Whipple and Tucker, 2002; Whittaker et al., 2007a). Previously glaciated environments provide ideal and complementary natural laboratories for such analyses.

A large body of literature focuses on sediment dynamics within and out of paraglacial systems—those in which sediment dynamics are directly conditioned by glaciation (sensu Church and Ryder, 1972)—but much of this literature is focused on understanding the slope processes occurring within these settings (e.g., Ballantyne, 2002b) or quantifying the sediment yields from them, as opposed to quantifying the geomorphic responses of fluvial networks across glacial cycles. Such sediment yield studies have shown that typical response times for large basin systems tend to fall in the region of 1–10 k.y. (e.g., Ashmore, 1993; Brooks, 1994; Church and Slaymaker, 1989; Ferguson, 1984; Lamoureux, 1999; Slaymaker and McPherson, 1977), although primary glacial sediment mobilization is thought to decrease on time scales perhaps one to two orders of magnitude shorter than this (e.g., Ballantyne and Benn, 1994; Cruden and Hu, 1993; Friele et al., 1999; Hinchliffe and Ballantyne, 1999; Meigs et al., 2006; Ryder, 1971), indicating the importance of sediment storage within the paraglacial realm. Modeling studies have also been used to investigate

sediment output from paraglacial systems, and these have reported time scales of sediment flux decay between 3 and 50 k.y. (e.g., Braun et al., 1999; Dadson and Church, 2005). Typically, the fluvial transport rules in these models are implemented in a simple way, assuming sediment mobility to be limited by the river's transport capacity and ignoring difficulties in lifting the sediment from the bed. However, few studies have considered the geomorphic response of these systems on medium to longer time scales (~10^5–10^6 yr). These time scales are of great interest because they are on a similar order to known response time scales for tectonically forced erosional-depositional catchment-fan systems (Allen, 2008; Baldwin et al., 2003; Carretier and Lucazeau, 2005; Densmore et al., 2007; Whipple, 2001). Responses on these longer time scales are also important since they match or exceed the time scales of most Milankovich-type climatic forcing, and thus determine the reactivity of landscape elements to such changes.

A number of studies have contrasted glacially sculpted basins with purely fluvial ones, but generally these have focused on the effects of the glaciers themselves rather than examining the postglacial fluvial dynamics (Amerson et al., 2008; Brocklehurst and Whipple, 2002, 2006; Brook et al., 2008; Montgomery, 2002). The inverse approach has been taken in some cases, using streams in glaciated landscapes to examine reach-scale fluvial geomorphology and stream structure and response (e.g., Brardinoni and Hassan, 2006, 2007; Brocard et al., 2003; Herman and Braun, 2006; Mueller and Pitlick, 2005), with the latter authors also emphasizing the impact that glacial sculpting of a basin has on distribution of channel type within it. However, no previous study has examined catchment-scale response of streams to variable degrees of glacial alteration. Therefore, the key geomorphic domain that modulates the influence of fully glaciated mountainous catchments on sedimentary basins at the edge of alpine mountain ranges has not been adequately characterized in terms of processes, rates, or time scales.

We use a suite of tributaries in a previously glaciated environment to describe and quantify the effects of glacial modification of catchments on their first-order channel hydraulics during postglacial recovery. We chose the field site using the

following criteria: (1) numerous catchments for comparison; (2) known tectonic forcing, and well-quantified, uniform base-level history; (3) uniform substrate; (4) quantifiable, variable extent of glacial alteration; (5) known glacial chronology; (6) minimal anthropogenic alteration; and (7) availability of remote-sensed digital elevation model and supporting imagery. On this basis, we selected 70 channels draining the Ladakh Batholith, northwest Indian Himalaya, southward into the Indus valley (Fig. 2.1). We use a combination of remotely sensed data, incorporating both 3 arc-second (90 m) resolution digital elevation models (DEMs) from the Shuttle Radar Topography Mission (SRTM; see Appendix A) and satellite imagery (Landsat 7 and Google Earth), and field-based investigation to assess the process geomorphology of the paraglacial environment of these tributaries, with particular emphasis on the trunk streams of each catchment. We first describe these field observations in order to assess the role of riverine processes and to provide evidence for controls on channel hydraulic scaling, which are not accessible from the remotely sensed data. Subsequently, we examine the hydraulic scaling of these streams using the satellite data, with emphasis on their slope-area relationships. We then synthesize both field and remotely sensed data to demonstrate that river scaling is directly controlled by glacial sculpting of the upper reaches of the valleys. We also show that the response time scale for these systems exceeds half a million years, but that incision into the substrate proceeds at rates on the order of 1 mm/yr. Both values are comparable to those observed during transient landscape response to tectonic forcing.

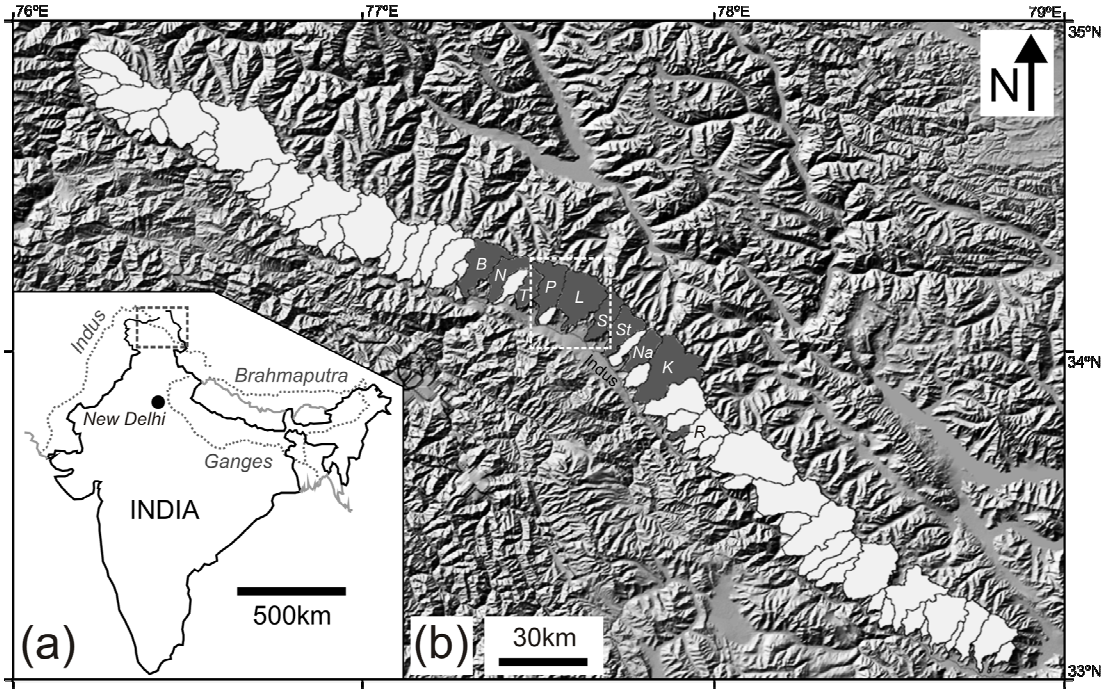

Figure 2.1. **(a)** Summary map of India. Dotted box indicates location of field area shown in b. **(b)** Hillshade digital elevation model (DEM) of field area. The Ladakh Batholith runs NW-SE, corner to corner, through the center of the image, north of the Indus River, picked out faintly in gray. Catchments flowing southward into the Indus Valley analyzed in this study are indicated. Those colored darker gray have been explored in the field, and are, from west to east, Basgo (B), Nimmu (N), Tharu (T), Phyang (P), Leh (L), Sobu (S), Stakma (St), Nang (Na), Karu (K), and Ratatse (R) valleys. The area of the paleolake referred to in the Regional Setting section corresponds broadly to the prominent valley flats around the Indus, approximately between the outlets of Basgo and Karu catchments. Area shown in Figure 2.2a is marked by white box.

2.2 Methodology

Our analysis is based around the framework of the stream power model. This approach has been widely used in fluvial analysis (e.g., Anderson, 1994; Howard, 1980; Howard and Kerby, 1983; Parker and Izumi, 2000; Snyder et al., 2000, 2003a; Whipple and Tucker, 1999, 2002) and provides a means of investigating the catchment-scale architecture of river channels and relating it to their erosive capacity, assuming that the evolution of the channel bed is rate limited by the ability

of the stream to detach elements of it. Many formulations of this relationship exist; however, almost all of them may be recast in the form

$$E = k_r k_c k_{\tau c} \mathrm{f}(Q_s)\, A^m\, S^n \tag{2.1}$$

where E is rate of channel incision, k_r and k_c are erosivity parameters based on substrate resistance and climate, respectively, $k_{\tau c}$ and $\mathrm{f}(Q_s)$ are threshold for erosion and relative sediment flux terms (both likely to be strongly nonlinear), A and S are upstream drainage area and channel slope, respectively (Whipple, 2004), and m and n are parameters that convolve the effects of channel width and basin hydrology responses, and are presumed constant. It may be shown that no matter what the details of the formulation, for all points in a river channel, we may write

$$S = k_s A^{-\theta} \tag{2.2}$$

where k_s and θ are parameters known as the channel steepness and channel concavity indices, respectively (e.g., Whipple and Tucker, 1999). This equation has been shown to be widely applicable within river channels on both a reach and catchment scale, it provides a mechanism for understanding river evolution without demanding an understanding of all of the parameters within a given incision law formulation, and it is applicable to both incisional and depositional systems (e.g., Whipple, 2004). However, working explicitly with the detachment-limited Equation 2.1, it may be shown that the value of concavity, θ, is governed only by m and n, and it may be further shown that based on known scaling of these two components, concavities for most natural channels ought to lie in the range 0.3–0.6, with a preferred value of 0.5 (Whipple and Tucker, 1999). This value ought to be the concavity measurable from field data for channels in topographic steady state under uniform forcing conditions. Similar arguments apply for the steady-state concavities of channels hypothesized to be limited by the rate at which the river can transport away material, rather than detach it, i.e., “transport-limited” channels, and these give an indistinguishable range

of predicted values (Whipple and Tucker, 2002). In contrast, the channel steepness, k_s, convolves very many effects, including climatic erosivity, rock uplift, channel bed resistance, width scaling and basin hydrology, sediment flux, incision thresholds, bed friction, and, crucially, whether the channel bed itself is in both flux and topographic steady state. If any of these controls also varies systematically downstream, this has the potential to create changes in the measured channel concavity (e.g., VanLaningham et al., 2006). Hence, the form of Equation 2.2 provides a sensible means of both displaying slope and drainage area data, and also investigating whether channels obey or indeed violate these expected scaling relations.

For our data, we also carry out power-law regression on plots of slope versus distance downstream, x, as opposed to upstream drainage area, A, giving correlation of the form

$$S = k_{\phi} x^{-\phi} \tag{2.3}$$

where ϕ is here defined as the channel curvature, and k_ϕ is a steepness term analogous to k_s. Hack (1957) first recognized a power-law correlation between downstream distance and upstream drainage area, and this curvature method allows us to discount changes in this power-law relation—Hack's exponent—as a potential cause of variation in channel concavity, that is, to isolate changes in the drainage architecture of the valleys caused by glacial resculpting as a mechanism for changing θ. A response in terms of drainage structure will lead to changes in θ while leaving ϕ unaltered. In other words, if the glaciers have little altered the preexisting channel form but have altered the structure of the drainage into the channels, comparing θ and ϕ should reveal this. This provides a complementary analysis to one based purely on concavity. An analogous approach has been previously exploited by other authors, though without explicitly considering variations in the value of curvature (e.g., Bishop et al., 2005). This method will also help prevent issues such as

dependence of rainfall on elevation (Anders et al., 2006; Bookhagen and Burbank, 2006) from clouding the analysis.

2.3 Field Area – Regional Setting

2.3.1 Geology

The Ladakh Batholith is part of the western end of the Transhimalayan Batholith system, and it represents the predominantly granodioritic plutonic core of part of the Cretaceous to Eocene arc batholiths that developed between India and Asia, and that are now ensnared into the collisional zone (Weinberg and Dunlap, 2000). The batholith is sandwiched between the Shyok suture zone to the north and the Indus-Tsangpo suture zone to the south (Searle et al., 1990), and both contacts are inferred to be presently tectonically inactive. The northwest-trending Indus River exploits the position of the contact with sediments to the south, following it fairly closely for the whole of the length of the Ladakh Range.

2.3.2 Topography

The present maximum elevation of the range above the floor of the Indus Valley varies from 2.3 km (west) to 4.1 km (east), while the ridgeline forms an almost horizontal divide, with summit elevations in the east around 6 km and in the west around 5.8 km. The ridgeline runs some 350 km broadly southeast-northwest, although there is a distinct kink in the center of the batholith in the vicinity of Leh, northwest of which the batholith trends more west-northwesterly (Fig. 2.1). Coinciding with this kink, the width of the batholith also decreases from ~40 km across both the southeastern and northwestern arms to 33 km. This narrowing is also associated with a slight decrease in summit elevation on the ridgeline of around 100 m.

2.3.3 Climate

The High Himalaya to the south of Ladakh blocks much of the northerly penetration of the annual Indian monsoon, creating arid desert conditions. Humidity in the summer months averages only 40 % (Fort, 1983), and modern precipitation at Leh is only ~80–100 mm/yr (Holmes, 1993; Spate et al., 1976), falling largely as snow in winter (Fort, 1983). Average monthly temperatures range from −8.2 °C to +17 °C (Spate et al., 1976), although diurnal temperature fluctuations are on the order of 25 °C (Cunningham, 1853), with winter temperatures frequently below −40 °C (Fort, 1983). This harshness of climate means that vegetation cover is scarce and discontinuous, although floors of river valleys are typically well cultivated, particularly at lower altitudes, due to human irrigation.

2.3.4 Geomorphology

The geomorphology of the Ladakh Batholith and Indus valley has been described by several authors (Bürgisser et al., 1982; Cunningham, 1853; Fort, 1983; Holmes, 1993; Jamieson et al., 2004; Owen et al., 2006). However, many of them have focused mostly or entirely on glacial geomorphology and, in particular, the geomorphology of the Indus Valley, rather than on the tributary catchments draining the batholith. The importance of glacial and periglacial action—that is, the effects of both flowing ice and other ice-mediated cold-region processes—on the landscape has been emphasized, along with reworking by snowmelt, glacial runoff, and mass movement processes. Jamieson et al. (2004) reported that some of these channels have developed knickzones due to the growth of valley glaciers in their middle to upper reaches, but the extent of this alteration varies with position and thus mean altitude of the individual catchments along the range. This arrangement provides a spectrum of data reflecting different degrees of glacial influence in the valleys.

Owen et al. (2006) provided a glacial chronology for these catchments, having measured cosmogenic ^{10}Be exposure ages from suites of boulders on the surfaces of moraines in seven of the valleys. Despite some scatter in their data, they argued that

the date of maximum advance was from 100 to 200 ka, and more probably between 100 and 150 ka. These dates imply that this is the oldest glacial sequence in the Himalaya, allowing us to examine the landscape response to overall glacial retreat on a time scale that is rarely available. In the Indus Valley around Leh, lake sediments have been dated at older than 50 ka (Phartiyal et al., 2005). This lake was formed by blockage of the Indus by ice and glacial debris emerging from the catchments draining the batholith (e.g., Bürgisser et al., 1982), and thus maximum glacial advance and lake initiation are believed to have been contemporaneous. Incision into the paleolake sediments upstream of Leh has been minimal, on the order of 20 m; downstream evidence is less clear but is unlikely to have exceeded 100 m since the last local glacial maximum. The geomorphic effect of base-level change is discussed in subsequent sections, but is minimal.

2.4 Field Observations and Interpretations

We undertook detailed field analyses in 10 of the valleys in the Leh area—Basgo, Nimmu, Tharu, Phyang, Leh, Sobu, Stakma, Nang, Karu, and Ratatse valleys (Fig. 2.1)—in order to establish a generalized geomorphologic structure (Table 2.1).

Figure 2.2 (next page). Generalized geomorphic structure for all significantly glaciated catchments. **(a)** Satellite imagery taken from Google Earth; images ©2009 GeoEye, DigitalGlobe, and TerraMetrics. Field of view is ~20 km across. Full catchments shown are Phyang (west) and Leh (east), with their drainage divides picked out with white dashes. Both drain southward into the anastamosing Indus River, which is visible at the bottom of the image. Leh airport is labeled and lies southwest of Leh town. White dotted lines demarcate the three domains that run along the range, as described in the text. Between the two dotted lines in each valley note in particular the gorges cut into the valley floors, which define domain 2 (c.f., Fig. 2.4). White V's show locations and directions of fields of view for photos shown in Figures 2.3-2.5, with the field of view arranged as if looking out along the arms of the V; solid lines indicate actual positions, while dashed lines indicate equivalent positions in Leh valley of images taken in catchments not shown in this figure. Inset shows in greater detail the hillslopes and valley floor in domain 1; the repeated sequence of valley-transverse rock ridges and associated fans as described in the text is very clear. **(b)** Cartoon of generalized glaciated catchment structure. Note that the boundaries between the domains are defined by the start and end of the gorge cut into the valley floor sediments in the middle reaches.

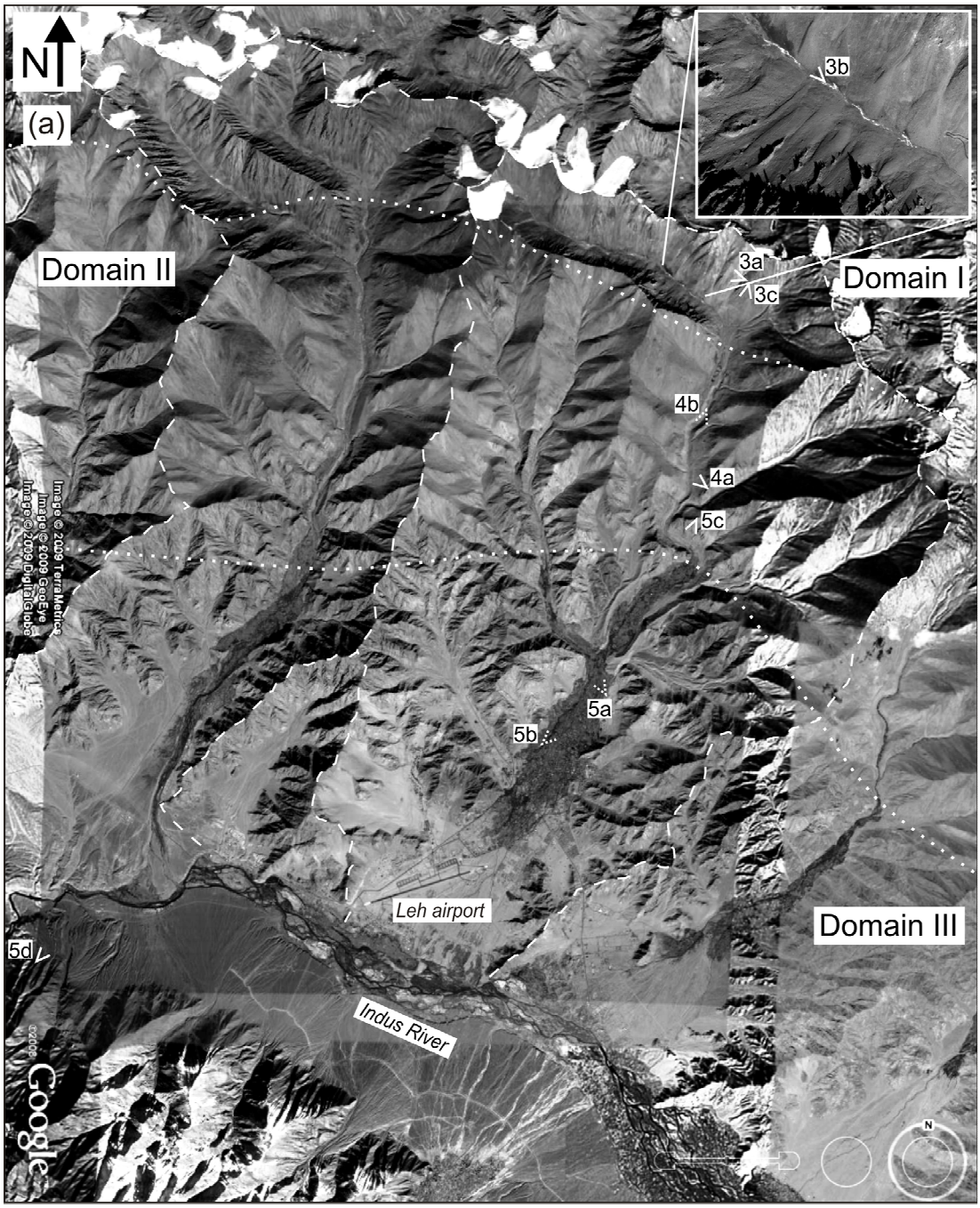
N
(a)
3b
Domain II
3a
3c
Domain I
4b
4a
5c
5a
5b
Leh airport
Domain III
5d
Indus River
Google

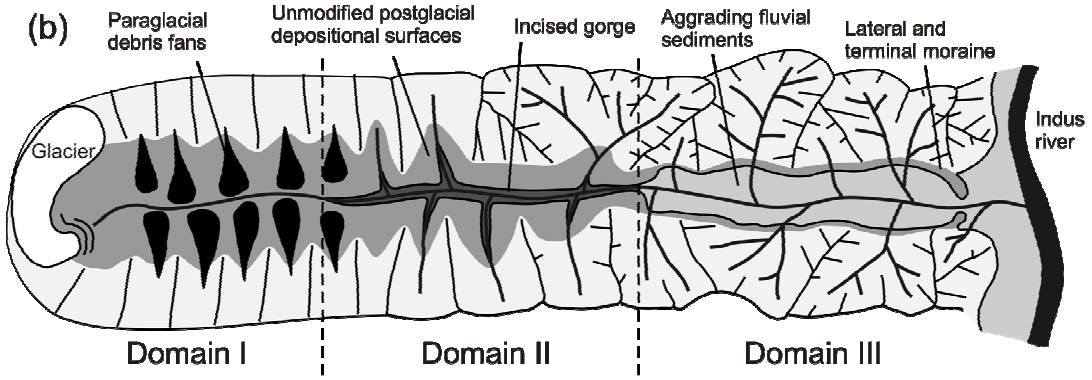
(b)
Paraglacial debris fans
Unmodified postglacial depositional surfaces
Incised gorge
Aggrading fluvial sediments
Lateral and terminal moraine
Glacier
Indus river
Domain I
Domain II
Domain III

TABLE 2.1. FIELD OBSERVATIONS OF PROPERTIES OF GLACIALLY ALTERED CATCHMENTS

Property	Domain 1 – the upper reaches (Glacially dominated)	Domain 2 – the middle reaches (Fluvial incision)	Domain 3 – the lower reaches (Fluvial aggradation)
Hillslopes			
Valley cross section	U-shaped; walls often dip >40°.	U-shaped, defined by facets on spurs between tributaries; V-shaped gorge inset into valley floor.	Convex spurs between side tributaries meet almost level valley floor at oblique angle; valley floor sediments onlap sidewalls. Spurs have marked break in slope 150-200 m above valley floor (Fig. 2.5a).
Hillslope morphology and tributaries	Transverse rock ridges every ~100m give crenulations perpendicular to valley; end abruptly 100-200m above valley floor (Figs. 2.2a, 2.3a); lichen & desert varnish common*. No tributary catchments.	Large tributary catchments, with ~km spacing; within these, linear hillslopes dip 30-40°.	Large side tributary catchments with ~km spacing, containing occasional bedrock landslide scars on 30-40° linear hillslopes.
Hillslope sediments	Gullies between rock ridges filled with loose, angular, lichen-poor*, very poorly sorted sediment, some blocks > 1 m; below ridges, debris fans cover most of sidewalls & project over valley floor.	Debris flow fans rare; in side catchments slopes covered with poorly sorted sediment with some lichen (like diamicton), accumulating more thickly at slope bases; some steeper surfaces are bare rock.	Side catchment slopes have some bedrock exposure & thin sediment drape; surfaces partly dissected; mean hillslope elevation ~1 km lower than in domain 1; bottoms of tributary valleys filled up to 10s of m depth†.
Hillslope-channel coupling	Debris fans intersect channel every 300-500 m (Fig. 2.3b). No direct coupling.	Direct coupling in side tributaries; valley sidewalls uncoupled from main axial channel; gorge walls are fully coupled.	Slopes not directly coupled to any channels, except at higher elevations in side catchments.
Valley floor			
Surface form	Hummocky§ sediment surface (Fig. 2.3c); ridges of thickly lichenous sediment transverse & parallel to valley axis (described as moraines dated by Owen et al. (2006)). Rare low bedrock outcrops present, most obvious in main channel.	V-shaped gorge cuts into same hummocky§ surface as in domain 1; sidewalls dip 32°; depth of gorge varies from 0 to 50-80 m just before halfway down domain 2, to 2-3m at domain 3 transition; length 4-8 km; floor width ~50m. Bedrock occasionally exposed in sidewalls; never in valley floor.	Broad, flat, alluviated, cultivated & artificially terraced plain extends across valley width (>500 m); surface is relatively flat, without hummocks, gorge incision, levees or sediment lobes around channels; active channel incised 0.5-3m (Fig. 2.5b), however, local incision increasing downstream to >20m exists at valley toes between Basgo & Phyang. Valley marginal or horseshoe-shaped ridges & mounds up to 80 m high sometimes present (Fig. 2.5c); tops are lichen rich, flanks lichen poor.
Sediment properties	Densely lichen coated*, sub-angular granodioritic sediment with bimodal sand-cobble particle distribution & occasional large (1-5m) blocks (diamicton) covers valley floor (Fig. 2.3b). Small glaciers often present at maximum elevations.	Valley-mantling sediment is lichenous diamicton as in domain 1; gorge sidewall sediment is lichen-poor*. Gorge floor often grassy, covering moderately well sorted subrounded sediment. In steepest reaches, channel may pass between 5-10 m wide, 1-2 m high bouldery sediment mounds, poorly defined though typically spanning valley floor#.	Entrenchment exposes valley fill of imbricated, well sorted cobbles interbedded with planar-laminated sands. Ridges & mounds composed of diamicton; later downcutting reveals that several m fill sediment covers mound toes (also noted by Fort (1983)). Where valley floors widen downstream near Leh (Fig. 2.1), sedimentation becomes fan-like; small divergent channels run across depositional surface (Fig. 2.5d); lichen & varnish cover is variable, but always less on sediment adjacent to active & recently active channels.
Channel			
Incision/Aggradation	Does not consistently aggrade or incise.	Incises, cutting gorge.	Aggrades; in downstream reaches deposition becomes fan-like (Fig. 2.5d).
Channel morphology & sediment	Narrow (<10 m) & steep (>0.1) single thread flow over cobbles & small boulders arranged in step-pool sequences & cascades along side debris fans; between fans, slope reduces to <0.05 with wide 30-100 m, shallow (~10cm), fine (D_{50} down to 2 cm) plane bed braided reaches (Fig. 2.3b). Lack of lichen demarks a high water line.	Braided channel contains 1-3 courses, abandoned channels common (Fig. 2.4b). Bedforms include steps & pools; moderately well-sorted pebble-small cobble surface. Spring head sapping starts occasional small channels joining main flows. Where S > ~0.15, D_{50} often increases abruptly to cobbles & boulders, with locked lichenous* boulders covering flow in cavity network beneath.	Commonly ~10 m wide, less steep (<0.08) single channel, gradually becoming less steep downstream; step-pool morphology, though tending towards plane bed with reducing gradient. Set within floodplain ~10 times wider (we observed inundation during 2006 storm flows). Channel grain size remains pebble-small cobble.

*An orange lichen of unknown species colonizes rock surfaces & a desert varnish forms, both of which provide a qualitative means of estimating sediment mobility, & hence exposure age of a surface.
†Estimated by extending exposed hillslopes beneath the surface in cross section, & assuming direct coupling to buried bedrock channels.
§Gently undulating, patchy topography, amplitude 1-2 m, wavelength several 10s of meters.
#Dissection of such mounds by the channel is clear in Phyang valley, where debris flow deposits associated with a major flood in 2006 have been cut through by subsequent fluvial activity within two years between visits.

2.4.1 Interpreted Catchment Structure—Glacially Modified Valleys

Inspection of remotely sensed imagery suggests that the form of the geomorphic domains outlined here is applicable to all catchments where U-shaped valley cross profiles are developed in their upper reaches (Fig. 2.2). We recognize three distinct domains sequentially present down the valleys, each of which reflects the locally dominant mode of channel behavior—from glacially overwhelmed, to incisional, to aggradational. The field-based descriptions of the geomorphic properties of each domain are recorded in Table 2.1. Next, we interpret the process geomorphology of each domain based on these field observations.

2.4.1.1 Domain 1, Upper Reaches—Glacially Dominated (Table 2.1; Fig. 2.3)

Almost all of the features described for this domain are consequences of the recent occupation of the upper reaches of these catchments by valley glaciers and the accompanying periglacial acceleration of weathering on exposed bedrock. The U-shape of the valleys indicates the action of warm-based subglacial abrasion and plucking (Bennett and Glasser, 1996). The abrupt termination of the transverse rock ridges some 100–200 m above the valley floor probably constitutes a paleosurface of the valley glaciers—a trimline—and suggests that significant arêtes were exposed above the ice, shedding large amounts of debris onto the surface of the glacier (e.g., Ballantyne, 1998). Along with the hummocky nature of the unmodified valley floor, this implies that much of the diamicton now mantling the valley is supraglacial in origin (Boulton and Eyles, 1979; Clayton et al., 2008), i.e., derived from material accumulated mainly on the surface of the glacier rather than at its bed, and this material mantles an irregular bedrock floor. However, the fresh debris fans shed from the sidewalls and characteristics of the river demonstrate that there has been significant paraglacial modification of this environment since glacial retreat. The angular, poorly sorted material of the fans is suggestive of frost-shattered debris being released from the hillslopes onto the valley floors, with localized extremely

Figure 2.3a,b. Figure continues on next page.

Figure 2.3 (see also previous page)**.** Field photos illustrating key geomorphic features for domain 1. **(a)** Classically U-shaped valley, looking west up toward glacier from dogleg in valley plan form, Leh catchment (compare Fig. 2.2). Transverse rock ridges and associated debris fans are particularly clear on the south flank. Note that these fans meet the channel thalweg, and that the channel is not incising. **(b)** Valley floor view of a typical point where a debris fan impinges on the channel, Leh valley. Main fan descends from right of image and meets the stream in the center left of the mid-distance. The steepness of the channel as it crosses the fans in contrast to the low gradient reach immediately downstream is obvious; for scale, this jammed cascade is ~5 m high. Many of the blocks comprising the fan material are in excess of 1 m across; the sediment in the low gradient reach is much finer, as also described in the text. **(c)** View southward from the dogleg in Leh valley. Trucks in foreground and military station of South Pullu in midground (left of image) provide scale. Note the hummocky texture of the valley bottom surface here. The gorge defining domain 2 begins around South Pullu and deepens southward. The irrigated valley fill of domain 3 and eventually the Indus Valley are visible in the far distance.

large blocks suggesting episodic sidewall collapse rather than a diffusive process (c.f., Augustinus, 1995; Dadson and Church, 2005). Moreover, the form of the river itself suggests that it is incapable of mobilizing much of the coarser material supplied by these debris fans where they impinge on the thalweg, and this has resulted in the mesoscale (300–500 m) reorganization of channel profile form. The river steepens to maximize its power over these coarse deposits and winnows out much of the finer sediment within the consequent cascades, resulting in the very high cobble-boulder D_{50} values. The channel then compensates for these steep reaches by aggrading between the cascades to reduce gradient, and much of the finer winnowed sediment is redeposited here. We note that this channel form is very similar to the process domain organization described by Brardinoni and Hassan (2006) for coastal glaciated British Columbia and that the inferred processes are similar to those suggested by Mueller and Pitlick (2005) for Halfmoon Creek, Colorado.

2.4.1.2 Domain 2, Middle Reaches—Fluvial Incision (Table 2.1; Fig. 2.4)

The basic relict valley structure mirrors the glacial influence already observed in domain 1. The presence of well-developed side tributary catchments points to a reduced glacial influence compared to the upper reaches. These side catchments have no evidence of remolding by flowing ice and are considered relics of the fluvial drainage structure before glaciation, lacking sufficient area to gather enough snow to form glaciers. The sediment mantling their present slopes is tentatively attributed to the action of periglacial freeze-thaw processes on these preexisting colluvial surfaces, partly retained within the sub-basins due to their reduced hillslope gradients compared to the sheer sidewalls of domain 1. The lichen covering on these blocks confirms the relatively immobility of these surfaces, and we suggest an average exposure time of several tens of thousands of years—their color is only a little lighter than that of the hummocky valley floor, which is known to be of the order of 100–50 k.y. old (Owen et al., 2006). However, it is the gorge cut into the trunk valley floor

that provides the defining distinction from domain 1. The dip of the sidewalls of the gorge is equal to the angle of repose for loose sand (Bagnold, 1966), and along with the lack of lichen cover on the sediment here, this indicates that these surfaces are being actively denuded by coupling to the incising river at their base (Burbank et al., 1996; Caine and Swanson, 1989; Strahler, 1950). Without the very coarse debris fans directly loading the channel that were present in domain 1, and with gradually increasing discharges and slopes in the channel, the transition to domain 2 represents the first time the stream power has become high enough to fully mobilize enough of the sediment to initiate incision (c.f., Parker and Klingeman, 1982; Wilcock, 1993; Wilcock and McArdell, 1993). This transition point represents the location at which a threshold for fluvial transport and erosion has been exceeded, and the river downstream may be regarded as self-formed, i.e., it has not inherited its channel properties purely from the relict surface left by the glacier, but instead has begun to form its own profile by sediment reorganization under the hydrologic regime or regimes active since glacial retreat. The coarser, less mobile sediments in the steeper reaches, especially where associated with mounds of this sediment at the sides of the channel, are interpreted as deposits from debris flows traveling down the gorge. However, these mounds appear on either side of the channel and seem to have been cut through by the flow, and, along with direct evidence of incised recent debris flow activity in Phyang Valley, this suggests that the fluvial processes active in these channels are dominant over the debris-flow activity on the medium to long term.

Figure 2.4 (next page). Field photos illustrating key geomorphic features for domain 2. **(a)** Well-developed gorge midway down domain 2 at a tributary confluence, Leh catchment. Gorge is ~60 m deep at this point, and some bedrock is exposed in the sidewalls at this location. Note the contrast in shade between unincised valley floor (orange) and non-bedrock gorge sidewalls (gray). Break in slope is picked out. **(b)** Typical channel form and floodplain within gorge. Image is from Basgo Valley, looking downstream. Yaks for scale.


(a)


(b)

2.4.1.3 Domain 3, Lower Reaches—Fluvial Aggradation (Table 2.1; Fig. 2.5)

This domain is a region of long-term fluvial aggradation, shown by the flat-lying fluvial sediments filling the valley (sorted cobbles and sandy laminated overbank deposits), and evidence for channel avulsion in the form of abandoned channels lower down the domain. The diamicton mounds in this domain are interpreted as terminal (horseshoe-form) and lateral (linear) moraines of the former glacier, consistent with the work of others in the region (Fort, 1983; Owen et al., 2006). The freshness of their sides indicates that the modern river periodically couples directly to their slopes. The drape of fluvial sediments onto the toes of these structures indicates that a major episode of aggradation postdates the maximum advance of the glaciers at ca. 100 ka (Owen et al., 2006). We relate the deep channel entrenchment between Basgo and Phyang to breaching of the glacial dam system around Basgo and Nimmu (see Regional Setting) and the propagation of this signal up the Indus and the associated side tributaries. Elsewhere, we link minor incision present in the tributaries to minor, ~10 m entrenchment into the valley floor by the Indus unrelated to the dam breach. However, we emphasize that these landscapes remain significantly active, and recent aggradation has occurred, as indicated by the freshness of portions of the fan surfaces in the lower parts of this domain. This aggradation also occurs in valleys where there is no good evidence for significant base-level change on the Indus, implying that it is a behavior driven primarily by processes occurring upstream, and not just governed by downstream base level. The main channels of the tributaries and the fan surfaces lack evidence of levees and inverse grading (sediment coarsening upward), characteristic of debris flows, and are interpreted as purely alluvial settings, in spite of the coarseness of some of the channel loads (c.f., Owen, 1991). This interpretation is corroborated by the observations from the remotely sensed data that the fans are also concave-up rather than planar, and they exhibit slope-drainage area relations more typical of fluvial than debris-flow processes (see next section). On the hillslopes and in the side catchments within the tributaries, colluvial processes are active. The paucity of sediment drape on these slopes in these side catchments relative to the side catchments in domain 2 is perhaps linked to decreasing efficiency of periglacial

weathering action with altitude, or to an increase in the amount of precipitation falling as rain rather than snow, removing the buffer on peakedness of flood discharge provided by ice (Fountain and Tangborn, 1985; Jansson et al., 2003) and allowing better mobilization of larger clasts.

2.4.2 Generalized Catchment Structure—Less Glacially Modified Valleys

Where U-shaped valley cross profiles are not present in the upper reaches, valley form is different. These catchments are smaller than the contrasting three domain valleys described already. They do not reach the main drainage divide and are confined to lower mean basin altitudes. Glaciers or major accumulations of interannual snow (firn) are never present in these today. Such catchments provide a reference case against which to compare the observations presented in Table 2.1. Generalized catchment form is more variable, and the description given here is based largely on the Ratatse catchment in the east of the accessible field area (Fig. 2.1).

2.4.2.1 Observations of Hillslopes and Valley Floor

The flow is confined to a single channel that is coupled directly to the surrounding slopes, meeting bare rock hillslopes in the upper reaches. Flattened, diamicton-draped surfaces a few meters thick are occasionally present, but they are not associated with widened valley form, are preserved only perched above the modern river base level, and are a minor component in the landscape. Lower in the catchments, the channel incises down several meters into crudely bedded, poorly sorted cobbles (D_{50} ~5 cm), which are coarser and more poorly sorted than the present channel material (Section 2.4.2.2). This sediment forms flat surfaces already filling the valley in its lower reaches. Satellite imagery indicates that there is a

continuum from catchments more heavily sediment flooded in their lower reaches, especially around the Leh paleolake, to much less sediment-flooded catchments, with good coupling to the surrounding bedrock hillslopes and well-developed V-shaped valleys.

2.4.2.2 Observations of Channel and Sediment Load

The lack of a glacier or firn in the valley headwaters means that these catchments are ephemeral, and there is no flow when there has been no rain. They show very coarse (D_{50} > 20 cm), jammed, angular blocks combined with very steep channel slopes (0.2–0.5) in the uppermost reaches, fining very rapidly into a moderately well-sorted veneer of medium- to coarse-grained (D_{50} < 2 mm) sand mixed with occasional gravel and cobble clasts as the slope falls beneath ~0.15. Below this (generally <50 cm) is bedrock. Almost all of the sediment in the channels is angular, subangular, or subrounded and lacks flat faceted faces.

Figure 2.5 (next two pages). Field photos illustrating key geomorphic features for domain 3. **(a)** Aggradational valley flats in Karu valley, looking north. Notice the drape onto the rocky sidewalls of this well-irrigated surface, and also the convex valley sides, with a break in slope clear toward the left of the image. Moraines are visible in the mid-distance (light tan structures), and eventually domain 2 and a hanging valley at the head of domain 1. **(b)** Channel entrenched a few meters into top surface of valley floor, Basgo valley. Channel is ~5 m wide. An artificial dry stone wall has been constructed on the far side of the channel. River is shown in flood, several days after exceptionally heavy rains in summer 2006. **(c)** Lateral and terminal moraines in Leh valley domain 3, looking southward. Indus Valley and Indus molasse sediments of the Zanskar Range beyond it are visible in the distance. **(d)** Indus Valley and fan of Phyang Valley from airplane, looking north. Notice entrenchment of modern channel into slightly (10–20 m) raised fan surface, and abandoned channel courses across fan.

Figure 2.5a,b. Figure continues overleaf; caption on previous page.

Figure 2.5c,d. See previous page for caption.

2.4.2.3 Interpreted Geomorphic Structure

The differences between this form and the valley form described previously can be ascribed to the fact that no glacially molded reach had developed in these catchments. Glaciers have been present in these valleys, as demonstrated by the accumulations of diamicton on undissected surfaces perched above the modern channel, but they have not carved significant U-shaped sections or widened the valley floors. Consequently, the amount of glacially processed sediment apparent in these valleys is also much smaller, with very rarely glacially faceted sediment and much more commonly angular slope failure debris in the channels. This is most apparent in the topmost, steepest reaches of the channels, where a true colluvial, debris-flow–dominated process regime has developed (angular, jammed coarse blocks giving way suddenly downstream to moderately well-sorted fluvial sands and gravels, indicating that flows of these blocks have frozen). This arrangement is typical of unglaciated, unperturbed, steep bedrock channel systems in other mountainous areas (Montgomery and Foufoula-Georgiou, 1993; Stock and Dietrich, 2003). We interpret the accumulations of poorly sorted cobbles forming incised terraces in the lower reaches as broadly analogous to the aggradational domain 3 in the glaciated catchments described previously, in that they represent a proximal storage site for material mobilized from the higher parts of the catchment, though they lack the inset morainal landforms seen in those cases. These older sediments are coarser than the modern channel material, and are perhaps debris-flow influenced. This material may be derived from early stage postglacial mobilization of the small amounts of loose diamicton present higher up these catchments.

2.5 Remotely Sensed Data

Methodology for the acquisition and processing of the DEM is described in Appendix A. For each trunk stream in the studied catchments, we derived data covering downstream distance (x), elevation (z), drainage area (A), and channel slope (S), smoothed across a 500 m window to remove finer scale noise in the data. We then used these extracted variables to examine the long profile for each trunk stream (plotting z versus x), and the concomitant variation in A and S with x. Prompted by the form of Equation 2.2, we also plotted slope versus area for each stream. Where discontinuities were present in the S-x and S-A plots, we subdivided the profiles into discrete segments, on the basis of local maxima in slope (see Fig. 2.6). These "points of curvature" were identified analytically for each stream, allowing unbiased comparison. Data were also visually inspected to ensure that the magnitude of the slope maximum peak was larger than the inherent scatter in the slope values surrounding it; where it was not, the point of curvature was set to the top of the profile or to a better-defined smaller peak. Where two or more slope peaks of similar magnitude were present, the one furthest downstream was selected. The point of curvature defines the position of a knickzone within a profile, a broad convexity (sensu Zaprowski et al., 2001), rather than a localized reach-scale feature. The location of each point defines an associated distance downstream, x_{PC}, and upstream drainage area, A_{PC}, for the downstream channel segment (Fig. 2.6). We also recorded the corresponding values of downstream distance and drainage area at the end of the downstream segment, x_{tot} and A_{tot}. On the basis of Equation 2.2, we then fit power laws to each of these segments downstream of x_{PC} on the slope versus area graphs, iteratively minimizing the sum of the squares error in the predicted value of slope. In some cases, a distinct but slight steepening is observed in the lowest few kilometers or less of the channels, of which the data presented in Figure 2.6 provide a typical example. We attribute this to minor base-level change occurring in the Indus Valley and propagating upstream as already described in the field observations, and where apparent, this oversteepened reach was excluded from the analysis. However, we also repeated the analysis without removing these sections and were able to show

that this removal does not significantly affect any of the conclusions drawn herein. The effect of this short oversteepened reach is typically just to increase the error on the fitted power laws, rather than to systematically alter them.

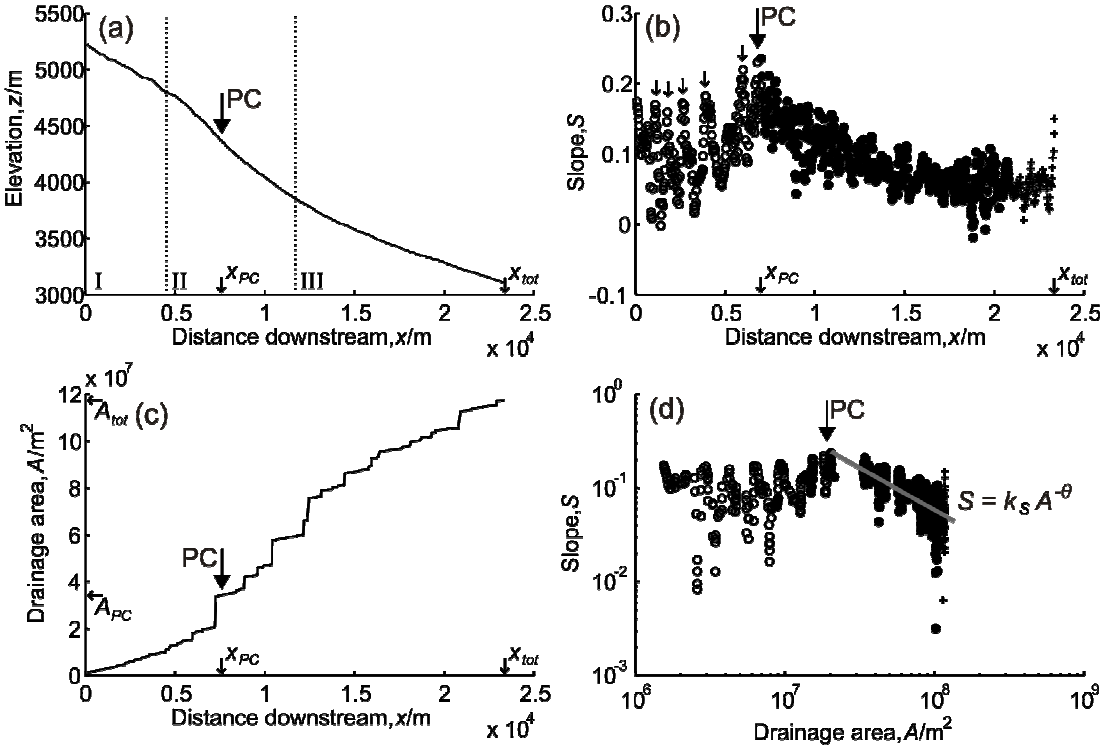

Figure 2.6. Example plots for a typical catchment showing derivation of θ from digital elevation model (DEM) data. See text for full explanation. **(a)** Long profile. Domains, known from field observations, are indicated with Roman numerals. **(b)** Slope of long profile. Point of curvature, PC, the slope maximum where long profile becomes concave on a long wavelength, is defined here. Open circles upstream of this point are excluded from numerical analysis. Steepening data at the toe of the channel, interpreted as related to base-level change in the Indus, are plotted as crosses and were also excluded from analysis. Small arrows pick out sawtooth pattern of steepening and shallowing reach segments within domain 1—these correspond to the large-scale step-pool channel structure as described in the field observations. **(c)** Drainage area evolution downstream. **(d)** Slope-area plot. Symbology as in b. Line represents least squares best fit to filled circles; θ is the exponent on A from this fit.

These fitted power laws yield a value of steepness (k_s) and concavity (θ) for each channel segment (see Equation 2.2). Note that we have deliberately chosen not to fit normalized steepness indices based on a reference concavity (see, e.g., Wobus et al., 2006b) to our data, since we shall show that significant and meaningful variations in measured channel concavity systematically occur, rendering the idea of a constant reference concavity meaningless for these catchments. We also do not discuss further variations in k_s within this data set, since it is known to be strongly correlated with θ (Wobus et al., 2006b), and if we cannot use a reference concavity to deconvolve this effect, this correlation will overwhelm any other signal not related to the concavity in the data. The same rationale has been applied to fit Equation 2.3 to the data set, providing values of channel curvature (ϕ) alongside our concavity values.

We constructed acceptable power-law regressions on the data for 58 trunk streams in 50 different catchments. This full data set is presented in Appendix B as Figures B1 and B2. The remaining streams are either too short (significantly less than one order of magnitude change in abscissa downstream of knickzone), have too many artifacts present in the SRTM data, or clearly do not follow a power-law relationship in slope versus area in their lower segments. These latter two cases are represented by 95% confidence intervals exceeding 50% of the calculated concavity value. There is no spatial pattern to the distribution of these poorly fit catchments along the batholith, and we hypothesize that they record areas where the glacially inherited form of the catchment has not been significantly modified by the subsequent fluvial system.

We recognize two distinct channel forms amongst the analyzed long profiles. The first represents a reference case, where the steepest reaches of the catchment are in the headwaters, and the whole stream is described as a single segment with a single power law fit through the slope-area data. These catchments correspond exactly to those lacking U-shaped valleys in their upper reaches, as described in the field observations. In the second case, each catchment shows a major knickzone

somewhere in the middle of its long profile, which divides it into discrete segments. Upstream of this knickzone, the valley form is commonly convex-up on a large scale, although on a finer scale, it can sometimes be subdivided into a number of short consecutive concave reaches (see Fig. 2.6). Downstream of the knickzone, the channel may be modeled as a single concave reach, with a well-defined power-law regression line. This second catchment form corresponds to the three-domain catchment type recognized in the field and described in the previous section. The point of curvature corresponds to the position of the knickzone, and it is always present within the gorged section of domain 2. The convex reach upstream of the knickzone thus corresponds to domain 1 and the upper part of domain 2, and we correlate the finer-scale concave reaches here with the pool-riffle type sequences observed in domain 1. Downstream of the point of curvature, the river flows entirely on a mobile sediment bed, either incising (domain 2) or depositing (domain 3)—the channels are self-formed downstream of the point of curvature. Visual inspection of the satellite imagery suggests that a point of curvature further downstream is associated with more extensive expression of domain 1, and in those catchments the transition from domain 2 to 3 is nearer the catchment outlet.

We checked the accuracy of our remote-sensed channel bed slope measurements by comparing them directly to field measurements of slope on a 30 m scale taken for the catchments of Basgo and Leh (see Figs. B3 and B4 in Appendix B). Within domains 2 and 3, field slopes match slopes extracted from the DEM well, though they tend toward the low end of observed values. Within domain 1, there is more variability, reflecting the rapid variation of true slope induced by the pool-riffle morphology on a scale much less than the 500 m averaging of DEM slope. However, field- and DEM-derived values are correlated 1:1 within error (Fig. B4 in Appendix B), and this leads to no differences in calculated concavities using either one data set or the other.

Our concavity data for all analyzed catchments fall in the interval $0.22 < \theta < 5.57$, and many values are significantly elevated above the expected theoretical range for streams in erosional steady state. A *t*-test confirms that these data are not

consistent with the highest expected steady-state value of $\theta = 0.6$ (Whipple and Tucker, 1999), to 95% confidence. Instead, we observe from the remotely sensed imagery that the significantly elevated values of concavity are associated with more extensive expression of domain 1 in the upper reaches, i.e., with a heavier glacial influence on the catchments. Moreover, concavity values remain high throughout the lower half of domains 2 and 3, with no apparent change as the system switches from incisional to aggradational behavior (see following). Those catchments that do not develop domain 1 at all, however, i.e., those that are not noticeably glacially beveled in their headwaters, retain concavities consistent with the expected theoretical range of $0.3 < \theta < 0.6$. We are able to investigate this hypothesized relationship quantitatively by plotting concavity (θ) versus A_{PC}/A_{tot} for each analyzed catchment (Fig. 2.7); this value determines the relative position of the glacially induced knickzone within each catchment, and so quantifies the relative impact of major glacial alteration downstream (see Figs. 2.6 and 2.7). A catchment lacking development of domain 1 will have an extremely low value of A_{PC}/A_{tot}, while a catchment where domain 1 extends far downstream would have a value of A_{PC}/A_{tot} approaching 1. Note, however, that as A_{PC}/A_{tot} increases, the amount of data on which our concavities are fitted also falls, increasing the analytical error on this value. This is reflected in the 95% confidence error bars shown in Figures 2.7 and 2.8, but even considering this error, we are still able to show a systematic increase in θ with A_{PC}/A_{tot}. Notice that we could equally well have plotted θ versus x_{PC}/x_{tot}, expressing extent of glaciation in terms of downstream distance instead of drainage area. We have chosen the drainage area plot because we wish to go on to attribute these trends to disequilibrium response of the systems to water discharge flowing into and through domains 2 and 3 (see Discussion).

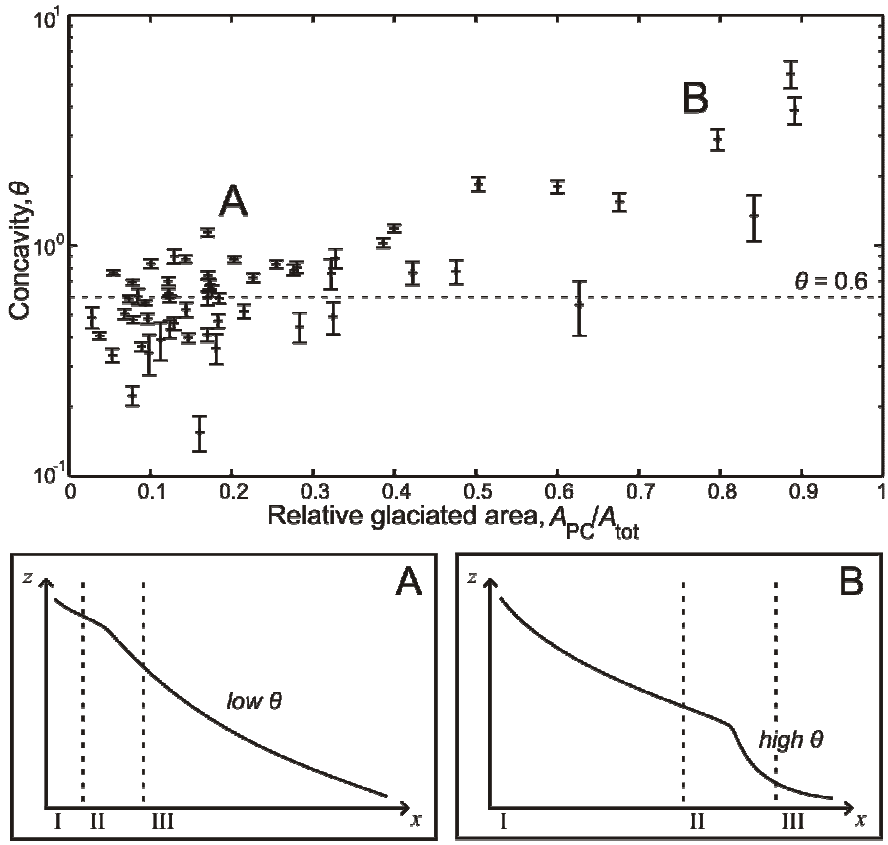

Figure 2.7. Relation of channel concavity to relative area upstream of point of curvature. Error bars are 95% confidence limits; note log scale on the *y*-axis. Data points represent individual catchments along the batholith. Cartoons illustrate effect of this concavity change on channel long profile form for channels showing little alteration by glaciers (A) and greater alteration (B), and also show schematic relative positions of domains downstream (denoted with Roman numerals).

We may also isolate the role of changes in catchment drainage structure, i.e., Hack's law, in causing these effects by plotting channel curvature ϕ versus A_{PC}/A_{tot}, as described in the Methodology. We also plot ϕ versus x_{PC}/x_{tot}, since this is more geometrically and dimensionally consistent. These two plots are shown in Figures 2.8a and 2.8b. Notice that broadly the same trend is evident in this figure as was shown in Figure 2.7, but that the fit is poorer and the data are less well grouped, especially for Figure 2.8a. This is to be expected, however, as we have removed the controlling effect of discharge on channel form by plotting curvature not concavity, and this problem is amplified by the mismatch of variables in the former of the two

plots. Note that we consider trend shown in Figure 2.7 to be stronger than that shown in Figure 2.8b, because the data are less scattered, and also because the relationship in Figure 2.8b suggests a maximum theoretical value for the curvature, which seems less physically reasonable than the asymptotic trend suggested by Figure 2.7. Even so, the broad similarity between Figures 2.7 and 2.8a–2.8b informs us that the river channels are indeed responding to increased amounts of glaciation by varying their slopes, as opposed to responding to altered drainage structure. This result is consistent with the field evidence we have presented for active aggradation of and incision into the valley floor in domains 2 and 3. We also note that no correlations are seen with either absolute catchment size, or absolute area above the point of curvature (Figs. 2.8c and 2.8d).

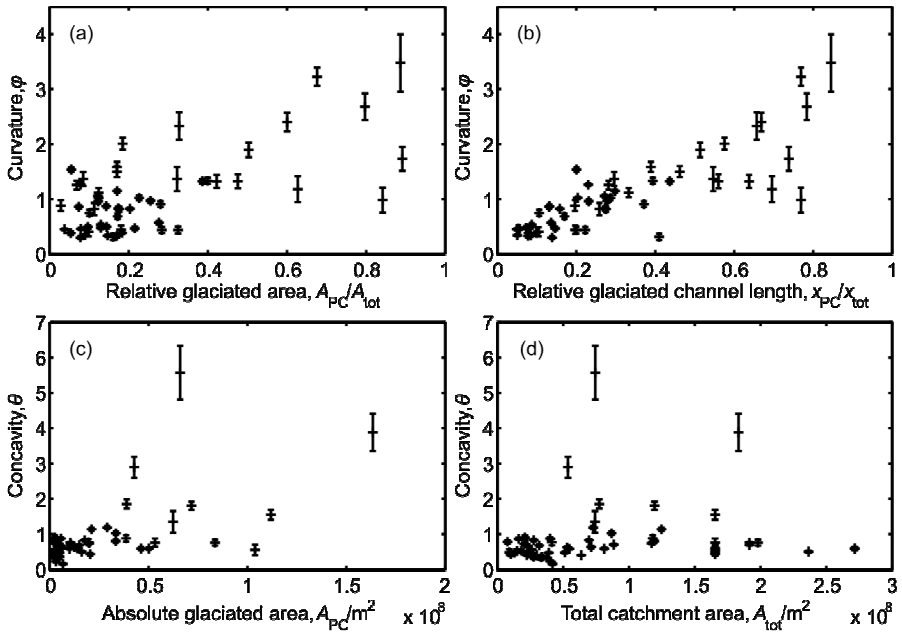

Figure 2.8. Analyses of other channel scaling metrics versus measures of relative amounts of glacial alteration in channel headwaters. All error bars are 95% confidence limits; note linear scales on the *y*-axes. Data points represent individual catchments along the batholith. Graphs contrast with Figure 2.7. **(a)** Channel curvature versus relative area upstream of point of curvature. **(b)** Channel concavity versus relative channel length upstream of point of curvature: notice occasional significantly depressed values of ϕ at elevated values of x_{PC}/x_{tot}. **(c)** Channel concavity versus absolute area upstream of point of curvature. **(d)** Channel concavity versus total catchment area.

Unfortunately, there is neither enough independent change in drainage area within domain 2, nor enough surety as to the precise location of its lower boundary across multiple catchments, to fully assess the possibility that domains 2 and 3 have different concavity values. However, we examined the convergence of the values of θ and ϕ to assess whether they systematically increase or decrease downstream, as presented in Appendix Section B3. The data suggest that this is not the case (see Fig. B5), and this implies (though cannot demonstrate) that there is not a significant and uniform scaling change either between domains 2 and 3 or more generally within either domain.

2.6 Discussion

2.6.1 Causes of Observed Concavity Trends

We suggest four possible reasons for the systematic increases in downstream segment concavity with point of curvature (and hence knickzone) position in the profile, as seen in Figure 2.7:

1) The signal is an artifact of either (a) systematically incorrect values of slope in the remotely sensed data, or (b) an increase in the relative importance of data scatter as the channel segment being analyzed becomes proportionally smaller.

2) The signal is glacial, carved in by the passage of ice into the lower regions of the catchment, and is unaffected by subsequent return to fluvial conditions.

3) Altered hydrologic conditions in the river are responsible for the signal, either (a) changes in the stochasticity of discharge in the channel caused

by the presence of a glacier in the upper reaches of the valley, or alternatively (b) orographic rainfall effects.

4) The signal is a consequence of the glacially generated knickzone in the middle reaches of the channel. The knickzone alters the expected scaling of variables such as channel width or sediment flux in the system, violating the assumptions behind the slope-area relationship.

We preclude hypothesis 1a on the basis that excellent correlation is obtained between field derived and remotely sensed slope values where known (see also Figs. B3 and B4), and values of concavity obtained for these catchments using each type of slope data are within error of each other. The role of processes in hypothesis 1b is also unlikely to be large, since there is no reason to assume that error introduced by scatter should be systematically positive, and no correlation is seen with the absolute parameters shown in Figures 2.8c and 2.8d.

We do not favor hypothesis 2 for this field area since the channel shows characteristics of being self-formed downstream of the point of curvature, as previously discussed in the field observations, meaning the signal is not purely glacially inherited. Moreover, due to the log-log scaling, much of the concavity signal is accommodated by changes at low gradient, that is, in the depositional regime of domain 3. Thus, only small changes in bed elevation, and hence in volume of sediment redistributed, are required to allow these small changes in slope. This strongly implies that the channel can readily adjust its concavity. However, similar work in nonglaciated regions will be required to conclusively falsify this hypothesis.

Modified hydrologic conditions induced by the upstream glacier (hypothesis 3a) may play some role. The exact effects, however, will depend strongly on the river response time scale. On interannual time scales, the presence of glaciers covering some intermediate proportion of the catchment will reduce the variability of runoff (Fountain and Tangborn, 1985; Jansson et al., 2003), since there is almost always background runoff from the melting glacier onto which precipitation spikes are

superimposed, and moreover the amplitude of each precipitation spike will be reduced as much of the precipitation arrives as snow, which will be released into the rivers gradually. However, melting glaciers can increase the magnitude of the individual largest flood events if glacial floods coincide with peak summer runoff (Braun et al., 2000), and the snowmelt will significantly alter the shapes of the associated flood hydrographs. Other authors have previously demonstrated that such changes can alter the responses of an incising river network, including channel concavity, largely by changing the frequency of breaching of erosion thresholds or by interacting with any nonlinearity in control of erosion by discharge within the models (Craddock et al., 2007; Molnar et al., 2006; Snyder et al., 2003b; Sólyom and Tucker, 2004; Tucker and Bras, 2000). These effects may also be enhanced by the aridity of this environment noted in the regional overview (Molnar et al., 2006). However, these studies have indicated that these changes, which make the flood hydrographs more spiky and less like the uniform, constant rain regime assumed by a standard stream power approach, should reduce, not increase, concavity, and thus this seems unlikely to be a first-order control on the concavity trends observed here. We note though that these studies have been carried out only on incising channels and cannot directly explain the behavior of the aggrading reaches, though we anticipate that similar arguments would apply in such regions, based on sediment mobility thresholds. Additionally, none of these modeling approaches explicitly considers disequilibrium scaling, instead only analyzing landscapes under topographic steady state, so we cannot preclude hypothesis 3a entirely.

The other alternative, hypothesis 3b, is that rainfall itself may be a function of altitude in these catchments, with more arid conditions higher up (Anders et al., 2006; Bookhagen and Burbank, 2006; Craddock et al., 2007). Such effects do have the capacity to increase concavities, as seen here by increasing erosivity at lower altitudes for a given drainage area. However, we note that this effect should also somewhat increase the concavities of those catchments that do extend to higher altitudes but do not develop major knickzones (e.g., Tharu valley in Fig. 2.1), which does not appear to be the case in our data.

We thus attribute the observed concavity trends mainly to hypothesis 4, and we suggest that conventional scaling relations must be altered during transient river response in these settings. Detailed analysis of quantitative field data, for instance, channel width or measured sediment fluxes, will be necessary to conclusively show the nature of this change, but since we have observed nonlinear amplification of concavity with relative knickzone position, we infer that k_s must itself be a nonlinear function of discharge, and we anticipate that the scaling change will primarily be within the nonlinear elements of Equation 2.1, i.e., in the sediment flux or threshold parameters. A stream power incision law method cannot capture the dynamics of the river in the aggrading zone, but the very fact that this trend is evident so strongly within the depositional domain 3 implicates the interaction of sediment flux and caliber with carrying capacity of the river as the ultimate cause of this effect.

2.6.2 Implications

2.6.2.1 Direct Control of Downstream Channel Hydraulic Scaling by Upstream Glacial Modification

We have demonstrated that for the catchments draining south into the Indus River from the Ladakh Batholith, the rate of change of local channel slope of each river below a glacially induced knickzone is set according to both contributing upstream drainage area and relative position of the knickzone within that catchment. This predictable pattern provides insight into the route by which such perturbed channels approach an equilibrium state. We may then test whether existing incision law and sediment deposition formulations successfully map out this path. An appropriate formulation will allow us to forward model this response, both within the conventional frameworks applicable to incising systems specifically where the gorge is developed in domain 2, and also continuously throughout the whole length of the river in domains 1, 2, and 3.

2.6.2.2 Rates and Time Scales of Paraglacial Recovery

Variations in the concavity of these systems also have implications for understanding the distribution of postglacial sediment fluxes out of these channels and into the Indus though time. During glacial retreat, we expect a coarse sediment (pebble-boulder fraction) production spike, as the glacially buttressed and oversteepened bedrock side walls of the valleys have their ice support removed and are exposed for the first time to the intense freeze-thaw cycles of the periglacial environment (Church and Ryder, 1972; Dadson and Church, 2005; Harbor and Warburton, 1993). However, we have shown here that in order for the postglacial valley floors to adjust their slopes in line with Equation 2.2, they must both incise into these floors around the point of curvature and aggrade in their furthest downstream reaches. This means that some significant fraction of the coarse sediments produced during glacial retreat does not reach the Indus, but is initially locked up in the more proximal lower reaches of the tributary valleys. If not flushed out by subsequent glacial readvance, this sediment will only be released following significant base-level fall on the trunk stream, which need not be coupled to glacial dynamics at all, or by significant relaxation of the knickzone in the upper reaches back toward a concave profile. Thus, we should expect to observe release of glacial sediments into basins further downstream across time scales much longer than those created by the movement of the ice masses themselves—both as discrete pulses, driven by bottom-up base-level changes, and gradually, driven by relaxation of the glacial modification of the catchment.

We can obtain a lower bound estimate for this postglacial recovery time by predicting the elevation of the hypothetical channel with curvature $\phi = 0.5$ for the example catchments of Basgo, Leh and Sobu using the channels' current maximum and minimum elevations, and then comparing the elevation of the point of curvature now with that predicted in the hypothetical channel (see Fig. 2.9). We work with curvature as opposed to concavity here since this allows us to handle the long profile without assuming a drainage structure, and we select a value of 0.5 on the basis of

the minimally altered catchments in Figure 2.8b. We know the approximate 100 ka age of the postglacial surface (Owen et al., 2006), the maximum amounts of incision into this surface in that time, and the equivalent heights of the hypothetical "steady-state" profiles at the same points. If we then assume that rates of recovery toward equilibrium are likely to exponentially decay (e.g., Ballantyne, 2002a; Howard, 1988), as indicated in the inset to Figure 2.9, then we may calculate an approximate relaxation time scale for these catchments by solving the equation

$$z = \frac{k_t}{\lambda} e^{-\lambda t} \tag{2.4}$$

where z is the elevation above our steady-state profile, t is the time elapsed since deglaciation, λ is the decay constant (equal to the inverse of the e-folding time scale, τ), and k_t a constant. Table 2.2 presents these data and the calculated rates and time scales. Thus, under the extremely optimistic assumption that this early rate of recovery will be sustained throughout the relaxation, especially if and when the incising river strikes bedrock rather than cutting into loose sediment, we quote a lower bound of ~500 k.y. for the response time of this system, with perhaps a factor of two error reflecting known error in the time elapsed since glacial retreat. Thus, if these catchments are not tectonically perturbed, we can expect to see significant quantities of sediment actually produced during glacial retreat being locally stored and then subsequently and gradually released into the Indus River and beyond throughout at least the next half a million years, assuming that no further glacial readvances occur.

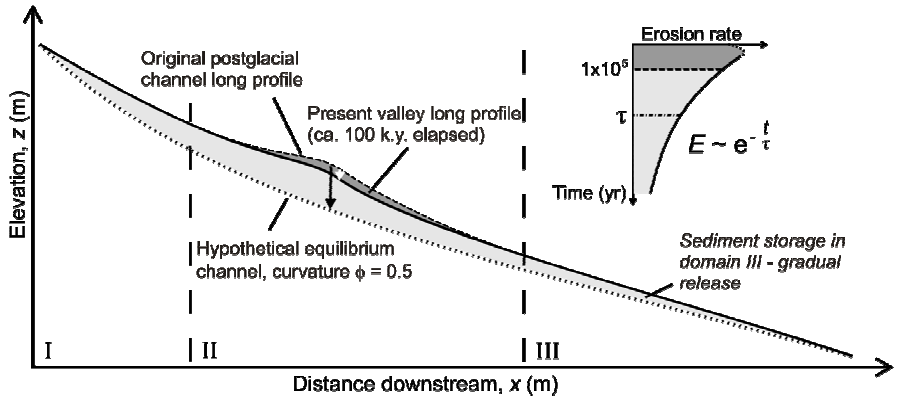

Figure 2.9. Schematic of method for estimating catchment recovery time. Solid black line represents present channel profile; dashed line represents reconstructed profile immediately after deglaciation based on gorge sidewall elevations. Present-day positions of domains are demarked and labeled with Roman numerals. Dotted line represents hypothetical idealized unperturbed profile for catchment of this drainage area, based on a curvature of 0.5 and a pinned point at the head of the catchment. This approach requires the removal of the minimum amount of material (light shading). Arrows indicate maximum amounts of lowering known to have taken place since the local last glacial maximum (white arrow) and that must occur in total to reach this hypothetical profile (black arrow). We may then calculate recovery times based on dates provided in the literature for the local last glacial maximum, and an assumed exponential decrease in incision rates (see text and inset).

TABLE 2.2. RATES AND TIMESCALES OF RESPONSE FOR SAMPLE CATCHMENTS

Catchment	Basgo	Leh	Sobu
Data used			
Max. depth of gorge (m)	53	65	78
Present elevation of max. depth point above equilibrium profile (m)	360	260	350
Time since deglaciation (k.y.)	100	100	100
Calculated values			
Decay constant, λ (/k.y.)	0.00137	0.00223	0.00206
Time constant (e-folding time), τ (k.y.)	730	450	490
95 % recovery time (k.y.)	2180	1340	1460
Max. incision rate (mm/yr)	0.53	0.65	0.78

This calculation and interpretation evoke the conclusions of both Church and Slaymaker (1989), who argued the importance of secondary remobilization of sediments in Quaternary landscape evolution, and Dadson and Church (2005), who used a coupled fluvial and landslide landscape evolution model of a postglacial U-shaped valley to demonstrate that a pulse of sediment out of this system could be delayed from the actual time of deglaciation by several to many thousand years. We note also the results of Brocard et al. (2003), who calculated a response time scale of 20 k.y. for the Drac River in response to glacial retreat from its lower reaches, and the similar but even more rapid response times (~10^2 – 10^3 yrs) reported by Meigs et al. (2006) for a similar scenario, but emphasize that both of these studies examined readjustment occurring by the fundamentally different mechanism of "bottom-up" glacially controlled base-level fall rather than the "top-down" response to glacial carving of the headwaters of a catchment discussed here. Perhaps the closest match to our data is to the modeling work of Braun et al. (1999), who reported time scales on the order of 50 k.y. for fluvially transported paraglacial sediment fluxes out of a mountain range–scale erosion model (see their Fig. 5a). However, our results indicate that sizable volumes of glacial sediment will continue to be stored on time scales at least one order of magnitude longer than this. This constitutes the first recorded instance of such long time scales for a catchment-scale paraglacial response. It may be argued that this is partly due to the aridity of this environment, but we note that the maximum incision rates calculated here are not particularly slow (see following discussion), and aridity probably cannot account for the whole order of magnitude difference from the Braun et al. results. We suggest that some of the mismatch is also due to overly simplistic implementation of fluvial transport laws within such models, probably related to the difficulty in mobilizing the large boulder clasts present within the diamicton mantling such landscapes.

This time scale is however directly comparable to those suggested for tectonically perturbed landscapes. Whipple (2001) gave a response time of between 0.25 and 2.5 m.y. for detachment-limited river channels; Densmore et al. (2007) have reported time scales of 10^5–10^6 yr for coupled catchment-fan systems. Our result also

conforms with response time estimates from Whittaker et al. (2007b) of between 1 and 3 m.y. for relaxation of a tectonically forced knickzone back to a smooth concave-up profile, a situation featuring a very similar channel long profile geometry but with dissimilar forcing mechanism. We also note that the peak time-averaged incision rate within the gorges of both Leh and Basgo valleys is between 0.5–1.0 mm/yr, which is typical of rivers in many actively uplifting regions (Milliman and Syvitski, 1992), but perhaps surprising in a landscape containing so many ancient landscape elements. Both of these similarities—in rate and time scale—further emphasize that the long-term geomorphic response of a landscape recovering from glaciation is likely to look very much like the response to any other perturbation, be it tectonic or climatic, since beyond the spatially and temporally restricted domain of periglacial processes, the same suite of landscape processes are responsible for change in both.

2.7 Conclusions

We have described the generalized geomorphic structure of catchments draining southward from the Ladakh Batholith into the Indus River. Each catchment where glacial erosion has lowered the down-valley gradient of the valley floor at higher elevations consists of three domains arranged sequentially downstream (Fig. 2.2). The upper domain is characterized by smooth U-shaped valley cross sections and small-scale postglacial sediment reorganization by the modern river, the middle domain is characterized by the incision of a large postglacial gorge into the diamicton mantling the floor of the valley, and the lower domain is characterized by the onset of fluvial aggradation over the glacial valley floor. This clear, repeated pattern makes these catchments an ideal natural laboratory for the study of fluvial dynamics in a transient setting.

By comparing drainages with differing degrees of glacial sculpting, we show that past glacial modification of the upper reaches of a catchment in the form of subglacial abrasion can have profound first-order influence on the hydraulic scaling

of the channel downstream. Channel concavities downstream of any convexity in the channel long profile are systematically and nonlinearly elevated above the expected value range of 0.3–0.6, where more elevated values are associated with the presence of the convexity proportionally further downstream. This effect is associated with increasing relative sediment flux through the channel system and is independent of possible drainage restructuring induced by glaciation and of the influence of inherited relict glacial landform, making it a true paraglacial response.

We demonstrate that the response times of these paraglacial systems must exceed 500 k.y., but nevertheless that implied time-averaged maximum rates of fluvial incision are on the order of 1 mm/yr, comparable with rates in many tectonically active settings. Furthermore, we emphasize that the coupled incisional-depositional nature of these systems means that large volumes of glacially derived sediments may be held within previously glaciated mountain belts on time scales on the order of 10^5–10^6 yr post-deglaciation. These time scales are at least an order of magnitude longer than any previously reported. If tapped by subsequent tectonic perturbation of the chain, this may have significant consequences for understanding the stratigraphic architecture of neighboring basins.

PAPER ACKNOWLEDGEMENTS

This work was supported by a National Environment Research Council studentship NER/S/A/2005/13851. We are very grateful to Tim Ivanic, Martin Hurst, and Jenny Rapp for assistance in the field, and especially to Fida Hussein of Leh for logistical support. Many thanks are also due to Alex Whittaker, Mikael Attal, Simon Mudd, and Mark Naylor for many stimulating discussions helping with the development of ideas for this work. We would also like to thank Simon Brocklehurst, Alison Anders, and Joan Florsheim for their very helpful and constructive reviews of this manuscript.

3. RIVER SCALING IN TRANSIENT LANDSCAPES[1]

CHAPTER ABSTRACT

The scaling of the slope of a river channel against upstream drainage area is a widely used metric in fluvial geomorphology, and is well understood for steady state conditions. However, the scaling in landscapes that have been perturbed by climate or tectonics is poorly characterized and not well understood. We compare the slope-area scaling of three sets of catchments in the east Himalaya/Tibetan plateau, West Himalaya and Carpathian Alps, which are all responding transiently to differing tectonic or climatic perturbations. In all these examples, downstream of channel long profile convexities (knickzones), the exponent in this scaling relationship (the concavity) is elevated above values that characterize topographic steady state. Uniquely, we show that its value is systematically and nonlinearly related to knickzone position in the catchment. Such scaling is best explained by sediment flux dependent channel incision and aggradation. We show how these results impact on the application of slope-area scaling to the interpretation of relative uplift histories from transiently responding rivers.

3.1 Introduction

The scaling exponent that relates the slope of a river bed to its upstream drainage area defines the concavity, θ, of a long river profile such that

$$S = k_s A^{-\theta} \tag{3.1}$$

where S is local channel gradient, A is upstream drainage area (acting as a proxy for channel discharge), and k_s and θ are defined as the steepness index and concavity respectively (Flint, 1974). In many landscapes, θ is found to be relatively invariant, ranging from 0.3 to 1.2, averaging 0.5 (Knighton, 1998; Whipple, 2004; Whipple and Tucker, 1999). This observation forms a key calibration for numerical landscape evolution models and underlies many quantitative analyses of river systems. For

[1] A version of this paper has been submitted to *Geology*:
Hobley, D.E.J., Sinclair, H.D., and Cowie, P.A., in review, River scaling in transient landscapes: Geology.

example, it is commonly used to interpret variations in rock uplift rate affecting different channels in a region (e.g., inter alia, Cyr et al., 2009; Harkins et al., 2007; Kirby and Whipple, 2001; Kirby et al., 2003; Kobor and Roering, 2004; Snyder et al., 2000; Wobus et al., 2006b). This approach generates a normalized steepness index assuming a constant concavity for all channels and that all channels have reached erosional steady state. Another application of assumed concavities is the reconstruction of pre-glacial valley long profiles, enabling quantification of glacial downcutting by the upstream projection of an assumed fluvial profile (Brocklehurst and Whipple, 2002).

The form of Equation (3.1) is often explicitly linked to the stream power law (Kobor and Roering, 2004; Whipple, 2004),

$$E = k_r k_c k_{\tau c} f(Q_s) \; A^m S^n \tag{3.2}$$

where E is rate of channel incision, k_r and k_c are erosivity parameters based on substrate resistance and climate respectively, and $k_{\tau c}$ and $f(Q_s)$ are threshold for erosion and relative sediment flux terms (both likely to be strongly non-linear). This assumes erosional steady state across the landscape, and that k_r, k_c, $k_{\tau c}$ and $f(Q_s)$, m and n are all constant and nonzero, and yields, where K is a constant,

$$K = k_r \, k_c \; k_{\tau c} \, f(Q_s), \quad \theta = m/n. \tag{3.3}$$

In field areas thought to be in steady state, the observed average $\theta = 0.5$ matches well with independently derived ratios of m and n (Whipple and Tucker, 1999).

However, channels which are in disequilibrium with their climatic or tectonic environment – transiently responding channels – may have significantly elevated values of θ, often exceeding 1. Such concavities are generally associated with broad

wavelength convexities, or knickzones, in the channel long profiles, and with downstream transitions to fully alluvial conditions (Hobley et al., 2010; Schoenbohm et al., 2004; VanLaningham et al., 2006; Whipple, 2004), but their origin has not been fully explained. Disequilibrium channels are important for discriminating between the processes of landscape evolution (e.g., Whipple and Tucker, 2002). Furthermore, Zhang et al (2001) have claimed transient landscape response plays a vital role in global sediment budgets.

This study uses remotely sensed data from three contrasting, transiently responding landscapes to investigate the causes of high concavities downstream of first-order convexities in river long profiles. Based on very similar scaling trends in the three sites we argue that this scaling is only compatible with channel evolution which is sediment flux dependent, especially where the channels incise. We then discuss the potential influences of such scaling on attempts to read past tectonic changes from modern topography.

3.2 Field Areas

We compare the scaling of sets of broadly linear, subparallel, perturbed river channels in three distinct environments, two glacially perturbed, one tectonically perturbed (Fig. 3.1 & Table 3.1).

3.2.1 South Flank of the Ladakh Batholith, NW Indian Himalaya

Along-strike variation in glaciation has resulted in knickzones carved into the present channel long profiles at varying positions along their lengths. The catchments comprise an upstream domain of lower river gradients where the channel does not incise down into the substrate, a middle domain straddling the knickzone where the channel responds by downcutting, and a lower domain where the river aggrades (Fig. 3.2a). The reduction of gradients upstream of the knickzone is the result of subglacial

abrasion above the equilibrium line altitude for the former glaciers (Jamieson et al., 2004). Bedrock is homogenous and crystalline, but the catchments are thickly draped with loose glacial debris and colluvium, which decouple the channel from the bedrock hillslopes. All the incision since the local last glacial maximum (LLGM) remobilizes these sediments (Hobley et al., 2010; see also Chapter 2).

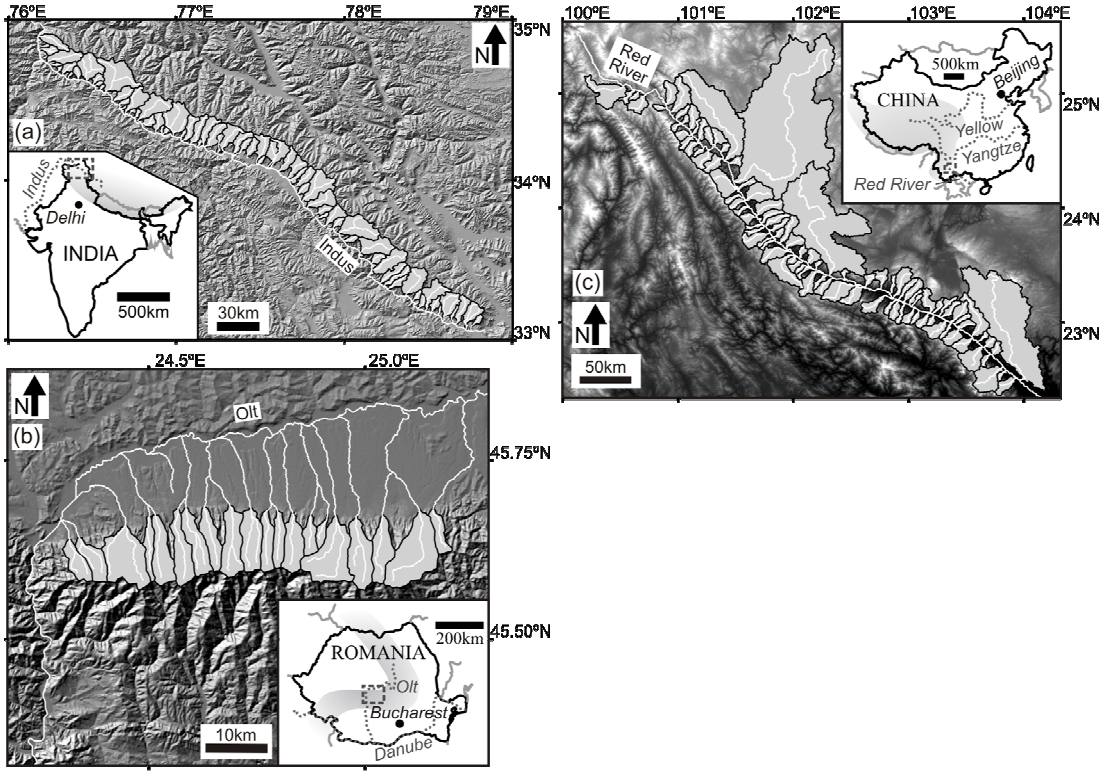

Figure 3.1. Field area overviews of the **(a)** Ladakh, **(b)** Făgăraş and **(c)** Red River sites. Catchments studied are shaded, and analyzed trunk streams within them shown in white. Axial rivers downstream are labelled. Surrounding topography is shown as hillshade for a and b, elevation for c. Insets show location maps.

TABLE 3.1. KEY GEOMORPHIC CHARACTERISTICS FOR EACH FIELD LOCALITY

Locality	Ladakh Batholith	Făgăraş Alps	Red River Region
Perturbation type	Glacial (LLGM ca.100 k.a.)*	Glacial (LLGM ca. 15 k.a.)†	Tectonic (base level fall post Pliocene)§
Present climate	High altitude desert	Temperate continental	Monsoonal tropical
Present precipitation (mm/yr)	c. 100#	>600**	c. 800††
No. of catchments	70	28	97
Median catchment length (km)	30	10	25§§
Catchment peak elevations (m)	6000	2500	2000-3000
Outlet elevations (m)	2000-4000	370-430	100-1300
Axial river	Indus	Olt	Red River

Note: Data drawn from – *Hobley et al., 2010 and Owen et al., 2006; †Bartmus, 1994; §Schoenbohm et al., 2004; #Holmes, 1993; **Tantau et al., 2006; ††Yunnan Province Meteorological Bureau Information Office, 1982.

§§Four catchments breach northern drainage divide and exceed 100 km.

3.2.2 North Flank of the Făgăraş Alps, Carpathians, Romania

The range is developed in a metamorphic anticline that has been thrust southwards; the north flank of the range is not fault bounded, but is presently uplifting relative to the Transylvanian basin to the north (Fielitz and Seghedi, 2005). As in Ladakh, the channels divide into three domains characterised by upper valley channel stability, followed by incision, and then aggradation (Fig. 3.2b). However, these catchments are less heavily glacially altered, with a smaller upper domain and presence of the knickzones higher up the systems, if at all. These rivers contain much less sediment compared to Ladakh, and incision occurs directly into channel bedrock – accumulations of glacial debris are only observed in the upper domain. The channel is coupled to vegetated hillslopes in domain 2 (Table 3.1). Transition to the depositional regime occurs close to the mountain front, with extensive piedmont alluvial fans extending north from this, largely excluded from this analysis (Fig. 3.1).

3.2.3 Red River Region, Yunnan Province, China

Data and observations for this field site are drawn directly from Schoenbohm et al. (2004). This landscape has not been glaciated. Channels are tributaries to the Red River and display knickzones in their long profiles, typically as two major profile convexities with some smaller knickzones between these (Fig. 3.2c). These discontinuities are the product of a ~1400 m relative base level fall on the Red River, with the two major knickzones reflecting punctuated vertical motions driven by faults. They are not lithologically controlled. The headwaters are dominated by meandering alluvial channels flowing through a deeply weathered, low relief, relict landscape. Below the first knickzone the channels pass into incised gorges, cut up to 1 km into bedrock and coupled to soil-rich hillslopes. Below the second knickzone the gorges become steep, landslide-dominated, soil-sparse V-shaped canyons with bedrock channels. This field site permits the investigation of channel scaling for a system with similar dimensions and geometries to the Ladakh examples, but tectonically forced, and with pure bedrock channels below the knickzones.

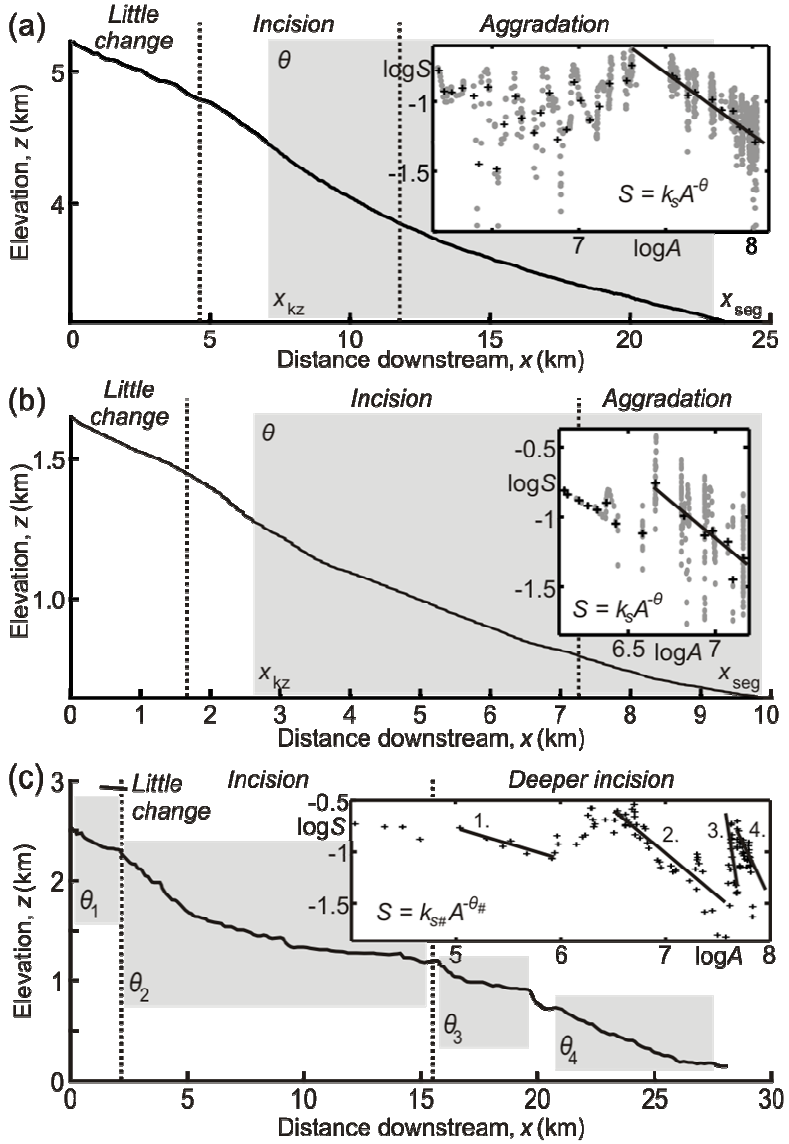

Figure 3.2. Example plots of stream data for each field site – **(a)** Ladakh, **(b)** Făgăraş, **(c)** Red River region (after Schoenbohm et al., 2004). Main plots show long profiles; inset boxes show associated slope(S)-area(A) scaling in log-log space. Crosses represent log-binned data. Note variable scales; aspect ratio is maintained in S-A plots. Dashed lines in main plots demark geomorphic domains as indicated in italics and described in the text. Shaded boxes show intervals over which concavities, θ, are determined, also shown as solid lines in S-A plots. Note that (c) has several local slope maxima and hence several values of θ, each associated with unique values of x_{kz} and x_{seg}.

3.3 Methods

The remotely sensed data used consist of 90 m resolution digital elevation models (DEMs) derived from the NASA Shuttle Radar Topography Mission (SRTM). The data for the Ladakh and Romania field sites comprise extracted long profiles smoothed on a 500 m scale, giving distance, x, elevation, z, and channel slope, S, along each stream, as well as concomitant drainage area, A, following the detailed methodology presented in Hobley et al. (2010) (see also Chapter 2 and Appendix A). Stream segments are separated by knickzones, defined by local slope maxima – where not present, the whole stream is treated as a single segment, and where multiple local maxima occur and the channel is smoothly concave downstream between them, several segments are defined for one channel (Fig. 3.2). Below and between these maxima, power laws are fitted to the slope-area data by a least-squares method, yielding steepness index, k_s, and concavity, θ, for each segment, recorded against the relative downstream positions of the segment start (x_{kz}) and end (x_{seg}). We reject fits where confidence intervals exceed 50% of the calculated θ value, often indicating that a power law fit is not appropriate for this reach. Data for the Red River site is drawn directly from Schoenbohm et al. (2004), whose processing parallels the above methods allowing direct comparison of the data sets (Fig. 3.2c). Note that in the Ladakh and Făgăraş Alps data, defined channel segments run across the transition from dominantly bedrock to alluvial channels; in Ladakh the concavities of these two process domains are indistinguishable (Hobley et al., 2010; see also Appendix B).

3.4 Results

In order to examine the variability of slope-area scaling in different channel segments and between field sites we plot the concavity value of each segment against the proportion of the channel upstream of the associated profile convexity, as measured by the fraction $F_{kz} = x_{kz}/x_{seg}$ (Fig. 3.3). This ratio uses x not A for consistency with existing data; expressing the position using A produces very similar results, since almost all catchments share the same form (Fig. 3.1; Hobley et al., 2010). All three data sets indicate that concavity values rise nonlinearly with position of the knickzone further downstream, and the trends for the glaciated field sites are contained within the data from the Red River. We describe the form of this trend with the empirical equation

$$\theta = \frac{F_{kz}}{1 - F_{kz}} \zeta + \theta_0 , \tag{3.4}$$

where θ_0 and ζ the fitting parameters, representing unperturbed channel concavity and the rate of divergence from this respectively (Fig. 3.3). This equation makes θ asymptotic approaching $F_{kz} = 1$, and also defines the intrinsic concavity θ_0, while still requiring only two parameters. t-testing indicates that the ζ values for each region as shown in Figure 3.3 are distinct from each other to 95% confidence, though are of similar magnitude. The θ_0 values are all indistinguishable however, and are within the range 0.3-0.6, which corresponds to the theoretical concavity for a steady state eroding system (Whipple and Tucker, 1999).

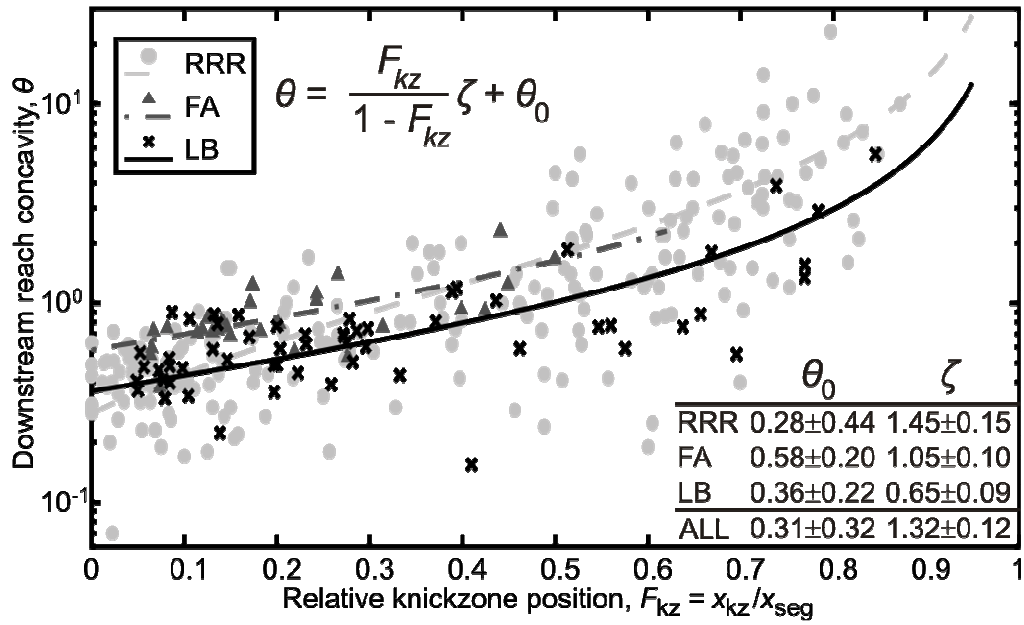

Figure 3.3. Data describing variation of reach concavity with relative knickzone position downstream for Red River Region (RRR), Făgăraş Alps (FA) and Ladakh Batholith (LB). Note logarithmic scale on y-axis. Trend lines are maximum likelihood best fits for each data series, giving parameters listed in inset table; errors are 95% confidence intervals.

3.5 Discussion

3.5.1 Causes of Concavity Scaling

Concavity of substantial reaches of rivers can be systematically elevated above the range 0.3-0.6 while they are undergoing transient response to perturbation (Fig. 3.3). There are a number of theoretical mechanisms which could produce this trend; here, we use the shared form of response in these three sites to test these hypotheses.

River hydrology. Changes in the stochasticity of river discharge driven by glaciation or other processes could drive changes in channel concavity (e.g., Sólyom and Tucker, 2004). However, the upper Red River Region records no significant glacial presence, and the trends in Figure 3.3 are shared between sites in very different climates, making hydrology an unlikely first order control.

Regional variation in channel uplift. In a river system in topographic steady state, higher uplift rates in the headwaters (i.e., tectonic rotation) can create elevated concavities (Kirby and Whipple, 2001). However, no realistic uplift gradients would be compatible with the nonlinear trends seen in Figure 3.3. Moreover, analysis carried out by Schoenbohm et al. (2004) to reconstruct past landscape form implicitly demonstrated that that field site has remained level. Similarly, the shared trend also makes it highly unlikely that downstream changes in lithology play an important role (c.f., VanLaningham et al., 2006).

Transition from incising to aggrading conditions. Previous authors have argued that the transition from incision to deposition and the associated change in channel process is responsible for increasing concavities in some systems (e.g., Whipple, 2004). While in Ladakh and the Făgăraş Alps we do see this transition, we do not in the Red River, which is a purely bedrock system in many of the analyzed reaches. Moreover, the concavities of purely alluvial systems tend to be lower than those in equilibrated bedrock systems (Voller and Paola, 2010), and sharp S-A scaling breaks between the two regimes are rarely observed in real systems (Densmore et al., 2007), including the Ladakh example seen here (Hobley et al., 2010; see Appendix B).

Width or sediment flux dependent scaling in transient landscapes. Perturbations to expected concavity scaling in transiently responding channels can be produced by unexpected scaling of channel width, of threshold of mobility or erosion, or of river response to relative sediment flux with drainage area. In incising reaches this is best illustrated by consideration of stream power, where changes to m/n (driven by channel width variation), $k_{\tau c}$ (threshold) or f(q_s) (sediment flux dependency) could alter the expected concavity scaling (Equ. 3.2). However, in order for variations in

channel width scaling to create elevated concavities, the channel aspect ratio must rise or the roughness fall considerably with changing A (Finnegan et al., 2005). Neither of these mechanisms is satisfactory, since comparing terms in the Finnegan and concavity equations shows the sensitivity required to produce concavities >>1 as seen here would be so extreme as to be immediately obvious in grain size changes in the field. Thus the elevated concavities seen in this study must be driven by sedimentary effects – either falling thresholds of sediment mobility, or decreasing f(q_s) downstream caused by sediment cover on the bed. We infer that sediment flux dependent incision is primarily responsible, because: (a) strong downstream trends in grain size are not observed in Ladakh (Hobley et al., 2010; Chapter 2); (b) similar sensitivity of concavity to realistic forms of f(q_s) has been reported from modelling (Gasparini et al., 2006); (c) transitions into depositional conditions in Ladakh and Făgăraş confirm that sediment flux is increasing downstream in these cases.

Although such arguments cannot account for behaviour in the aggrading reaches of Ladakh and the Făgăraş Alps, the response in these systems is very similar to that in the Red River Region (Fig. 3.3) where such arguments do apply. Also, the bedrock-alluvial transition makes little impact on the trends in Figure 3.3 in the Ladakh and Făgăraş examples. We infer on the grounds of these similarities that sediment flux dependent effects analogous to those during incision must apply during aggradation. This would be consistent with the underlying physics of transport-limited channel processes (Whipple and Tucker, 2002).

3.5.2 Reading Uplift from Topographic Data

The trends recorded in Figure 3.3 highlight a key issue in trying to interpret the nature of past perturbations from transiently responding river systems. Typical approaches essentially solve Equations (3.1), (3.2) and (3.3) to calculate k_s, assuming erosional steady state and constant K and θ. This is recorded as the concavity-

normalized steepness index, k_{sn}, which proxies uplift (see, e.g., Wobus et al., 2006b). However, we have shown that in these examples K is variable, since sediment flux sensitivity and/or threshold variability must change downstream (Equ. 3.3). It is well recognized in the literature that analyzing transient landscapes is more challenging than those at steady state, but our results demonstrate a consistent, quantifiable, nonlinear signal in this variation in K and hence k_{sn}, if it is calculated for a transient landscape. By comparison of equations (3.1) and (3.4) under assumed constant reference concavity we can show that for these disequilibrium channels

$$k_{sn} = k_s A^{\frac{-F_{kz}}{1-F_{kz}}\zeta}, \tag{3.5}$$

where k_s is the "true" channel steepness which accurately reflects the relative uplift rate. This equation demonstrates that where knickzones are present in the middle reaches of transiently responding river systems, relative changes in k_{sn} are driven primarily by the nonlinear response captured by the exponent on A, swamping real changes in k_s. Encouragingly however, where knickzones are not present ($F_{kz} = 0$), concavities are consistent with the assumptions of the steepness index method and will produce results that reflect k_s as intended (e.g., Snyder et al., 2000).

3.6 Conclusions

In three contrasting river systems responding transiently to differing climatic or tectonic perturbations, the concavity of a channel reach downstream of a long profile convexity increases nonlinearly and systematically above expected equilibrium values as the knickzone is located proportionally further downstream. The magnitude and form of this response is similar in each field location as well as

being present in both incising and aggrading river reaches. In the incising reaches, this response is most consistent with sediment flux dependent channel dynamics. Such slope-area scaling means that channel steepness indices derived in transiently responding rivers with prominent long profile knickzones will not accurately reflect relative channel uplift, instead convolving tectonic signals with sediment flux dependent adjustments.

PAPER ACKNOWLEDGEMENTS

This work was supported by a National Environment Research Council studentship NER/S/A/2005/13851. We are very grateful to Tim Ivanic, Martin Hurst, Ciaran Beggan and Jenny Rapp for assistance in the field, and especially to Fida Hussein of Leh for logistical support. Many thanks also to Alex Whittaker, Mikaël Attal and Simon Mudd for many stimulating discussions helping with the development of ideas for this work.

4. FIELD CALIBRATION OF SEDIMENT FLUX DEPENDENT RIVER INCISION[1]

CHAPTER ABSTRACT

Theoretical and laboratory studies suggest that the dynamics of eroding river systems may be strongly modulated by their sediment load, allowing both promotion and inhibition of bed incision at different relative sediment fluxes. Testing this hypothesis in the field has proven difficult, however, since establishing both the long-term sediment budget and erosion record in a channel where the style of erosion is well-known has hitherto been extremely difficult. This paper presents a new framework for understanding channel erosion style as either detachment- or transport-limited, and for revealing the relative importance of sediment flux in modulating incision rates. We show that downstream distribution of shear stress forms the key discriminator between detachment- and transport-limited models when compared to measured patterns of resulting incision across a short timestep in a transiently responding channel network. We use this framework to demonstrate that incision proceeding into a coarse, loose, poorly sorted substrate in a postglacial setting in the Ladakh Himalaya, NW India should be modelled as a detachment-limited process, though modulated by both tools and cover effects driven by evolving relative sediment flux downstream. We then go on to model how incision varies as a function of sediment flux in this setting, and are uniquely able to describe the detailed form of this sediment flux function in each analyzed catchment. The resulting functions show many features which are compatible with previous theoretical and laboratory studies but which have not before been independently verified from real field data. Our results suggest that the peak in incision efficiency may occur at lower relative sediment flux values than widely assumed in the literature.

4.1 Introduction

River dynamics in upland settings are a key element in the Earth surface system, redistributing large volumes of sediment into basins (Milliman and Syvitski, 1992), coupling climate and tectonic processes (Molnar and England, 1990; Willett

[1] This paper is to be submitted to the *Journal of Geophysical Research (Earth Surface)*:
Hobley, D.E.J., Sinclair, H.D., Cowie, P.A., and Mudd, S.M., in prep., Field Calibration of Sediment Flux Dependent River Incision.

and Brandon, 2002), transmitting information from downstream into highlands (Rodriguez-Iturbe et al., 1992) and controlling the form of mountain belts themselves (Burbank, 2002; Zeitler et al., 2001). However, significant uncertainty still remains over how real river systems are likely to evolve through time. Numerous models of river erosion have been proposed (see, e.g., Tucker and Hancock, 2010), but much doubt remains over how we should distinguish between these models and whether factors such as thresholds and sediment-flux dependent incision are important in real settings. This is vital to establish, since the long term tempo, style and patterns of landscape evolution under each modelling approach can be very different (e.g., Whipple and Tucker, 2002).

In particular, several authors have drawn attention to the probable importance of sediment flux dependent incision in natural channels, arguing that it is likely to create a strongly nonlinear erosional response, as sediment may both promote incision by acting as tools and inhibit it by covering the bed (Cowie et al., 2008; Gilbert, 1877; Sklar and Dietrich, 2001; Turowski et al., 2007). Sediment flux dependent erosion has also been shown to significantly alter the styles and patterns of channel response to changes in boundary conditions (e.g., Gasparini et al., 2006). However, it has proven difficult to unequivocally demonstrate the form of this "tools and cover" effect in real environments.

We set out to discriminate between incision models and assess the role of sediment flux in catchments in Ladakh, northwest Indian Himalaya. These catchments have been perturbed by glacial resculpting of their upper reaches (Hobley et al., 2010). This location is ideal for such a study as we may tightly constrain through time both average incision rates and average sediment fluxes downstream as the channels respond. However, the "bedrock" of these channels consists of very poorly sorted glacial sediment, which although consisting of loose material, contains many clasts which in any given flood will be immobile, and which may interact in an unpredictable way with the surrounding clasts. Thus it is unclear just from the nature of the substrate whether this system is essentially transport-limited, where incision proceeds as a function of divergence of sediment carrying capacity of the flow, or

detachment-limited, where incision is a function of the ability of the channel to mobilize the bed.

Thus this paper seeks to address two related objectives. Firstly we present a novel analysis of the detachment- and transport-limited frameworks for fluvial erosion, using shear stress distribution downstream to demonstrate that these channels are responding in a sediment flux dependent, detachment-limited manner above an incision theshold. Secondly, we use field observations to constrain the resulting sediment flux functions for each analyzed catchment using a Monte Carlo Markov Chain model. The resulting curves show the detailed interaction of the tools and cover effects in a real setting and allow investigation of the factors controlling their expression.

4.2 Modelling Framework

In the past fluvial systems have often been described as either detachment-limited (DL), governed by resistance of the bed to erosion, or transport-limited (TL), governed by capacity of the flow to carry away material which is freely available on the bed (Anderson, 1994; Beaumont et al., 1992; Howard, 1994; Kooi and Beaumont, 1994; Tucker and Bras, 1998; Whipple and Tucker, 1999, 2002; Willgoose et al., 1991). These mutually exclusive descriptions of incision are advantageous as they allow modelling of channels in mountain belts across geologically relevant timescales (> 10^4 years), and represent relatively simple approaches which allow us to understand the first order kinematics of such systems through time. Both have been shown to produce realistic results when compared to real landscapes (Attal et al., 2008; Cowie et al., 2006; Kooi and Beaumont, 1994; Stock and Montgomery, 1999; Valla et al., 2010; van der Beek and Bishop, 2003; Whittaker et al., 2008).

4.2.1 Detachment-Limited and Transport-Limited River Incision

Many different formulations of the detachment-limited approach exist in the literature; however, perhaps the most general has been outlined by Whipple (2004), as

$$E = k_r k_c k_{\tau c} f(q_s, q_c) A^m S^n \tag{4.1}$$

where E is bed erosion rate, k_r, k_c and $k_{\tau c}$ are parameters reflecting bed erodability, climatic influence and threshold of incision, respectively, $f(q_s,q_c)$ is a parameter reflecting the influence of sediment load which we shall term the sediment flux function, A and S are the upstream drainage area and local channel slope, and m and n are dimensionless parameters reflecting incision process in the channel, basin hydrology and channel hydraulic geometry. This equation can also be stated explicitly in terms of mean bed shear stress, τ, giving

$$E = Kf(q_s, q_c)(\tau - \tau_c)^a \tag{4.2}$$

where a reflects the dominant incision process (Whipple et al., 2000), τ_c is a threshold below which no incision occurs, and K is a parameter reflecting the combined influences of bed erodability, climatic influence and erosion process (Hancock et al., 1998; Howard and Kerby, 1983). Despite the existence of numerous forms of the basic law, all preserve this power law dependence of erosion rate on shear stress or a direct equivalent to it, and it is widely recognized that all generally accepted forms of the model can give rise to effectively indistinguishable topographic outputs, given tuning of parameters which cannot be directly measured (e.g., Tucker and Hancock, 2010).

Importantly, existing real-world tests of the detachment-limited model indicate that this $f(q_s,q_c)$ term is likely to be non-linear, allowing for both promotion and/or inhibition of erosion by sediment flux (Cowie et al., 2008; Sklar and Dietrich, 2001; Turowski and Rickenmann, 2009; Valla et al., 2010; Whittaker, 2007). This is because, in rivers, sediment acts as tools to detach bed material, but increasing quantities of bedload sediment in transport will act to cover a greater proportion of the bed, reducing the likelihood of impact against the bed. The ratio of sediment flux, q_s, to carrying capacity of the channel, q_c, appears to control the variation in erosional efficiency (e.g., Johnson and Whipple, in press; Sklar and Dietrich, 2004). This "tools and cover" effect should produce a humped form of $f(q_s,q_c)$ when plotted against q_s/q_c, where the maximum value of $f(q_s,q_c) = 1$ occurs at intermediate values of relative sediment flux within the available range $q_s/q_c = 0$ to 1. However, no actual example of this relation has been well constrained either experimentally or in the field, with authors tending to assume a parabolic or almost parabolic form based on consideration of normal kinetic energy flux to the bed and a static bed cover proportion (Gasparini et al., 2006; Sklar and Dietrich, 1998, 2004). A notable exception is the formulation of Turowski et al. (2007), who noted that parabolic-type forms do not match laboratory studies of bed abrasion. They showed that allowing for dynamic covering of the bed by sediment and spatial heterogeneity of the armouring of the bed creates an exponential decrease for the cover term. Such an adjustment allowed them to more accurately model the original Sklar and Dietrich (2001) experimental results.

The transport-limited model in contrast postulates that rates of incision in a channel depend on divergence of sediment carrying capacity, q_c, in the channel, and thus assumes that enough sediment is always available on the channel bed to be incorporated into the flow (Tucker and Bras, 1998; Willgoose et al., 1991). Such models may be written in general form as

$$E = \frac{1}{1-\lambda_p}\frac{d}{dx}\left(\frac{1}{w}q_c\right) \tag{4.3}$$

where λ_p is sediment porosity (which we shall treat in our approach as a constant), x is the downstream direction, w is the channel width and q_c is the sediment carrying capacity (Whipple and Tucker, 2002). Importantly, we note that q_c can be expressed as some function of shear stress, τ, in the channel (see also Davy and Lague, 2009).

Under equilibrium conditions in which channel erosion is everywhere equal to uplift in the landscape, these end member erosion laws give rise to indistinguishable longitudinal channel profiles. However, they lead to fundamentally distinct response styles as landscapes undergo transient response to changes in boundary conditions, such as in climate or tectonics acting on the catchments (Whipple and Tucker, 2002). This is extremely important, since these transient conditions are those which hold promise for reconstructing past conditions affecting a landscape, and will likely also be reflected most strongly in the stratigraphic record (Whittaker et al., in press; Zhang et al., 2001). They also underpin predictions of landscape response to future climate change. When perturbed by a step change in relative base level, pure detachment-limited models of channel incision where $f(q_s,q_c) = 1$ and any thresholds are negligible typically lead to a wave-like response propagating up through a channel network. A sharp break in channel slope demarks a boundary between a downstream reach where the channel is fully adjusted to the new boundary conditions and an upstream reach where the channel has not felt the effects of boundary condition changes in the system at all. This contrasts sharply with the predictions of the simple transport-limited end member model, which existing analyses suggest will give a diffusive response in the network where all points will respond gradually and together to a change in boundary conditions (Whipple and Tucker, 2002; Wobus et al., 2006a).

However, work focussed on the response of systems which lie between these two erosion styles is less well advanced. Figure 4.1 illustrates graphically the interaction of the pure detachment-limited, pure transport-limited and hybrid erosion laws. Erosion in channels where clast transport downstream and clast detachment from the bed are of comparable difficulty is generally treated within the detachment-limited erosion law, where the $f(q_s/q_c)$ term models the effects of the sediment in the channel. Gasparini et al. (2006; 2007) have explored the transient dynamics of a such a system in which $f(q_s,q_c)$ is allowed to vary, modelling both just the cover effect in isolation (linearly falling $f(q_s,q_c)$ with q_s/q_c) and also an almost-parabolic form of the function incorporating both tools and cover. They demonstrated more complex responses combining elements of both diffusive and advective behavior.

Other authors have also approached this problem without employing the DL-TL framework described here. Such models (e.g., Beaumont et al., 1992; Braun and Sambridge, 1997; Davy and Lague, 2009) tend to instead treat erosion and deposition in the stream as independent but linked processes, with a characteristic travel length for a particle once it is in transit. We acknowledge the potential of such methods to describe these intermediate cases, but choose not to consider them here, partly on the grounds of frequent difficulty in replicating scaling relations (particularly channel concavity) seen in natural systems using such approaches (e.g., Whipple, 2004). However, these alternative methods should be seen as complementary to the DL-TL system – the same kinematics can arise from both treatments, and they represent contrasting idealized descriptions of the same underlying real processes. We anticipate that a better understanding of channel response within one framework will lead to better understanding of the mechanics of the other.

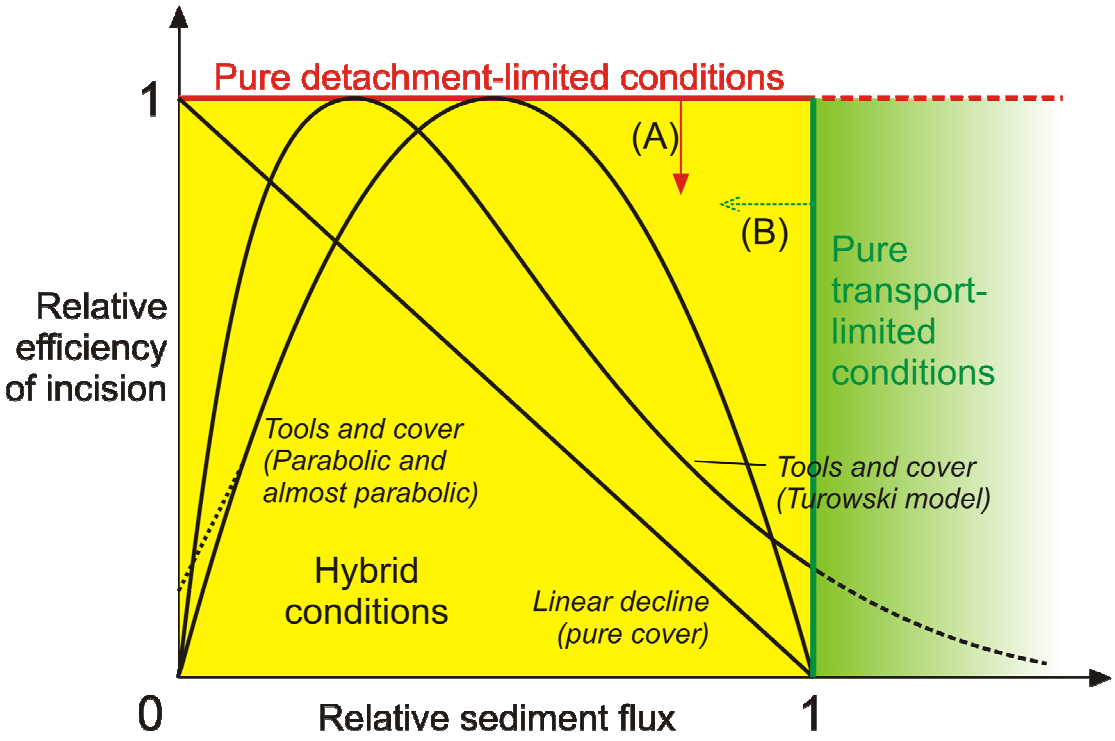

Figure 4.1. Model space for stream power-based incision laws. Hybrid models shown are linear decline (Beaumont et al., 1992), and three versions of "tools and cover"-type models, parabolic (Sklar and Dietrich, 2004), almost parabolic (Gasparini et al., 2006), and Turowski's (2007) dynamic cover model; all three are based upon detachment-limited-type assumptions (i.e., Equs. 4.1, 4.2), though note the Turowski et al. formulation depends on relative sediment supply rather than flux. The figure emphasizes that the pure detachment- (red) and transport-limited (green) domains are orthogonal. Transport-limited conditions are not simply the "end-point" of a pure detachment-limited system, and all efficiencies of incision are possible in a sediment-saturated channel (depending on sediment flux divergence downstream, as opposed to its magnitude). Small arrows indicate that it is possible to consider the space where incision efficiency is controlled by relative sediment flux (yellow; the main body of the diagram) both from the traditional hybrid detachment-limited perspective (A) but also from a hybrid transport-limited perspective (B).

4.2.2 A Hybrid Transport-Limited Model

As outlined above, within the DL-TL framework almost all models which describe "hybrid" erosion behavior – i.e., that which falls between the end-members of detachment- and transport-limited – do so from a fundamentally detachment limited footing, where erosion is modelled as direct function of shear stress on the bed (Fig. 4.1). The equivalent formulation of what could be termed a "hybrid transport-limited" system is missing from the literature, and we here provide this.

If sediment transport capacity, q_c, in the channel is some function of bed shear stress or a close equivalent, as it is in very many published derivations (see, e.g., Bagnold, 1977, 1980; Einstein, 1950; Fernandez Luque and van Beek, 1976; Meyer-Peter and Muller, 1948; Parker et al., 1982; Schoklitsch, 1962; Yalin, 1963), then we may simply use the chain rule and quotient rule to express the transport-limited Equation (4.3) as

$$E = \frac{1}{(1-\lambda_p)} \frac{1}{w} \left(\frac{dq_c}{d\tau} \cdot \frac{d\tau}{dx} - \frac{q_c}{w} \frac{dw}{dx} \right) \tag{4.4}$$

This new format of the transport-limited erosion law has several advantages over Equation (4.3). We can now see the relative effects of variation in each of the primary controlling variables of transport capacity, shear stress and channel width separately, and the form of Equation (4.4) mirrors that of the hybrid detachment-limited equivalent (Equ. 4.2) – erosion rate is now in both cases modelled as a constant multiplied by the product of a sediment transport capacity dependent term and a shear stress dependent term, which are independent of each other.

Thus, this new expression allows direct comparison of the predictions of the two models under known variations of shear stress and channel width with field data

describing channel incision. This forms a theoretical basis for qualitatively distinguishing between detachment- and transport-limited erosion occurring in real settings (see Section 4.2.3). Equation (4.4) also however clarifies that the transport-limited erosion law may be hybrid – that is, erosion rate responds both to shear stresses and sediment flux, and these effects can operate independently. If the $dq_c/d\tau$ term varies, we may model sediment flux dependent channel incision without initially assuming that erosion rate is described as a power of bed shear stress.

If existing sediment transport relations (e.g., Bagnold, 1977; Bagnold, 1980; Einstein, 1950; Fernandez Luque and van Beek, 1976; Meyer-Peter and Muller, 1948; Parker et al., 1982; Schoklitsch, 1962; Yalin, 1963 - see also Section 4.5.1.3) are used to describe the transport capacity, in most cases these predict that the $dq_c/d\tau$ term in Equation (4.4) should be a constant. However, such transport relations already implicitly incorporate the assumption that the sediment on the bed may be freely incorporated into the flow, in that the sediment considered for transport is often already known to be potentially mobile under "normal" experimental conditions, either in the laboratory or in an alluvial field setting. This may not be true of natural rivers responding on longer timescales than typically reflected in such experiments, or in settings where fluvially unsorted material may be fed directly into the flow. We suggest that to account for this the $dq_c/d\tau$ term be allowed to vary with τ in an analogous manner to $f(q_s,q_c)$ varying with relative sediment flux. This would constitute what we term a "hybrid transport-limited" channel. Such an extension to the framework fills out our understanding of sediment flux dependent incision and can also address some of the criticisms that can be levelled at an explicitly DL-TL modelling framework regarding poor treatment of the intermediate, sediment flux dependent conditions away from the pure end-members (e.g., Davy and Lague, 2009).

4.2.3 Discrimination Between Models

The restatement of the transport limited erosion law presented as Equation (4.4) is also advantageous because it allows examination of how channel incision varies as a function of channel width and shear stress. Furthermore, for a given pattern of shear stress and channel width the two incision rules predict quite different distributions of channel incision (Fig. 4.2). This is true regardless of the forms of the sediment flux dependent terms $f(q_s,q_c)$ and $dq_c/d\tau$, neither of which are well established. Thus, field measurements of channel incision, shear stress and channel width can be used to determine if a channel is behaving in a fundamentally transport- or detachment-limited manner.

We illustrate this idea by a hypothetical example (Fig. 4.2). The form of each of the instantaneous incision responses shown by the curves in Figure 4.2c-f is uniquely associated with the shear stresses producing it (Fig. 4.2a,b). Varying the sediment flux dependent term ($f(q_s,q_c)$) allows for the incision maxima to be translated up or downstream (solid gray arrows), but it cannot affect the location in the channel where incision transitions to deposition. Varying channel width systematically can translate the pattern of incision up or downstream in the case of the transport-limited model (dashed and toothed gray arrows), but field data can be used to examine this effect, using the sense and magnitude of channel width change to constrain translation of the function. Thus comparison between positions of maxima, minima and zero points in the downstream distributions of incision and shear stress in natural channels forms a key diagnostic tool for differentiating between these two incision models. While Figure 4.2 presents only an instantaneous channel response under each of these models, as long as the cumulative incision remains relatively small (i.e., little change in long profile form since incision began), we can reliably use direct comparison between shear stresses, channel widths and cumulative incision patterns to discriminate between models. In line with other authors, however (see, e.g., Valla et al., 2010), we emphasise that the patterns of incision downstream alone are not sufficient to differentiate amongst the models –

for example note the strong similarity between Figs. 4.2c and 4.2f under different incision laws.

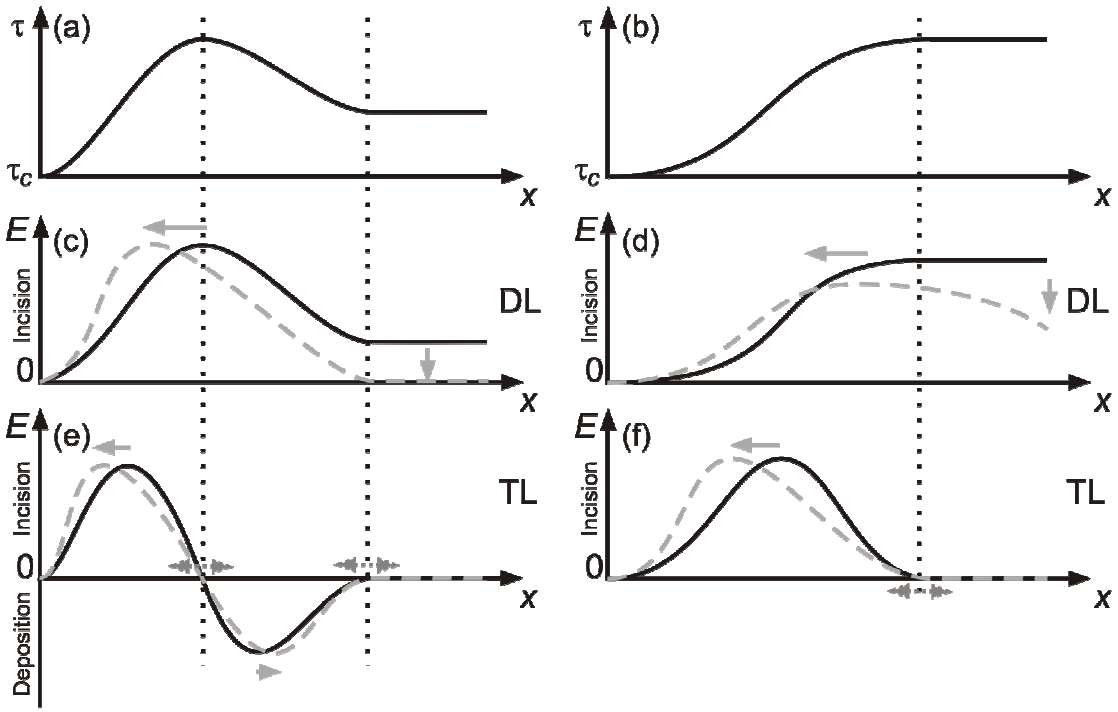

Figure 4.2. Erosive responses under contrasting erosion models to two hypothetical downstream shear stress distributions. **(a,b)** Two contrasting hypothetical shear stress distributions which might be seen in a real mountain river channel which is transiently responding to a perturbation. Lower plots show the form of corresponding instantaneous incision patterns under the detachment-limited model **(c,d)** and the transport-limited model **(e,f)**. Black curves correspond to the case where only variations in shear stress occur downstream; channel width is invariant and $f(q_s,q_c) = dq_c/d\tau = 1$. This is the simplest possible reference case for both models. Gray dashed curve and associated marker arrows represent the general case; channel width varies downstream and sediment flux dependent terms are both humped functions analogous to the tools and cover-type $f(q_s,q_c)$ proposed for the detachment-limited law. Where the transport-limited model predicts deposition to occur, magnitude is schematic, and assumed to behave simply as "negative incision", i.e., deposition is also governed by Equation (4.4). Location of the start of an aggrading reach remains unaffected by this assumption.

4.3 Field Data

4.3.1 Field Area

We use this modelling framework to understand incision occurring in catchments on the Ladakh batholith in the northwest Indian Himalaya (Fig. 4.3). The site comprises a set of around 70 broadly subparallel and linear catchments cut into the exhumed batholith. These drain from the ridgeline of the range down its southwest flank into the river Indus, which flows northwest along the foot of the massif. The batholith itself is effectively monolithologic, composed of granodioritic crystalline rocks, but the floors of the valleys are thickly mantled with coarse, loose, poorly sorted postglacial debris which creates a relatively flat, easily traceable surface (Fig. 4.4). Everywhere the channels incise, they do so into this material, and never downcut into bedrock. This creates the ambiguity in choice between detachment- and transport-limited erosion referred to in the introduction: the looseness and small grain size of a large fraction of the substrate suggests a transport-limited approach, but a detachment-limited approach is also possible due to the immobility of the coarse fraction.

The upper reaches of those catchments which extend all the way to the drainage divide all show signs of significant carving by flowing ice, with prominent U-shaped valleys developed and reduced valley gradients compared to the lower reaches (Figs. 4.4 and 4.5). This has created a knickzone in the long profile of these channels. The extent of this glacial remolding is variable along the batholith, probably primarily driven by variations in the altitude of each catchment (Jamieson et al., 2004). This glacial alteration of valley form, and particularly development of the knickzone, has perturbed the fluvial network and induced the transient response which we focus on in this work.

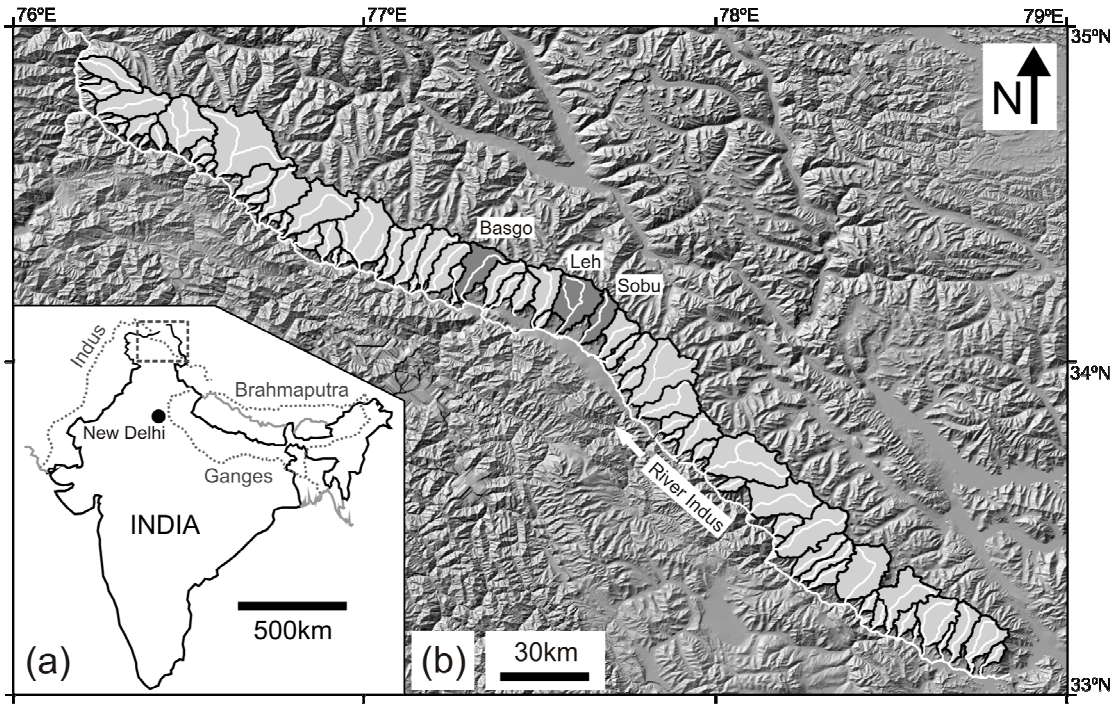

Figure 4.3. **(a)** General location map for Ladakh field site. **(b)** Catchments draining the southeast flank of the Ladakh batholith. Trunk streams are shown in white. The three catchments considered in more detail later in this study, Basgo, Leh and Sobu, are shown in darker gray. The River Indus is shown, and drains northwest along the foot of the batholith (white arrow).

The present form of the landscape is best described as three distinct downstream divisions: a domain in the headwaters where the present long profile has changed little from the original postglacial surface, a domain in the middle reaches where a gorge records past incision into the sediment substrate, and a lower domain where fluvial sediment aggrades above the original postglacial surface (Hobley et al., 2010) (Figs. 4.4, 4.5). The gorge in the middle reaches forms the focus of this study, and is decoupled from the bedrock sidewalls of the surrounding glacial trough by the intervening flat, terrace-like surface of the postglacial valley fill. Field evidence does however suggest that the lower aggrading domain onlaps this postglacial surface, implying that the point where aggradation begins has migrated up the channel through time, but also that the modern channel is slightly inset into the older

depositional surface by a couple of meters (Hobley et al., 2010). This hints at a somewhat complex movement of this boundary through time, with the aggradational front first advancing up the river system, and then later retreating back down it.

Figure 4.4. Panoramic view of Leh catchment, looking northwest, taken from Google Earth. Coloration change in the lower right corner of the image is due to stitching of two images, and can be ignored. Field of view is roughly 6 km across. Trunk stream drains southwards (left). The postglacial sediment surface described in the main text is clear, running down from the upper reaches in the U-shaped valley (top right) round the dogleg, through the middle reaches of the valley and disappearing under the broad alluvial depositional domain just after the rock spur which creates a kink in the river planform (lower arrow). Note that this depositional domain now fills the prominent terminal moraine complex in this valley (bottom left corner, downstream of lower arrow). The incised gorge surrounding the trunk stream which we primarily focus on in this work is visible cutting into the postglacial surface in the middle reaches, the start and end of which are out by the two arrows.

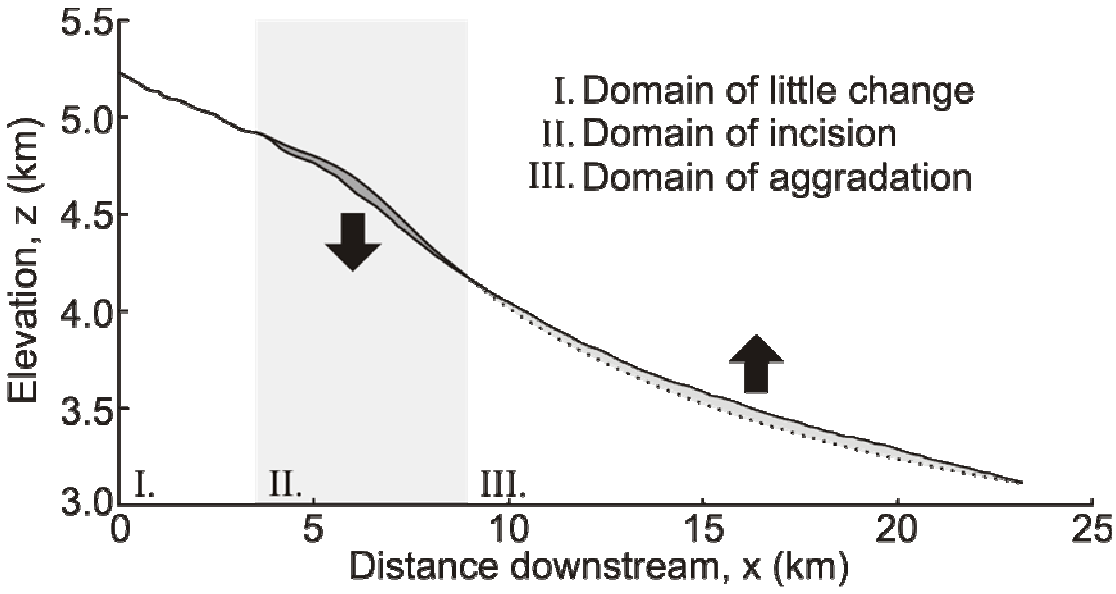

Figure 4.5. Present long profile form for Leh valley, as example of general form. The three domains are illustrated, with black arrows indicating sense of motion of the river through time. Dark shading in the middle reaches indicates material removed, and picks out the gorge incised below the postglacial surface. Light shading in the lower reaches indicates material deposited above the original postglacial valley floor (dotted line, shown schematically); likely complexity in the motion of the boundary between these two domains through time is not shown here. Little change through time in the long profile occurs in the upper reaches.

4.3.2 Data Collection Methodology

We have collected detailed field data in three of the catchments draining the batholith – Basgo, Leh, and Sobu valleys (Fig. 4.3). The dataset incorporates measurements made in all three of the domains described above, but focuses largely on the incising reaches. The data consist of systematic measurements spaced approximately every 300-500 m downstream (where possible) of channel slope on a 30 m scale, current channel depth and width, and the gorge dimensions of depth on either side of the channel and slope of the gorge walls, all measured using a laser range finder. Bankfull depth and width were determined using the height of a sharp boundary between lichen-free and lichen-covered surfaces of boulders in the stream,

which was found to be approximately level with the channel banks in the depositional reaches of the channels. To complete the data set we later used remote sensed imagery of the sites freely available through Google Earth to establish variability of channel and valley floor width downstream in the catchments. Shear stress was then calculated with

$$\tau = \rho_w g h S, \tag{4.5}$$

where ρ_w is the density of water, g the gravitational acceleration and h the flow depth at bankfull. The reasonableness of these shear stress values was checked by ensuring that the stream discharges calculated from these values using a Darcy-Weisbach friction factor approach and known channel dimensions appeared to increase downstream. Allowing for some noise, this was the case.

4.3.3 Gorge Dimensions and Shear Stress (Fig. 4.6)

As suggested in Section 4.2.3, shear stress data combined with an incision history can discriminate between known incision models. Depth of the gorge in the middle reaches shows clearly the expected increase from zero to a maximum then decrease downstream noted qualitatively, but suffer from variations across and down valley introduced by (a) the fact the surface the gorge incises is hummocky and not perfectly flat, (b) valley-perpendicular ridges and moraines, and (c) locations where the gorge sidewalls coincide with the rock walls of the glacial trough. To reduce the impact of these variations, we present gorge depth as a five point moving average downstream of the maximum gorge depth present at each site (Fig. 4.6). This also has the advantage of smoothing the data to an appropriate level to stabilize the numerical simulations performed in the later parts of this paper.

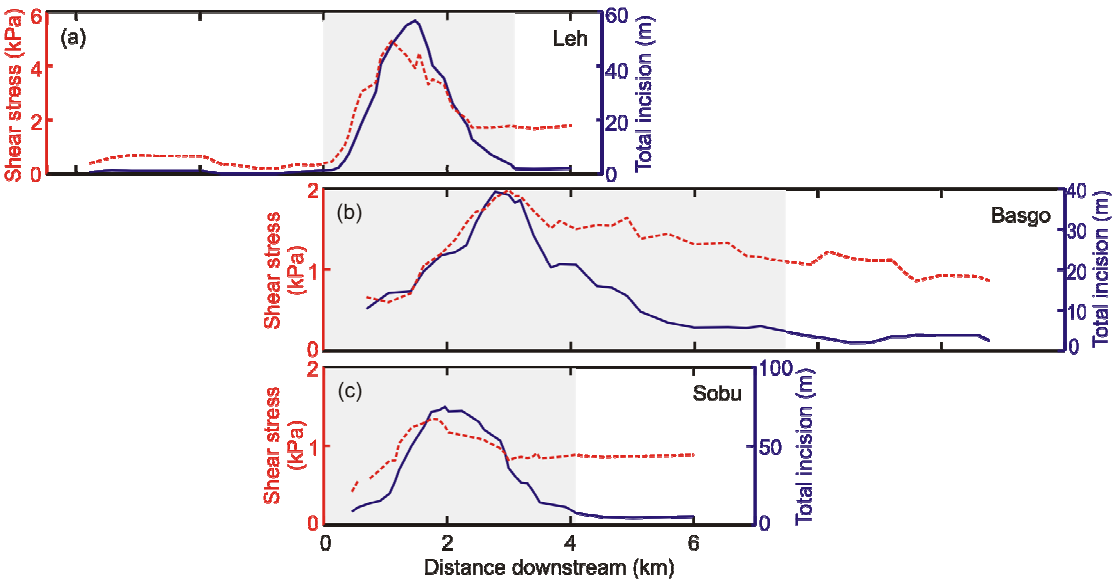

Figure 4.6. Downstream distributions for shear stress (red dotted line) and gorge depth (blue solid line) for trunk streams in four catchments, Leh **(a)**, Basgo **(b)**, and Sobu **(c)**. Approximate extent of the gorge is shown by gray shading, and profiles are displayed with the gorge starting points aligned. Note the approximate coincidence of the maximum gorge depth with a shear stress maximum in each case. Shear stress values at the gorge feet are also often significantly higher than they are at the gorge heads.

Calculated shear stresses (Equ. 4.5) are plotted alongside these gorge depth data (Fig. 4.6), and are similarly smoothed with a five point moving average to allow direct comparison between the datasets. In all the valleys, maximum shear stresses broadly coincide with maximum gorge depth. Shear stresses rise from a roughly constant value in the headwaters, and return to a roughly constant value just before the end of the gorge, but the stable value of shear stress is three or four times higher downstream of the gorge than the value upstream – this is particularly clear for the Leh valley data.

We have also analyzed data describing the gorge sidewall angles, focussing on Basgo and Leh valleys, and discarding any measurements taken where bedrock was known to be exposed in these slopes. These data have a mean of 31.4° and a

median of 32.3°, and these values are indistinguishable between valleys. Similarly, analysis of remotely sensed imagery suggests that the width of the valley floor within the gorge is relatively invariant with distance downstream, and approximately 40 m in all cases.

In the Leh and Sobu valleys, rates of change of shear stress downstream suddenly fall to almost zero (Fig. 4.6) beginning approximately 1 km before the end of the currently exposed gorge. This change is less extreme, but still present for Basgo. We infer that this change is related to the onset of aggradation in the channel and associated changes in channel dynamics, and the position of this point is consistent with field evidence that the postglacial surface is onlapped by the fluvial sediments. If this is the case, then within this reach shear stresses are likely to have changed over time, as the downstream decrease associated with ongoing downcutting has been replaced by the more even downstream distribution associated with aggradation. We discuss the role of this effect as we proceed.

4.3.4 Channel Width and Substrate Grain Size

An understanding of channel width variation is also an essential component in discriminating between incision models (Fig. 4.7). The distribution of channel widths varies markedly between the three process domains of glacial-incisional-aggradational outlined above. In the upper glacial domain large variation is present, reflecting changing substrate grain size as the channel passes over and between debris flow fans (c.f., Hobley et al., 2010). In the aggradational domain and within the gorge, channel width is more uniform, with occasional high outliers. Qualitative field observations indicate that localized width maxima within the gorge are sometimes associated with recent debris flow activity. Importantly, there is only a slight hint of systematically increasing downstream width in these lower domains, an observation borne out by inspection of the remote sensed imagery. This indicates that downstream changes in channel width will not significantly translate the predicted transport-limited incision distribution for these channels (c.f., Fig. 4.2).

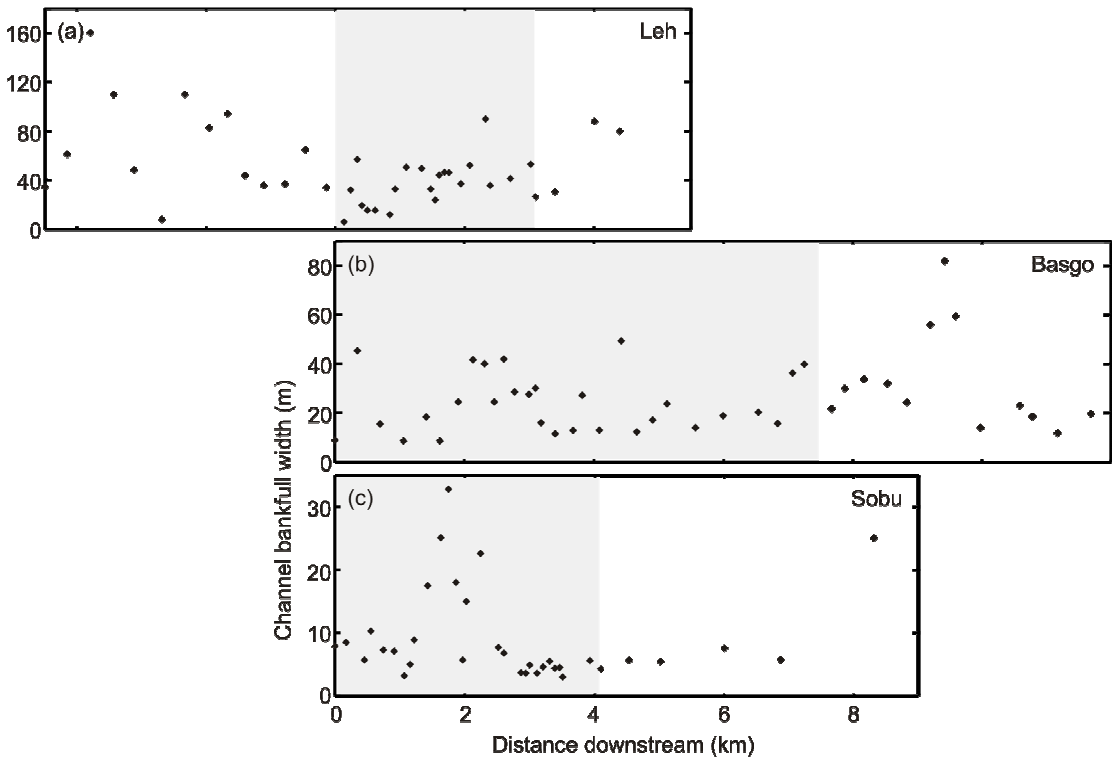

Figure 4.7. Field measurements of channel bankfull widths for trunk streams, again for the catchments Leh **(a)**, Basgo **(b)** and Sobu **(c)**. Approximate extent of the gorge is shown by gray shading, and profiles are displayed with the gorge starting points aligned.

We have also considered variation in the grain size of the substrate using the Wolman values measured at two different exposures in the Leh valley, approximately 2.5 km apart (see Appendix C and Fig. C1). Substrate size distribution is identical between the sites measured (95 % confidence; Kolmogorov-Smirnov test), and we assume that this is true of the glacial debris substrate throughout the catchments, consistent with semi-quantitative field observations elsewhere, including field photographs. This observation forms a basis for our treatment of channel aspect ratio variation in the past (Section 4.5.1.5), and demonstrates that the substrate has a uniform resistance to erosion.

4.4 Channel Response Style

Direct visual comparison of Figures 4.2 and 4.6 allows discrimination between detachment- and transport-limited response in these catchments. Figure 4.6 indicates that the maxima in shear stress, and hence the points where $d\tau/dx = 0$, are associated with the maximum gorge depths and not with points of zero incision. This result is incompatible with the transport-limited model, unless (a) channel width were to fall significantly downstream to compensate, or (b) shear stress distributions have evolved significantly through time. We have demonstrated in Section 4.3.4 that channel width does not fall significantly downstream so are able to discount the former case, and reject the latter both on grounds of parsimony and from consideration of likely past variation in shear stress from the small changes in overall long profile form seen here (e.g., Fig. 4.5), corroborated by the output of the modelling presented in Section 4.5.

The patterns in Figure 4.6 are however entirely consistent with the detachment-limited model (c.f., Figure 4.2c). Shear stresses downstream of the gorge are several times greater than those upstream, but in both cases there is almost no incision, and the peaks in shear stress in some of the cases may be offset with respect to the incision peaks. These are the hallmarks of a sediment flux dependent, detachment-limited response, as shown schematically in Figure 4.2c. The raised shear stresses downstream indicate that work is being done in the stream which is not associated with downcutting, and we attribute this to work done moving sediment. Similarly if the peaks are significantly displaced this would indicate that the incision efficiency maxima in the systems are offset with respect to the shear stress maxima, with sediment flux a likely means of mediating this process. Moreover, the fact no incision occurs in the upper domain of Leh valley despite non-zero shear stresses also strongly suggests that this response also involves a shear stress threshold below which no erosion occurs.

To invoke sediment flux dependent variation in incision rates, we also need to constrain the actual evolution of sediment flux downstream in the gorge. Sediment flux in the channel can be supplied from upstream and from valley sidewalls. There is no evidence for significant amounts of erosion or sediment transport upstream of the gorge, as large scale postglacial reshaping of the valley floor has not occurred (Hobley et al., 2010). Within the gorge, hillslopes are at the angle of repose, with a median of 32.3° (c.f., Bagnold, 1966). Slopes of loose material at the angle of repose will fail as their base is lowered (Roering et al., 1999; Strahler, 1950), and this appears to be the case within the gorge because of the lack of lichen cover on these slopes compared to the hummocky glacial surface (Hobley et al., 2010). We can therefore calculate sediment flux to the channel by determining the amount of material that must be removed from the hillslope to maintain angle of repose as the channel lowers.

4.5 Incision Model

We have now inferred in Section 4.4 that the Ladakh channels we have studied respond in a detachment limited manner, in which incision depends on sediment flux and shear stress must exceed a threshold if incision is to occur. However, the exceptional quality of the preservation of the incision history in this landscape and the consistency of the form across several examples in fact means we can go beyond this and calibrate the forms of the sediment flux function active in each channel. We use a finite element approach to model the incision occurring under an excess shear stress incision model modulated by a sediment flux function, and vary the inputs to this using a Monte-Carlo Markov Chain method. This technique allows us both to establish the most likely form of the sediment flux function for each catchment, and to rigorously assess the uncertainties associated with these solutions.

4.5.1 Approach

The finite element model tracks the progressive incision history at each measurement point in the gorge, and gorge dimensions for each timestep are integrated with the incision rates to calculate the sediment flux for each iteration. Because incision rate evolves in time, so does gorge depth as well as shear and Shields stresses.

4.5.1.1 Initial Model Setup

Model input consists of downstream distances, the smoothed modern slope and gorge depth data already discussed, and flow depth measurements for each locality. Using the known gorge depths, the original downstream slope distribution of the initial channels before incision began was also reconstructed and forms the starting condition for the model. At the gorge head, all available data points within the gorge are included, as well as some just upstream of its start where available. However, in the lower gorge reaches we have interpreted the prominent levelling off of the shear stress data in Leh and Sobu valleys c. 1 km up from the gorge end (Fig. 4.6) as indicating the onset of depositional behaviour (Section 4.3.3). We do not include data for localities downstream of these transitions, as the model does not account accurately for aggradation on the valley floor. Similarly we do not consider data points in the final kilometer of Basgo valley, which also shows a levelling off around this point, though less distinctly. We acknowledge that this transition point can migrate as the model evolves and the gorge deepens, but our results indicate that this makes little difference for these catchments.

4.5.1.2 Sediment Flux Function

We model the gorge incision over 100 ka (Δt = 0.5 yrs) using an assumed sediment flux function. A $Kf(q_s/q_c)$ curve forms the main variable input for the model, assigned between $0 \leq q_s/q_c \leq 1$. The form is given by

$$Kf(q_s / q_c) = \kappa\left(\left(\frac{q_s}{q_c}\right)^n + c\right)\exp\left(-\phi\frac{q_s}{q_c}\right) \tag{4.6}$$

where κ, n, ϕ and c are all positive constants. This equation is adopted explicitly for its generality; it allows us to fit a wide variety of peaked, smoothly increasing or smoothly decreasing curve shapes, including a broadly symmetrical form as favoured by Sklar and Dietrich (2004), as well as optionally allowing a nonzero value of $Kf(q_s/q_c)$ at $q_s/q_c = 0$ as has been suggested in some models (e.g., Gasparini et al., 2006). The form of the equation is also analogous to the dependence of erosion on sediment supply proposed by Turowski et al. (2007), though their analysis was not cast explicitly within a shear stress driven, detachment-limited framework and it is nontrivial to compare the detailed predictions of the two models.

4.5.1.3 Sediment Flux and Capacity

The value of $Kf(q_s/q_c)$ is allocated using q_s produced by mass balance directly within the model from the gorge form and the incision rate, and also a value for q_c determined from a slightly modified version of the Meyer-Peter-Muller (MPM) transport equation (see below). The calculation of q_s assumes that no sediment enters the gorge from upstream of its head or from side tributaries but rather that it is sourced entirely from the gorge hillslopes and channel bed. The three catchments presented here were selected specifically to minimize the impact of sediment brought

in from side tributaries, and the geomorphology of the upper reaches of the valleys beyond the gorge head also indicates that little sediment transport is transported significantly downstream in this domain (Hobley et al., 2010).

The transport capacity, q_c, for these channels is calculated from

$$q_c = 8C\left(\frac{\rho_s - \rho_w}{\rho_w} g D_{char}^3\right)^{0.5} \left(\tau^* - \tau_c^*\right)^{1.5} \tag{4.7}$$

where ρ_s is the density of the sediment, 2700 kgm^{-3}, C an empirical constant, D_{char} a characteristic critical grain size for the system, and τ^* and τ^*_c the bed Shields stress and critical Shields stress respectively (Meyer-Peter and Muller, 1948). Note that this formulation gives a volume flux, not mass flux. D_{char} replaces the median diameter of the sediment in the subsurface, which is inappropriate across such a broad range of grain sizes. Instead, it is calculated to give a consistent relationship between the critical shear stress observed in the field and the critical Shields stress which we calculate using the Lamb equation (Lamb et al., 2008; see below, Section 4.5.1.4). C is unity in the MPM equation senso stricto, but here is a free parameter reflecting changing transport stage in the channel (e.g., Fernandez Luque and van Beek, 1976). We calculate its value heuristically for each catchment, adjusting the input value for successful model runs until the sediment capacity matches the sediment flux at the known modern transition points to depositional behaviour at the end of the simulation.

We have chosen to use the MPM relation instead of one of the very many alternative sediment capacity equations since (1) it is of simple form, (2) it makes predictions based on a small set of variables of which we believe we understand the distribution back through time, and (3) most previous studies of the tools and cover effect have used this formulation. We do recognize that we are using the MPM relation under a circumstance it was not derived to explicitly describe – that of a

heterogeneous grain mixture. However, we note that most other transport laws which we could have selected (e.g., Bagnold, 1977; Bagnold, 1980; Einstein, 1950; Fernandez Luque and van Beek, 1976; Meyer-Peter and Muller, 1948; Parker et al., 1982; Schoklitsch, 1962; Yalin, 1963) rely on a similar form, analogous to excess shear stress raised to a power of 1.5. The multiplier in front of this tends to be only a weak function of variables which we expect may evolve downstream in our channels. Thus we expect a similar downstream form from many of the relations, and since we know absolute value of sediment flux at the point of sediment saturation from our field observations we independently calibrate the function magnitude at capacity, so the choice of specific function is much less of an issue.

4.5.1.4 Thresholds

We require threshold values for both shear stress and Shields' stress for our equations. We use the Lamb equation (Lamb et al., 2008) to derive the critical Shields stress, which makes this value a weak function of slope:

$$\tau^*_c = 0.15S^{0.25} \tag{4.8}$$

We derive values for τ_c for our channels based on consideration of past values of shear stress in the channels, but also incorporating this threshold sensitivity to slope, since Shields stress is given by

$$\tau^* = \frac{\tau}{g(\rho_s - \rho_w)D_{char}} \tag{4.9}$$

We thus calculated the shear stresses that would have been present in the gorge head at the start of its evolution using the calculated initial values of channel slope, correcting for this slope sensitivity, and adjusted the value of D_{char} uniformly

for all streams in order to allow incision everywhere within all gorges but forbid it at all points upstream. The critical value of D_{char} was calculated as 0.229 m, which seems feasible based on the known caliber of the bed sediment at the gorge head. In fact, without this slope sensitivity, it is not possible to select a single value to predict τ_c everywhere at once, providing support for our use of the Lamb equation.

4.5.1.5 Model Output

The model output is determined by a slightly modified version of Equation (4.2), the general detachment-limited erosion equation:

$$E\left(1+\frac{2H}{W_V \tan 32°}\right) = tKf\left(q_s / q_c\right)\left(\tau - \tau_c\right) \tag{4.10}$$

where E is the incision rate, H is the total accumulated gorge depth, W_V is the gorge floor width, and t the total time since incision. Since the standard tools-and-cover detachment-limited model treats $0 < f(q_s/q_c) < 1$, we can then rescale the solution to give both K, presumed constant within each valley, and $f(q_s/q_c)$ separately. Note that we assume $a = 1$ in Equation (4.2) to derive Equation (4.10) – this is the value typically associated with erosion proceeding by plucking of clasts from the bed (Whipple et al., 2000) as is occurring here, and authors using higher values in the incision law tend to be aiming to implicitly incorporate sediment or threshold effects which we treat here explicitly (Whipple and Tucker, 2002). τ evolves as a function of S throughout the run, which assumes constancy of discharge and channel aspect ratio through time – the latter being a reasonable assumption given the uniform grain size distribution in the glacial substrate (Finnegan et al., 2005). We take t = 100000 years (Owen et al., 2006), which is a significant approximation with a large uncertainty, but as long as the glacier retreat time is the same in each valley, the absolute value is of little importance as fractional error will be subsumed into the

erodability parameter K. The term inside the brackets on the left hand side of the equation reflects the complexity that as we cut down in a v-shaped gorge, for a unit of downwards incision we must also simultaneously mobilize all the material shed into the channel from the angle of repose hillslopes. We treat the addition of this material as instantaneous and assume it is effectively spread evenly across the valley floor. The uniformity of the substrate, demonstrated 32° hillslopes (Sections 4.3.3, 4.3.4) and long time scale considered serve to make these assumptions reasonable.

4.5.1.6 Optimal Solutions

Our goal is to determine the form of Equation (4.6), or in other words to constrain the coefficients κ, n, ϕ and c. We treat these coefficients as unknown, and determine their values and the uncertainties in their values using a Monte Carlo Markov Chain method. This method involves selecting values of the coefficients from a probability distribution, and then accepting or rejecting these values using an acceptance criterion. This process is iterated upon several thousand times in order to constrain the posterior distribution of the model coefficients (e.g., Berg, 2004). The acceptance criterion is based on the Metropolis-Hastings algorithm (Hastings, 1970). The proposed values of the model coefficients are used to drive the finite difference model of channel evolution of the 100,000 year span of gorge development. The model predicts the depth of gorge incision. This model prediction is then compared to the measured gorge to determine the likelihood of the coefficients in Equation (4.6). The likelihood of the current iteration is compared to the previous iteration. If the ratio likelihood of the new iteration to the previous iteration is > 1, then the new coefficient values are accepted. If this ratio is < 1, then the new coefficients are accepted with a probability equal to the ratio. To generate the posterior distribution of coefficient values, each iteration in the Markov Chain is weighted by the likelihood of the combination of parameter values, creating a probability distribution of each coefficient. This can be used to determine both mean and 95% credibility limits on the parameter values (Fig. 4.8).

4.5.2 Optimal Results from the Forward Model

Figure 4.8 shows the most likely forms of the sediment flux function for our channels. We solve for $Kf(q_s/q_c)$ (Fig. 4.8a), and derive the value of K and the form of $f(q_s/q_c)$ by rescaling the latter to give a peak magnitude of unity (Fig. 4.8b). We note that the erosivity, K, of Sobu is much higher than the other two channels. The associated values of κ, n, ϕ and c are quoted in Table 4.1. We plot predicted vs. modelled incision patterns (Fig. 4.9) to illustrate the quality of fit of the sediment flux functions. The matches to the field data are excellent.

We also illustrate the evolution in $f(q_s/q_c)$ values used at each node in the model and resulting changes in incision rates as the best fit runs proceed (Fig. 4.10). Somewhat surprisingly, the value of $f(q_s/q_c)$ used by the model, and hence the relative sediment flux itself, is relatively stable at most points downstream. We interpret this to reflect interplay between the evolving gorge form, erosion rates and channel slopes, balancing out the tendency for the deepening gorge to increase the sediment flux per unit incision. In particular the point of maximum erosional efficiency ($f(q_s/q_c) = 1$) moves very little through time, and does not always migrate in the same direction, up- or downstream (Fig. 4.10a-c). This runs counter to the expected behaviour that would be assumed if slope and erosion rates could not evolve during the run, which would predict advance of both the point of maximum erosional efficiency and the transition to alluvial conditions upstream through time. Such stability in the erosional efficiencies through time may account for the difficulties in demonstrating conclusively the existence of the tools and cover effect in many other real landscapes. The model output also indicates that the rates of incision at most points in the gorge are either approximately constant or gradually decrease through time (Fig. 4.10d-i). This general tendency to decreasing response speeds as the system matures is what would intuitively be expected for a perturbed geomorphic system (e.g., Church and Ryder, 1972).

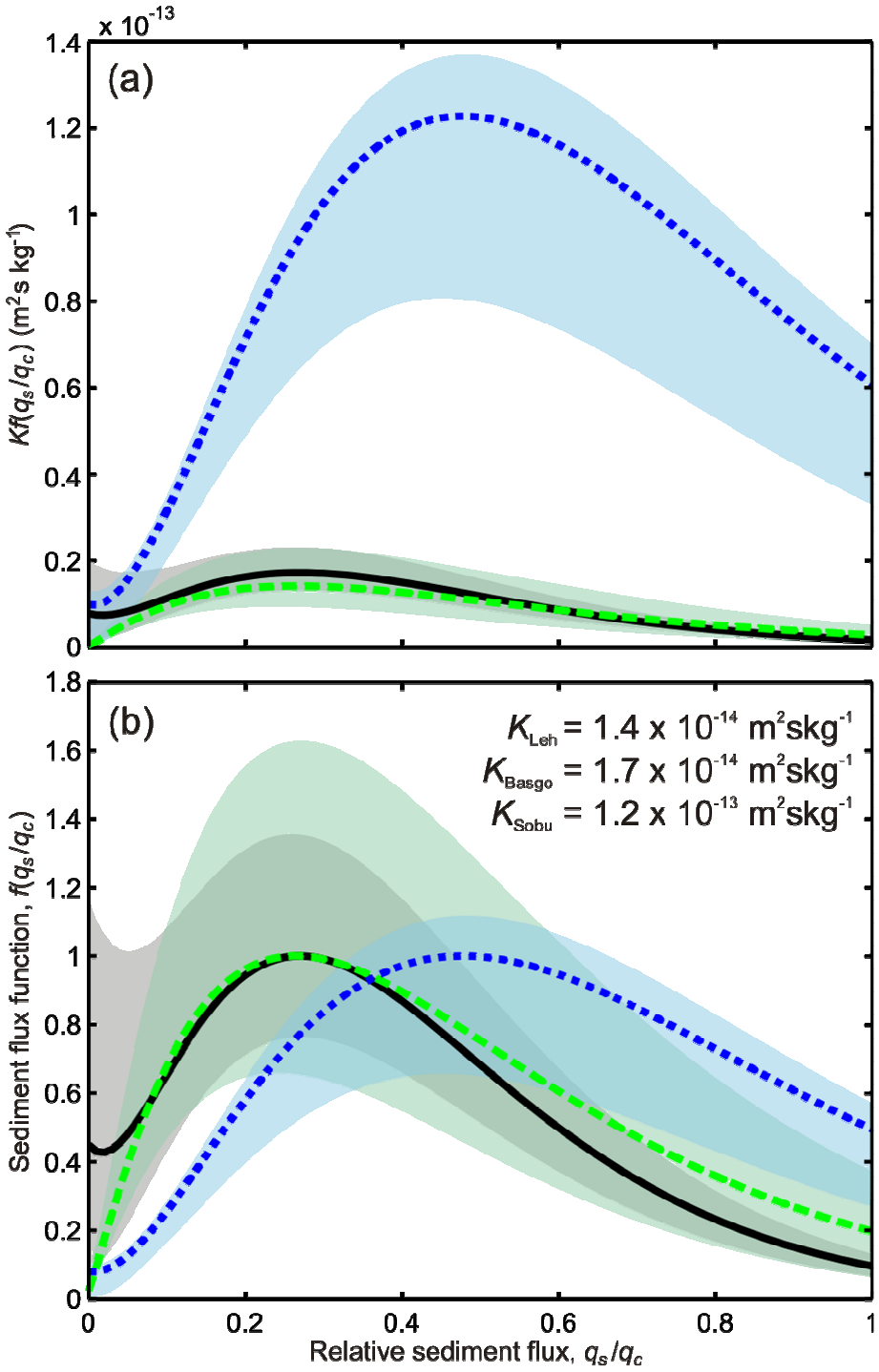

Figure 4.8. Most likely sediment flux functions for Leh (dashed green line), Basgo (solid black line) and Sobu (dotted blue line) valleys. Shaded areas represent 95% credibility limits for these curves. **(a)** Comparison of functions preserving best fit magnitude, *K*. **(b)** Comparison of functions rescaled to a relative magnitude of 1, consistent with theory. Implied values of *K* for each catchment are also shown.

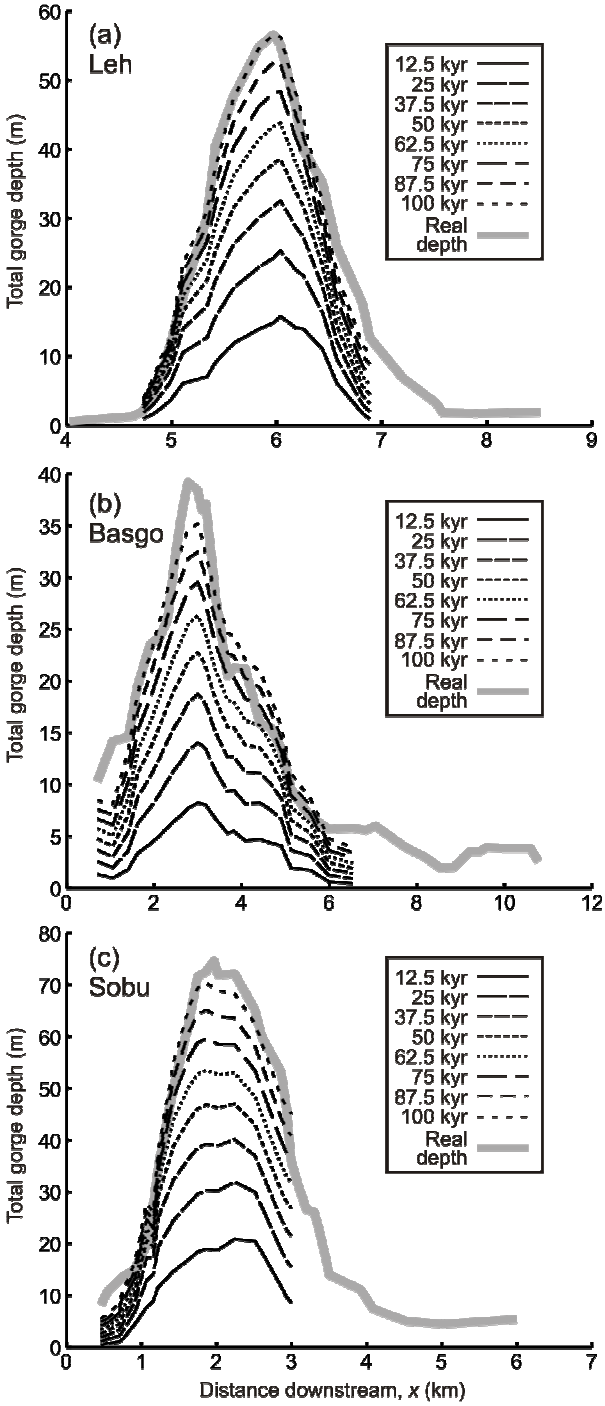

Figure 4.9. Outputs from the forward model using most likely solutions shown in Figure 4.8. Thinner black lines represent the total accumulated incision every eighth of the total runtime, i.e., 12.5 ka. Thicker gray lines are the known field observations of gorge depth. Modelled curves are truncated at the known real transition to depositional behavior in the modern channel.

TABLE 4.1. BEST FIT VALUES FOR PARAMETERS IN EQUATION 10 FOR EACH CHANNEL

Channel	κ	n	ϕ	c
Leh	$4.22\text{x}10^{-6} < 6.07\text{x}10^{-6} < 9.74\text{x}10^{-6}$	$1.02 < 1.13 < 1.37$	$7.30\text{x}10^{-4} < 1.81\text{x}10^{-3} < 4.20\text{x}10^{-3}$	$3.64 < 4.24 < 4.89$
Basgo	$2.77\text{x}10^{-5} < 3.56\text{x}10^{-5} < 4.73\text{x}10^{-5}$	$1.69 < 1.91 < 2.05$	$1.81\text{x}10^{-3} < 6.83\text{x}10^{-3} < 1.76\text{x}10^{-2}$	$6.33 < 6.54 < 6.72$
Sobu	$8.76\text{x}10^{-5} < 1.26\text{x}10^{-4} < 1.39\text{x}10^{-4}$	$1.84 < 2.02 < 2.08$	$1.88\text{x}10^{-4} < 2.44\text{x}10^{-3} < 3.22\text{x}10^{-3}$	$3.85 < 4.19 < 4.31$

We also illustrate the evolving transport stage, the ratio of the Shields stress of the flow to the critical Shields stress, down each channel under these optimal solutions (Fig. 4.11). The different lines shown for each catchment indicate variation in transport stage throughout the model runs as slope and sediment load evolve, but overall these values are relatively stable. These values are important since relative transport stage is also thought to play a role in controlling erosivity in sediment flux dependent incising systems (Sklar and Dietrich, 2004; Whittaker, 2007), and we go on to discuss its possible effects in Sections 4.6.1 and 4.6.2. We note that Basgo has slightly higher peak transport stages than Sobu, and Leh has much higher values than both of these. This ordering is consistent with the idea that lower transport stages can be associated with increased erosivity, but the large change in erosivity occurs between Basgo and Sobu, while the large change in transport stage occurs between Basgo and Leh.

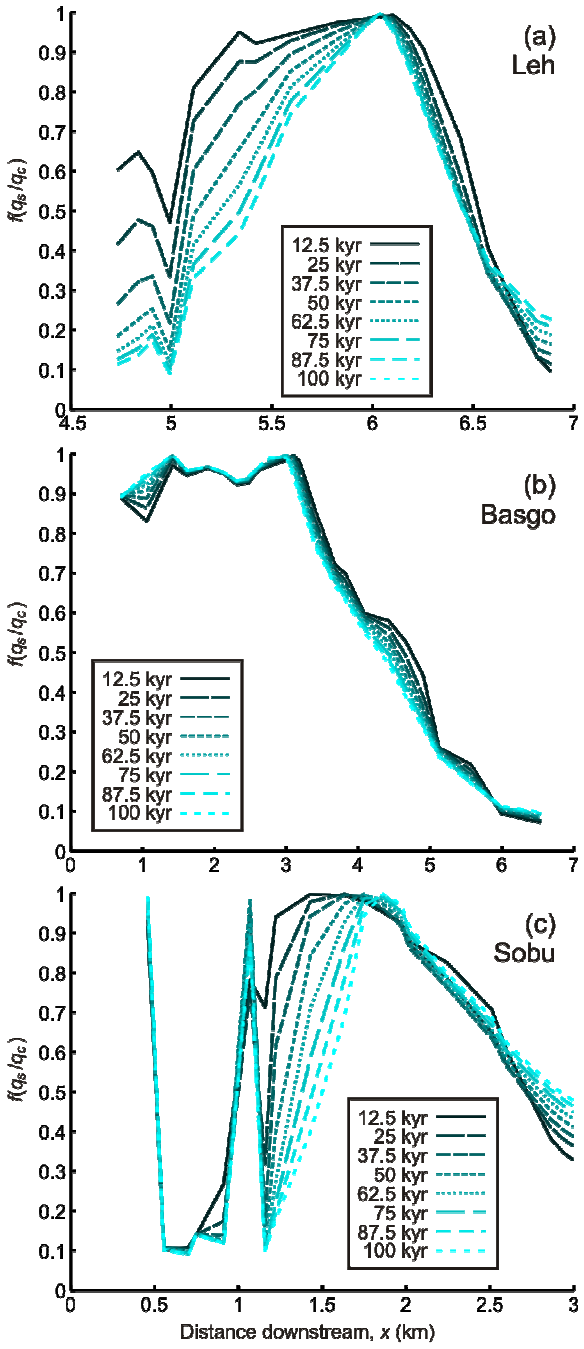

Figure 4.10. (a-c) Model data reflecting evolution of $f(q_s/q_c)$ at each node downstream during model run for each catchment using most likely solutions (Fig. 4.8). The sharp spike in the Sobu data is a point with high error driven by initially low shear stresses in the gorge head. **(d-i)** (Overleaf) Model data reflecting evolution of gorge depth through time for each node in each catchment using best fit solutions (Fig. 4.8). These data are shown both as true depths (d-f) and normalized to total incision at that node at the end of the run (g-i). Note that most nodes show a tendency to incise more slowly later in the model run, but a few increase their rates of incision slightly through time. These accelerating nodes are typically either at the head or foot of the gorge, but are not intuitively distributed.

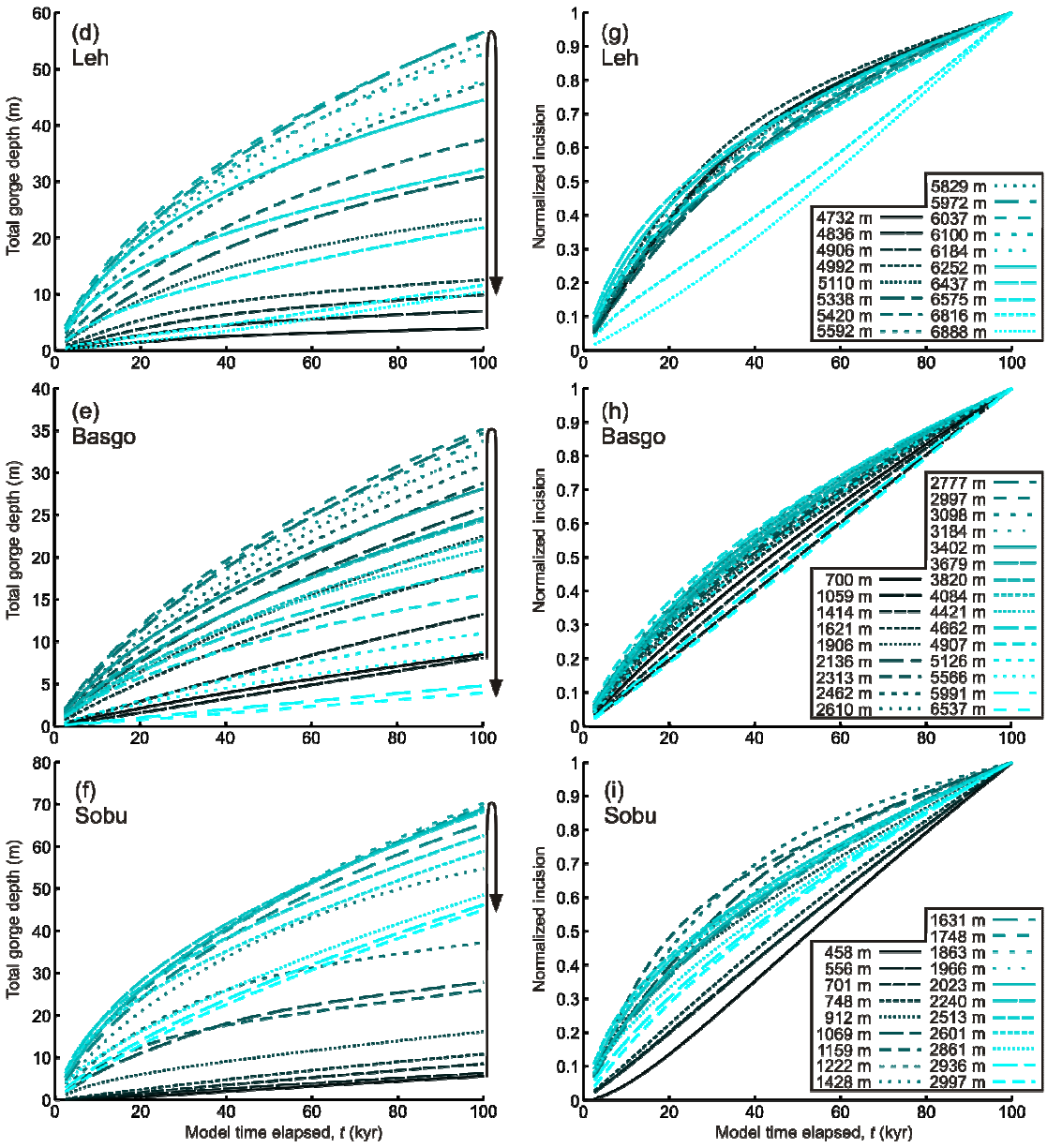

Figure 4.10 (cont.).

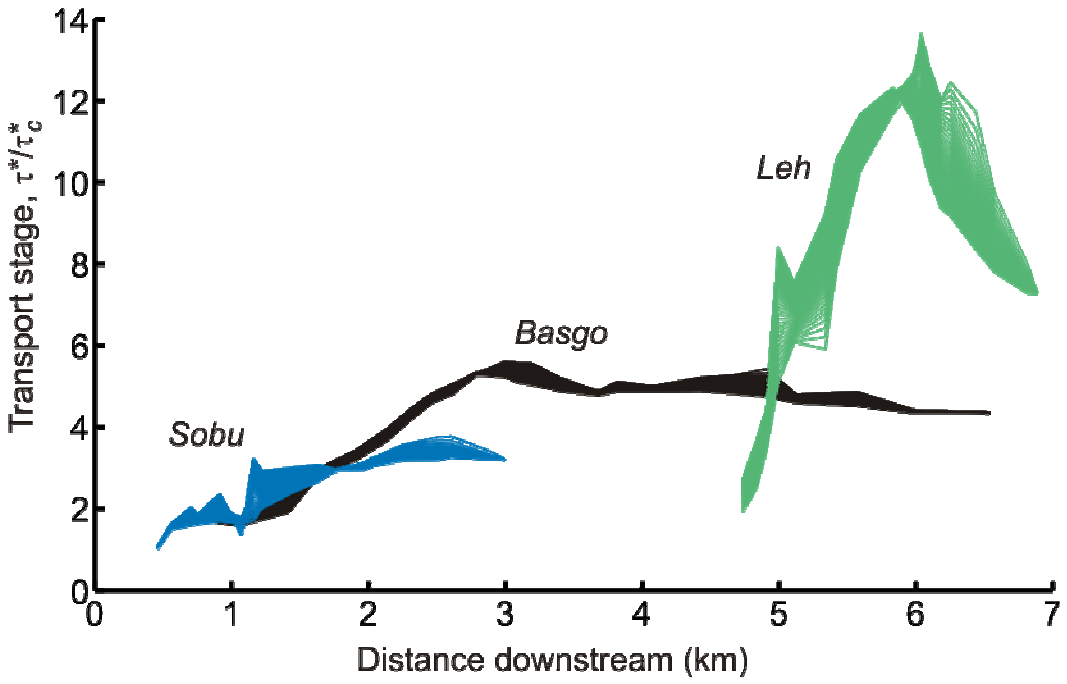

Figure 4.11. Distributions of transport stage downstream for Leh, Basgo, and Sobu valleys for the most likely sediment flux functions (Fig. 4.8). Each fine line represents transport stage at a single 2.5 ka time-slice in during each run; note that although transport stages do evolve during the model runs, they do not vary greatly. The peak transport stages in Leh valley are much (3-5 times) higher than in either Basgo or Sobu valleys, whereas the difference between the Basgo and Sobu distributions is much smaller (< twofold variation).

4.6 Discussion

4.6.1 General Form of the Sediment Flux Function

This study has demonstrated that incision proceeding into loose, poorly sorted substrate material across long timescales can and should be modelled as a detachment-limited process, but modulated by a sediment flux function which incorporates both tools and cover effects. Figure 4.8 shows that the sediment flux function is not always of the parabolic form originally proposed by Sklar and Dietrich (2004). We identify some general differences to this model: the transition point between the tools and cover effects, which represents the maximum efficiency of erosion, occurs at low q_s/q_c = 0.25-0.5, the rising limb of the tools effect is steep, and the decreasing limb of the cover effect falls off less rapidly at high relative sediment flux, giving a quasi-exponential decrease. These features are all reminiscent of the form of the sediment flux sensitive erosive response proposed by Turowski et al. (2007), indicating that their dynamic treatment of bed cover is probably a sensible revision of theoretical models of the cover effect.

Peak erodability occurs at reduced relative sediment flux in the Basgo and Leh catchments compared to the Sobu catchment (Fig. 4.8b). This pattern has in fact already been reported from experimental studies of bedrock abrasion in a flume, where increasing asymmetry is associated with increasing transport stage in the flow, across a similar to slightly lower range of transport stages to that reported here (Whittaker, 2007). This outcome is also consistent with results from modelling using cellular automata to constrain sediment transport and erosion (R. A. Hodge, unpubl. data). The relative transport stages in our channels (Fig. 4.11) are consistent with this explanation, but demand that the sensitivity to variation in τ^*/τ^*_c is much greater at low transport stages than it is at high. The extent to which the skew of the sediment flux function towards low relative sediment flux values will be mirrored in other incising systems is not clear however, as it may reflect the specific dominance of the cover effect in a loose sediment system (see also section 4.6.3). We do however note

that this skew matches that suggested by Turowski et al.'s (2007) dynamic cover model, and is consistent with previous experimental abrasion studies (Whittaker, 2007), including the original Sklar and Dietrich results (Sklar and Dietrich, 2001).

4.6.2 The K Parameter, Absolute Sediment Flux and the Sobu Curve

Our method has allowed us not only to isolate the form of the sediment flux function, but also the absolute magnitude of the expression $Kf(q_s/q_c)$ for each analyzed channel (Fig. 4.8). The magnitudes of $Kf(q_s/q_c)$ for the Leh and Basgo data sets are significantly lower than that for Sobu. Since the function $f(q_s/q_c)$ varies only between zero and one, this means that the value of K is varying strongly between catchments, with a higher value – more efficient erosion – in Sobu valley. Traditionally, within the stream power law (e.g., Equ. 4.1) the value of K is thought to depend primarily on substrate erodability, climatic erosivity, and perhaps a threshold effect (e.g., Whipple, 2004). However, Leh and Sobu are adjacent, subparallel valleys, their outlets only some 6 km apart, and are of similar dimensions (Fig. 4.3). Both share the same postglacial substrate within the gorge, and similar elevation spans for each geomorphic domain. It seems unlikely that either the substrate or climate could vary significantly between these valleys.

Our data suggest that some other parameter not captured by the conventional erosion expression must affect the value of K. Studies of the tools and cover effect in flumes as well as theoretical approaches have suggested that this missing expression is transport stage (Sklar and Dietrich, 2004; Whittaker, 2007). The transport stage is on average lowest for Sobu (Fig. 4.11), but in order for this effect to be solely responsible for the enhanced erosivity in Sobu valley we would require a very strong decrease in erosivity across a very narrow window in transport stage. In contrast, the most obvious factor that varies strongly between the valleys is absolute sediment flux (Fig. 4.12). We suggest that the erosivity term within the hybrid detachment-limited erosion law should also be sensitive to the absolute bedload flux. Such sensitivity would be consistent with the underlying physics of a bed abrasion model

for the tools effect, and has previously been incorporated into theoretical models of sediment dependent incision (Sklar and Dietrich, 2004; Turowski et al., 2007).

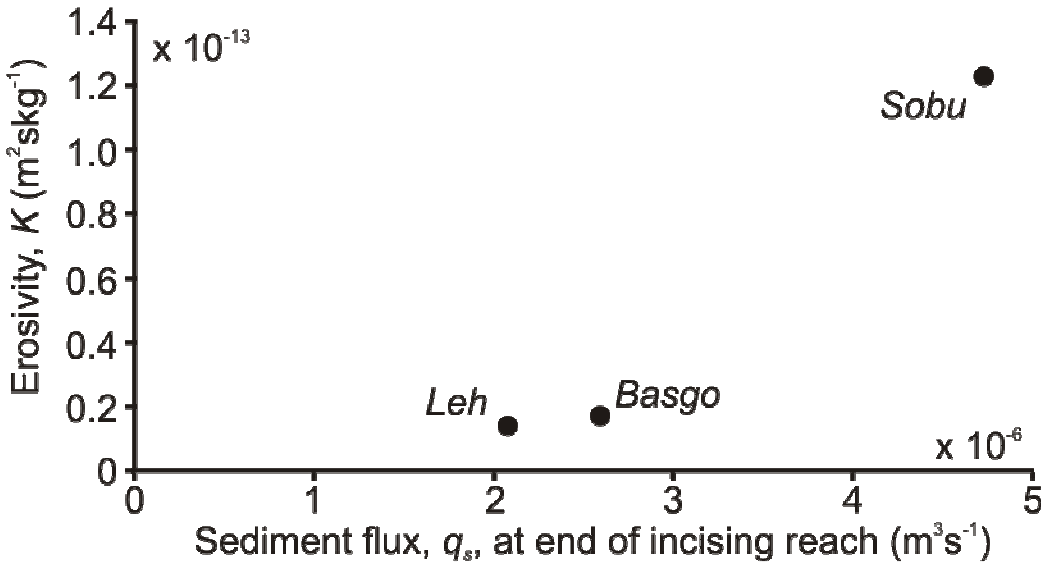

Figure 4.12. Sediment flux function erosivity, K, as a function of modelled total sediment flux at the transition to depositional behavior, measured at the end of model runs using the most likely sediment flux functions (Fig. 4.8).

4.6.3 Tools and Cover - If Here, Then Everywhere?

The prominent cover effect in these results is consistent with results from a number of natural bedrock erosional systems (e.g., Cowie et al., 2008; Johnson et al., 2009; Valla et al., 2010). The mechanism of draping of the bed with sediment already in transport applies here, and we had already observed the transition downstream to full alluvial conditions which implied the channel approached then exceeded the limit $q_s/q_c = 1$. However, the presence of the tools effect in our study area is more unexpected, as most formulations for tools theory assume erosion of a

bedrock substrate. This indicates that clasts already in transport play an important role in dislodging clasts that were previously immobile on the bed and allowing them to be incorporated more easily into the flow (c.f., Chatanantavet and Parker, 2009; Schmeeckle et al., 2001). Indeed, very recent experimental work has confirmed that erosion rates of a loose sediment can be enhanced by the addition of sediment to the flow, providing direct support for the existence of a tools effect in such systems (Venditti et al., 2010).

This study comprises the first documented example of the tools effect arising from changing downstream sediment flux from within single channels, and the best constrained examples of any previously documented sediment flux functions. However, this incision is occurring in a non-bedrock system. We speculate that if the tools and cover effect is occurring here, it is probably also occurring in any channel, bedrock or otherwise, which is downcutting while also transporting a significant coarse bedload. This behavior should at least be considered in all bedrock channels, and many of the implications discussed below may well apply in a large number of incising systems in a wide variety of settings.

4.6.4 Implications

In a transiently responding landscape undergoing sediment flux dependent incision, different reaches of the same channel with differing relative sediment fluxes will experience different erosional efficiencies (Fig. 4.10a-c). This has several profound consequences for how we understand the long term evolution of landscapes, particularly in terms of how we use the stream power law.

4.6.4.1 Modelling Channel Erosion

If the channel element of landscape evolution is modelled with a stream power law approach, then in order to correctly predict both the pace of topographic

change and sediment flux from basins one must include the effects of incision thresholds and the sediment flux function. Other authors have already highlighted many of these effects in isolation – we note amongst others the contributions of Gasparini et al. (2006) discussing the effects of sediment flux on transient response of a modelled landscape and the differences from simpler stream power models, and those of Baldwin et al. (2003) and Wobus et al. (2006a) discussing the profound (order of magnitude) extensions in landscape response time that seemingly small changes in erosion model complexity can produce, including simply implemented sediment flux effects. However, further work is needed to explicitly explore how varying downstream erosional efficiency fits into this picture, especially the tools effect, and how sediment flux dependency interacts with thresholds on the system, the stochasticity of the imposed climate, and downstream depositional regimes, especially those developing ephemerally during transient channel response. We anticipate that in many cases nonlinear sediment flux functions may significantly extend the response times of perturbed rivers (c.f., Fig. 4.10d-i), though for relatively sediment starved channels it is also possible that the tools effect may shorten response times compared to predictions from more simply implemented erosion models (c.f., Gasparini et al., 2007).

4.6.4.2 Channel Scaling

It has previously been noted that rivers in transient landscapes tend to develop anomalous scaling metrics, especially in terms of the slope-area scaling exponent, or concavity (e.g., Hobley et al., in review; VanLaningham et al., 2006; Whipple, 2004). Similarly, a number of studies have addressed the theory behind how perturbations to these scaling relations can be produced, with reference typically to a specific effect such as model formulation, catchment-scale variation in forcing, or sediment flux effects (e.g., Gasparini et al., 2006; Sinha and Parker, 1996; Sólyom and Tucker, 2004; Tucker and Whipple, 2002; Wobus et al., 2006a). However, the link between the theory and real field studies is rarely made. Uniquely, we are here able to demonstrate that the tools and cover effect is active in a channel system

which has previously been documented to have systematically elevated concavity values (Hobley et al., 2010). This provides good evidence that variation in relative sediment flux in natural systems is one of the prime drivers of altered scaling in natural channels. We also note that concavities can evolve significantly in channel networks even following quite modest bed elevation changes, as are occurring in this field site. It is the distribution of this change downstream which is the important driving parameter for channel concavity.

4.6.4.3 Reading Past Changes in Boundary Conditions From Landscapes

It has previously been argued that an understanding of the dynamics of channel incision can allow past boundary conditions affecting a landscape to be read from its present form (e.g., Kirby and Whipple, 2001; Snyder et al., 2000; Wobus et al., 2006b). These approaches have met with some impressive success when applied to landscapes where this past forcing is known and the landscape is believed to have reached topographic steady state. However, some more recent studies have extended the method into landscapes which are responding transiently (e.g., Cyr et al., 2009; Harkins et al., 2007; Kirby et al., 2007; Wobus et al., 2006a). Such methods typically assume a simple form of the detachment-limited erosion law without sediment flux effects when deriving the mathematical inversion required to reconstruct the past changes. We suggest that if sediment flux dependent incision is widespread in bedrock channels (Section 4.6.3), then applying such methods in transiently evolving landscapes in particular may create significant systematic errors in any results (c.f., Chapter 3). We would advocate caution in applying the simplest form of detachment-limited erosion law to transient landscapes until further work has more fully established the prominence and forms of the sediment flux function across a wider variety of mountain channels.

4.7 Conclusions

We have presented a framework under which the erosion style of an incising channel may be understood as either detachment- or transport-limited. We have also demonstrated that both styles can incorporate a sediment flux dependent term as well as a shear stress dependent term, allowing extension of the idea of a "hybrid" incision response into the transport-limited erosion model. Shear stress distribution downstream forms the key discriminator between these two erosion models when compared to known patterns of resulting incision in a transiently responding channel network.

We have applied this framework in a postglacial landscape where we have direct measurements of shear stress and where incision is well constrained due to the presence of a dated terrace. We demonstrate for the first time that incision proceeding into a coarse, loose, poorly sorted substrate can and should be modelled as a sediment flux dependent, detachment-limited system. This sediment dependency must incorporate both a tools effect, where increasing relative sediment flux from initially low values promotes more efficient incision of the bed, and also a cover effect, where as the relative sediment flux continues to rise it begins to inhibit incision of the substrate. Uniquely, we are able to calibrate the precise form of the resulting sediment flux function in three different catchments in the field site, and model how transient variations in relative sediment flux control the development of a gorge and the transition to the downstream aggrading system as these catchments develop through time, accurately matching these outcomes to real field data. The resulting sediment flux functions show many features which are compatible with previous theoretical and laboratory studies but which have not before been independently verified from real field data, but also suggest that the peak in incision efficiency may occur at lower relative sediment flux values than widely assumed in the literature. We also show that the erosivity (K) of hybrid detachment-limited systems is not described sufficiently by extrinsic controls of climate and lithology, and may also depend on absolute values of sediment flux in the channel. The

presence of the tools and cover effects working in concert in this environment suggests that they are also likely to important in any eroding river channel carrying significant quantities of coarse bedload.

Paper Acknowledgements

This work was supported by a NERC studentship NER/S/A/2005/13851. We are very grateful to Tim Ivanic, Martin Hurst and Jenny Rapp for assistance in the field, and especially to Fida Hussein of Leh for logistical support. Many thanks also to Alex Whittaker, Mikaël Attal and Dimitri Lague for many stimulating discussions helping with the development of ideas for this work.

5. DISCUSSION AND SYNTHESIS

5.1 Overview and Synthesis

This thesis has used an integrated study of field and remotely sensed data combined with analytical and computer modelling to investigate the long term transient response of mountain rivers to changes in their boundary conditions. This addresses an outstanding challenge in modern quantitative geomorphology (c.f., Whipple, 2004), allowing us to discriminate between incision models, to understand the dynamics and style of the response, and to better read past environmental changes from the landscape record. We have presented the previous three chapters in a stand-alone paper style, but together they form a coherent narrative which makes significant forward progress on several deeper unsolved questions in geomorphology. Amongst others, these include:

- Is there anything special about the perturbation experienced by a postglacial landscape compared to a landscape perturbed by changing tectonics?
- How reliable is the steepness index method for reconstructing past tectonics when applied in transient landscapes?
- What is the role of sediment flux in controlling river incision?
- How can we tell the difference between detachment- and transport-limited responses of river channels from field data? How does sediment flux fit into this picture?

The next section provides a detailed account of how the work presented in chapters 2, 3 and 4 addresses these major challenges in the field, and makes explicit how the material in this thesis significantly advances our understanding of transient river dynamics. The subsequent section outlines questions which this thesis has in turn raised and suggests possible avenues of approach for some of these. The thesis then concludes with a short summary of the key elements of this study.

5.2 Importance, Impact and Implications

5.2.1 Postglacial Landscapes as Transient Landscapes – Differences, but Mainly Similarities

The literature describing geomorphic response to and recovery from glaciation – "paraglacial response" – tends to leave the reader with the strong impression of the "special-ness" of postglacial landscapes. New, ice mediated ("periglacial") processes may be active, and the accelerated rates of change and short response time scales of small and intermediate scale geomorphic features compared to nonglaciated environments tend to be emphasized (see Section 2.1). However, the geomorphic response of the landscape to glaciation at the catchment scale, perhaps the most relevant to the impact of glaciation in the geologic record, has been rarely considered in this literature. Are the rates and styles of response at this scale distinctively "glacial", or are the landscape dynamics more or less equivalent to any transiently perturbed landscape?

This question is addressed in Chapters 2 and 3 of this work, looking first at the exceptionally ancient postglacial landscape of the Ladakh Himalaya (Chapter 2), then more explicitly at the contrast between this case and two differently perturbed river systems elsewhere (Chapter 3). It has been shown that while the geomorphology of the Ladakh landscape is filled with features which are clearly relics of the glaciation and unique to such a postglacial environment, the first order characteristics and divisions of the landscape are defined by the style of response (or indeed non-response) of the trunk streams draining the catchments (Section 2.4). This is vital, as it indicates that on the catchment scale, exotic processes driven by the effects of ice are of minor importance, and it is the channel response which determines the long term evolution of the system after deglaciation, both geomorphologically and in terms of its sediment output to downstream stores. A simple approach, based on the known rate of river downcutting into the landscape, has been used to suggest a minimum response time for the landscape on the order of 10^6 years and a rate of downcutting on the order of 0.5 mm/y, values which are both

entirely consistent with examples of nonglacial transient landscape response from the literature (Section 2.6.2.2). However, this time scale of response is an order of magnitude longer than any previous value quoted for any system responding to a glacially driven perturbation, i.e., a paraglacial response.

This thesis also looks into the first order scaling of channels perturbed by glaciation. Chapter 2 draws attention to the existence of concavity (slope-area scaling) values which are sharply elevated above those expected at steady state for the glacially perturbed landscapes in Ladakh. The magnitude of the displacement away from steady state values reflects the extent of the glacial alteration of the landscape, as measured by the position of the glacially carved knickzone within the catchment (Section 2.5). This might instinctively be interpreted as a unique consequence of some aspect of the system specifically forced by the glaciation (e.g., altered channel hydrology), but this is not supported by existing work on the effects of altered stochasticity on river scaling (Section 2.6.1). Instead, Chapter 3 demonstrates that such an altered scaling is a consequence of the presence of a knickzone within the catchment, rather than by the fact it is glacially carved. Since a migrating knickzone is a common feature of many transiently responding landscapes (e.g., Whipple and Tucker, 2002), this scaling is probably widespread in very many channel systems in a wide variety of climatic and tectonic settings. It is possible that many instances of atypically high concavity values previously reported in the literature (see, e.g., Whipple, 2004 for a review) also reflect this same sensitivity of river scaling to presence of a knickzone in a river system.

This conclusion – that at the catchment scale, glacially perturbed catchments can be regarded as equivalent to transiently responding catchments in other settings – has not previously been well articulated, and forms the foundation for the subsequent approach taken in this work exploring the style of response of the channels in these environments within a purely fluvial framework.

5.2.2 Transient Landscapes, River Scaling and the Reading of Tectonics from Landscape

Chapters 2 and 3 have described the existence of a systematic and nonlinear perturbation in the measured concavity value for reaches downstream of knickzones in the long profile of a river. Chapter 3, with its documentation of this trend in a variety of tectonoclimatic settings and the arguments from first principles laid out in Section 2.6.1 together make the case that this behaviour is not driven by extrinsic forcing on the systems – be it stochastic, climatic, tectonic or paraglacial. Instead, the evidence suggests that the effect is forced by catchment geometry, and an inevitable consequence of the existence of the knickzone in the channel perturbing some property of the flow, such as width or sediment flux scaling, as it passes over the break in slope. Section 5.2.3 returns to the nature of this perturbation, but here it is noted that the nonlinearity in concavity scaling reported here is not predicted by simple versions of the stream power law, where erosion is effectively modelled as a direct function of the shear stress on the bed (Figure 5.1).

This previously unrecognized but yet widespread trend is in fact of vital importance. Almost all attempts to read past changes of tectonics from landscape assume this simple form of the stream power law somewhere in their derivation, and if the scaling of river channels deviate from this then systematic error in the calculations is to be expected. This idea is dealt with thoroughly in Section 3.5, which describes in detail the errors that this altered scaling will introduce into the steepness index method of channel analysis. That chapter concludes that the effect will make little difference where the channels have reached steady state (e.g., Snyder et al., 2000), but will introduce phantom zones of increased inferred uplift downstream of long profile convexities in transiently responding landscapes where the method been recently applied. The effect will be exacerbated by considering individual reaches of the channel, which has also recently become common practice when using this method (e.g., Harkins et al., 2007). A clear, unequivocal demonstration of the stability of the slope-area scaling of channels on the scale that

they are analyzed is essential if the results of such studies in transient landscapes are to be believed.

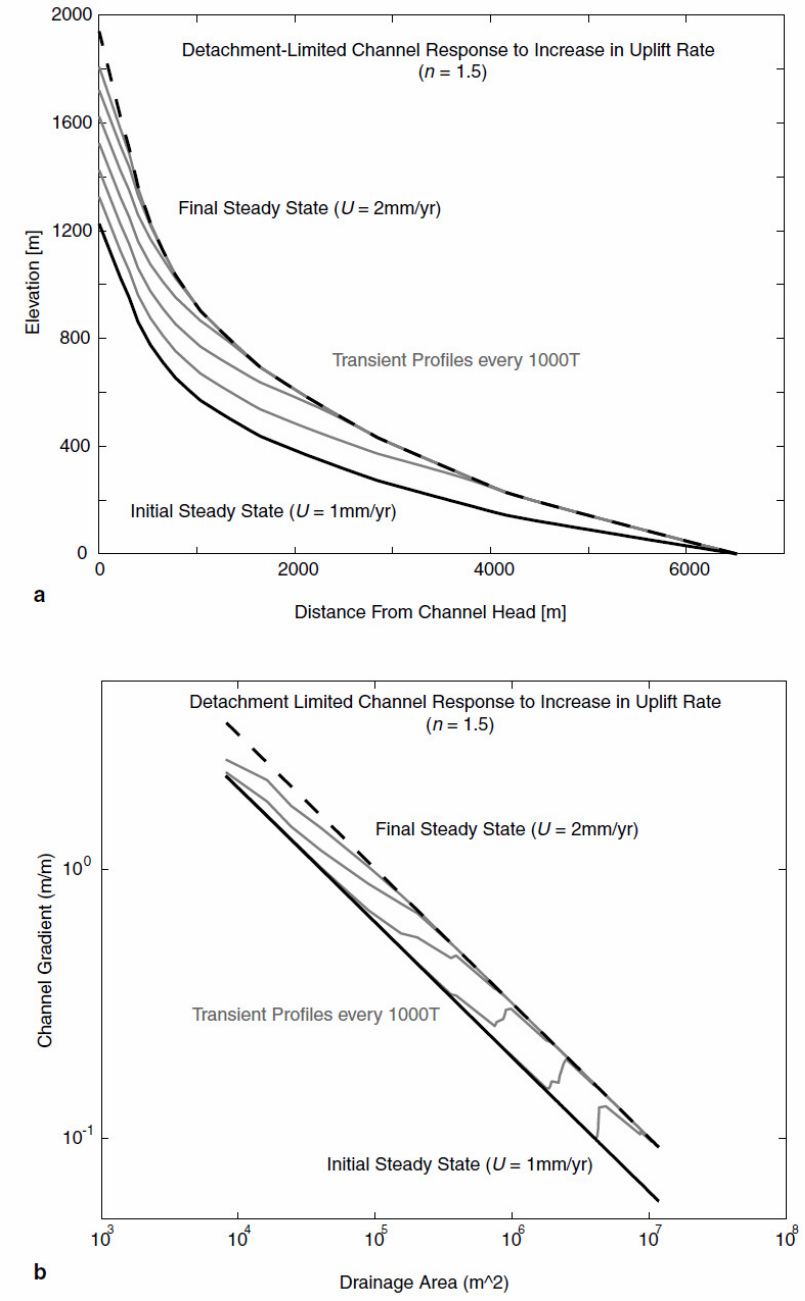

Figure 5.1. From Whipple and Tucker (2002). Modelled long profile **(a)** and slope-area scaling **(b)** for a channel responding transiently to an increase in uplift rates, assuming a simple detachment limited erosion law. Light gray lines indicate profile at regular timesteps during the response. A migrating knickzone sweeps up through the system as time advances, but note that the slope area scaling of the reach downstream of the knickzone does not deviate from the expected concavity value of 0.5 (dashed black line in b), the same as that before perturbation (solid black line in b).

This conclusion echoes general concerns previously raised by others over the applicability of the steepness index method in transient landscapes (see Section 3.5.2), but provides an entirely novel explanation for how systematic error can enter the calculations and provides a framework for understanding its likely impacts and for avoiding interpretations biased by its effects. Demonstration of the presence of the signal across a variety of different environments also means that these conclusions have the potential to impact very many future studies of transient river response to past changes in boundary conditions.

5.2.3 Sediment Flux and River Incision

The idea that the rate of erosion in a natural river system ought to be sensitive to the flux of sediment it carries has now been present in the literature for some time. Working from both theory and experimental modelling studies, it has been suggested that sediment entrained in the flow has the capacity to act both as tools to promote incision by impacts on the bed, and also as cover, where increased volumes of sediment form a protective layer over the bed. This existing work (see Section 4.2.1) suggests that the tools effect should be dominant at low relative sediment fluxes and will give way to the limiting effects of cover at higher relative sediment fluxes, giving a peak in erosional efficiency at some intermediate value of relative sediment flux. This means that of the various possible controlling factors modulating the simple stream power type approach – e.g., climate, lithology, threshold effects – the effect of sediment flux is likely to be most important, both due to the strongly nonlinear, humped, form of the response and also due to its ubiquity – all eroding rivers must carry sediment, and in transient landscapes the relative sediment flux must vary downstream. However, despite all this an astonishingly small body of work has attempted to calibrate or detail this effect in real, natural settings.

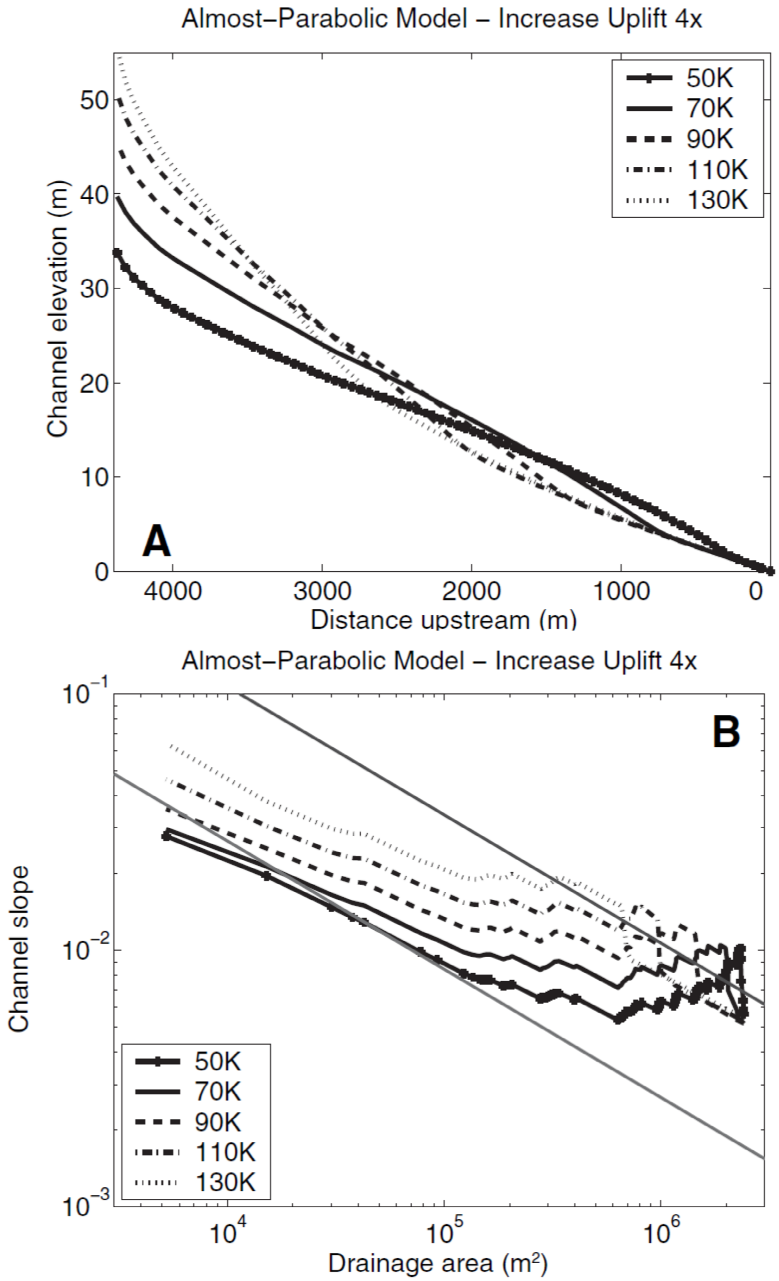

Figure 5.2. From Gasparini et al. (2006). Change in modelled channel long profile **(A)** and associated slope area-plot **(B)** for catchment perturbed by a fourfold increase in uplift rates, assuming an almost-parabolic form of the sediment flux function. Data lines represent time intervals as shown in B, as model years. Straight lines running through slope-area plot are the equilibrium relationships, i.e., θ = ~0.5, for old (lower) and new (upper) uplift rates. Note that this model generates a migrating knickzone in the long profile (local slope maxima in B), and that downstream of this the concavities are significantly elevated. These concavities relax back towards equilibrium values as the knickzone moves up the system. Compare Fig. 5.1.

The role of sediment flux forms perhaps the strongest theme running through this thesis. Chapter 2 begins by describing the qualitative field evidence that in the Ladakh field site, the relative sediment flux in the river system must be varying downstream – the mobile boundary between incising reaches upstream and depositing reaches downstream in the glaciated catchments is perhaps the best evidence for this. The altered river scaling then described in Section 2.5 and further documented in other tectonoclimatic settings in Chapter 3 is also shown to be entirely compatible with the long term effects expected from this downstream increase in relative sediment fluxes (see, e.g., Sections 2.6.1 and 3.5). It has previously been documented that elevated concavity values may be associated with downstream transitions to alluvial river behaviour, but uniquely here we have shown this only to be a sufficient, not necessary condition – the transition to alluvial reaches is driven by evolving relative sediment flux downstream, at the same time as it drives increases in concavity. It has been asserted here that evolving sediment flux would still drive increased concavity without the transition to full alluvial conditions, as we see in the Red River region in Chapter 3. The close match between field sites of the increased concavity trend downstream of profile convexities also argues that this is an intrinsic feature of river dynamics, shared between eroding and depositing reaches and relatively invariant in different settings. Long term relative sediment flux is the most parsimonious choice for the driver of this effect, since sediment variations will occur in all transient landscapes independent of forcing mechanism, can be demonstrated for the Ladakh and Făgăraş regions by the downstream transitions to alluvial reaches, and have been suggested from theory to be capable of producing elevated concavity trends downstream of knickzones in eroding systems (c.f., Sections 2.6.1 and 3.5; Fig. 5.2).

Having suggested in Chapters 2 and 3 that evolving relative sediment flux is sufficiently important to perturb first order slope-area scaling in transient river networks, it is essential that the effects of sediment flux also be demonstrated from the detailed reach scale channel response of the Ladakh field site. This provided the original motivation behind Chapter 4. Working from within a detachment-limited erosion framework (justified by consideration of the distribution of downstream

shear stress; see Section 5.2.4), this chapter demonstrates that the patterns of incision observed in the field in the incisional Domain 2 of the Ladakh catchments are most consistent with an erosion law modulated by both tools and cover sediment flux effects. This field site presents a unique opportunity to go beyond this however and to fully calibrate the form of this sediment flux function, using the exceptionally clear and continuous form of the postglacial gorge and the ability here to produce an almost comprehensive sediment budget through time for the stream within it. Section 4.5 presents this material. Figure 4.8 presents the resulting unprecedented curves describing the relative erosional efficiency at varying relative sediment fluxes for three different Ladakh catchments. These results provide an unmatched opportunity to test theoretical ideas of how the tools and cover effect works against real data (see Section 4.6) and represent a very important contribution to our wider understanding of this process.

Although the Ladakh site is somewhat atypical to many transiently responding landscapes in terms of the loose substrate incised and the aridity of the environment, this thesis has emphasized the similarity of the response rates, styles and time scales to other environments (c.f., Section 5.2.1). It is in fact likely that the role of the sediment flux function presented here is widely applicable in incising transient landscapes of all types, especially considering that this work has demonstrated that the Ladakh system is responding in a detachment-limited fashion, in line with most other bedrock upland systems (next section).

5.2.4 Distinguishing Incision Models Using Field Data

A wide variety of models to describe river incision have been proposed in the literature (see, e.g., Section 4.2). However, as has been widely noted, distinguishing between these is challenging, since under equilibrium channel conditions many of the models achieve a similar concave-up form. Looking at the river response while it is transiently adjusting to a change in forcing conditions is now recognized as the best hope for model discrimination, since the response style (e.g.,

diffusive/advective/hybrid) has been shown to vary from theory to theory. However, to be able to reconstruct the long profile form in sufficient detail across a long enough time window to definitely identify this response style can prove difficult in a real world setting.

This study has taken a novel approach to this problem by returning to the basic mathematics used to frame a river incision model as either detachment limited, (where erosion proceeds as a function of shear stress on the bed) or transport limited (where it proceeds as a function of divergence of carrying capacity in the flow). Chapter 4 has argued that by making explicit the dependence of the transport capacity of the channel on shear stress, we can make direct comparison between these two formulations where each incision equation depends on the product of two independent terms, one a function of sediment flux, the other a function of bed shear stress. This treatment allows us not only to recognize a potential new class of hybrid transport-limited erosion response (Section 4.2.2), but also to distinguish between detachment- and transport-limited behaviour purely on the basis of downstream shear stress distribution and the resulting pattern of channel downcutting.

We have used this framework to test the style of response occurring in Ladakh, an environment in which the choice between incision model is ambiguous. Incision is known to be proceeding into the coarse, loose, but very poorly sorted substrate of glacial debris. This material is not attached to the bed and a lot of it is quite fine grained, so we might expect a transport-limited response, but equally there are many blocks in the grain mixture which the channel will not be able to freely incorporate into the flow, which would argue against this. On the basis of the shear stress and gorge depth data (Figure 4.6), we are able to demonstrate that these channels are adjusting to the glacial sculpting of the catchments in a sediment flux dependent, detachment-limited fashion on catchment response ($> 10^3$ yrs) time scales. Presumably, a similar response should be expected in analogous situations in other mountain catchments, for instance where debris flow or landslide deposits directly impinge on channels, or where river beds are composed of jointed or otherwise fragmented bedrock.

This shear stress based approach to understanding erosive response style across the whole spectrum of detachment-limited and transport-limited behaviour is entirely new, and has great potential to allow us to distinguish between river incision models in other environments and settings where long profile form may not be sufficient to distinguish between them. The addition of the new hybrid transport-limited response style also fills a theoretical gap in our understanding of this spectrum of behaviour, and provokes further questions regarding when and if such modified diffusive behaviour would be seen. The ability to demonstrate that a channel is responding in a detachment-limited fashion is also a key step in the reconstruction of a channel's response to relative sediment flux, as described in Section 5.2.3. Providing this framework may also stimulate further attempts to understand this important parameter in other settings.

5.3 Research Opportunities and Future Work

The novel results and conclusions from this work have in turn triggered a set of new research questions, both regarding the detailed evolution of the Ladakh catchments and on how we treat long term river dynamics more generally. This section outlines some of these questions as well as possible approaches to tackling them.

5.3.1 Landscape Evolution in an Ancient Postglacial Environment: Dynamics of the Other Domains

Chapter 2 of this work has presented a thorough field description of the catchments draining the Ladakh batholith. However, the detailed analysis conducted for these catchments in Chapter 4 focussed almost entirely on the dynamics of the incising channel in the gorged reaches. There is still abundant research to be done on

kinematics and dynamics of the lower, aggrading domain and in particular the upper, glacially dominated domain, some of which we outline below.

The lower domain is clearly an important part of the evolving concavity story outlined in Chapters 2 and 3. However, on the grounds of shared response, this study has only been able to hypothesize that evolving long term sediment flux modulates long term channel aggradation in the same way that it modulates long term channel incision in the better documented downcutting reaches. This is largely due to the fact that long term deposition in this reach has hidden beneath the surface any evidence of past landscape form – we need to know the stratigraphy to interpret the evolution of this domain. Surveys of the subsurface in such settings would be extremely valuable, perhaps exploiting subsequent downcutting, though this would not be possible in any of the Ladakh catchments documented here. An alternative might be to establish systematic modern sediment flux measurements throughout the systems to investigate how the material supplied to the depositing regime at the end of the gorge is dispersed today, or to use stable isotope systems in grains in this domain to see particle transport histories. Such approaches would allow us to test the extent to which standard sediment transport laws are appropriate in these settings, and to try to document the details of the coupling between the sediment flux dependent incising reaches and the downstream areas of deposition.

The upper domain however may yield more easy progress, since burial of the past landscape form is not so much of a problem. Chapter 2 has qualitatively documented some of the complexities of landscape evolution in this domain, but time and logistical difficulties prevented a fuller examination of the details of response in this area. The role of the paraglacial debris fans and unusual hillslope channel coupling in this domain presents an interesting problem, since while it is clear that material is reorganized on a 500 m scale between fans and the flats between them, it is not clear how this impacts and has impacted long term channel evolution in this domain. What would the landscape be like if more/fewer of these fans intersected with the channel? Do they prevent the channel from modifying the landscape more widely by forcing it to concentrate its power on these coarse bed regions? How old

are the fans, and what is the likely fate of this component of the landscape in the future? The role of the inherited valley width carved by the glaciers will form an important component of this problem. A field campaign focussed on taking finer scale field measurements than those presented in Chapter 4 in a number of the Ladakh valleys would rapidly make progress on these questions.

Further clarification of how these other elements within the such catchments operate would not only provide a clearer view of some of the processes described in this study and the links between them, but would also be an ideal study of the dynamics of the transition points between contrasting incisional and depositional channel processes, a topic of great importance within geomorphology but still poorly understood (c.f., Paola et al., 2009). It might also enable better understanding of the concavity trends seen in Chapters 2 and 3, and possibly allow for a correction to be applied when considering the calculation of past forcings from transient topography (Section 3.5).

5.3.2 The Hybrid Transport-Limited Erosion Model

Section 4.2 of this work introduced the theoretical concept of a hybrid transport-limited erosion model, where erosion is modelled as a function of the product of rate of change of sediment capacity with shear stress and rate of change of shear stress downstream (Equation 4.4). This formulation arose as a natural consequence of the framework under which we analyzed the transport-limited erosion law, and in fact was not found to be applicable in the Ladakh field site. However, this raises the questions of how such a formulation would respond in theory to equilibrium and perturbed boundary conditions, and whether or not it may be shown to be a real driver of channel behaviour rather than just a theoretical possibility.

Chapter 4.2.2 suggested that the hybrid transport-limited model would behave in a manner analogous to the hybrid detachment-limited law on the basis of similarity

of form. However, this has not been demonstrated. A thorough study is needed in the vein of those by Whipple and Tucker (2002) and Gasparini et al. (2006) (c.f., Figs. 5.1, 5.2) to document the details of the expected response of this erosion equation. This will also require an examination of the likely form of the $dq_s/d\tau$ term, which it was suggested in Chapter 4 may well diverge away from the linear relation predicted from the form of many laboratory derived transport equations when considered in real landscapes over long time periods. An approach based on predicted proportions of a mixed substrate to move under certain imposed shear stress conditions may be a good place to start with this (c.f., Wong and Parker, 2006). A very simple trial attempt at doing this (conducted during this study but not reported in the main text) using field data on the Ladakh glacial sediments and a Shields particle mobility calculation suggested it may be possible to produce a strongly nonlinear form of $dq_c/d\tau$ like that for the detachment-limited sediment flux function. However, the precision of the sediment data already collected cannot support a robust conclusion on this topic, and a more definitive study on well-constrained substrate sediment grain size data would be needed. Examples of good locations for such a study would be those in which the incising substrate were to be composed of homogenous blocks, such as glacial, jointed or landslide material, where detailed measurements of the substrate and subsequent predictions of its mobility under sediment flux laws could be compared to documented long term incision trends.

It would also be interesting to test other real incising fluvial landscapes to see if hints of this hybrid transport-limited behaviour can actually be seen in the field. The method used in Chapter 4 would allow a first order indication of whether it is acting. Since we have already discounted its importance in a coarse, loose and poorly sorted postglacial substrate, the next most obvious place to look might well be for incision occurring into pre-existing fluvial deposits, for example, an entrenched fan. Such a site would not have a heavy load of essentially immobile clasts, as in the Ladakh case, but the channel would still have to shift material not entirely optimized to its current flow regime. It may also be that the style of response changes

according to the magnitude and speed of perturbation, and this idea could also be explored.

The existence or otherwise of a hybrid transport-limited erosion regime could shed important light on the nature of the interaction between detachment-limited and transport-limited erosion and transport processes, both temporally and spatially. A fuller understanding of the "best" way to describe incision processes in a wide variety of settings will also significantly improve our ability to computationally model landscape evolution.

5.3.3 Interaction of Sediment Flux and Threshold

This study has demonstrated that in the Ladakh catchments, incision can only be modelled adequately with both a threshold and a tools-and-cover type sediment flux function incorporated into the detachment-limited incision law (Chapter 4). However, in drawing such a conclusion this field-based study has now outstripped the theoretical background describing how such a system will evolve in the long term. Modelling work has addressed both the role of thresholds (Attal et al., 2009; Snyder et al., 2003b) and the role of varying sediment flux (Gasparini et al., 2006) independently, but no previous research has attempted to examine how having both of these effects active together will change the long term evolution of fluvial systems. This is a particularly important gap in the literature to close, since it seems likely that any river system loaded with enough sediment to experience the tools and cover effects may also have imposed upon it an incision threshold driven by the threshold of motion of that sediment (c.f., Section 4.5.1.4).

A systematic study of the way in which a both thresholded and sediment flux dependent detachment-limited system would respond to a perturbation in its boundary conditions (e.g., increased uplift), again after Tucker and Whipple (2002) or Gasparini et al. (2006), would serve to fill this gap. Such a study could also be

combined with the investigation of a hybrid transport-limited system as proposed in Section 5.3.2.

5.3.4 Landscape and Climate

One of the original motivations for this study was the observation that erosion rates have seemingly intensified globally over the last few million years, and that this is probably linked to transience imposed on the landscape by oscillating climate (Molnar and England, 1990; Zhang et al., 2001; see also Section 1.2). This work has examined the particular role in this story that glacial growth and retreat can play in inducing transience in mountain river systems, but we have quite deliberately ignored the possible role played by evolving climate itself. An important counterpart to studies such as this will be to examine the effect that more globally relevant climatic change (i.e., in rainfall distribution, quantity and intensity) can have on driving increased erosion of landscapes. Such changes have the potential to drive global erosion signals, not just those in glaciated regions, and will also modulate the effects of glaciers on landscapes such as that studied here. They will also shed light on the landscape change, including natural hazards, likely to be induced by modern anthropogenic climate perturbation.

Chapter 2 has presented a response time scale for the Ladakh system of the order of 10^6 years, much longer than the time scales of Milankovich-type climate cyclicity (Lisiecki and Raymo, 2005). This prompts several specific research questions which we might ask: To what extent are landscapes buffered against climatically induced cycles (c.f., Allen, 2008, and references therein)? Is the landscape more sensitive to climatic variation with a certain characteristic period? What, if anything, could make landscapes more reactive to climatic changes, for instance, sediment effects or thresholds? An obvious angle of attack on such problems will be to numerically model the consequences for the landscape of likely climate change scenarios, both modern and past, but the conclusions of such studies will also need to be field tested to establish their robustness. A methodology

focussed on an ideal real natural laboratory like the approach taken in this work will again prove invaluable. An appropriate natural laboratory will consist of a landscape with a strong climatic gradient on a relatively short lengthscale, combined with some understanding of how this gradient varies through time. A combined approach using global climate modelling or, more likely, well constrained orographic rainfall variation and atmospheric flow kinematics alongside detailed field work describing the form of channels (and hillslopes) crossing and within climatic zones will probably yield immediate gains in our understanding of the response of landscape to a changing climate.

6. CONCLUSIONS

The main conclusions of this thesis are as follows:

- The geomorphology of catchments draining the south flank of the Ladakh batholith follows a tripartite division, defined primarily by the dynamics of the trunk streams. In the upper domain the channels are controlled mainly by the inherited glacial and paraglacial structure of the landscape; in the middle domain the channels incise strongly down through postglacial sediments; in the lower domain the channels aggrade in a valley-filling floodplain above the postglacial surface. Field observations show that the lower domain is migrating up into the lower parts of the gorges previously cut by the channels. These observations demonstrate that the channel network is transiently adjusting to changing forcings on the system.

- The extent of glacial modification of the upper reaches of these catchments alters the hydraulic scaling of the downstream channel. The channel concavity measured downstream of the knickzone carved by the ice is systematically and nonlinearly elevated above the expected range of 0.3-0.6. Field observations suggest that this effect is associated with evolving relative sediment flux downstream in the channel, which would be consistent with its hypothesized role in some incision laws.

- The peak time-averaged incision rates in the Ladakh catchments surveyed are of the order of 0.5 mm/y, and catchment recovery times from the glaciation must significantly exceed 1 Ma. These values are consistent with rates and time scales from catchments elsewhere undergoing transient response induced by a change in tectonics. However, when interpreted strictly as glacially induced – "paraglacial" – responses, this response time scale exceeds any other previously reported by an order of magnitude. This is interpreted as being due to the previously underexplored whole catchment scale of this response.

- Comparison of the altered hydraulic scaling in Ladakh with river scaling in catchments elsewhere of similar form but responding transiently to different tectonoclimatic forcings demonstrates that the elevation of channel concavities downstream of knickzones is a widespread phenomenon, linked to some intrinsic property of the transiently eroding systems. This property is interpreted as evolving relative sediment flux downstream of the knickzone in each case.

- The existence of significantly perturbed slope-area river scaling relations in transiently responding landscapes creates significant complications for attempts to read past changes in tectonics from topography in these environments. The documented trends will create phantom zones of apparent uplift downstream of long profile convexities due to locally elevated concavity indices if a steepness index methodology is applied unthinkingly. This effect will be exacerbated by the presence of such convexities progressively further downstream in a catchment and by subdivision of the channel into smaller segments for analysis. Attempts to use such a method must take care to document the stability of measured channel concavities on the length scale appropriate to the channel segment length.

- Transport-limited and detachment-limited styles of erosion may be distinguished in real settings based on comparison between downstream shear stress distribution, channel width and erosion rates. This method also allows qualitative assessment of the relative importance of relative sediment flux effects on incision rate in each case. This process also highlights the possible existence of a previously unappreciated class of sediment flux dependent, transport-limited incision responses.

- Long term incision into a coarse, loose, poorly sorted but homogeneous substrate occurs as a detachment-limited process. Rates of downcutting in these settings are modulated by both an erosion threshold, below which

erosion does not occur, and a nonunity sediment flux function. Accurate modelling of this process requires that the sediment flux function incorporates both a tools effect at low relative sediment flux and a cover effect at high relative sediment flux.

- It is possible to fully calibrate the detailed form of this sediment flux function in this setting. This is the first description of the shape of the curve from a natural eroding system. The shape is not compatible with the simple parabolic form of the original Sklar and Dietrich (2004) theoretical suggestion, and instead shows nonzero erosion rates at zero sediment flux, a rapid rise and peak at relative sediment fluxes of less than 0.5 and a quasi-exponential decrease in erosional efficiency beyond this. Both the position of the erosional efficiency peak in relative sediment flux space and the magnitude of the curve are shown to be variable between catchments explored and correlated with transport stage and absolute sediment flux in the streams.

7. REFERENCES

Allen, P. A., 2008, Time scales of tectonic landscapes and their sediment routing systems, *in* Gallagher, K., Jones, S. J., and Wainwright, J., eds., Landscape Evolution: Denudation, Climate and Tectonics Over Different Time and Space Scales: Geological Society, London, Special Publications, v. 296, p. 7-28.

Amerson, B. E., Montgomery, D. R., and Meyer, G., 2008, Relative size of fluvial and glaciated valleys in central Idaho: Geomorphology, v. 93, no. 3-4, p. 537-547, doi: 10.1016/j.geomorph.2007.04.001.

Anders, A. M., Roe, G. H., Hallet, B., Montgomery, D. R., Finnegan, N. J., and Putkonen, J., 2006, Spatial patterns of precipitation and topography in the Himalaya, *in* Willett, S. D., Hovius, N., Brandon, M. T., and Fisher, D., eds., Tectonics, Climate, and Landscape Evolution: Geological Society of America Special Paper, v. 398, p. 39-53.

Anderson, R. S., 1994, Evolution of the Santa Cruz Mountains, California, through tectonic growth and geomorphic decay: Journal of Geophysical Research, v. 99, no. B10, p. 20161-20179.

Anderson, R. S., Molnar, P., and Kessler, M. A., 2006, Features of glacial valley profiles simply explained: Journal of Geophysical Research, v. 111, F01004, doi: 10.1029/2005JF000344.

Ashmore, P., 1993, Contemporary erosion of the Canadian landscape: Progress in Physical Geography, v. 17, p. 190-204.

Attal, M., Cowie, P. A., Whittaker, A. C., Hobley, D. E. J., Tucker, G. E., and Roberts, G. P., 2009, Integrated field and numerical test of stream erosion models using the transient response of bedrock rivers to tectonic forcing: Geological Society of America Abstracts with Programs, v. 41, no. 7, p. 335.

Attal, M., Tucker, G. E., Whittaker, A. C., Cowie, P. A., and Roberts, G. P., 2008, Modeling fluvial incision and transient landscape evolution: Influence of dynamic channel adjustment: Journal of Geophysical Research, v. 113, F03013, doi: 10.1029/2007JF000893.

Augustinus, P. C., 1995, Glacial valley cross-profile development: the influence of in situ rock stress and rock mass strength, with examples from the Southern Alps, New Zealand: Geomorphology, v. 14, p. 87-97.

Bagnold, R. A., 1966, The shearing and dilatation of dry sand and the 'singing' mechanism: Proceedings of the Royal Society of London. Series A, Mathematical and Physical Sciences, v. 295, p. 219-232.

-, 1977, Bedload transport by natural rivers: Water Resources Research, v. 13, no. 2, p. 303-312, doi: 10.1029/WR013i002p00303.

-, 1980, An empirical correlation of bedload transport rates in flumes and natural rivers: Proceedings of the Royal Society of London. Series A, Mathematical and Physical Sciences, v. 372, p. 453-473.

Baldwin, J. A., Whipple, K. X., and Tucker, G. E., 2003, Implications of the shear stress river incision model for the timescale of postorogenic decay of topography: Journal of Geophysical Research, v. 108, 2158, doi: 10.1029/2001JB000550.

Ballantyne, C. K., 1998, Age and Significance of Mountain-Top Detritus: Permafrost and Periglacial Processes, v. 9, p. 327-345.

-, 2002a, A general model of paraglacial landscape response: The Holocene, v. 12, no. 3, p. 371-376, doi: 10.1191/0959683602hl553fa.

-, 2002b, Paraglacial geomorphology: Quaternary Science Reviews, v. 21, p. 1935-2017.

Ballantyne, C. K., and Benn, D. I., 1994, Paraglacial slope adjustment and resedimentation following glacier retreat, Fåbergstølsdalen, Norway: Arctic and Alpine Research, v. 26, p. 255-269.

Barry, J. J., Buffington, J. M., and King, J. G., 2004, A general power equation for predicting bed load transport rates in gravel bed rivers: Water Resources Research, v. 40, W10401, doi: 10.1029/2004WR003190.

Bartmus, A., 1994, Die Spăteiszeitliche und Nacheiszeitliche Waldgeschichte Siebenbürgisches, *in* Heltmann, H., and Wendelberger, G., eds., Naturwissenschaftliche Forschungen über Siebenbürgen. V. Beiträge zur Flora, Vegetation und Fauna von Siebenbürgen: Siebenbürgisches ArchivKöln-Weimar-Wien, Böhlau Verlag, p. 1-10.

Beaumont, C., Fullsack, P., and Hamilton, J., 1992, Erosional control of active compressional orogens, *in* McClay, K. R., ed., Thrust TectonicsLondon, Chapman and Hall, p. 1-18.

Bennett, M. R., and Glasser, N. F., 1996, Glacial Geology: Ice Sheets and Landforms: Chichester, John Wiley & Sons Ltd., 364 p.

Berg, B. A., 2004, Markov Chain Monte Carlo Simulations and Their Statistical Analysis: Singapore, World Scientific.

Berger, A. L., Gulick, S. P. S., Spotila, J., Upton, P., Jaeger, J., Chapman, J. B., Worthington, L. A., Pavlis, T., Ridgway, K. D., Willems, B. A., and McAleer, R., 2008, Quaternary tectonic response to intensified glacial erosion

in an orogenic wedge: Nature Geoscience, v. 1, no. 11, p. 793-799, doi: 10.1038/ngeo334.

Bishop, P., Hoey, T. B., Jansen, J. D., and Lexartza Artza, I., 2005, Knickpoint recession rate and catchment area: the case of uplifted rivers in Eastern Scotland: Earth Surface Processes and Landforms, v. 30, no. 6, p. 767-778, doi: 10.1002/(ISSN)1096-9837.

Bookhagen, B., and Burbank, D. W., 2006, Topography, relief and TRMM-derived rainfall variations along the Himalaya: Geophysical Research Letters, v. 33, L08405, doi: 10.1029/2006GL026037.

Boulton, G. S., and Eyles, N., 1979, Sedimentation by valley glaciers; a model and genetic classification, *in* Schlüchter, C., ed., Moraines and VarvesRotterdam, Balkema, p. 11-23.

Boulton, S. J., and Whittaker, A. C., 2009, Quantifying the slip rates, spatial distribution and evolution of active normal faults from geomorphic analysis: Field examples from an oblique-extensional graben, southern Turkey: Geomorphology, v. 104, p. 299-316, doi: 10.1016/j.geomorph.2008.09.007.

Brardinoni, F., and Hassan, M. A., 2006, Glacial erosion, evolution of river long profiles, and the organization of process domains in mountain drainage basins of coastal British Columbia: Journal of Geophysical Research, v. 111, F01013, doi: 10.1029/2005JF000358.

-, 2007, Glacially induced organization of channel-reach morphology in mountain streams: Journal of Geophysical Research, v. 112, F03013, doi: 10.1029/2006JF000741.

Braun, J., and Sambridge, M., 1997, Modelling landscape evolution on geological time scales: a new method based on irregular spatial discretization: Basin Research, v. 9, p. 27-52.

Braun, J., Zwartz, D., and Tomkin, J. H., 1999, A new surface-processes model combining glacial and fluvial erosion: Annals of Glaciology, v. 28, no. 1, p. 282-290.

Braun, L. N., Weber, M., and Schulz, M., 2000, Consequences of climate change for runoff from Alpine regions: Annals of Glaciology, v. 31, p. 19-25.

Brocard, G. Y., van der Beek, P. A., Bourlès, D. L., Siame, L. L., and Mugnier, J. L., 2003, Long-term fluvial incision rates and postglacial river relaxation time in the French Western Alps from 10Be dating of alluvial terraces with assessment of inheritance, soil development and wind ablation effects: Earth and Planetary Science Letters, v. 209, no. 1-2, p. 197-214, doi: 10.1016/S0012-821X(03)00031-1.

Brocklehurst, S. H., and Whipple, K. X., 2002, Glacial erosion and relief production in the Eastern Sierra Nevada, California: Geomorphology, v. 42, p. 1-24.

-, 2006, Assessing the relative efficiency of fluvial and glacial erosion through simulation of fluvial landscapes: Geomorphology, v. 75, p. 283-299.

Brook, M. S., Kirkbride, M. P., and Brock, B. W., 2008, Temporal constraints on glacial valley cross-profile evolution: Two Thumb Range, central Southern Alps, New Zealand: Geomorphology, v. 97, no. 1-2, p. 24-34, doi: 10.1016/j.geomorph.2007.02.036.

Brooks, G. R., 1994, The fluvial reworking of Late Pleistocene drift, Squamish River drainage basin, southwest British Columbia: Géographie Physique et Quaternaire, v. 48, p. 51-68.

Burbank, D. W., 2002, Rates of erosion and their implications for exhumation: Mineralogical Magazine, v. 66, no. 1, p. 25-52.

Burbank, D. W., and Anderson, R. S., 2001, Tectonic Geomorphology: London, Blackwell Science.

Burbank, D. W., Leland, J., Fielding, E., Anderson, R. S., Brozović, N., Reid, M. R., and Duncan, C. C., 1996, Bedrock incision, rock uplift and threshold hillslopes in the northwestern Himalayas: Nature, v. 379, p. 505-510.

Bürgisser, H. M., Gansser, A., and Pika, J., 1982, Late Glacial lake sediments of the Indus valley area, northwestern Himalayas: Eclogae geol. Helv., v. 75, no. 1, p. 51-63.

Caine, N., and Swanson, F. J., 1989, Geomorphic coupling of hillslope and channel systems in two small mountain basins: Zeitschrift für Geomorphologie, v. 33, no. 2, p. 189-203.

Carretier, S., and Lucazeau, F., 2005, How does alluvial sedimentation at range fronts modify the erosional dynamics of mountain catchments?: Basin Research, v. 17, no. 3, p. 361-381, doi: 10.1111/bre.2005.17.issue-3.

Chatanantavet, P., and Parker, G., 2009, Physically based modeling of bedrock incision by abrasion, plucking and macroabrasion, Journal of Geophysical Research, v. 114, F04018, doi: 10.1029/2008JF001044.

Church, M., and Ryder, J. M., 1972, Paraglacial Sedimentation: A Consideration of Fluvial Processes Conditioned by Glaciation: Geological Society of America Bulletin, v. 83, no. 10, p. 3059-3072, doi: 10.1130/0016-7606(1972)83[3059:psacof]2.0.co;2.

Church, M., and Slaymaker, O., 1989, Disequilibrium of Holocene sediment yield in glaciated British Columbia: Nature, v. 337, p. 452-454.

Clayton, L., Attig, J. W., Ham, N. R., Johnson, M. D., Jennings, C. E., and Syverson, K. M., 2008, Ice-walled-lake plains: Implications for the origin of hummocky glacial topography in middle North America: Geomorphology, v. 97, no. 1-2, p. 237-248, doi: 10.1016/j.geomorph.2007.02.045.

Cowie, P. A., Attal, M., Tucker, G. E., Whittaker, A. C., Naylor, M., Ganas, A., and Roberts, G. P., 2006, Investigating the surface process response to fault interaction and linkage using a numerical modelling approach: Basin Research, v. 18, p. 231-266, doi: 10.1111/j.1365-2117.2006.00298.x.

Cowie, P. A., Whittaker, A. C., Attal, M., Roberts, G. P., Tucker, G. E., and Ganas, A., 2008, New constraints on sediment-flux dependent river incision: Implications for extracting tectonic signals from river profiles: Geology, v. 36, p. 535-538, doi: 10.1130/G24681A.1.

Craddock, W. A., Burbank, D. W., Bookhagen, B., and Gabet, E. J., 2007, Bedrock channel geometry along an orographic rainfall gradient in the upper Marsyandi River valley in central Nepal, Journal of Geophysical Research, v. 112, F03007, doi: 10.1029/2006JF000589.

Crave, A., and Davy, P., 2001, A stochastic "precipiton" model for simulating erosion/sedimentation dynamics: Computers and Geosciences, v. 27, p. 815-827.

Cruden, D. M., and Hu, X. Q., 1993, Exhaustion and steady-state models for predicting landslide hazards in the Canadian Rocky Mountains: Geomorphology, v. 8, p. 279-285.

Cunningham, A., 1853, Ladak: Physical, Statistical and Historical: New Delhi, Pilgrims Publishing, 483 p.

Cyr, A. J., Granger, D. E., Olivetti, V., and Molin, P., 2009, Distinguishing between tectonic and lithologic controls on bedrock channel longitudinal profiles using cosmogenic 10Be erosion rates and channel steepness index: Eos Trans. AGU, v. 90, no. 52, Fall Meet. Suppl., Abstract EP41B-0606.

Dadson, S. J., and Church, M., 2005, Postglacial topographic evolution of glaciated valleys: a stochastic landscape evolution model: Earth Surface Processes and Landforms, v. 30, no. 11, p. 1387-1403, doi: 10.1002/(ISSN)1096-9837.

Dahlen, F. A., and Suppe, J., 1988, Mechanics, growth and erosion of mountain belts, *in* Clark Jr., S. P., Burchfiel, B. C., and Suppe, J., eds., Processes in Continental Lithospheric Deformation: Geological Society of America Special Paper, v. 218, p. 161-178.

Dancey, C. L., Panayiotis, D., Papanicolaou, A., and Bala, M., 2002, Probability of Individual Grain Movement and Threshold Condition: Journal of Hydraulic Engineering, v. 128, no. 12, p. 1069-1075.

Davy, P., and Lague, D., 2009, Fluvial erosion/transport equation of landscape evolution models revisited: Journal of Geophysical Research, v. 114, F03007, doi: 10.1029/2008JF001146.

Densmore, A. L., Allen, P. A., and Simpson, G., 2007, Development and response of a coupled catchment fan system under changing tectonic and climatic forcing: Journal of Geophysical Research, v. 112, F01002, doi: 10.1029/2006JF000474.

Ehlers, T. A., Farley, K. A., Rusmore, M. E., and Woodsworth, G. J., 2006, Apatite (U-Th)/He signal of large-magnitude accelerated glacial erosion, southwest British Columbia: Geology, v. 34, p. 765-768, doi: 10.1130/G22507.1.

Einstein, H. A., 1950, The bed-load function for sediment transportation in open channel flows: Technical Bulletin, v. 1026, U.S. Department of Agriculture, Washinton, D.C., 73 p.

Ferguson, R. I., 1984, Sediment load of the Hunza River, *in* Miller, K. J., ed., The International Karakoram Project, v. 2: Cambridge, Cambridge University Press, p. 581-598.

Fernandez Luque, R., and van Beek, R., 1976, Erosion and transport of bed-load sediment: Journal of hydraulic Research, v. 14, p. 127-144.

Fielitz, W., and Seghedi, I., 2005, Late Miocene–Quaternary volcanism, tectonics and drainage system evolution in the East Carpathians, Romania: Tectonophysics, v. 410, p. 111-136.

Finnegan, N. J., Roe, G. H., Montgomery, D. R., and Hallet, B., 2005, Controls on the channel width of rivers: Implications for modeling fluvial incision of bedrock: Geology, v. 33, no. 3, p. 229-232, doi: 10.1130/G21171.1.

Flint, J. J., 1974, Stream Gradient as a Function of Order, Magnitude, and Discharge: Water Resources Research, v. 10, no. 5, p. 969-973.

Fort, M., 1983, Geomorphological Observations in the Ladakh Area (Himalayas): Quaternary Evolution and Present Dynamics, *in* Gupta, V. J., ed., Stratigraphy and structure of Kashmir and Ladakh, Himalaya, Hindustan Publishing, New Delhi, p. 39-58.

Fountain, A. G., and Tangborn, W. V., 1985, The Effect of Glaciers on Streamflow Variations: Water Resources Research, v. 21, no. 4, p. 579-586.

Friele, P. A., Ekes, C., and Hicken, E. J., 1999, Evolution of Cheekye fan, Squamish, British Columbia: Holocene sedimentation and implications for hazard assessment: Canadian Journal of Earth Sciences, v. 36, p. 2023-2031.

Gasparini, N. M., Bras, R. L., and Whipple, K. X., 2006, Numerical modeling of non-steady-state river profile evolution using a sediment-flux-dependent incision model, *in* Willett, S. D., Hovius, N., Brandon, M. T., and Fisher, D., eds., Tectonics, Climate, and Landscape Evolution: Geological Society of America Special Paper, v. 398, p. 127-141.

Gasparini, N. M., Whipple, K. X., and Bras, R. L., 2007, Predictions of steady state and transient landscape morphology using sediment-flux-dependent river incision models, Journal of Geophysical Research, v. 112, F03S09, doi: 10.1029/2006JF000567.

Gilbert, G. K., 1877, Report on the Geology of the Henry Mountains, U.S. Government Printing Office, Washington, D. C.

Hack, J. T., 1957, Studies of longitudinal stream profiles in Virginia and Maryland: U.S. Geological Survey Professional Paper, v. 294-B, United States Government Printing Office, Washington, 97 p.

Hallet, B., 1990, Spatial self-organization in geomorphology: from periodic bedforms and patterned ground to scale-invariant topography: Earth-Science Reviews, v. 29, no. 1-4, p. 57-75, doi: 10.1016/0012-8252(0)90028-T.

Hallet, B., Hunter, L., and Bogen, J., 1996, Rates of erosion and sediment evacuation by glaciers: A review of field data and their implications: Global and Planetary Change, v. 12, p. 213-235.

Hancock, G. S., Anderson, R. S., and Whipple, K. X., 1998, Beyond power: bedrock river incision process and form, *in* Tinkler, K. J., and Wohl, E. E., eds., Rivers Over Rock: Fluvial Processes in Bedrock Channels, Geophys. Monogr. Ser, vol. 107, v. Geophysical Monograph 107: Washington DC, AGU, p. 35-60.

Harbor, J. M., and Warburton, J., 1993, Relative rates of glacial and nonglacial erosion in alpine environments: Arctic and Alpine Research, v. 25, p. 1-7.

Harkins, N., Kirby, E., Heimsath, A., Robinson, R., and Reiser, U., 2007, Transient fluvial incision in the headwaters of the Yellow River, northeastern Tibet, China: Journal of Geophysical Research, v. 112, F03S04, doi: 10.1029/2006JF000570.

Hastings, W. K., 1970, Monte Carlo Sampling Methods Using Markov Chains and Their Applications: Biometrika, v. 57, no. 1, p. 97-109.

Herman, F., and Braun, J., 2006, Fluvial response to horizontal shortening and glaciations: A study in the Southern Alps of New Zealand: Journal of Geophysical Research, v. 111, F01008, doi: 10.1029/2004JF000248.

Hey, R. D., Bathurst, C. R., and Thorne, J. C., 1982, Gravel bed rivers: Fluvial processes, engineering and management: Chichester, J. Wiley, 995 p.

Hinchliffe, S., and Ballantyne, C. K., 1999, Talus accumulation and rockwall retreat, Trotternish, Isle of Skye, Scotland: Scottish Geographical Journal, v. 115, p. 53-70.

Hobley, D. E. J., Sinclair, H. D., and Cowie, P. A., 2010, Processes, rates and time scales of fluvial response in an ancient post-glacial landscape of the northwest Indian Himalaya: Geological Society of America Bulletin, v. 122, no. 9/10, p. 1569-1584, doi: 10.1130/B30048.1.

-, in review, River scaling in transient landscapes: Geology.

Holmes, J. A., 1993, Present and past patterns of glaciation in the northwest Himalaya: climatic, tectonic and topographic controls, *in* Shroder Jr., J. F., ed., Himalaya to the Sea: Geology, Geomorphology and the QuaternaryLondon, Routledge, p. 72-90.

Howard, A. D., 1980, Thresholds in river regimes, *in* Coates, D. R., and Vitek, J. D., eds., Thresholds in GeomorphologyLondon, Allen and Unwin, p. 227-258.

-, 1988, Equilibrium models in geomorphology, *in* Anderson, M. G., ed., Modelling geomorphological systemsNew York, John Wiley, p. 49-72.

-, 1994, A detachment-limited model of drainage basin evolution: Water Resources Research, v. 30, no. 7, p. 2261-2285.

Howard, A. D., and Kerby, G., 1983, Channel changes in badlands: Geological Society of America Bulletin, v. 94, p. 739-752.

Jamieson, S. S. R., and Hulton, N. R. J., 2007, Ice sheets: victims of their own success?: Geophysical Research Abstracts, v. 9, EGU2009-00336.

Jamieson, S. S. R., Sinclair, H. D., Kirstein, L. A., and Purves, R. S., 2004, Tectonic forcing of longitudinal valleys in the Himalaya: morphological analysis of the Ladakh Batholith, North India: Geomorphology, v. 58, no. 1-4, p. 49-65, doi: 10.1016/S0169-555X(03)00185-5.

Jansson, P., Hock, R., and Schneider, T., 2003, The concept of glacier storage: a review: Journal of Hydrology, v. 282, no. 1-4, p. 116-129, doi: 10.1016/S0022-1694(03)00258-0.

Johnson, J. P. L., and Whipple, K. X., in press, Evaluating the controls of shear stress, sediment supply, alluvial cover and channel morphology on experimental bedrock incision rate: Journal of Geophysical Research, doi: 10.1029/2009JF001335.

Johnson, J. P. L., Whipple, K. X., Sklar, L. S., and Hanks, T. C., 2009, Transport slopes, sediment cover, and bedrock channel incision in the Henry Mountains, Utah: Journal of Geophysical Research, v. 114, F02014, doi: 10.1029/2007JF000862.

Kaplan, M. R., Hein, A. S., Hubbard, A., and Lax, S. M., 2009, Can glacial erosion limit the extent of glaciation?: Geomorphology, v. 103, p. 172-179, doi: 10.1016/j.geomorph.2008.04.020.

Kirby, E., Johnson, J., Furlong, K., and Heimsath, A., 2007, Transient channel incision along Bolinas Ridge, California: Evidence for differential rock uplift adjacent to the San Andreas fault: Journal of Geophysical Research, v. 112, F03S07, doi: 10.1029/2006JF000559.

Kirby, E., and Whipple, K. X., 2001, Quantifying differential rock-uplift rates via stream profile analysis: Geology, v. 29, no. 5, p. 415-418.

Kirby, E., Whipple, K. X., Tang, W., and Chen, Z., 2003, Distribution of active rock uplift along the eastern margin of the Tibetan Plateau: Inferences from bedrock channel longitudinal profiles: Journal of Geophysical Research, v. 108, 2217, doi: 10.1029/2001JB000861.

Knighton, D., 1998, Fluvial Forms & Processes: A New Perspective: London, Hodder Arnold, 383 p.

Kobor, J. S., and Roering, J. J., 2004, Systematic variation of bedrock channel gradients in the central Oregon Coast Range: implications for rock uplift and shallow landsliding: Geomorphology, v. 62, p. 239-256, doi: doi:10.1016/j.geomorph.2004.02.013.

Kooi, H., and Beaumont, C., 1994, Escarpment evolution on high-elevation rifted margins: Insights derived from a surface processes model that combines diffusion, advection and reaction: Journal of Geophysical Research, v. 99, no. B6, p. 12191-12209.

Lamb, M. P., Dietrich, W. E., and Venditti, J. G., 2008, Is the critical Shields stress for incipient sediment motion dependent on channel-bed slope?, Journal of Geophysical Research, v. 113, F02008, doi: 10.1029/2007JF000831.

Lamoureux, S. F., 1999, Catchment and lake controls over the formation of varves in monomictic Nicolay Lake, Cornwall Island, Nunavat: Canadian Journal of Earth Sciences, v. 36, p. 1533-1546.

Lavé, J., and Avouac, J. P., 2001, Fluvial incision and tectonic uplift across the Himalayas of central Nepal: Journal of Geophysical Research, v. 106, no. B11, p. 26561-26591.

Lisiecki, L. E., and Raymo, M. E., 2005, A Pliocene-Pleistocene stack of 57 globally distributed benthic D18O records: Paleoceanography, v. 20, PA1003, doi: 10.1029/2004PA001071.

MacGregor, K. R., Anderson, R. S., Anderson, S. P., and Waddington, E. D., 2000, Numerical simulations of glacial-valley longitudinal profile evolution: Geology, v. 28, no. 11, p. 1031-1034.

Meigs, A. J., Krugh, W. C., Davis, K., and Bank, G., 2006, Ultra-rapid landscape response and sediment yield following glacier retreat, Icy Bay, southern Alaska: Geomorphology, v. 78, p. 207-221.

Meyer-Peter, E., and Muller, R., 1948, Formulas for bedload transport, *in* Research, I. A. f. H. S., ed., Proceedings of the 2nd Meeting of the International Association for Hydraulic Structures ResearchStockholm, Int. Assoc. for Hydr. Struct. Res., p. 39-64.

Milliman, J. D., and Meade, R. H., 1983, World-wide delivery of river sediment to the oceans: The Journal of Geology, v. 91, no. 1, p. 1-21.

Milliman, J. D., and Syvitski, J. P. M., 1992, Geomorphic/tectonic control of sediment transport to the ocean: the importance of small mountainous rivers: Journal of Geology, v. 100, p. 525-544.

Molnar, P., 2004, Late Cenozoic Increase in Accumulation Rates of Terrestrial Sediment: How Might Climate Change Have Affected Erosion Rates?: Annual Review of Earth and Planetary Sciences, v. 32, no. 1, p. 67-89, doi: 10.1146/earth.2004.32.issue-1.

Molnar, P., Anderson, R. S., Kier, G., and Rose, J., 2006, Relationships among probability distributions of stream discharges in floods, climate, bed load transport, and river incision: Journal of Geophysical Research, v. 111, F02001, doi: 10.1029/2005JF000310.

Molnar, P., and England, P., 1990, Late Cenozoic uplift of mountain ranges and global climate change: chicken or egg?: Nature, v. 346, p. 29-34.

Montgomery, D. R., 2002, Valley formation by fluvial and glacial erosion: Geology, v. 30, no. 11, p. 1047-1050.

Montgomery, D. R., and Foufoula-Georgiou, E., 1993, Channel network source representation using digital elevation models: Water Resources Research, v. 29, no. 12, p. 3925-3934.

Montgomery, D. R., and Stolar, D. B., 2006, Reconsidering Himalayan river anticlines: Geomorphology, v. 82, no. 1-2, p. 4-15, doi: 10.1016/j.geomorph.2005.08.021.

Mueller, E. R., and Pitlick, J., 2005, Morphologically based model of bed load transport capacity in a headwater stream: Journal of Geophysical Research, v. 110, F02016, doi: 10.1029/2003JF000117.

Owen, L. A., 1991, Mass movement deposits in the Karakoram Mountain: their sedimentary characteristics, recognition and role in Karakoram landform evolution: Zeitschrift für Geomorphologie, v. 35, no. 4, p. 401-424.

Owen, L. A., Caffee, M. W., Bovard, K. R., Finkel, R. C., and Sharma, M. C., 2006, Terrestrial cosmogenic nuclide surface exposure dating of the oldest glacial successions in the Himalayan orogen: Ladakh Range, northern India: Geological Society of America Bulletin, v. 118, no. 3, p. 383-392, doi: 10.1130/B25750.1.

Paola, C., Wolinsky, M., Voller, V. R., and Swenson, J. B., 2009, Moving-boundary methods as a unifying approach to linked erosional-depositional systems: Geophysical Research Abstracts, v. 11, EGU2009-6486.

Parker, G., and Izumi, N., 2000, Purely erosional cyclic and solitary steps created by flow over a cohesive bed: Journal of Fluid Mechanics, v. 419, p. 203-238.

Parker, G., and Klingeman, P. C., 1982, On why gravel bed streams are paved: Water Resources Research, v. 18, no. 5, p. 1409-1423.

Parker, G., Klingeman, P. C., and McLean, D. G., 1982, Bedload and size distribution in paved gravel-bed streams: Journal of the Hydraulic Division of the American Society of Civil Engineers, v. 108, p. 544-571.

Phartiyal, B., Sharma, A., Upadhyay, R., and Sinha, A. K., 2005, Quaternary geology, tectonics and distribution of palaeo- and present fluvio/glacio lacustrine deposits in Ladakh, NW Indian Himalaya - a study based on field observations: Geomorphology, v. 65, no. 3-4, p. 241-256, doi: 10.1016/j.geomorph.2004.09.004.

Rodriguez-Iturbe, I., Rinaldo, A., Rigon, R., Bras, R. L., Marani, A., and Ijjász-Vásquez, E., 1992, Energy dissipation, runoff production, and the three-dimensional structure of river basins: Water Resources Research, v. 28, no. 4, p. 1095-1103.

Roe, G. H., Whipple, K. X., and Fletcher, J. K., 2008, Feedbacks among climate, erosion, and tectonics in a critical wedge orogen: American Journal of Science, v. 308, p. 815-842, doi: 10.2475/07.2008.01J.

Roering, J. J., Kirchner, J. W., and Dietrich, W. E., 1999, Evidence for nonlinear, diffusive sediment transport on hillslopes and implications for landscape morphology: Water Resources Research, v. 35, no. 3, p. 853-870.

Ryder, J. M., 1971, The stratigraphy and morphology of paraglacial alluvial fans in south-central British Columbia: Canadian Journal of Earth Sciences, v. 8, p. 279-298.

Schmeeckle, M. W., Nelson, J. M., Pitlick, J., and Bennett, J. P., 2001, Interparticle collision of natural sediment grains in water: Water Resources Research, v. 37, no. 9, p. 2377-2391.

Schoenbohm, L. M., Whipple, K. X., Burchfiel, B. C., and Chen, L., 2004, Geomorphic constraints on surface uplift, exhumation, and plateau growth in the Red River region, Yunnan Province, China: Geological Society of America Bulletin, v. 116, no. 7, p. 895-909, doi: 10.1130/B25364.1.

Schoklitsch, A., 1962, Handbuch des wasserbaues, v. 1: Vienna, Springer-Verlag, p. 173-177.

Searle, M. P., Pickering, K. T., and Cooper, D. J. W., 1990, Restoration and evolution of the intermontane Indus molasse basin, Ladakh Himalaya, India: Tectonophysics, v. 174, no. 3-4, p. 301-314.

Sinha, S. K., and Parker, G., 1996, Causes of concavity in longitudinal profiles of rivers: Water Resources Research, v. 32, no. 5, p. 1417-1428.

Sklar, L. S., and Dietrich, W. E., 1998, River Longitudinal Profiles and Bedrock Incision Models: Strem Power and the Influence of Sediment Supply, *in* Tinkler, K. J., and Wohl, E. E., eds., Rivers Over Rock: Fluvial Processes in Bedrock Channels, Geophys. Monogr. Ser, vol. 107, Washington DC, AGU, p. 237-260.

-, 2001, Sediment and rock strength controls on river incision into bedrock: Geology, v. 29, no. 12, p. 1087-1090.

-, 2004, A mechanistic model for river incision into bedrock by saltating bed load: Water Resources Research, v. 40, W06301, doi: 10.1029/2003WR002496.

Slaymaker, O., and McPherson, H. J., 1977, An overview of geomorphic processes in the Canadian Cordillera: Zeitschrift für Geomorphologie, v. 21, p. 169-186.

Snyder, N. P., Whipple, K. X., Tucker, G. E., and Merritts, D. J., 2000, Landscape response to tectonic forcing: Digital elevation model analysis of stream profiles in the Mendocino triple junction region, northern California: Geological Society of America Bulletin, v. 112, no. 8, p. 1250-1263.

-, 2003a, Channel response to tectonic forcing: field analysis of stream morphology and hydrology in the Mendocino triple junction region, northern California: Geomorphology, v. 53, no. 1-2, p. 97-127, doi: 10.1016/S0169-555X(02)00349-5.

-, 2003b, Importance of a stochastic distribution of floods and erosion thresholds in the bedrock river incision problem: Journal of Geophysical Research, v. 108, 2117, doi: 10.1029/2001JB001655.{Whipple, 2000 #686}

Sólyom, P. B., and Tucker, G. E., 2004, Effect of limited storm duration on landscape evolution, drainage basin geometry, and hydrograph shapes: Journal of Geophysical Research, v. 109, F03012, doi: 10.1029/2003JF000032.

Spate, O. H. K., Learmonth, A. T. A., and Farmer, B. H., 1976, India, Pakistan and Ceylon (2nd revised edition): London, Methuen and Co., Ltd., p. 424-450.

Stock, J. D., and Dietrich, W. E., 2003, Valley incision by debris flows: Evidence of a topographic signature: Water Resources Research, v. 39, 1089, doi: 10.1029/2001WR001057.

Stock, J. D., and Montgomery, D. R., 1999, Geologic constraints on bedrock river incision using the stream power law: Journal of Geophysical Research, v. 104, no. B3, p. 4983-4993.

Strahler, A. N., 1950, Equilibrium theory of erosional slopes approached by frequency distribution analysis: American Journal of Science, v. 248, p. 673-696.

Tantau, I., Reille, M., De Beaulieu, J. L., and Farcas, S., 2006, Late Glacial and Holocene vegetation history in the southern part of Transylvania (Romania): pollen analysis of two sequences from Avrig: Journal of Quaternary Science, v. 21, no. 1, p. 49-61, doi: 10.1002/(ISSN)1099-1417.

Tomkin, J. H., Brandon, M. T., Pazzaglia, F. J., Barbour, J. R., and Willett, S. D., 2003, Quantitative testing of bedrock incision models for the Clearwater River, NW Washington State, Journal of Geophysical Research, v. 108, no. B6, 2308, doi: 10.1029/2001JB000862.

Tucker, G. E., and Bras, R. L., 1998, Hillslope processes, drainage density, and landscape morphology: Water Resources Research, v. 34, no. 10, p. 2751-2764.

-, 2000, A stochastic approach to modeling the role of rainfall variability in drainage basin evolution: Water Resources Research, v. 36, no. 7, p. 1953-1964.

Tucker, G. E., and Hancock, G. S., 2010, Modelling landscape evolution: Earth Surface Processes and Landforms, v. 35, p. 28-50, doi: 10.1002/esp.1952.

Tucker, G. E., and Whipple, K. X., 2002, Topographic outcomes predicted by stream erosion models: Sensitivity analysis and intermodel comparison: Journal of Geophysical Research, v. 107, 2179, doi: 10.1029/2001JB000162.

Turowski, J. M., Lague, D., and Hovius, N., 2007, Cover effect in bedrock abrasion: A new derivation and its implications for the modeling of bedrock channel morphology: Journal of Geophysical Research, v. 112, F04006, doi: 10.1029/2006JF000697.

Turowski, J. M., and Rickenmann, D., 2009, Tools and cover effects in bedload transport observations in the Pitzbach, Austria: Earth Surface Processes and Landforms, v. 34, p. 26-37, doi: 10.1002/esp.1686.

Valla, P. G., van der Beek, P. A., and Lague, D., 2010, Fluvial incision into bedrock: insights from morphometric analysis and numerical modeling of gorges incising glacial hanging valleys (western Alps, France): Journal of Geophysical Research, v. 115, F02010, doi: 10.1029/2008JF001079.

van der Beek, P. A., and Bishop, P., 2003, Cenozoic river profile development in the Upper Lachlan catchment (SE Australia) as a test of quantitative fluvial incision models: Journal of Geophysical Research, v. 108, 2309, doi: 10.1029/2002JB002125.

VanLaningham, S., Meigs, A. J., and Goldfinger, C., 2006, The effects of rock uplift and rock resistance on river morphology in a subduction zone forearc, Oregon, USA: Earth Surface Processes and Landforms, v. 31, no. 10, p. 1257-1279.

Venditti, J. G., Dietrich, W. E., Nelson, P. A., Wydzga, M. A., Fadde, J., and Sklar, L. S., 2010, Effect of sediment pulse grain size on sediment transport rates and bed mobility in gravel bed rivers, Journal of Geophysical Research, v. 115, F03039, doi: 10.1029/2009JF001418.

Weinberg, R. F., and Dunlap, W. J., 2000, Growth and Deformation of the Ladakh Batholith, Northwest Himalayas: Implications for Timing of Continental Collision and Origin of Calc-Alkaline Batholiths: The Journal of Geology, v. 108, p. 303-320.

Whipple, K. X., 2001, Fluvial landscape response time: how plausible is steady-state denudation?: American Journal of Science, v. 301, p. 313-325.

-, 2004, Bedrock Rivers and the Geomorphology of Active Orogens: Annual Review of Earth and Planetary Sciences, v. 32, no. 1, p. 151-185, doi: 10.1146/earth.2004.32.issue-1.

Whipple, K. X., Hancock, G. S., and Anderson, R. S., 2000a, River incision into bedrock: Mechanics and relative efficacy of plucking, abrasion, and cavitation: Geological Society of America Bulletin, v. 112, no. 3, p. 490-503.

Whipple, K. X., Snyder, N. P., and Dollenmayer, K., 2000b, Rates and processes of bedrock incision by the Upper Ukak River since the 1912 Novarupta ash flow in the Valley of Ten Thousand Smokes, Alaska: Geology, v. 28, p. 835-838, doi: 10.1130/0091-7613(2000)28<835:RAPOBI>2.0.CO;2.

Whipple, K. X., and Tucker, G. E., 1999, Dynamics of the stream-power river incision model: Implications for height limits of mountain ranges, landscape response timescales and research needs: Journal of Geophysical Research, v. 104, no. B8, p. 17661-17674.

-, 2002, Implications of sediment-flux-dependent river incision models for landscape evolution: Journal of Geophysical Research, v. 107, 2039, doi: 10.1029/2000JB000044.

Whittaker, A. C., 2007, Investigating Controls on Bedrock River Incision Using Natural and Laboratory Experiments [PhD thesis]: University of Edinburgh, 188 p.

Whittaker, A. C., Attal, M., and Allen, P. A., in press, Characterising the origin, nature and fate of sediment exported from catchments perturbed by active tectonics: Basin Research, doi: 10.1111/j.1365-2117.2009.00447.x.

Whittaker, A. C., Attal, M., Cowie, P. A., Tucker, G. E., and Roberts, G. P., 2008, Decoding temporal and spatial patterns of fault uplift using transient river long profiles: Geomorphology, v. 100, p. 506-526, doi: 10.1016/j.geomorph.2008.01.018.

Whittaker, A. C., Cowie, P. A., Attal, M., Tucker, G. E., and Roberts, G. P., 2007a, Bedrock channel adjustment to tectonic forcing: Implications for predicting river incision rates: Geology, v. 35, no. 2, p. 103-106, doi: 10.1130/G23106A.1.

-, 2007b, Contrasting transient and steady-state rivers crossing active normal faults: new field observations from the Central Apennines, Italy: Basin Research, v. 19, no. 4, p. 529-556, doi: 10.1111/bre.2007.19.issue-4.

Wilcock, P. R., 1993, Critical Shear Stress of Natural Sediments: Journal of Hydraulic Engineering, v. 119, no. 4, p. 491-505.

Wilcock, P. R., and McArdell, B. W., 1993, Surface-Based Fractional Transport Rates: Mobilization Thresholds and Partial Transport of a Sand-Gravel Sediment: Water Resources Research, v. 29, no. 4, p. 1297-1312.

Willett, S. D., and Brandon, M. T., 2002, On steady states in mountain belts: Geology, v. 30, no. 2, p. 175-178.

Willgoose, G., Bras, R. L., and Rodriguez-Iturbe, I., 1991, A Coupled Channel Network Growth and Hillslope Evolution Model, 1. Theory: Water Resources Research, v. 27, no. 7, p. 1671-1684.

Wobus, C. W., Crosby, B. T., and Whipple, K. X., 2006a, Hanging valleys in fluvial systems: Controls on occurrence and implications for landscape evolution: Journal of Geophysical Research, v. 111, F02017, doi: 10.1029/2005JF000406.

Wobus, C. W., Whipple, K. X., Kirby, E., Snyder, N. P., Johnson, J., Spyropolou, K., Crosby, B. T., and Sheehan, D., 2006b, Tectonics from topography: Procedures, promise, and pitfalls, *in* Willett, S. D., Hovius, N., Brandon, M. T., and Fisher, D., eds., Tectonics, Climate, and Landscape Evolution: Geological Society of America Special Paper, v. 398, p. 55-74.

Wong, M., and Parker, G., 2006, Reanalysis and Correction of Bed-Load Relation of Meyer-Peter and Müller Using Their Own Database: Journal of Hydraulic Engineering, v. 132, no. 11, p. 1159-1168.

Yalin, M. S., 1963, An expression for bed bed-load transportation: Journal of the Hydraulic Division of the American Society of Civil Engineers, v. 89, no. 3, p. 221-250.

Yunnan Province Meteorological Bureau Information Office, 1982, Meteorological Information of Land Surface for 30 years in Yunnan Province, vol. 4. Rainfall, Yunnan Province Meteorological Bureau (in Chinese).

Zaprowski, B. J., Evenson, E. B., Pazzaglia, F. J., and Epstein, J. B., 2001, Knickzone propagation in the Black Hills and northern High Plains: A different perspective on the late Cenozoic exhumation of the Laramide Rocky Mountains: Geology, v. 29, no. 6, p. 547-550.

Zeitler, P. K., Meltzer, A. S., Koons, P. O., Craw, D., Hallet, B., Chamberlain, C. P., Kidd, W. S. F., Park, S. K., Seeber, L., Bishop, M., and Shroder, J., 2001, Erosion, Himalayan Geodynamics, and the Geomorphology of Metamorphism: GSA Today, v. 11, no. 1, p. 4-9.

Zhang Peizhen, Molnar, P., and Downs, W. R., 2001, Increased sedimentation rates and grain sizes 2-4 Myr ago due to the influence of climate change on erosion rates: Nature, v. 410, p. 891-897.

APPENDIX A:

METHODOLOGY FOR ACQUISITION AND TREATMENT OF RAW DIGITAL ELEVATION MODEL DATA

A1. Ladakh

We have taken three arc-second resolution data freely available from NASA (ftp://e0srp01u.ecs.nasa.gov/srtm/version2/SRTM3/), derived from the Shuttle Radar Topography Mission (SRTM). Raw data were converted to ARCinfo GRID format for processing using IMAGEGRID.aml, developed by the United States Geological Survey (ftp://e0srp01u.ecs.nasa.gov/srtm/version2/Documentation/notes_for_ARCInfo_users.pdf). The data used here comprise one degree by one degree squares N33E077, N33E078, N34E076, N34E077 and N34E078 (see Figs. 2.1, 3.1a, 4.2). The data for this region are in fact well suited to DEM analysis, since the glaciers have widened and flattened the valley floors over much of the rivers' courses, meaning artifacts produced by the satellite's footprint catching the valley sides as well as the channel in the valley centre are much reduced. Minor holes in the data (<2 % of pixels in analyzed catchments, and rarely impinging on valley bottoms) were patched by converting the whole dataset into a point dataset then using ARCinfo to interpolate back into GRID form using a cubic spline algorithm. This process provided the base DEM on which subsequent analysis was carried out.

The base DEM was first filled to remove artificial internally draining patches – the affected area comprises <1 % of the total surface, almost entirely confined to regions of the Indus valley itself and not significantly changing the profiles of the tributaries. The drainage network was then predicted from a flow accumulation threshold of 200 pixels (a drainage area of approximately 1.4×10^6 m^2). This relatively high value was chosen to avoid the prediction of channels beneath the existing glaciers and recent moraine successions in the highest elevations of the catchments, and creates a channel network that agrees well with the known channel

forms seen in satellite imagery. The trunk streams for each of the 70 independent basins draining southwards into the Indus were then selected, taking more than one profile per valley if a major bifurcation of the trunk stream was present, and elevation, z, upstream drainage area, A, and distance downstream, x, data extracted for each pixel along the course of each trunk stream. MATLAB was then used first to smooth out high frequency noise in the elevation data with a low-pass filter on z, then to construct a value of channel slope, S, on a reach length scale of 500 m. Both these methods act to damp local (<500 m) variation in channel slope, whether an artifact of the DEM or due to fine scale river responses. This scaling is appropriate since we only sampled local slope and channel form in the field once every 300–500 m, and variability on a finer scale than this will not be revealed by the data. These methods and smoothing techniques correspond broadly to those chosen by Snyder et al. (2000) and recommended by Wobus et al. (2006), though with different absolute values chosen appropriate to the coarser resolution of our DEM data.

A2. Făgăraş

The treatment methods parallel exactly those described above for the Ladakh data to allow direct comparison between the datasets. The squares used in this case were N45E024 and N45E025 (Fig. 3.1b). A similar number of holes in the data were present as for Ladakh, and internally draining patches were even less of a problem.

A3. Red River Region

The data describing this DEM were drawn directly from material presented by Schoenbohm et al. (2004) and have not been reprocessed. However, the base DEM presented as Figure 3.1c was produced by me in order to compare directly with the earlier parts of the figure. The methods again parallel those described above for Ladakh, and the degree squares used were N22E100-N22E103, N23E100-N23E103, N24E100-N24E103 and N25E100-N25E103. Details of this processing clearly have

no impact on the quality of the associated data presented in Chapter 3, as this uses the Schoenbohm data directly.

APPENDIX B:

SUPPORTING MATERIAL FOR CHAPTER 2

B1. Long Profiles and Scaling Plots for All Analyzed Ladakh Catchments

An altered version of Figure 2.1 is presented as Figure B1 in order to illustrate which catchments provide acceptable slope-distance (curvature) and slope-area (concavity) regressions, as described in the Remotely Sensed Data section (2.5) of the main manuscript. Those which do are colored blue. Channels are numbered consecutively as they appear along the batholith going from west to east. Note that several catchments have more than one trunk stream, and these channels are each allocated their own number. The channels in question are 2/3, 7/8/9, 11/12, 17/18, 19/20/21 and 37/38, and the associated catchments are shown in a lighter blue in the Figure.

Figure B2 illustrates the long profile (z-x) and drainage structure (A-x) of each of these channels, along with associated slope plots S-x and S-A, plotted on logarithmic axes. The grayscale lines show the slope scaling relations fitted to these latter two plots by the method described in the main text, and the range of values over which the fit is made. The associated equations are also shown above these figures.

Table B1 collates all of these data, and is the source for Figures 2.7 and 2.8 in the main text.

B2. Field-DEM Slope Comparisons

Figure B3 shows plots of channel slope, S, versus distance downstream, x, for the valleys Basgo (a) and Leh (b). DEM-derived slopes (see Appendix A) are shown

as grey open circles and direct field measurements over 30 m intervals, every c. 500 m are shown as black closed squares.

Figure B4 displays these same data as a direct comparison for each catchment. Quoted errors on the lines of best fit are 95% confidence intervals, assuming direct linear correlation. Note that neither gradient is distinguishable from 1, but that there is a tendency for the DEM values to be slightly higher. This is probably an artifact of the different scales over which the gradient is averaged (500 m versus 30 m), especially in domain 1, where slope can be highly variable on a scale less than 500 m. This is particularly clear in Figure B3. For the same reason, we note that the fit for Leh is poorer, since a larger proportion of these data points come from within domain 1.

B3. Variation of Scaling Metrics between Domains

As noted in the main text, the data presented here do not extend across enough variation in drainage area to conclusively calculate the scaling metrics of concavity and curvature for the bottom of domain 2 and domain 3 separately. However, in order to investigate this issue further, we present here a semi-quantitative method examining the convergence towards the whole channel values as progressively larger proportions of the channel are included. This analysis is presented as Figure B5.

We plot calculated concavity and curvature values for each channel over the first 50, 100, 150, 200, etc. points downstream of the knickzone up to the end of the whole analyzed segment, then similarly plot the data in sections 50, 100, 150, etc. points long going from the downstream end of the channel up to the knickzone. This data is then displayed graphically on the same chart, where the fits established for the first 50 points (upper- and lower-most stream sections of the channel) are displayed to the left and the fits incorporating all of the data to the right. We then examine the manner in which the data converges to the right-hand side of the graph. The

measured values are clearly quite variable where fewer data points are used, but as more data is incorporated, the variability in the values tends to stabilize. We recognize three patterns in these tails as the final elements of data are incorporated: -

1) Magnitude of concavity (or curvature) becomes gradually greater as data is incorporated towards the downstream end of the channel (blue bars), and gradually smaller as data is incorporated towards the upstream end of the channel (red bars). This suggests that the scaling exponents are uniformly lower in the upstream reaches of the channel than in the downstream reaches.

2) Magnitude of concavity (or curvature) becomes gradually lesser as data is incorporated towards the downstream end of the channel (blue), and gradually greater as data is incorporated towards the upstream end of the channel (red). This suggests that the scaling exponents are uniformly greater in the upstream reaches of the channel than in downstream reaches.

3) Neither of the above is the case, with no trends in the scaling metrics, or with trends in the same direction incorporating data going both upstream and downstream in the catchment. This category also includes catchments with few points in total (<200). We interpret this to indicate that there is no demonstrable systematic difference in concavity (or curvature) in the upstream reaches versus the downstream reaches of the channel as a whole.

The pattern we assign for the concavity and curvature of each channel is noted above each graph as 1, 2 or 3. Note that we ignore the first three data points (50-150 data points) entirely, where random noise will certainly overwhelm any signal. This method is, at best, limited, but provides at least some indication of the variability of the scaling values quoted in the main text, and also avoids having to

pre-allocate domain boundaries for all of the catchments, which are not always easy to accurately fix from the satellite imagery.

We find that for both the concavity and curvature, very many channels (34 out of 58 for θ; 27 out of 58 for ϕ) show no uniform tendency for a changing value downstream. The remainder are split between a tendency for increase and a tendency for decrease downstream for both metrics (12 type 1, 12 type 2 for θ; 12 type 1, 19 type 2 for ϕ). We interpret this to mean that there is no tendency for upstream reaches to have uniformly higher or lower scaling exponents to downstream reaches, including across the boundary of domain 2 into domain 3, as discussed in the main text.

TABLE B1. DATA EXTRACTED FROM DEM FOR REACHES DOWNSTREAM OF KNICKZONES FOR LADAKH

Channel number	Area upstream of knickzone, A_{PC} (m^2)	Total area, A_{tot} (m^2)	Downstream distance of knickzone, x_{PC} (m)	Total channel length, x_{tot} (m)	A_{PC}/A_{tot}	x_{PC}/x_{tot}	k_θ	θ	Error on θ	k_ϕ	ϕ	Error on ϕ
1	6.60E+07	7.44E+07	15749	18633	0.887	0.845	7.04E+42	5.57	0.76	6.64E+13	3.48	0.52
2	3.26E+06	3.32E+07	779	7451	0.098	0.105	4.93E+01	0.34	0.07	4.66E+00	0.40	0.08
3	1.99E+06	3.73E+07	695	8804	0.053	0.079	4.11E+01	0.33	0.02	4.16E+00	0.38	0.03
4	7.17E+07	1.19E+08	13852	20710	0.600	0.669	2.68E+13	1.80	0.11	1.45E+09	2.40	0.17
5	2.88E+06	1.02E+07	878	3947	0.283	0.223	2.00E+02	0.44	0.07	5.46E+00	0.44	0.05
6	2.94E+06	9.07E+06	607	3036	0.325	0.200	3.98E+02	0.49	0.08	5.12E+00	0.44	0.06
7	1.41E+07	1.66E+08	4478	15142	0.085	0.296	5.76E+03	0.60	0.05	3.01E+04	1.36	0.13
8	5.33E+07	1.65E+08	10767	19692	0.322	0.547	1.44E+05	0.76	0.12	5.11E+04	1.36	0.22
9	2.05E+07	1.65E+08	5503	16546	0.124	0.333	3.32E+02	0.43	0.04	3.58E+03	1.11	0.08
10	3.06E+06	2.71E+07	1556	6024	0.113	0.258	1.37E+02	0.39	0.07	1.81E+02	0.82	0.11
11	4.63E+07	2.72E+08	11423	24730	0.170	0.462	5.09E+03	0.59	0.04	1.72E+05	1.50	0.10
12	5.01E+07	2.71E+08	13600	23642	0.185	0.575	5.13E+03	0.59	0.03	3.19E+07	2.01	0.11
13	6.51E+06	5.30E+07	2846	12300	0.123	0.231	5.26E+03	0.62	0.03	5.86E+02	0.96	0.04
14	3.20E+06	1.49E+07	683	4668	0.215	0.146	6.30E+02	0.52	0.04	6.62E+00	0.47	0.03
15	3.86E+07	1.18E+08	13411	20417	0.327	0.657	1.03E+06	0.88	0.09	6.41E+08	2.33	0.25
16	1.63E+08	1.83E+08	22297	30193	0.891	0.738	7.02E+30	3.88	0.53	2.98E+06	1.73	0.22
17	2.77E+06	2.75E+07	913	8629	0.101	0.106	9.61E+04	0.83	0.04	6.29E+01	0.74	0.05
18	4.98E+06	2.75E+07	1442	7324	0.181	0.197	3.24E+01	0.36	0.05	3.31E+00	0.44	0.07
19	4.67E+06	1.65E+08	2894	14724	0.028	0.197	5.60E+02	0.49	0.05	3.32E+02	0.88	0.10
20	1.12E+08	1.65E+08	17836	23187	0.676	0.769	3.48E+11	1.55	0.14	6.61E+12	3.22	0.17
21	5.73E+06	4.00E+07	1538	11648	0.143	0.132	3.31E+05	0.88	0.03	2.31E+02	0.87	0.03
22	2.91E+07	7.28E+07	8501	21593	0.399	0.394	1.31E+08	1.19	0.05	3.30E+04	1.33	0.05
23	3.90E+07	7.74E+07	10854	21138	0.503	0.513	1.90E+13	1.85	0.13	7.04E+06	1.89	0.13
24	3.35E+07	8.67E+07	9525	21821	0.386	0.437	1.06E+07	1.03	0.05	3.48E+04	1.32	0.04
25	1.08E+07	8.84E+07	5503	20265	0.122	0.272	2.08E+04	0.70	0.03	1.68E+03	1.05	0.03
26	2.62E+06	1.82E+07	949	11309	0.144	0.084	4.43E+02	0.53	0.04	6.12E+00	0.49	0.03
27	4.96E+06	5.13E+07	1152	13624	0.097	0.085	3.47E+02	0.48	0.02	6.98E+00	0.49	0.02
28	3.04E+06	3.40E+07	576	11451	0.089	0.050	4.04E+01	0.36	0.02	1.72E+00	0.34	0.02
29	1.25E+07	7.12E+07	5503	19999	0.176	0.275	7.10E+03	0.64	0.04	2.03E+02	0.81	0.05
30	2.00E+07	1.17E+08	6831	22921	0.171	0.298	5.87E+04	0.75	0.03	4.36E+03	1.14	0.03
31	6.73E+06	4.19E+07	3188	7780	0.161	0.410	1.83E+00	0.15	0.03	1.93E+00	0.31	0.06
32	1.78E+07	6.96E+07	4858	17457	0.255	0.278	1.92E+05	0.83	0.03	7.18E+02	0.97	0.03
33	2.40E+06	6.37E+07	646	13206	0.038	0.049	1.02E+02	0.41	0.01	4.72E+00	0.45	0.01
34	2.45E+06	2.61E+07	607	11613	0.094	0.052	1.05E+03	0.56	0.01	5.47E+00	0.46	0.01
35	4.04E+06	5.48E+07	1784	13624	0.074	0.131	2.03E+03	0.59	0.02	1.78E+02	0.86	0.03

(continued)

TABLE B1 (CONT.). DATA EXTRACTED FROM DEM FOR REACHES DOWNSTREAM OF KNICKZONES FOR LADAKH

Channel number	Area upstream of knickzone, A_{PC} (m^2)	Total area, A_{tot} (m^2)	Downstream distance of knickzone, x_{PC} (m)	Total channel length, x_{tot} (m)	A_{PC}/A_{tot}	x_{PC}/x_{tot}	k_θ	θ	Error on θ	k_ϕ	ϕ	Error on ϕ
36	2.71E+06	2.09E+07	607	6983	0.130	0.087	9.66E+04	0.90	0.06	5.24E+00	0.53	0.03
37	1.50E+07	1.92E+08	5313	23070	0.078	0.230	1.54E+04	0.69	0.02	8.14E+03	1.26	0.03
38	1.05E+07	1.91E+08	4802	23984	0.055	0.200	5.81E+04	0.76	0.02	1.06E+05	1.54	0.04
39	3.34E+07	1.19E+08	8368	22542	0.280	0.371	1.38E+05	0.80	0.05	3.36E+02	0.90	0.05
40	3.09E+06	3.91E+07	645	11385	0.079	0.057	3.14E+02	0.48	0.02	5.21E+00	0.46	0.01
41	2.38E+06	1.30E+07	607	6186	0.183	0.098	2.01E+02	0.47	0.03	2.56E+00	0.38	0.02
42	1.01E+07	8.12E+07	3545	17419	0.124	0.204	3.09E+03	0.59	0.02	1.04E+03	1.02	0.02
43	4.39E+06	2.99E+07	645	7623	0.147	0.085	1.03E+02	0.40	0.02	2.34E+00	0.33	0.02
44	1.62E+07	2.36E+08	6224	22119	0.069	0.281	9.69E+02	0.51	0.03	1.18E+04	1.25	0.08
45	3.89E+06	2.26E+07	1152	6777	0.172	0.170	1.05E+04	0.67	0.05	4.62E+01	0.68	0.05
46	8.36E+07	1.98E+08	15066	23632	0.422	0.638	1.43E+05	0.76	0.09	3.90E+04	1.32	0.12
47	3.17E+06	4.06E+07	1366	9863	0.078	0.139	6.33E+00	0.22	0.02	1.93E+00	0.30	0.03
48	6.24E+07	7.42E+07	15787	20531	0.842	0.769	4.25E+09	1.35	0.31	1.73E+03	0.98	0.23
49	4.27E+07	5.36E+07	15104	19274	0.797	0.784	1.67E+21	2.89	0.30	2.22E+10	2.68	0.25
50	1.97E+07	4.14E+07	7780	13890	0.476	0.560	7.30E+04	0.77	0.09	2.52E+04	1.32	0.13
51	1.04E+08	1.66E+08	14914	21441	0.627	0.696	2.49E+03	0.55	0.15	8.21E+03	1.18	0.24
52	4.64E+06	2.05E+07	2391	8349	0.226	0.286	2.46E+04	0.72	0.03	1.04E+03	1.02	0.04
53	3.06E+06	2.36E+07	607	8349	0.129	0.073	1.56E+02	0.46	0.03	4.61E+00	0.48	0.03
54	5.51E+06	3.18E+07	2353	8652	0.173	0.272	8.84E+03	0.68	0.03	1.50E+02	0.83	0.03
55	2.13E+06	7.70E+06	645	4744	0.276	0.136	2.18E+04	0.78	0.04	9.96E+00	0.57	0.03
56	2.12E+07	1.25E+08	6831	17571	0.170	0.389	3.98E+07	1.14	0.05	2.25E+05	1.58	0.09
57	3.27E+06	1.61E+07	1670	10552	0.203	0.158	1.54E+05	0.87	0.03	1.56E+02	0.82	0.02
58	3.80E+06	2.23E+07	576	7438	0.170	0.077	9.72E+01	0.41	0.03	1.67E+00	0.33	0.02

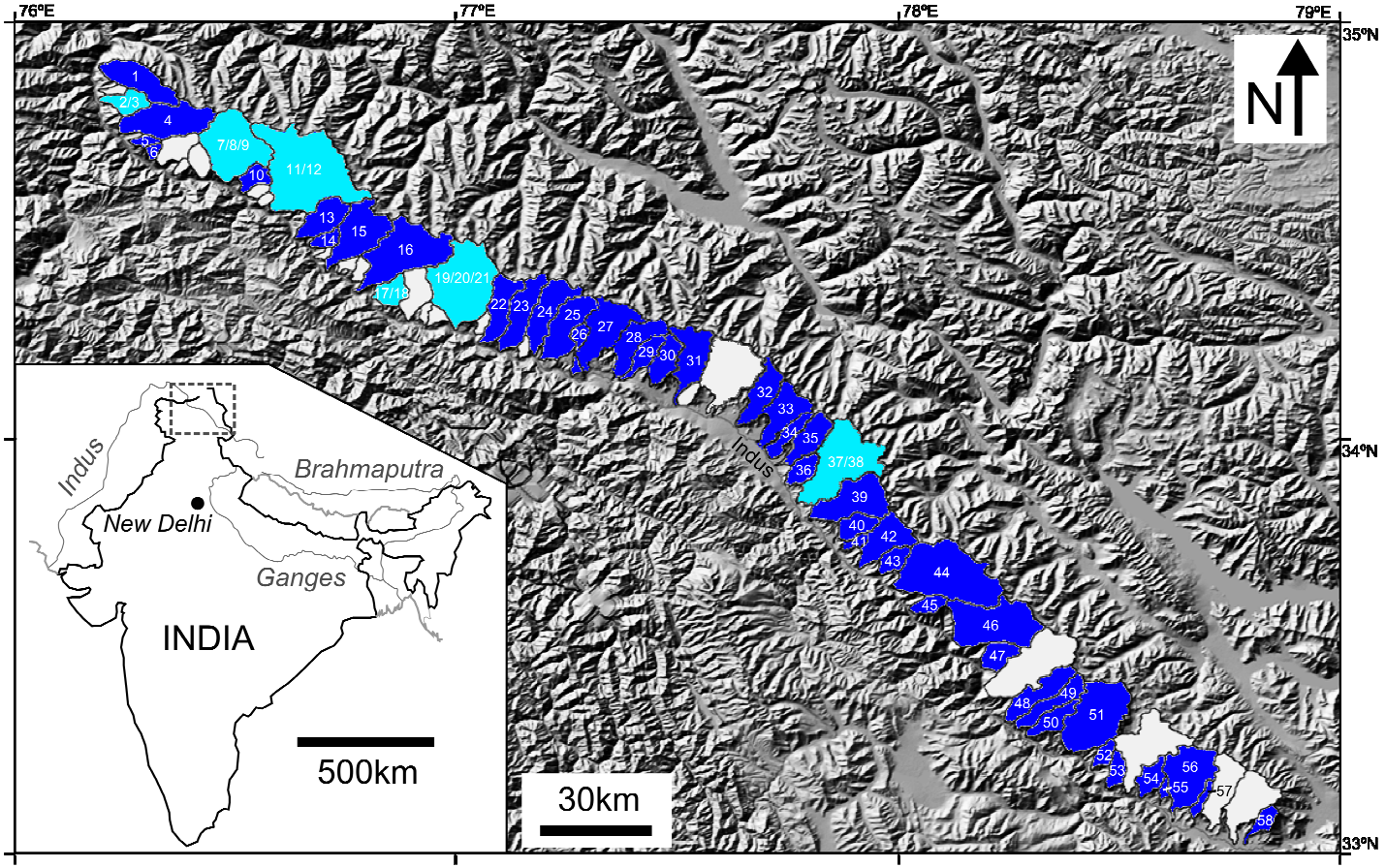

Figure B1. Summary map showing location of analyzed channels presented in Figs. B2 and B5. Deep blue catchments contain 1 trunk stream, Lighter blue catchments contain more than 1 major channel.

Figure B2 (subsequent pages). Plots of long profile (z-x) and drainage structure (A-x) of each analyzed channel, along with associated slope plots S-x and S-A, plotted on logarithmic axes. Grayscale lines show slope scaling relations fitted to these latter two plots by the method described in the main text of Chapter 2, and the range of values over which the fit is made. The associated equations are also shown above the figures.

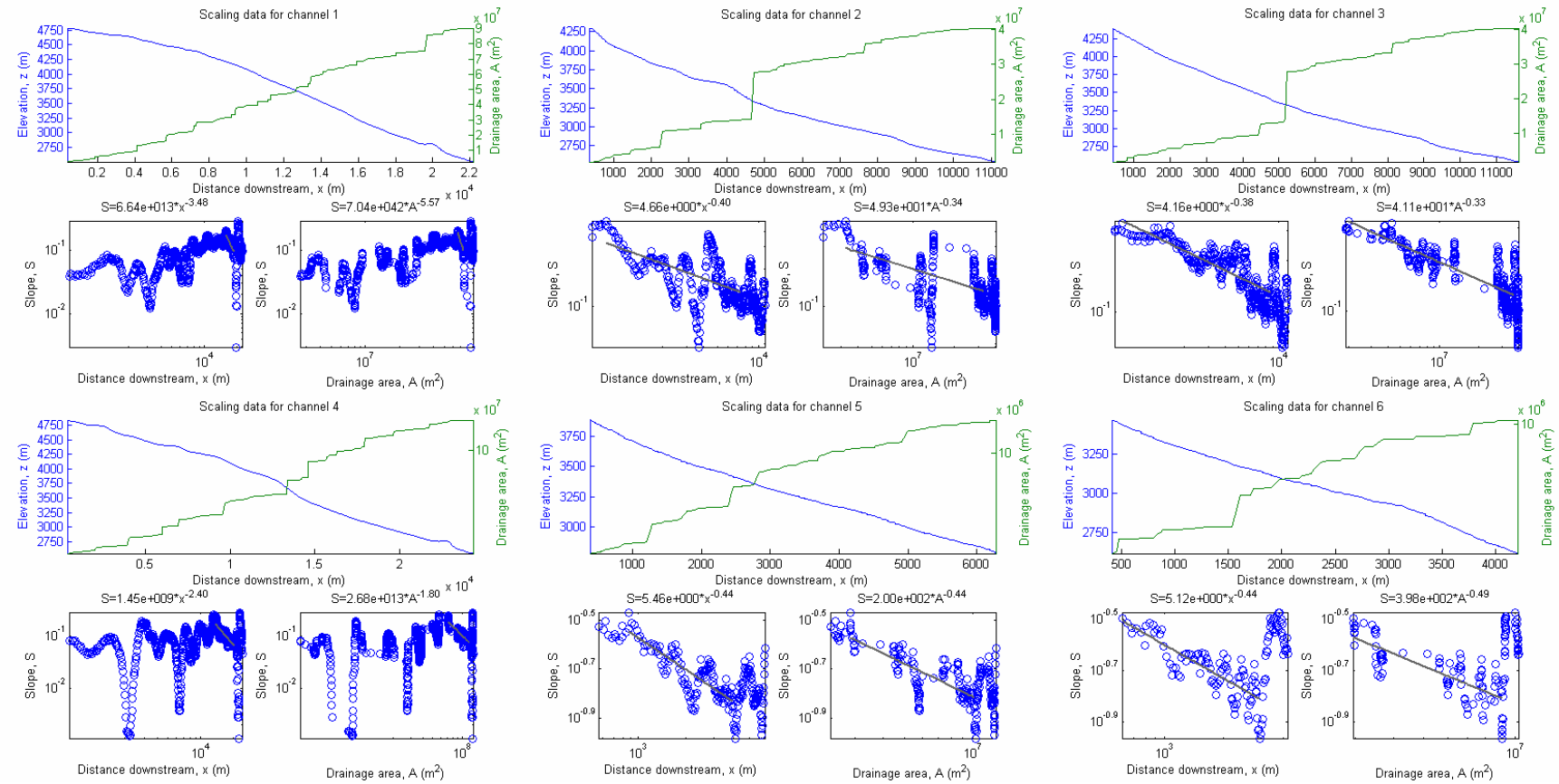
Scaling data for channel 1
Elevation, z (m)
Drainage area, A (m²)
Distance downstream, x (m)
S=6.64e+013*x^-3.48
S=7.04e+042*A^-5.57
Slope, S
Distance downstream, x (m)
Drainage area, A (m²)
Scaling data for channel 2
Elevation, z (m)
Drainage area, A (m²)
Distance downstream, x (m)
S=4.66e+000*x^-0.40
S=4.93e+001*A^-0.34
Slope, S
Distance downstream, x (m)
Drainage area, A (m²)
Scaling data for channel 3
Elevation, z (m)
Drainage area, A (m²)
Distance downstream, x (m)
S=4.16e+000*x^-0.38
S=4.11e+001*A^-0.33
Slope, S
Distance downstream, x (m)
Drainage area, A (m²)
Scaling data for channel 4
Elevation, z (m)
Drainage area, A (m²)
Distance downstream, x (m)
S=1.45e+009*x^-2.40
S=2.68e+013*A^-1.80
Slope, S
Distance downstream, x (m)
Drainage area, A (m²)
Scaling data for channel 5
Elevation, z (m)
Drainage area, A (m²)
Distance downstream, x (m)
S=5.46e+000*x^-0.44
S=2.00e+002*A^-0.44
Slope, S
Distance downstream, x (m)
Drainage area, A (m²)
Scaling data for channel 6
Elevation, z (m)
Drainage area, A (m²)
Distance downstream, x (m)
S=5.12e+000*x^-0.44
S=3.98e+002*A^-0.49
Slope, S
Distance downstream, x (m)
Drainage area, A (m²)

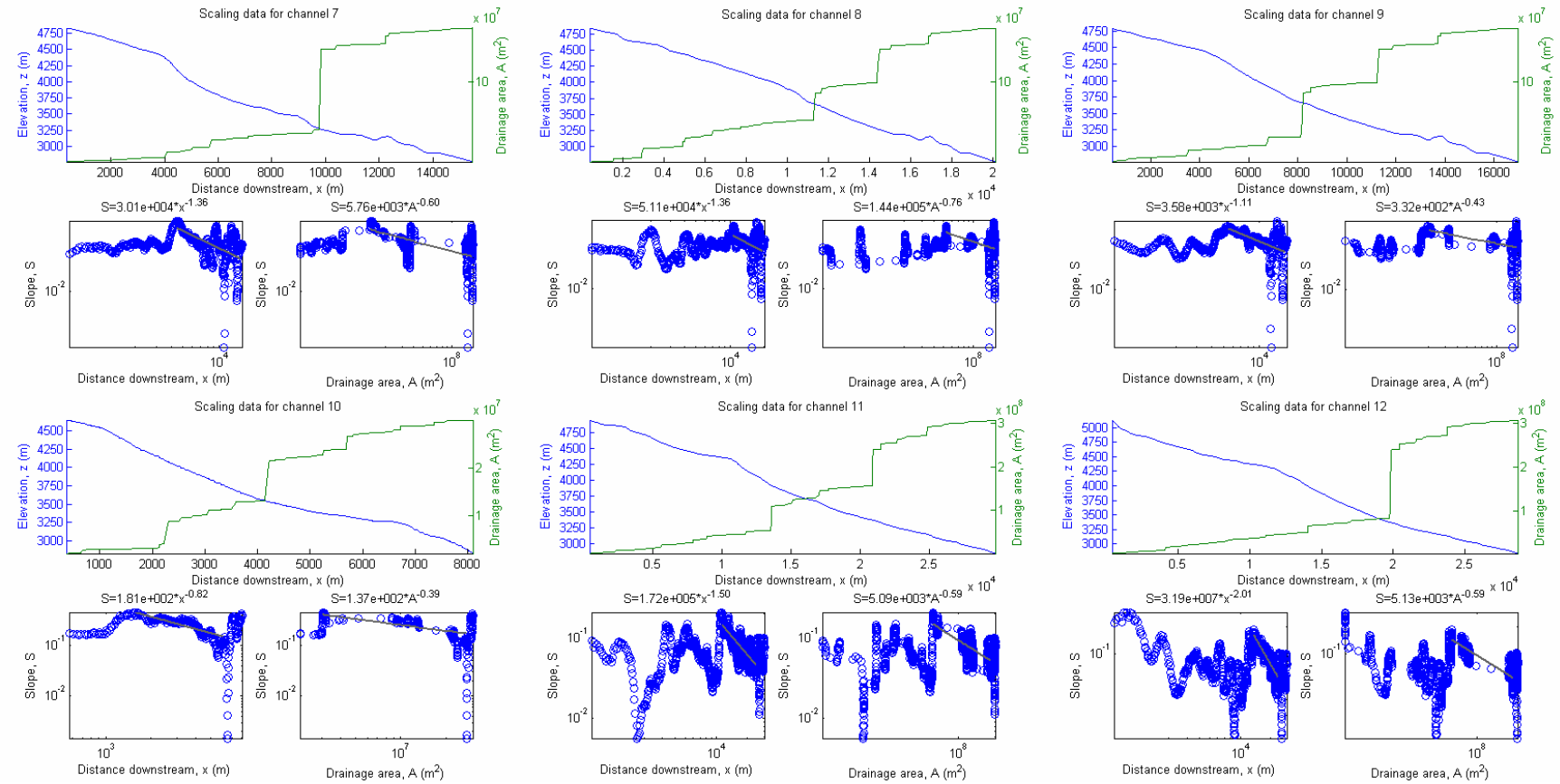
Scaling data for channel 7
Elevation, z (m)
Drainage area, A (m²)
Distance downstream, x (m)
S=3.01e+004*x^-1.36
S=5.76e+003*A^-0.60
Slope, S
Distance downstream, x (m)
Drainage area, A (m²)
Scaling data for channel 8
Elevation, z (m)
Drainage area, A (m²)
Distance downstream, x (m)
S=5.11e+004*x^-1.36
S=1.44e+005*A^-0.76
Slope, S
Distance downstream, x (m)
Drainage area, A (m²)
Scaling data for channel 9
Elevation, z (m)
Drainage area, A (m²)
Distance downstream, x (m)
S=3.58e+003*x^-1.11
S=3.32e+002*A^-0.43
Slope, S
Distance downstream, x (m)
Drainage area, A (m²)
Scaling data for channel 10
Elevation, z (m)
Drainage area, A (m²)
Distance downstream, x (m)
S=1.81e+002*x^-0.82
S=1.37e+002*A^-0.39
Slope, S
Distance downstream, x (m)
Drainage area, A (m²)
Scaling data for channel 11
Elevation, z (m)
Drainage area, A (m²)
Distance downstream, x (m)
S=1.72e+005*x^-1.50
S=5.09e+003*A^-0.59
Slope, S
Distance downstream, x (m)
Drainage area, A (m²)
Scaling data for channel 12
Elevation, z (m)
Drainage area, A (m²)
Distance downstream, x (m)
S=3.19e+007*x^-2.01
S=5.13e+003*A^-0.59
Slope, S
Distance downstream, x (m)
Drainage area, A (m²)

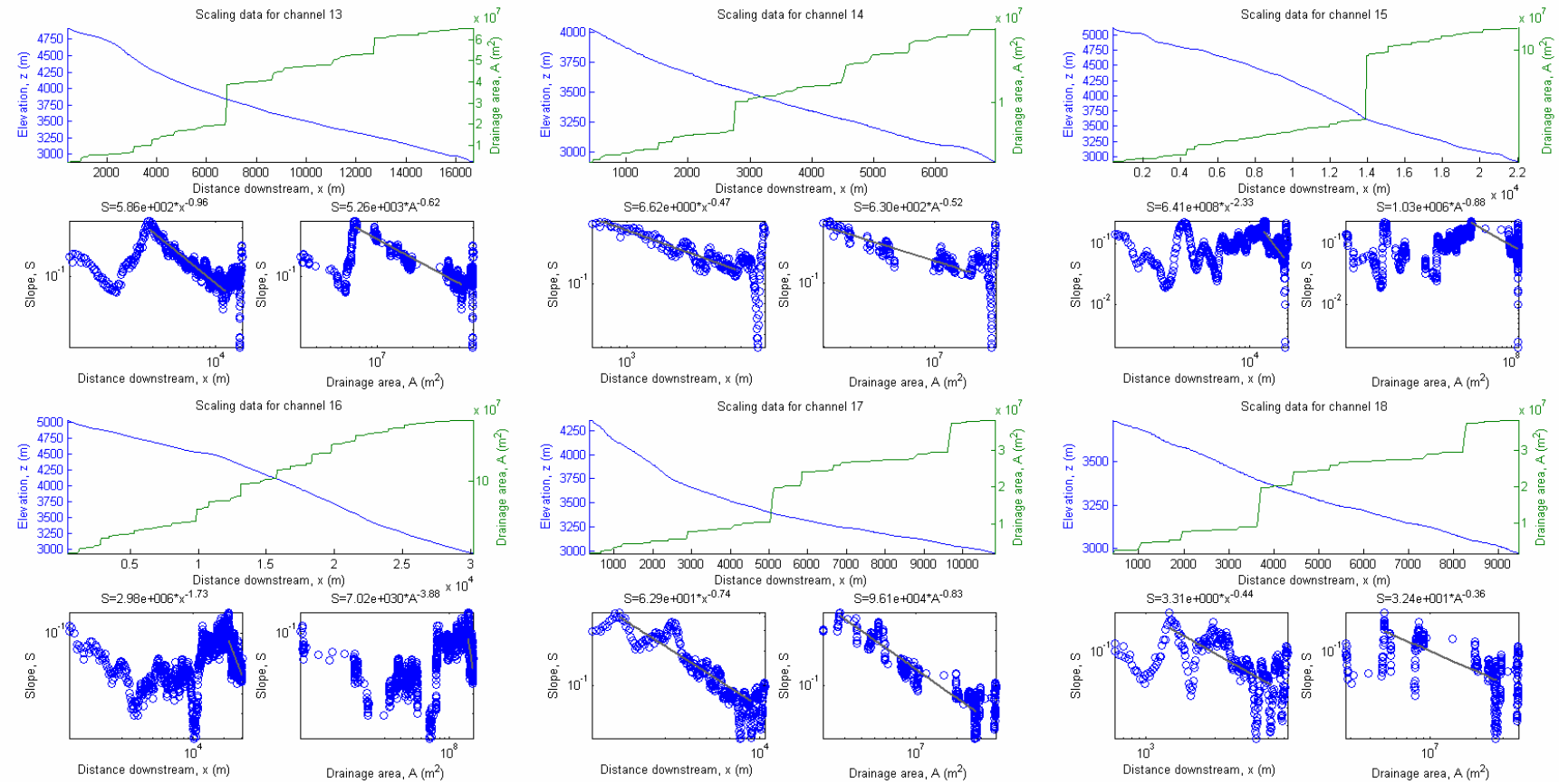
Scaling data for channel 13
Elevation, z (m)
Drainage area, A (m²)
Distance downstream, x (m)
S=5.86e+002*x^-0.96
S=5.26e+003*A^-0.62
Slope, S
Distance downstream, x (m)
Drainage area, A (m²)
Scaling data for channel 14
Elevation, z (m)
Drainage area, A (m²)
Distance downstream, x (m)
S=6.62e+000*x^-0.47
S=6.30e+002*A^-0.52
Slope, S
Distance downstream, x (m)
Drainage area, A (m²)
Scaling data for channel 15
Elevation, z (m)
Drainage area, A (m²)
Distance downstream, x (m)
S=6.41e+008*x^-2.33
S=1.03e+006*A^-0.88
Slope, S
Distance downstream, x (m)
Drainage area, A (m²)
Scaling data for channel 16
Elevation, z (m)
Drainage area, A (m²)
Distance downstream, x (m)
S=2.98e+006*x^-1.73
S=7.02e+030*A^-3.88
Slope, S
Distance downstream, x (m)
Drainage area, A (m²)
Scaling data for channel 17
Elevation, z (m)
Drainage area, A (m²)
Distance downstream, x (m)
S=6.29e+001*x^-0.74
S=9.61e+004*A^-0.83
Slope, S
Distance downstream, x (m)
Drainage area, A (m²)
Scaling data for channel 18
Elevation, z (m)
Drainage area, A (m²)
Distance downstream, x (m)
S=3.31e+000*x^-0.44
S=3.24e+001*A^-0.36
Slope, S
Distance downstream, x (m)
Drainage area, A (m²)

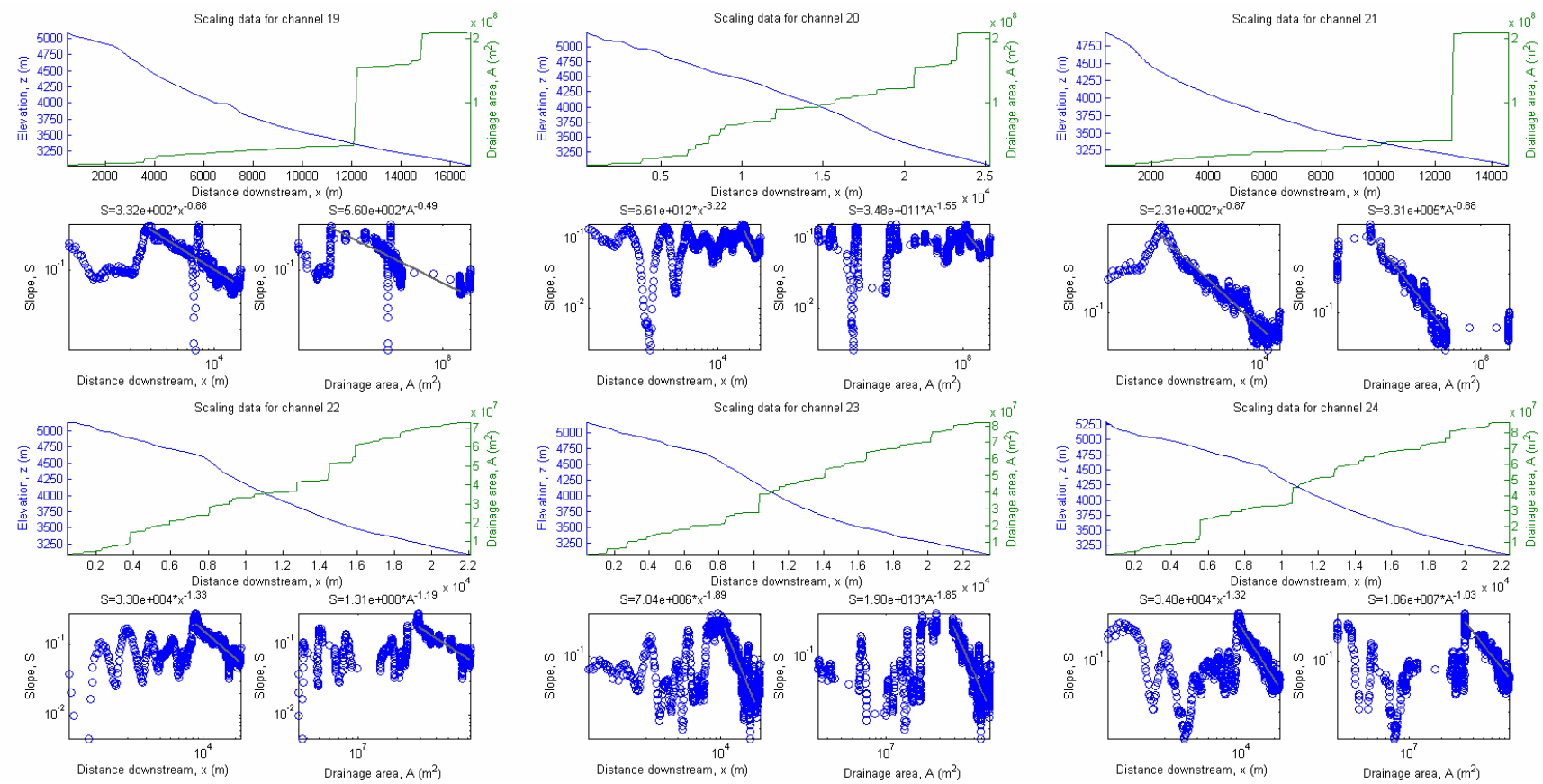
Scaling data for channel 19
Elevation, z (m)
Drainage area, A (m²)
Distance downstream, x (m)
S=3.32e+002*x^-0.88
S=5.60e+002*A^-0.49
Slope, S
Distance downstream, x (m)
Drainage area, A (m²)
Scaling data for channel 20
Elevation, z (m)
Drainage area, A (m²)
Distance downstream, x (m)
S=6.61e+012*x^-3.22
S=3.48e+011*A^-1.55
Slope, S
Distance downstream, x (m)
Drainage area, A (m²)
Scaling data for channel 21
Elevation, z (m)
Drainage area, A (m²)
Distance downstream, x (m)
S=2.31e+002*x^-0.87
S=3.31e+005*A^-0.88
Slope, S
Distance downstream, x (m)
Drainage area, A (m²)
Scaling data for channel 22
Elevation, z (m)
Drainage area, A (m²)
Distance downstream, x (m)
S=3.30e+004*x^-1.33
S=1.31e+008*A^-1.19
Slope, S
Distance downstream, x (m)
Drainage area, A (m²)
Scaling data for channel 23
Elevation, z (m)
Drainage area, A (m²)
Distance downstream, x (m)
S=7.04e+006*x^-1.89
S=1.90e+013*A^-1.85
Slope, S
Distance downstream, x (m)
Drainage area, A (m²)
Scaling data for channel 24
Elevation, z (m)
Drainage area, A (m²)
Distance downstream, x (m)
S=3.48e+004*x^-1.32
S=1.06e+007*A^-1.03
Slope, S
Distance downstream, x (m)
Drainage area, A (m²)

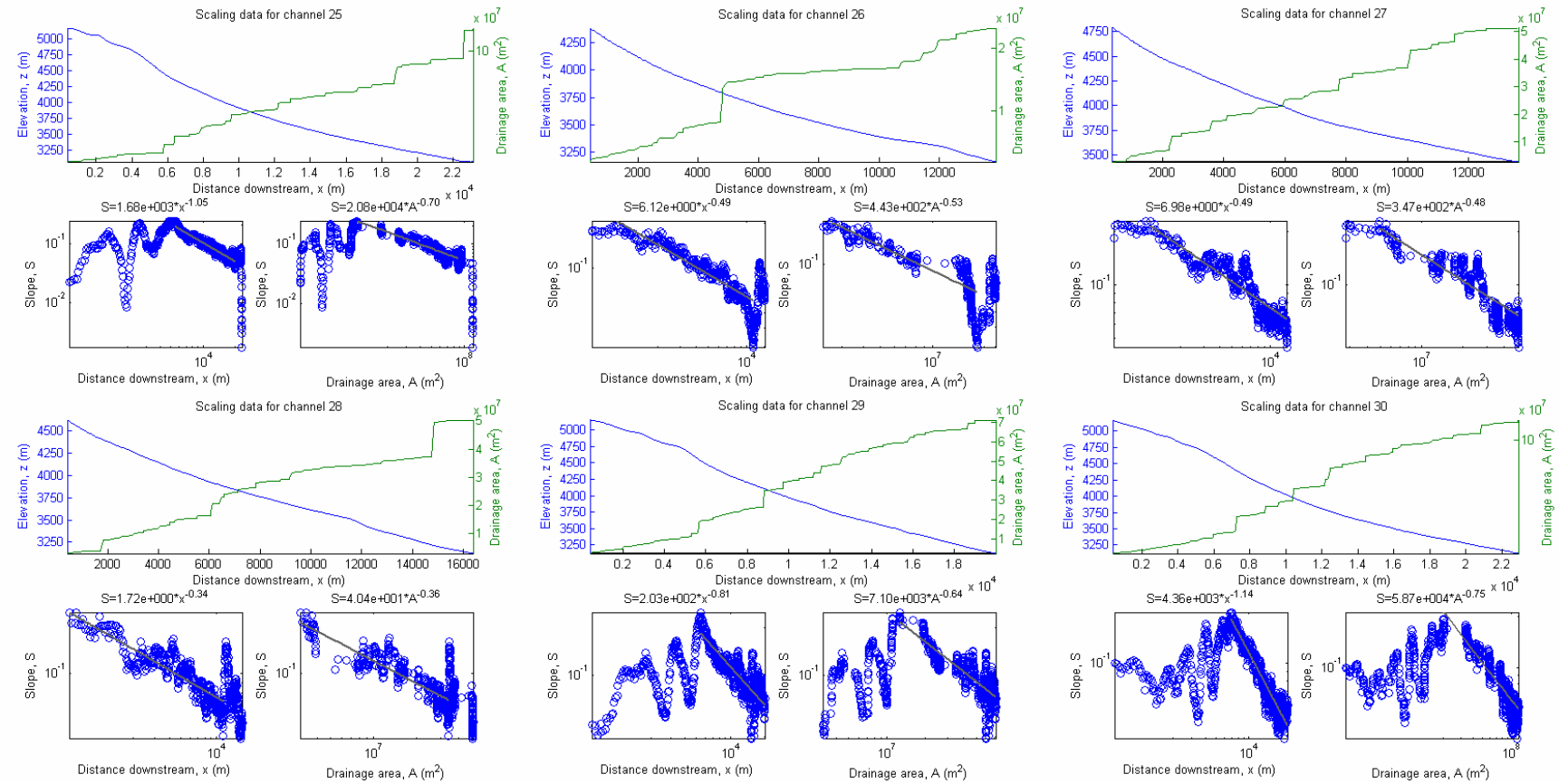
Scaling data for channel 25
Elevation, z (m)
Drainage area, A (m²)
Distance downstream, x (m)
S=1.68e+003*x^-1.05
S=2.08e+004*A^-0.70
Slope, S
Distance downstream, x (m)
Drainage area, A (m²)
Scaling data for channel 26
Elevation, z (m)
Drainage area, A (m²)
Distance downstream, x (m)
S=6.12e+000*x^-0.49
S=4.43e+002*A^-0.53
Slope, S
Distance downstream, x (m)
Drainage area, A (m²)
Scaling data for channel 27
Elevation, z (m)
Drainage area, A (m²)
Distance downstream, x (m)
S=6.98e+000*x^-0.49
S=3.47e+002*A^-0.48
Slope, S
Distance downstream, x (m)
Drainage area, A (m²)
Scaling data for channel 28
Elevation, z (m)
Drainage area, A (m²)
Distance downstream, x (m)
S=1.72e+000*x^-0.34
S=4.04e+001*A^-0.36
Slope, S
Distance downstream, x (m)
Drainage area, A (m²)
Scaling data for channel 29
Elevation, z (m)
Drainage area, A (m²)
Distance downstream, x (m)
S=2.03e+002*x^-0.81
S=7.10e+003*A^-0.64
Slope, S
Distance downstream, x (m)
Drainage area, A (m²)
Scaling data for channel 30
Elevation, z (m)
Drainage area, A (m²)
Distance downstream, x (m)
S=4.36e+003*x^-1.14
S=5.87e+004*A^-0.75
Slope, S
Distance downstream, x (m)
Drainage area, A (m²)

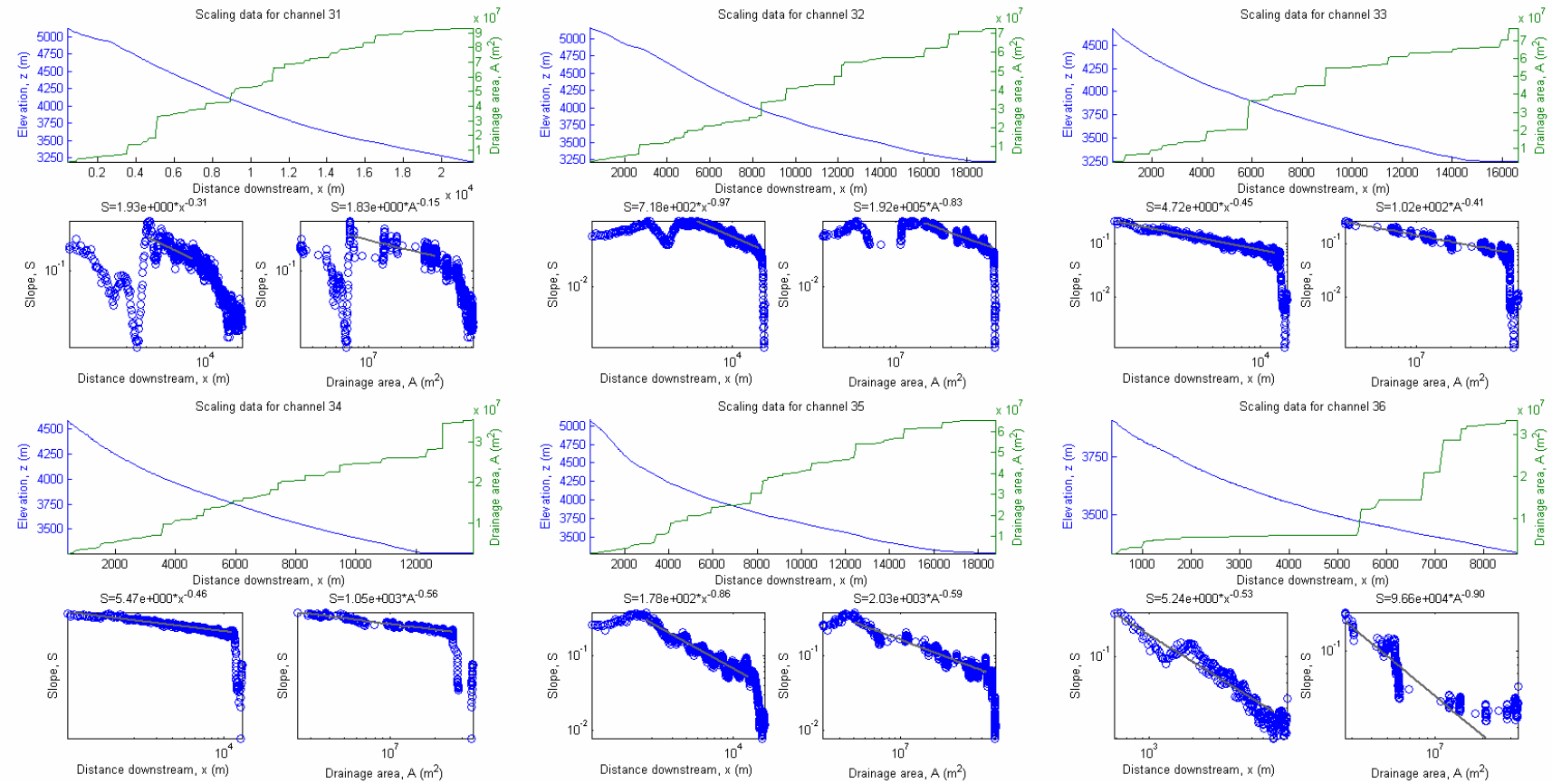
Scaling data for channel 31
Elevation, z (m)
Drainage area, A (m²)
Distance downstream, x (m)
S=1.93e+000*x^-0.31
S=1.83e+000*A^-0.15
Slope, S
Distance downstream, x (m)
Drainage area, A (m²)
Scaling data for channel 32
Elevation, z (m)
Drainage area, A (m²)
Distance downstream, x (m)
S=7.18e+002*x^-0.97
S=1.92e+005*A^-0.83
Slope, S
Distance downstream, x (m)
Drainage area, A (m²)
Scaling data for channel 33
Elevation, z (m)
Drainage area, A (m²)
Distance downstream, x (m)
S=4.72e+000*x^-0.45
S=1.02e+002*A^-0.41
Slope, S
Distance downstream, x (m)
Drainage area, A (m²)
Scaling data for channel 34
Elevation, z (m)
Drainage area, A (m²)
Distance downstream, x (m)
S=5.47e+000*x^-0.46
S=1.05e+003*A^-0.56
Slope, S
Distance downstream, x (m)
Drainage area, A (m²)
Scaling data for channel 35
Elevation, z (m)
Drainage area, A (m²)
Distance downstream, x (m)
S=1.78e+002*x^-0.86
S=2.03e+003*A^-0.59
Slope, S
Distance downstream, x (m)
Drainage area, A (m²)
Scaling data for channel 36
Elevation, z (m)
Drainage area, A (m²)
Distance downstream, x (m)
S=5.24e+000*x^-0.53
S=9.66e+004*A^-0.90
Slope, S
Distance downstream, x (m)
Drainage area, A (m²)

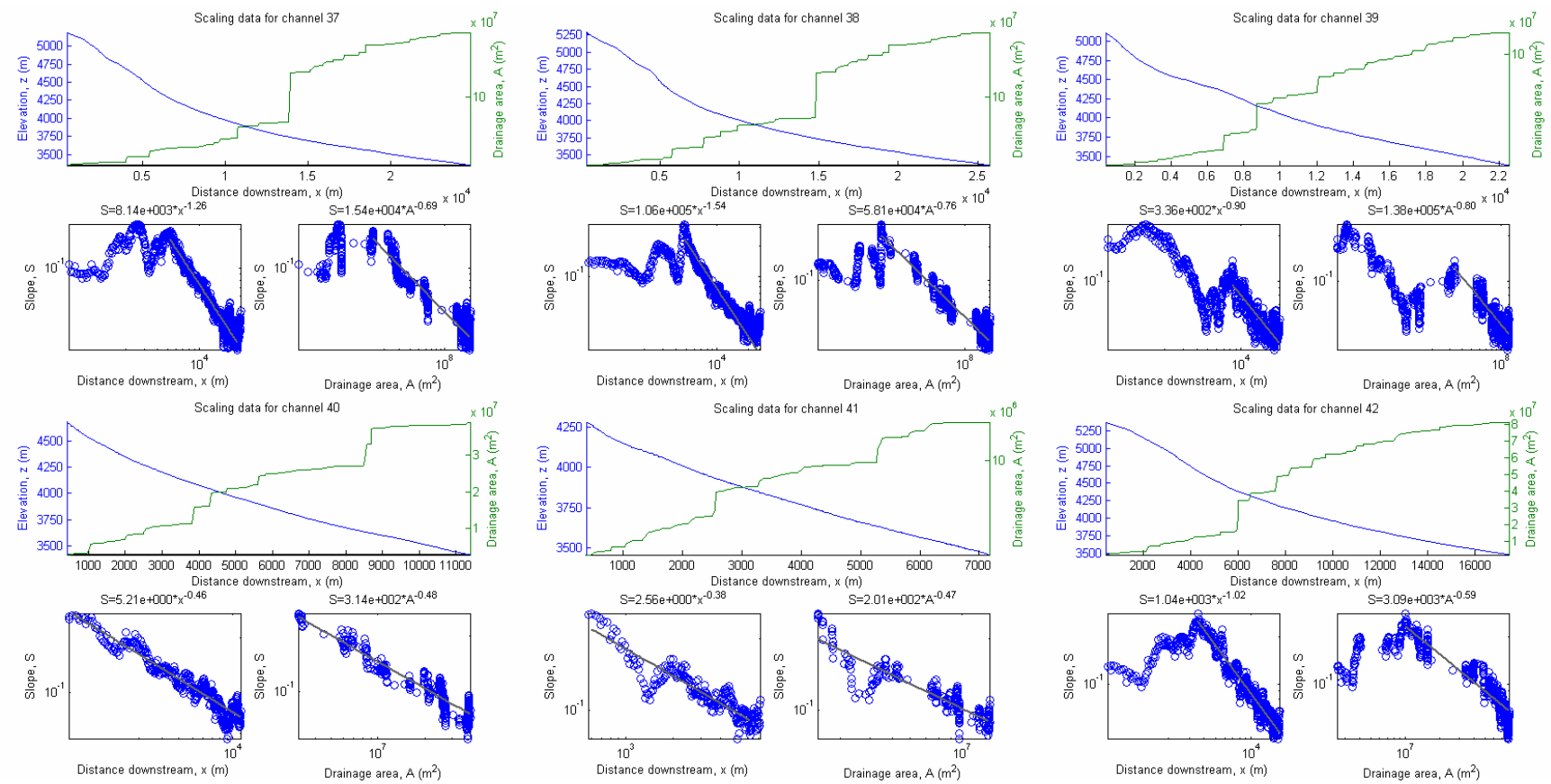
Scaling data for channel 37
Elevation, z (m)
Drainage area, A (m²)
Distance downstream, x (m)
S=8.14e+003*x^-1.26
S=1.54e+004*A^-0.69
Slope, S
Distance downstream, x (m)
Drainage area, A (m²)
Scaling data for channel 38
Elevation, z (m)
Drainage area, A (m²)
Distance downstream, x (m)
S=1.06e+005*x^-1.54
S=5.81e+004*A^-0.76
Slope, S
Distance downstream, x (m)
Drainage area, A (m²)
Scaling data for channel 39
Elevation, z (m)
Drainage area, A (m²)
Distance downstream, x (m)
S=3.36e+002*x^-0.90
S=1.38e+005*A^-0.80
Slope, S
Distance downstream, x (m)
Drainage area, A (m²)
Scaling data for channel 40
Elevation, z (m)
Drainage area, A (m²)
Distance downstream, x (m)
S=5.21e+000*x^-0.46
S=3.14e+002*A^-0.48
Slope, S
Distance downstream, x (m)
Drainage area, A (m²)
Scaling data for channel 41
Elevation, z (m)
Drainage area, A (m²)
Distance downstream, x (m)
S=2.56e+000*x^-0.38
S=2.01e+002*A^-0.47
Slope, S
Distance downstream, x (m)
Drainage area, A (m²)
Scaling data for channel 42
Elevation, z (m)
Drainage area, A (m²)
Distance downstream, x (m)
S=1.04e+003*x^-1.02
S=3.09e+003*A^-0.59
Slope, S
Distance downstream, x (m)
Drainage area, A (m²)

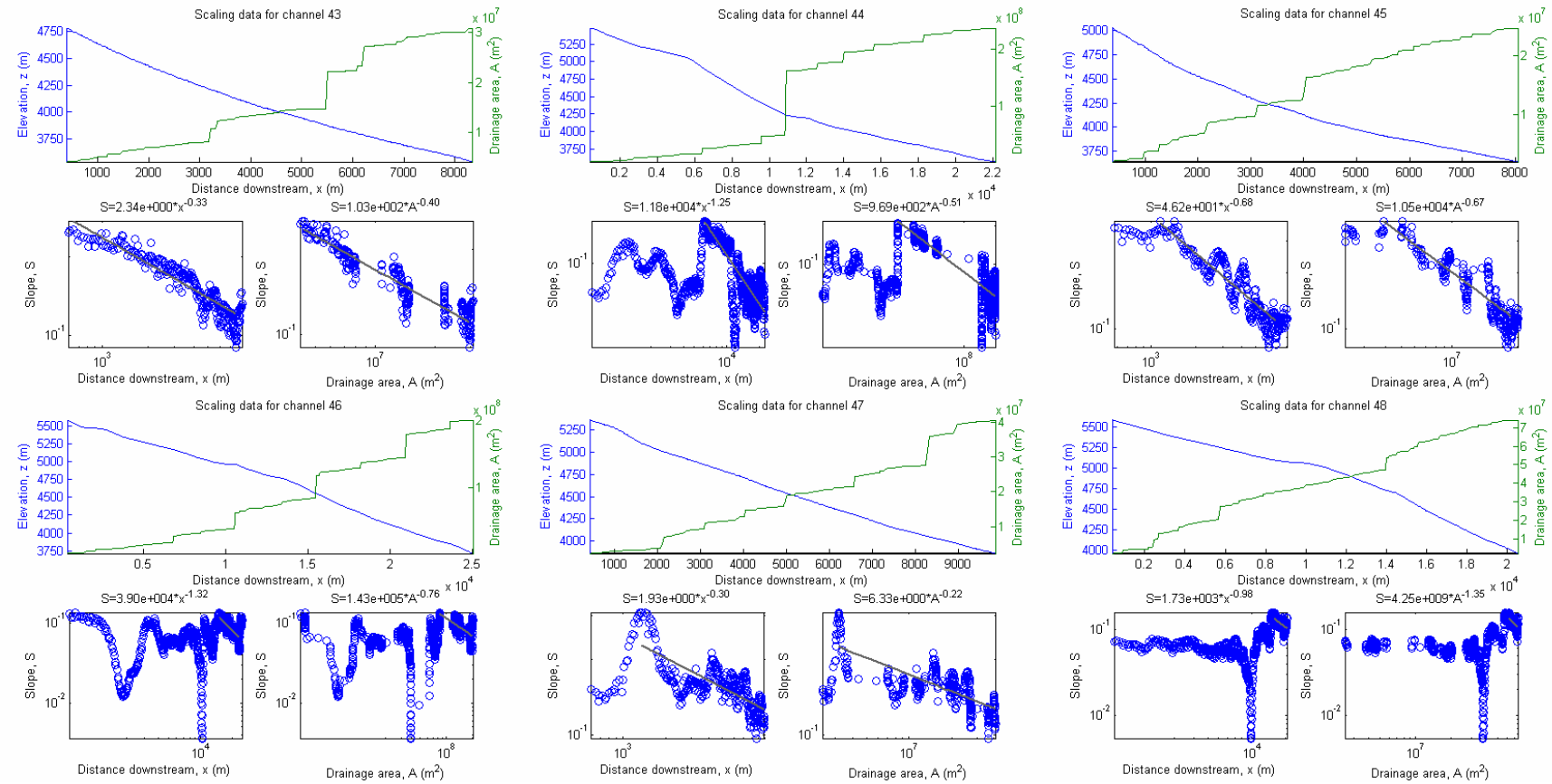
Scaling data for channel 43
Elevation, z (m)
Drainage area, A (m²)
Distance downstream, x (m)
S=2.34e+000*x^-0.33
S=1.03e+002*A^-0.40
Slope, S
Distance downstream, x (m)
Drainage area, A (m²)
Scaling data for channel 44
Elevation, z (m)
Drainage area, A (m²)
Distance downstream, x (m)
S=1.18e+004*x^-1.25
S=9.69e+002*A^-0.51
Slope, S
Distance downstream, x (m)
Drainage area, A (m²)
Scaling data for channel 45
Elevation, z (m)
Drainage area, A (m²)
Distance downstream, x (m)
S=4.62e+001*x^-0.68
S=1.05e+004*A^-0.67
Slope, S
Distance downstream, x (m)
Drainage area, A (m²)
Scaling data for channel 46
Elevation, z (m)
Drainage area, A (m²)
Distance downstream, x (m)
S=3.90e+004*x^-1.32
S=1.43e+005*A^-0.76
Slope, S
Distance downstream, x (m)
Drainage area, A (m²)
Scaling data for channel 47
Elevation, z (m)
Drainage area, A (m²)
Distance downstream, x (m)
S=1.93e+000*x^-0.30
S=6.33e+000*A^-0.22
Slope, S
Distance downstream, x (m)
Drainage area, A (m²)
Scaling data for channel 48
Elevation, z (m)
Drainage area, A (m²)
Distance downstream, x (m)
S=1.73e+003*x^-0.98
S=4.25e+009*A^-1.35
Slope, S
Distance downstream, x (m)
Drainage area, A (m²)

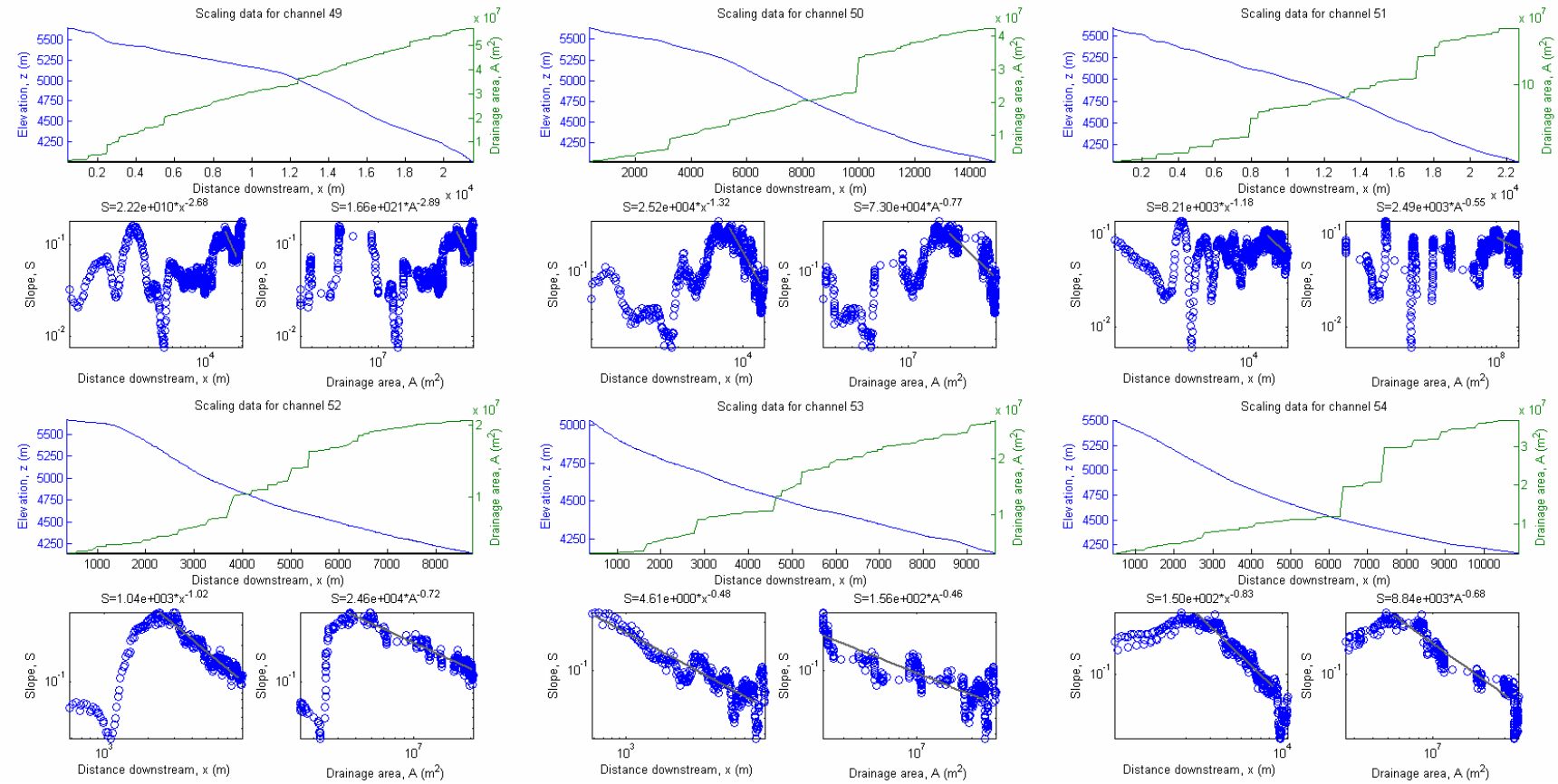
Scaling data for channel 49
Elevation, z (m)
Drainage area, A (m²)
Distance downstream, x (m)
S=2.22e+010*x^-2.68
S=1.66e+021*A^-2.89
Slope, S
Drainage area, A (m²)
Scaling data for channel 50
S=2.52e+004*x^-1.32
S=7.30e+004*A^-0.77
Scaling data for channel 51
S=8.21e+003*x^-1.18
S=2.49e+003*A^-0.55
Scaling data for channel 52
S=1.04e+003*x^-1.02
S=2.46e+004*A^-0.72
Scaling data for channel 53
S=4.61e+000*x^-0.48
S=1.56e+002*A^-0.46
Scaling data for channel 54
S=1.50e+002*x^-0.83
S=8.84e+003*A^-0.68

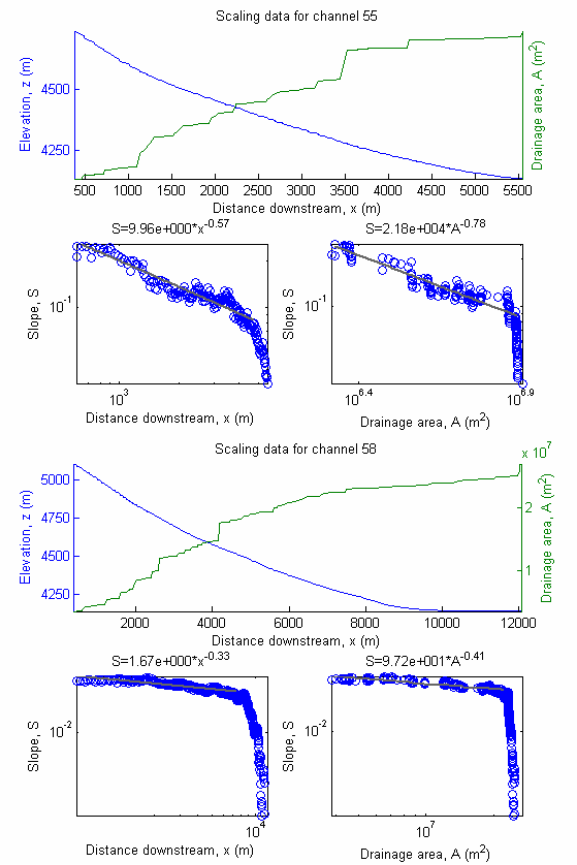
Scaling data for channel 55
Elevation, z (m)
Drainage area, A (m²)
Distance downstream, x (m)
S=9.96e+000*x^-0.57
S=2.18e+004*A^-0.78
Slope, S
Distance downstream, x (m)
Drainage area, A (m²)

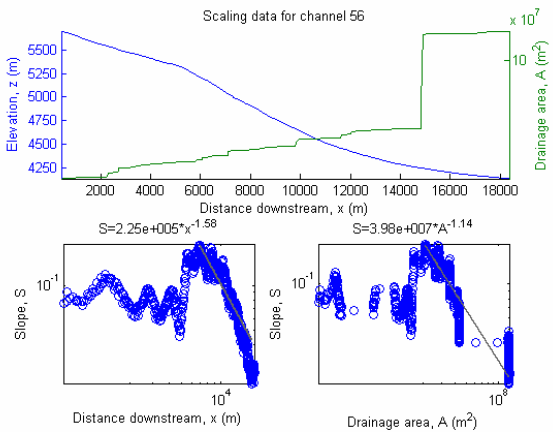
Scaling data for channel 56
Elevation, z (m)
Drainage area, A (m²)
Distance downstream, x (m)
S=2.25e+005*x^-1.58
S=3.98e+007*A^-1.14
Slope, S
Distance downstream, x (m)
Drainage area, A (m²)

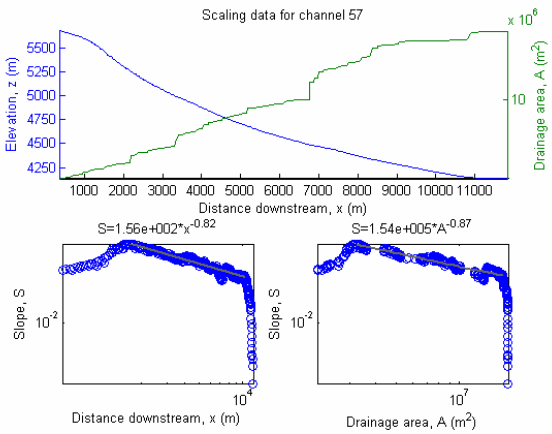
Scaling data for channel 57
Elevation, z (m)
Drainage area, A (m²)
Distance downstream, x (m)
S=1.56e+002*x^-0.82
S=1.54e+005*A^-0.87
Slope, S
Distance downstream, x (m)
Drainage area, A (m²)

Scaling data for channel 58
Elevation, z (m)
Drainage area, A (m²)
Distance downstream, x (m)
S=1.67e+000*x^-0.33
S=9.72e+001*A^-0.41
Slope, S
Distance downstream, x (m)
Drainage area, A (m²)

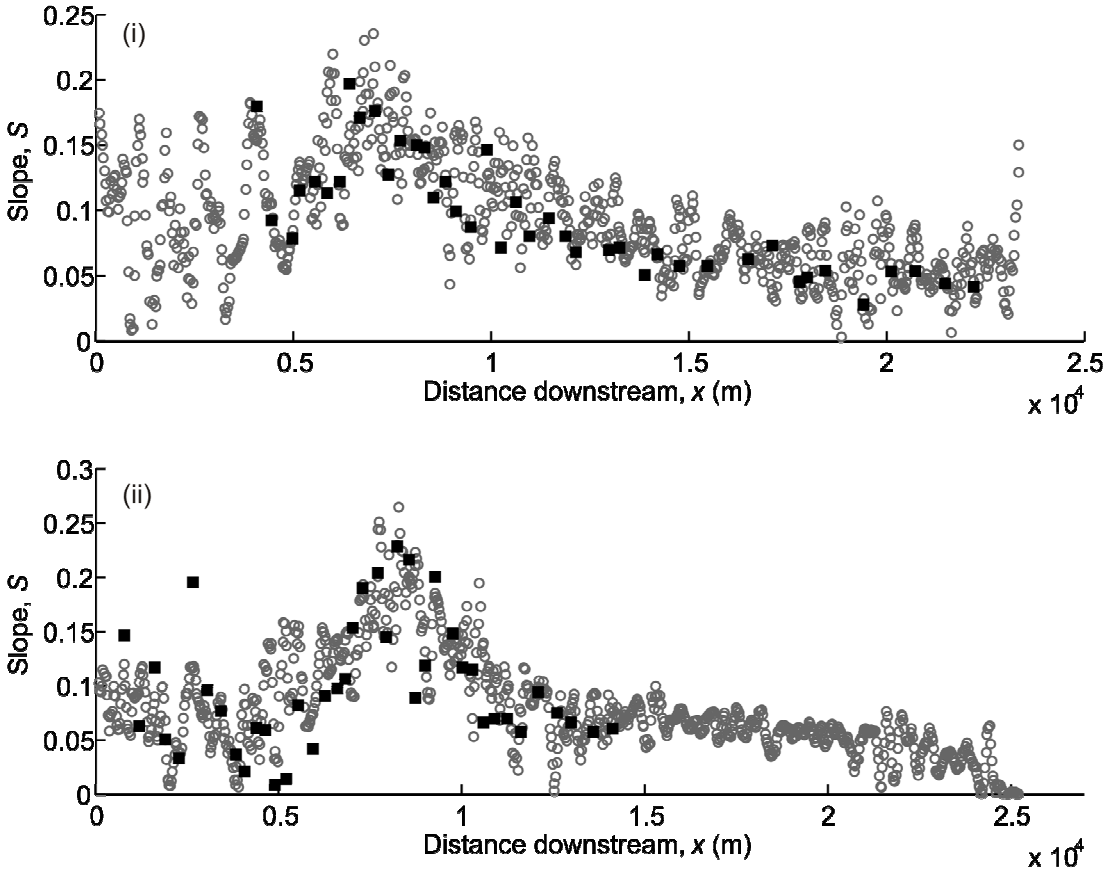

Figure B3. Comparison of field (black squares) and DEM (gray circles) derived slopes as measured downstream for **(i)** Basgo valley and **(ii)** Leh valley.

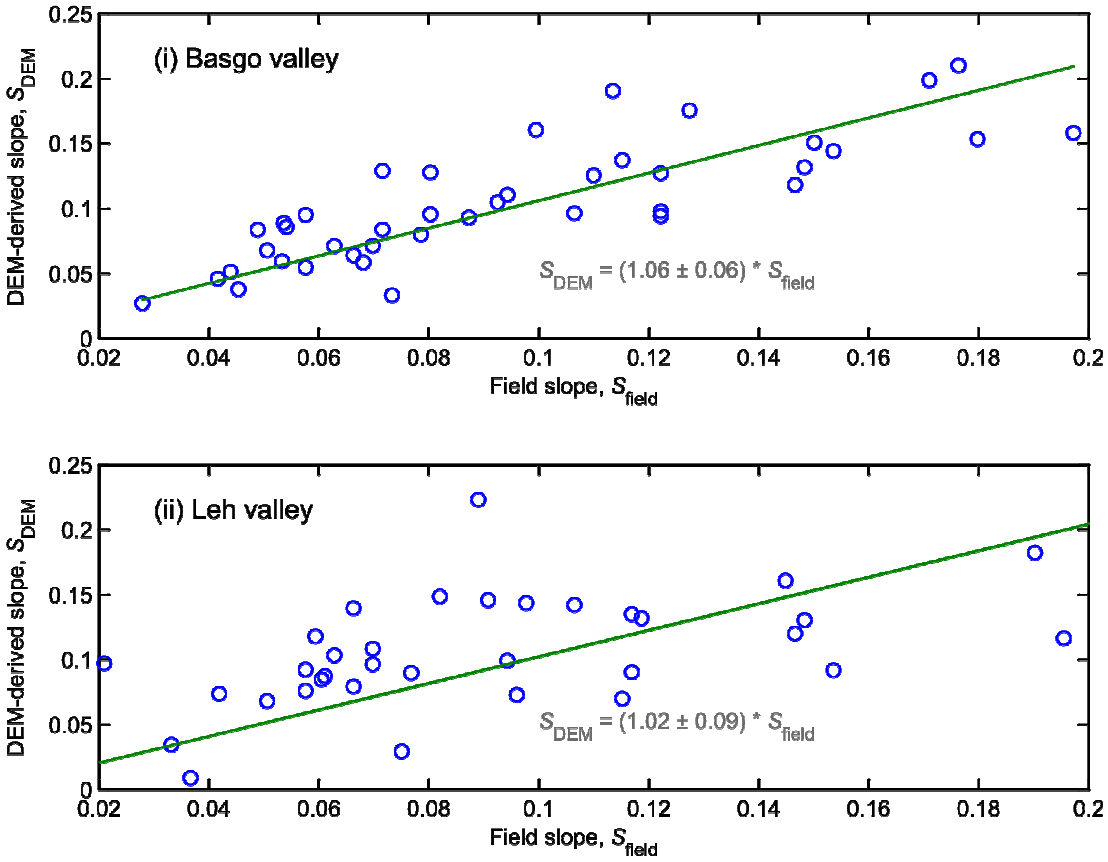

Figure B4. Field slopes versus DEM slopes for two catchments in Ladakh, **(i)** Basgo valley, **(ii)** Leh valley

Figure B5 (subsequent pages). Plots of calculated concavity and curvature values for each catchment, subdividing the data to investigate possible variations in the values downstream. Data is plotted incorporating different numbers of sets of 50 data points, working both from upstream to downstream (blue) and downstream to upstream (red). The pattern of convergence as described in the accompanying supporting text is noted above each graph. See Appendix section B3 for full explanation.

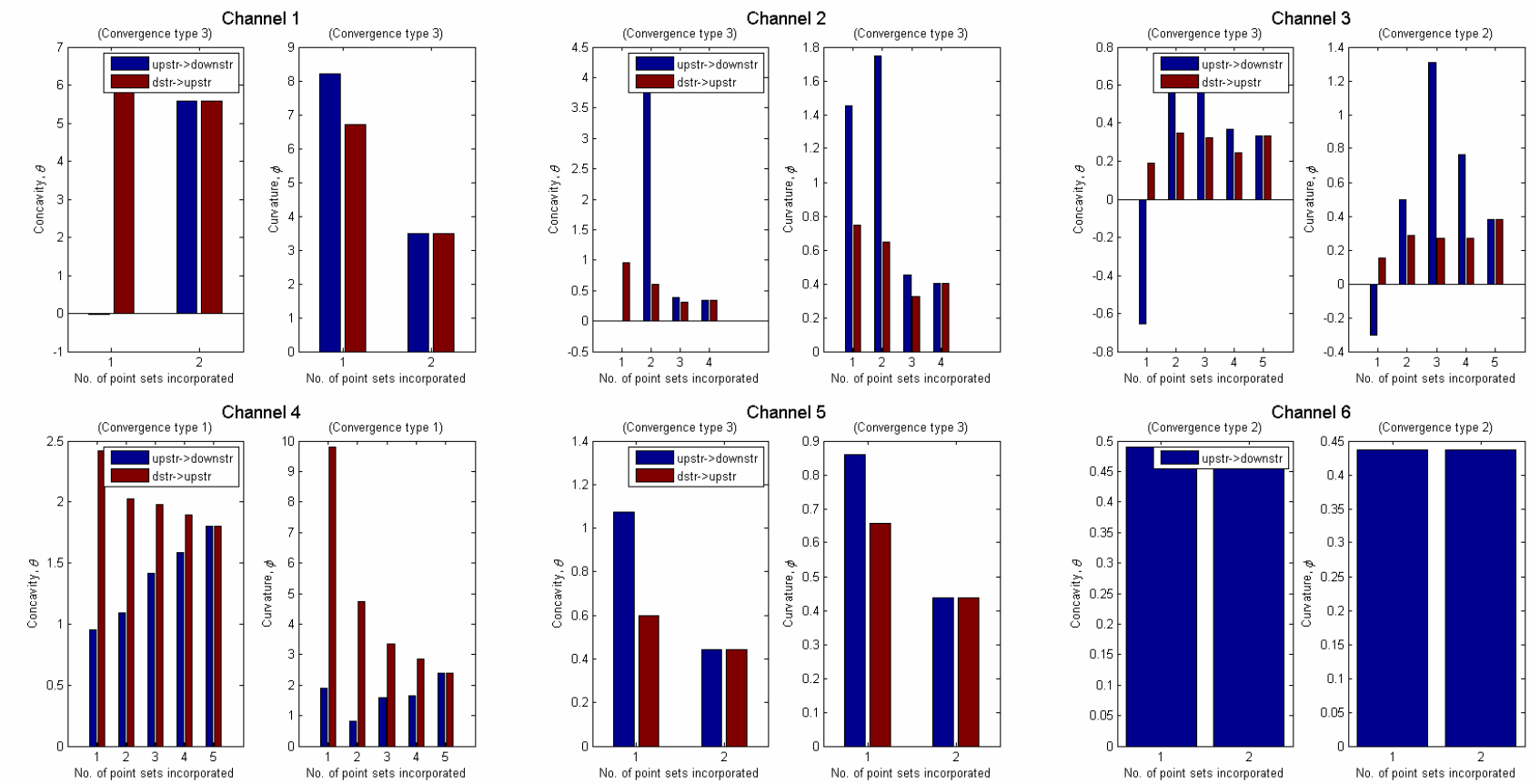
Channel 1
(Convergence type 3)
upstr->downstr
dstr->upstr
Concavity, θ
No. of point sets incorporated
(Convergence type 3)
Curvature, ϕ
No. of point sets incorporated
Channel 2
(Convergence type 3)
upstr->downstr
dstr->upstr
Concavity, θ
No. of point sets incorporated
(Convergence type 3)
Curvature, ϕ
No. of point sets incorporated
Channel 3
(Convergence type 3)
upstr->downstr
dstr->upstr
Concavity, θ
No. of point sets incorporated
(Convergence type 2)
Curvature, ϕ
No. of point sets incorporated
Channel 4
(Convergence type 1)
upstr->downstr
dstr->upstr
Concavity, θ
No. of point sets incorporated
(Convergence type 1)
Curvature, ϕ
No. of point sets incorporated
Channel 5
(Convergence type 3)
upstr->downstr
dstr->upstr
Concavity, θ
No. of point sets incorporated
(Convergence type 3)
Curvature, ϕ
No. of point sets incorporated
Channel 6
(Convergence type 2)
upstr->downstr
Concavity, θ
No. of point sets incorporated
(Convergence type 2)
Curvature, ϕ
No. of point sets incorporated

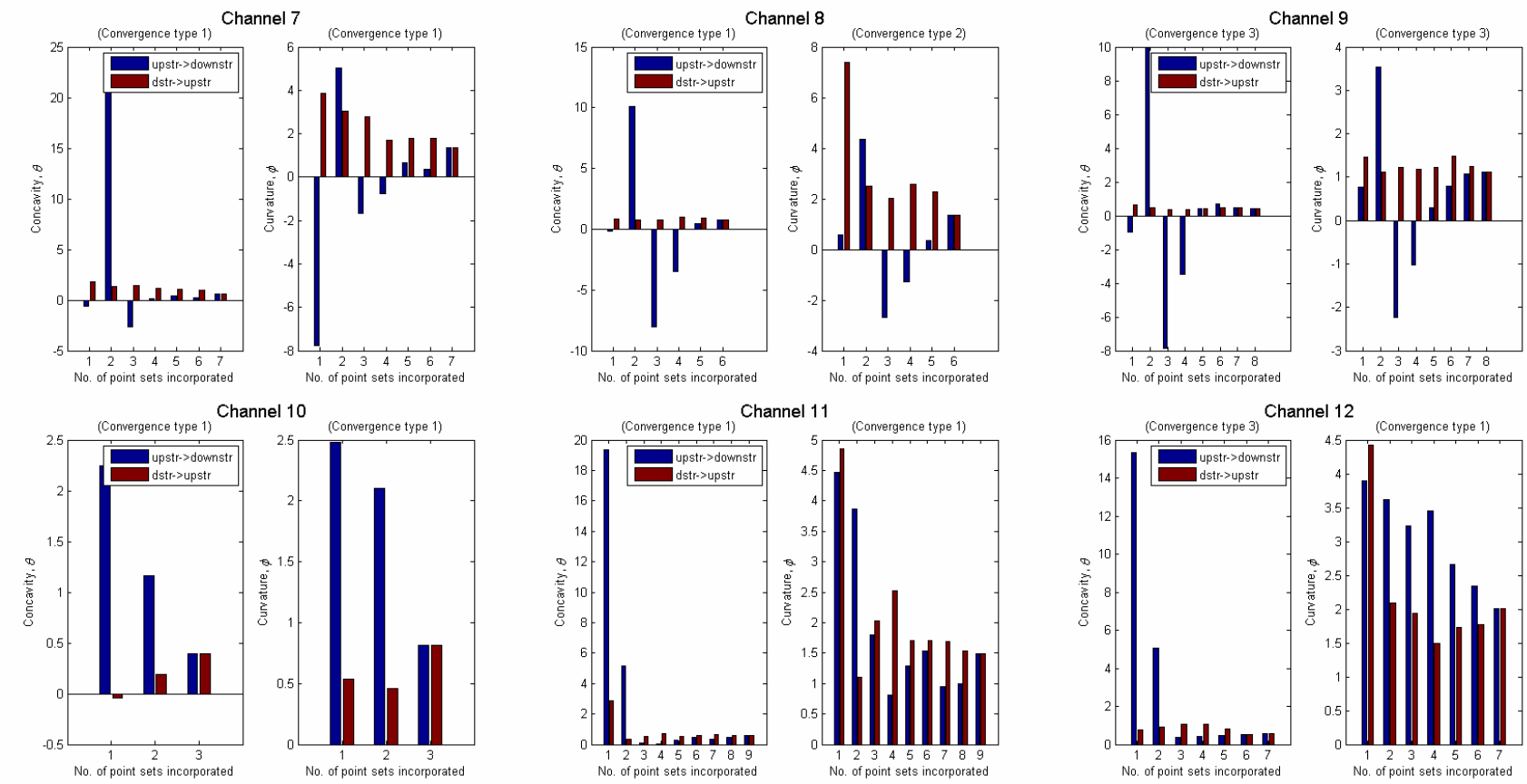
Channel 7
(Convergence type 1)
upstr->downstr
dstr->upstr
Concavity, θ
No. of point sets incorporated
(Convergence type 1)
Curvature, φ
No. of point sets incorporated
Channel 8
(Convergence type 1)
upstr->downstr
dstr->upstr
Concavity, θ
No. of point sets incorporated
(Convergence type 2)
Curvature, φ
No. of point sets incorporated
Channel 9
(Convergence type 3)
upstr->downstr
dstr->upstr
Concavity, θ
No. of point sets incorporated
(Convergence type 3)
Curvature, φ
No. of point sets incorporated
Channel 10
(Convergence type 1)
upstr->downstr
dstr->upstr
Concavity, θ
No. of point sets incorporated
(Convergence type 1)
Curvature, φ
No. of point sets incorporated
Channel 11
(Convergence type 1)
upstr->downstr
dstr->upstr
Concavity, θ
No. of point sets incorporated
(Convergence type 1)
Curvature, φ
No. of point sets incorporated
Channel 12
(Convergence type 3)
upstr->downstr
dstr->upstr
Concavity, θ
No. of point sets incorporated
(Convergence type 1)
Curvature, φ
No. of point sets incorporated

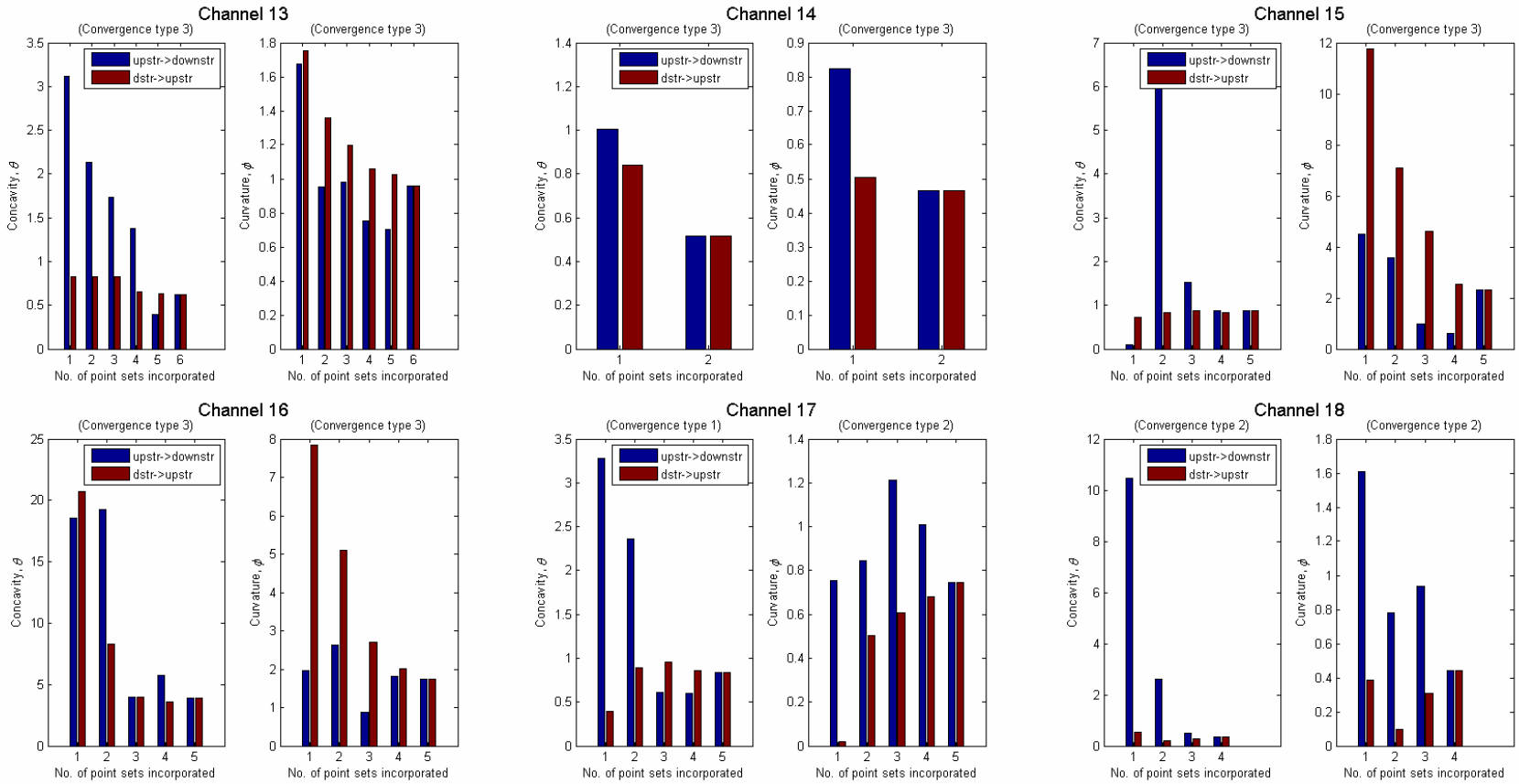
Channel 13
(Convergence type 3)
(Convergence type 3)
upstr->downstr
dstr->upstr
Concavity, θ
Curvature, ϕ
No. of point sets incorporated
No. of point sets incorporated
Channel 14
(Convergence type 3)
(Convergence type 3)
upstr->downstr
dstr->upstr
Concavity, θ
Curvature, ϕ
No. of point sets incorporated
No. of point sets incorporated
Channel 15
(Convergence type 3)
(Convergence type 3)
upstr->downstr
dstr->upstr
Concavity, θ
Curvature, ϕ
No. of point sets incorporated
No. of point sets incorporated
Channel 16
(Convergence type 3)
(Convergence type 3)
upstr->downstr
dstr->upstr
Concavity, θ
Curvature, ϕ
No. of point sets incorporated
No. of point sets incorporated
Channel 17
(Convergence type 1)
(Convergence type 2)
upstr->downstr
dstr->upstr
Concavity, θ
Curvature, ϕ
No. of point sets incorporated
No. of point sets incorporated
Channel 18
(Convergence type 2)
(Convergence type 2)
upstr->downstr
dstr->upstr
Concavity, θ
Curvature, ϕ
No. of point sets incorporated
No. of point sets incorporated

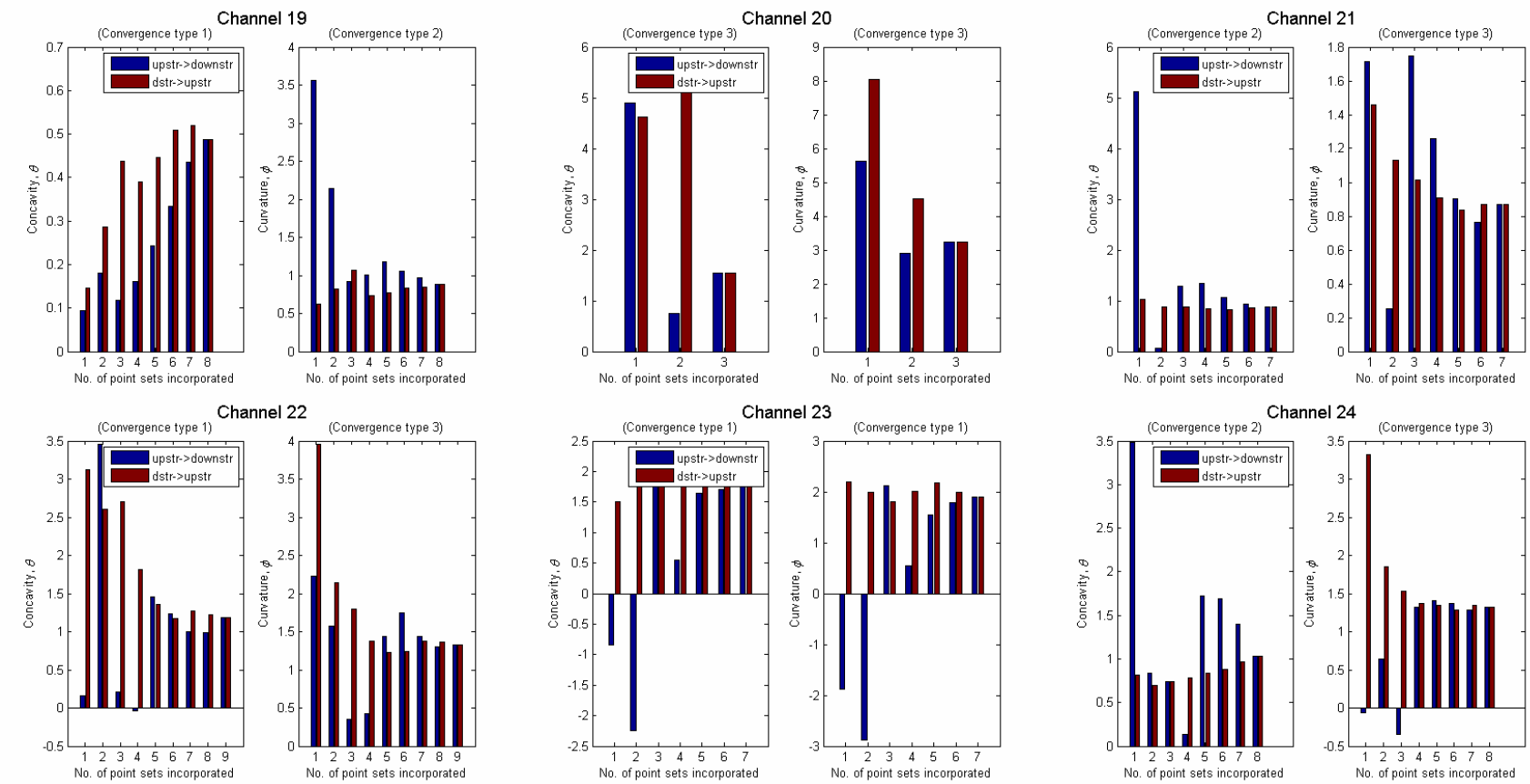
Channel 19
(Convergence type 1)
(Convergence type 2)
upstr->downstr
dstr->upstr
Concavity, θ
Curvature, ϕ
No. of point sets incorporated
Channel 20
(Convergence type 3)
(Convergence type 3)
Channel 21
(Convergence type 2)
(Convergence type 3)
Channel 22
(Convergence type 1)
(Convergence type 3)
Channel 23
(Convergence type 1)
(Convergence type 1)
Channel 24
(Convergence type 2)
(Convergence type 3)

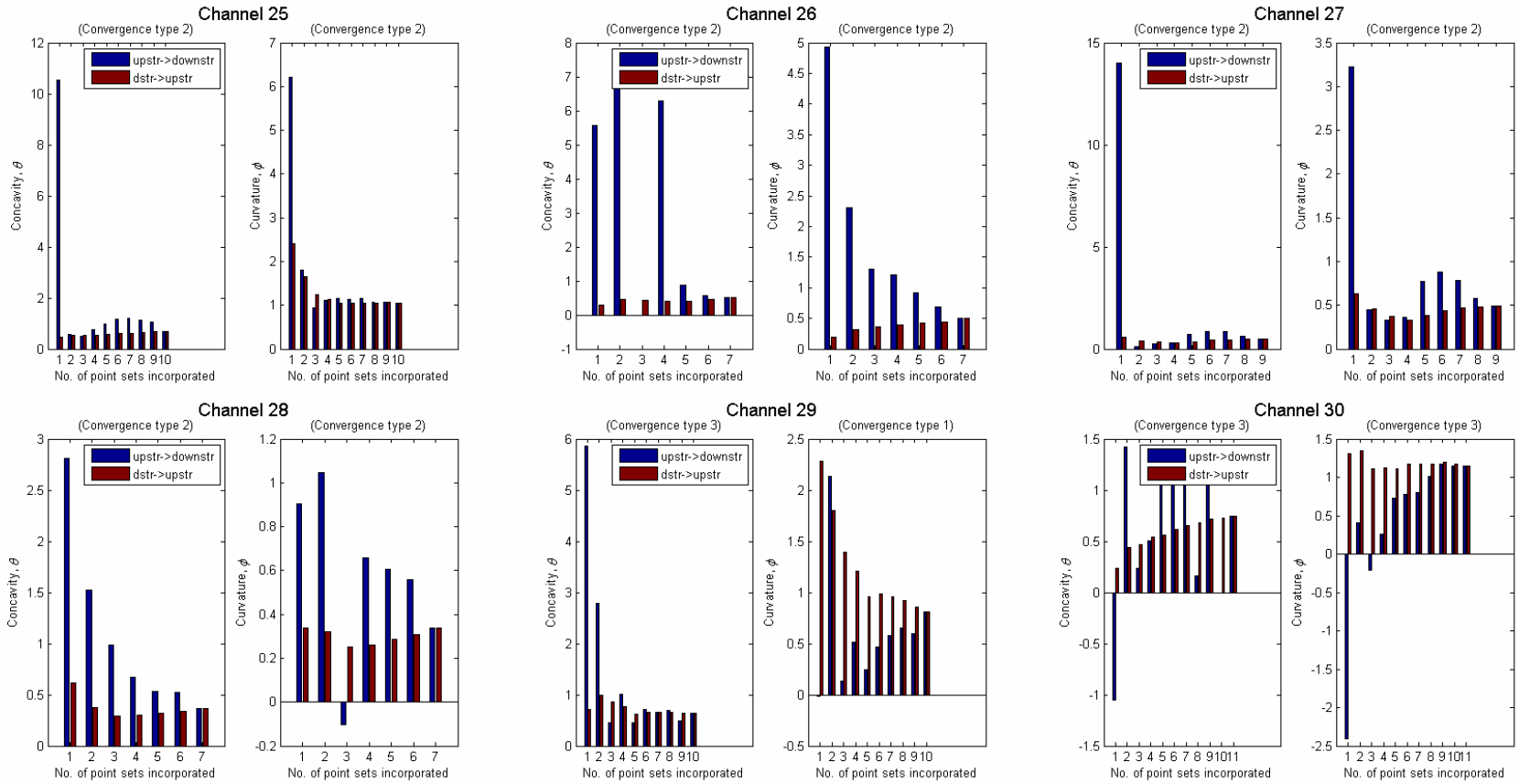
Channel 25
(Convergence type 2)
upstr->downstr
dstr->upstr
Concavity, θ
No. of point sets incorporated
(Convergence type 2)
Curvature, ϕ
No. of point sets incorporated
Channel 26
(Convergence type 2)
upstr->downstr
dstr->upstr
Concavity, θ
No. of point sets incorporated
(Convergence type 2)
Curvature, ϕ
No. of point sets incorporated
Channel 27
(Convergence type 2)
upstr->downstr
dstr->upstr
Concavity, θ
No. of point sets incorporated
(Convergence type 2)
Curvature, ϕ
No. of point sets incorporated
Channel 28
(Convergence type 2)
upstr->downstr
dstr->upstr
Concavity, θ
No. of point sets incorporated
(Convergence type 2)
Curvature, ϕ
No. of point sets incorporated
Channel 29
(Convergence type 3)
upstr->downstr
dstr->upstr
Concavity, θ
No. of point sets incorporated
(Convergence type 1)
Curvature, ϕ
No. of point sets incorporated
Channel 30
(Convergence type 3)
upstr->downstr
dstr->upstr
Concavity, θ
No. of point sets incorporated
(Convergence type 3)
Curvature, ϕ
No. of point sets incorporated

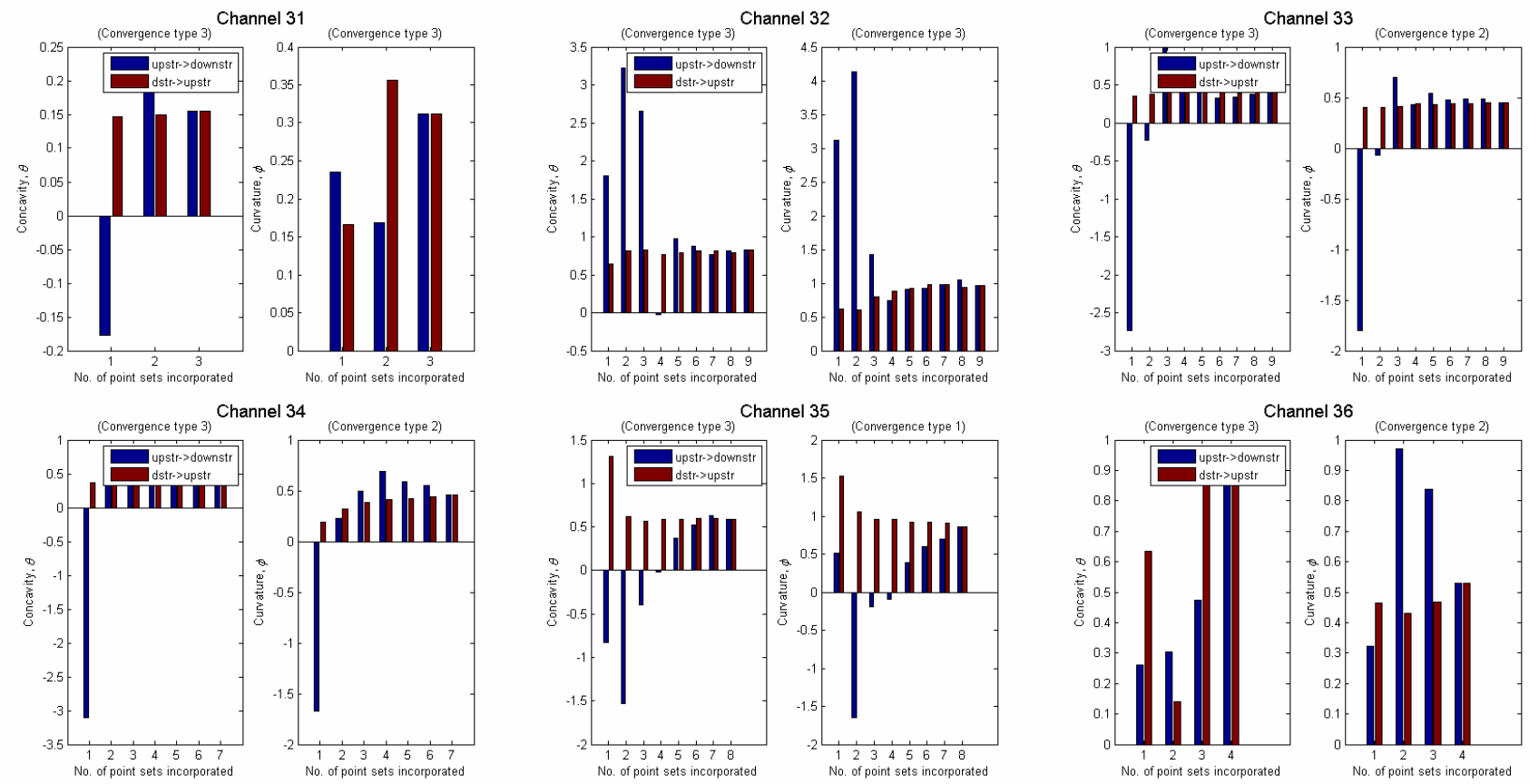
Channel 31
(Convergence type 3)
upstr->downstr
dstr->upstr
Concavity, θ
No. of point sets incorporated
(Convergence type 3)
Curvature, ϕ
No. of point sets incorporated
Channel 32
(Convergence type 3)
upstr->downstr
dstr->upstr
Concavity, θ
No. of point sets incorporated
(Convergence type 3)
Curvature, ϕ
No. of point sets incorporated
Channel 33
(Convergence type 3)
upstr->downstr
dstr->upstr
Concavity, θ
No. of point sets incorporated
(Convergence type 2)
Curvature, ϕ
No. of point sets incorporated
Channel 34
(Convergence type 3)
upstr->downstr
dstr->upstr
Concavity, θ
No. of point sets incorporated
(Convergence type 2)
Curvature, ϕ
No. of point sets incorporated
Channel 35
(Convergence type 3)
upstr->downstr
dstr->upstr
Concavity, θ
No. of point sets incorporated
(Convergence type 1)
Curvature, ϕ
No. of point sets incorporated
Channel 36
(Convergence type 3)
upstr->downstr
dstr->upstr
Concavity, θ
No. of point sets incorporated
(Convergence type 2)
Curvature, ϕ
No. of point sets incorporated

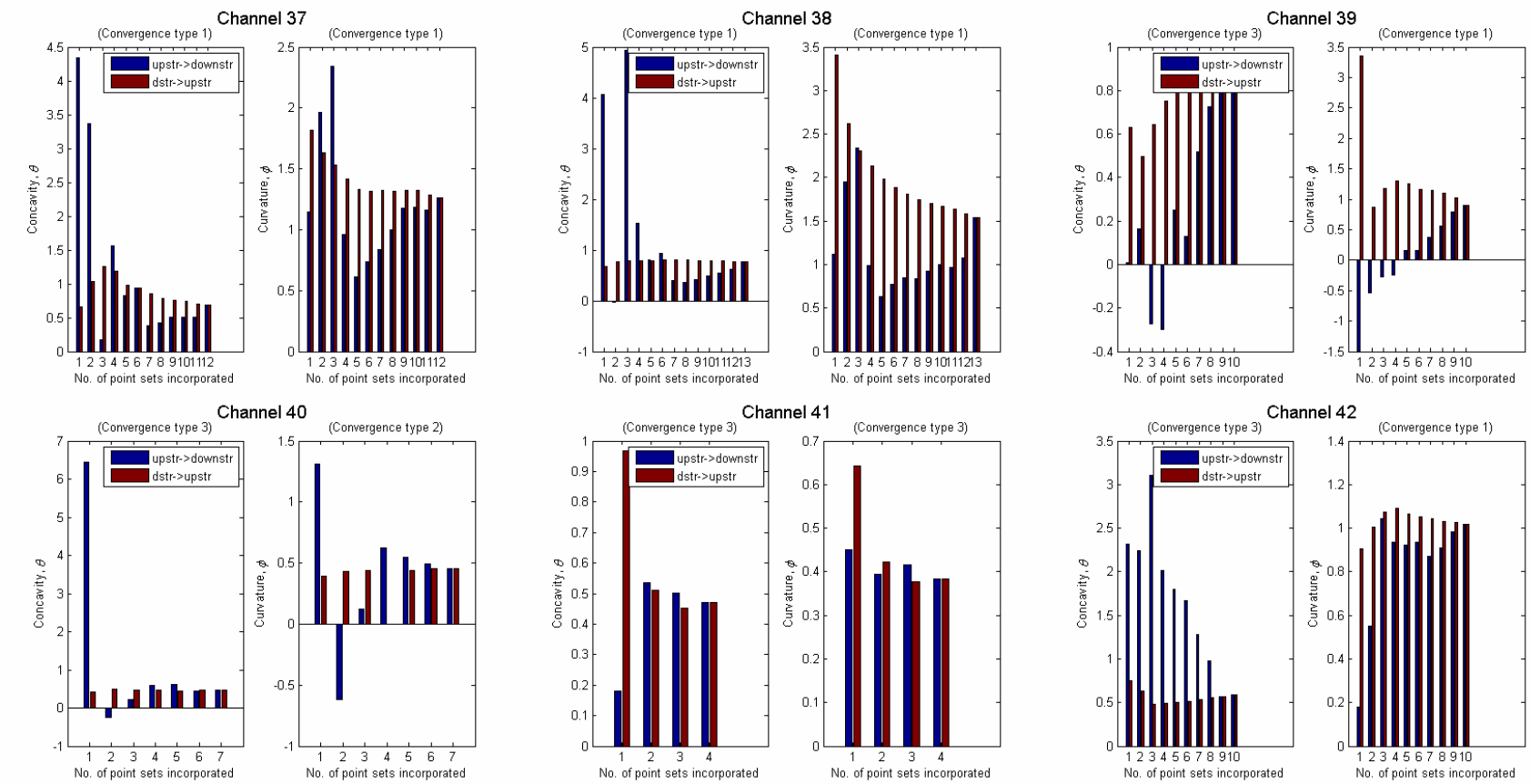
Channel 37
(Convergence type 1)
upstr->downstr
dstr->upstr
Concavity, θ
No. of point sets incorporated
(Convergence type 1)
Curvature, ϕ
No. of point sets incorporated
Channel 38
(Convergence type 1)
upstr->downstr
dstr->upstr
Concavity, θ
No. of point sets incorporated
(Convergence type 1)
Curvature, ϕ
No. of point sets incorporated
Channel 39
(Convergence type 3)
upstr->downstr
dstr->upstr
Concavity, θ
No. of point sets incorporated
(Convergence type 1)
Curvature, ϕ
No. of point sets incorporated
Channel 40
(Convergence type 3)
upstr->downstr
dstr->upstr
Concavity, θ
No. of point sets incorporated
(Convergence type 2)
Curvature, ϕ
No. of point sets incorporated
Channel 41
(Convergence type 3)
upstr->downstr
dstr->upstr
Concavity, θ
No. of point sets incorporated
(Convergence type 3)
Curvature, ϕ
No. of point sets incorporated
Channel 42
(Convergence type 3)
upstr->downstr
dstr->upstr
Concavity, θ
No. of point sets incorporated
(Convergence type 1)
Curvature, ϕ
No. of point sets incorporated

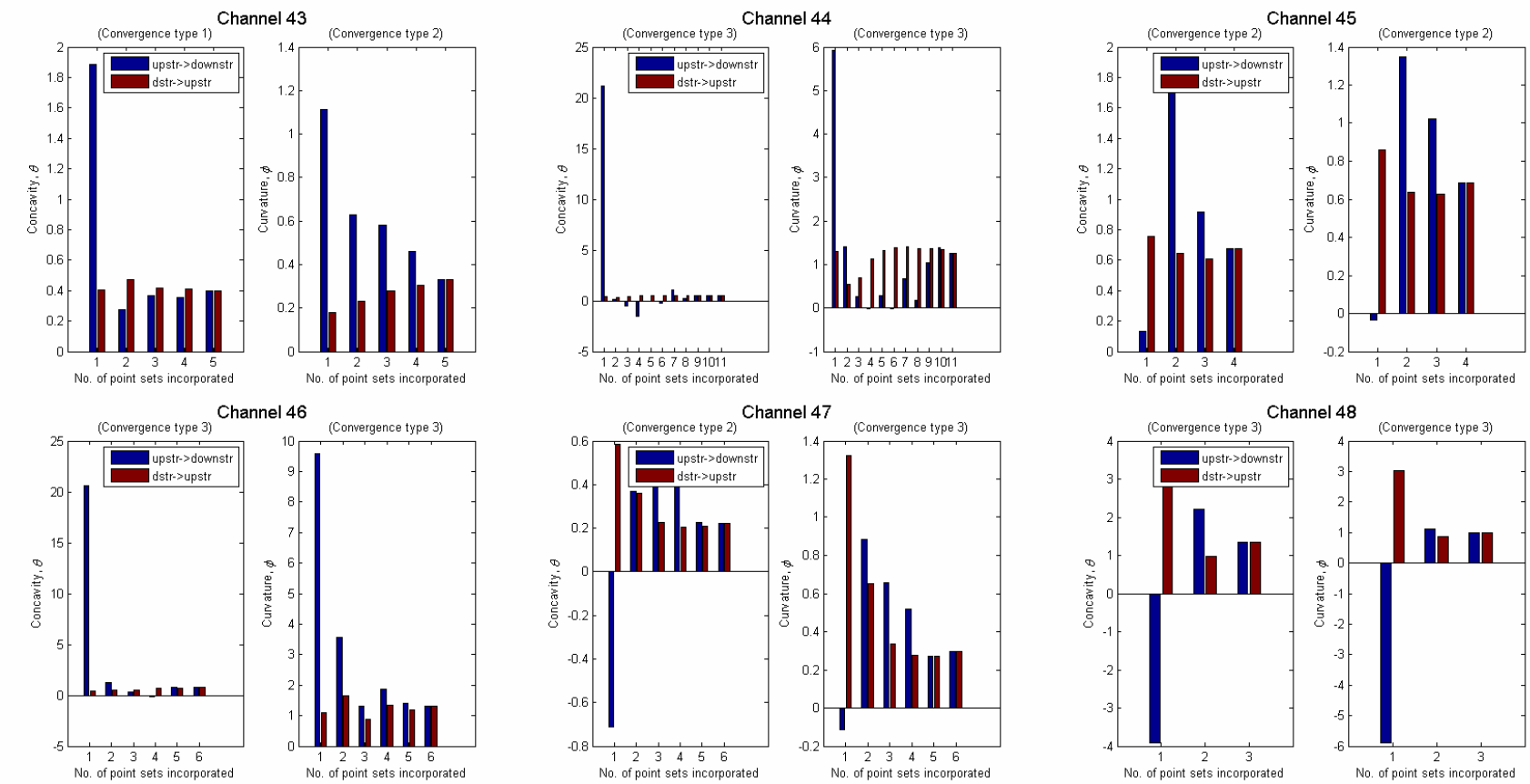
Channel 43
(Convergence type 1)
(Convergence type 2)
upstr->downstr
dstr->upstr
Concavity, θ
Curvature, ϕ
No. of point sets incorporated
Channel 44
(Convergence type 3)
(Convergence type 3)
Channel 45
(Convergence type 2)
(Convergence type 2)
Channel 46
(Convergence type 3)
(Convergence type 3)
Channel 47
(Convergence type 2)
(Convergence type 3)
Channel 48
(Convergence type 3)
(Convergence type 3)

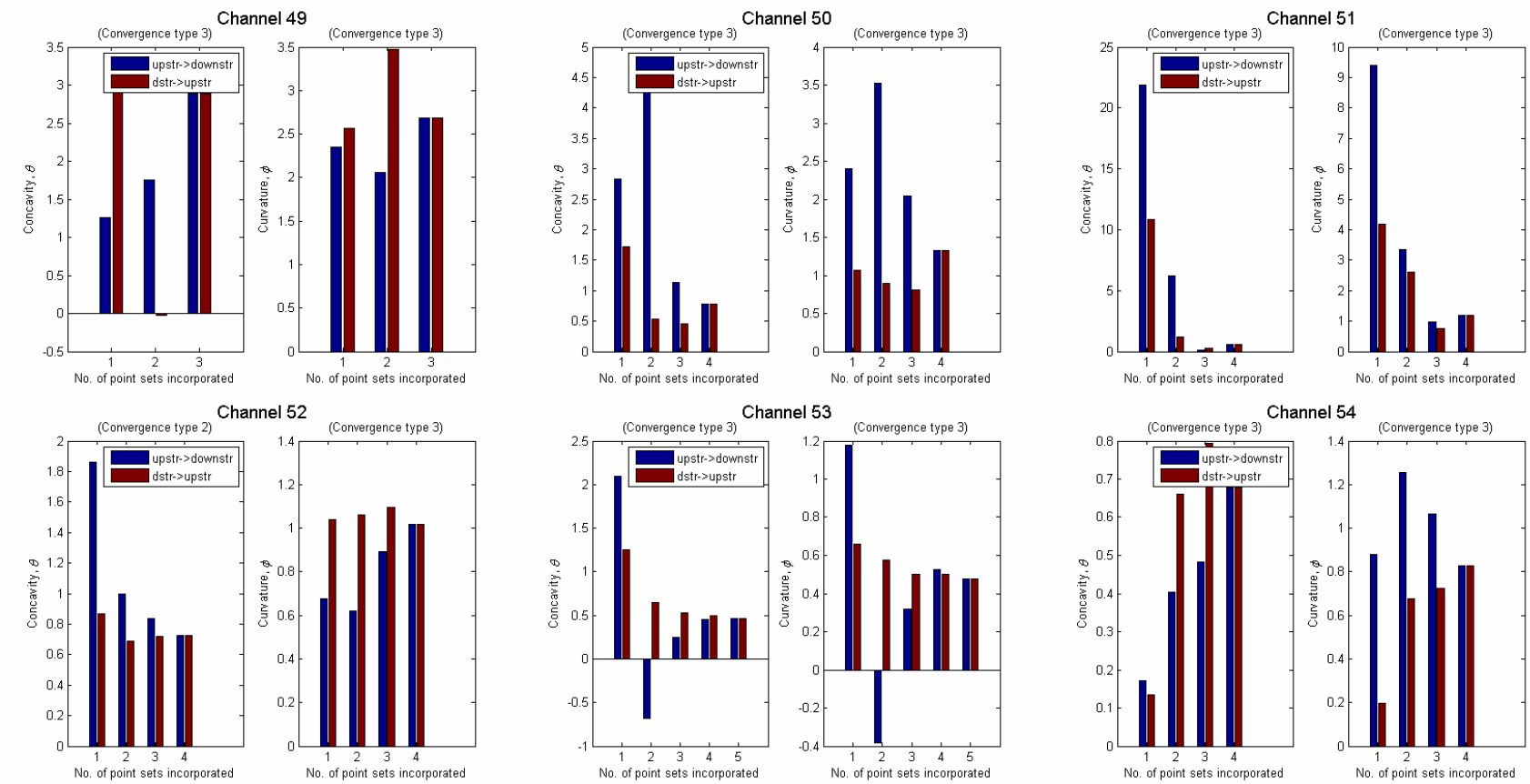
Channel 49
(Convergence type 3)
(Convergence type 3)
upstr->downstr
dstr->upstr
Concavity, θ
Curvature, ϕ
No. of point sets incorporated
No. of point sets incorporated
Channel 50
(Convergence type 3)
(Convergence type 3)
upstr->downstr
dstr->upstr
Concavity, θ
Curvature, ϕ
No. of point sets incorporated
No. of point sets incorporated
Channel 51
(Convergence type 3)
(Convergence type 3)
upstr->downstr
dstr->upstr
Concavity, θ
Curvature, ϕ
No. of point sets incorporated
No. of point sets incorporated
Channel 52
(Convergence type 2)
(Convergence type 3)
upstr->downstr
dstr->upstr
Concavity, θ
Curvature, ϕ
No. of point sets incorporated
No. of point sets incorporated
Channel 53
(Convergence type 3)
(Convergence type 3)
upstr->downstr
dstr->upstr
Concavity, θ
Curvature, ϕ
No. of point sets incorporated
No. of point sets incorporated
Channel 54
(Convergence type 3)
(Convergence type 3)
upstr->downstr
dstr->upstr
Concavity, θ
Curvature, ϕ
No. of point sets incorporated
No. of point sets incorporated

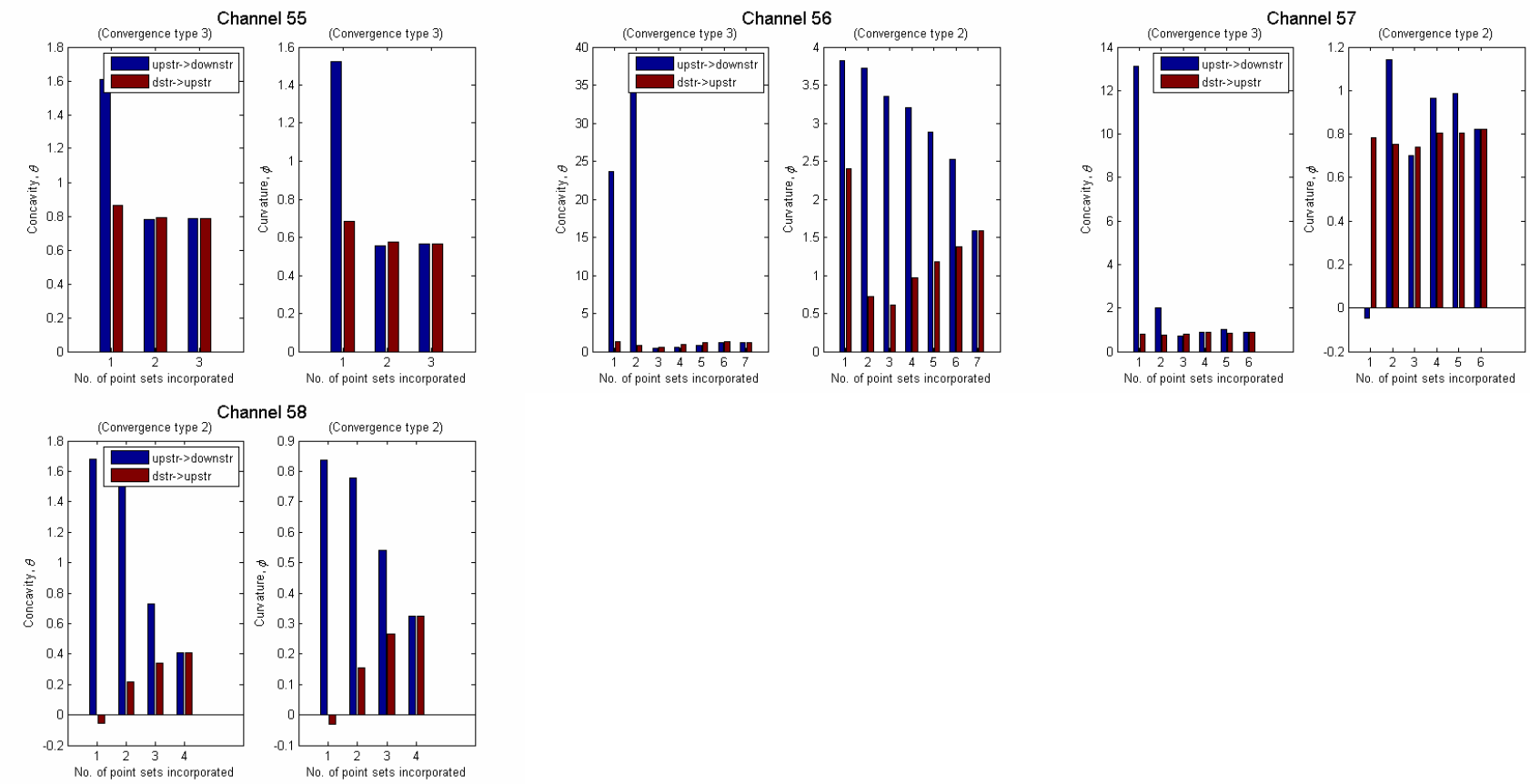
Channel 55
(Convergence type 3)
upstr->downstr
dstr->upstr
Concavity, θ
No. of point sets incorporated
(Convergence type 3)
Curvature, ϕ
No. of point sets incorporated
Channel 56
(Convergence type 3)
upstr->downstr
dstr->upstr
Concavity, θ
No. of point sets incorporated
(Convergence type 2)
Curvature, ϕ
No. of point sets incorporated
Channel 57
(Convergence type 3)
upstr->downstr
dstr->upstr
Concavity, θ
No. of point sets incorporated
(Convergence type 2)
Curvature, ϕ
No. of point sets incorporated
Channel 58
(Convergence type 2)
upstr->downstr
dstr->upstr
Concavity, θ
No. of point sets incorporated
(Convergence type 2)
Curvature, ϕ
No. of point sets incorporated

APPENDIX C:

SUPPORTING MATERIAL FOR CHAPTER 4

Grain Size Distributions for Glacial Sediments

Figure C1 presents histograms describing the distribution of sediment grain size in the glacial material for two sites in Leh valley, both within the lateral/terminal moraine complex but >2.5 km apart. Data was collected using a Wolman point counting method and the data binned into intervals between the values of 1, 2, 4, 6, 8 and 12 cm, keeping a separate record of the b-axis length of clasts larger than 12 cm. 250 clasts where measured at each site. The distributions are indistinguishable between sites to 95% confidence, using a Kolmogorov-Smirnov test.

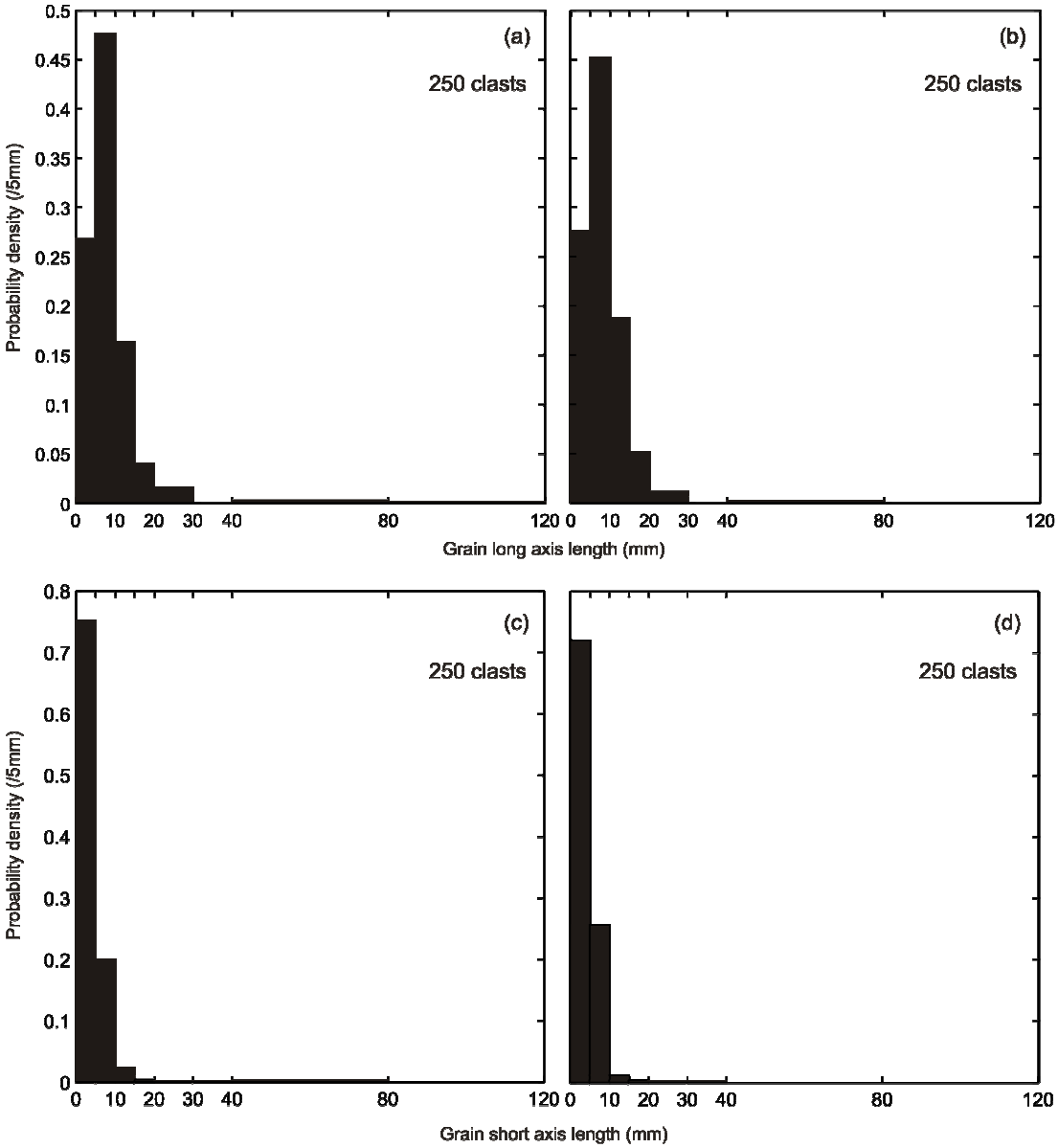

Figure C1. Grain size distributions for two sites in Leh valley, **(a,c)** 34.20598N, 77.61563E; **(b,d)** 34.18933N, 77.59868E. (a) and (b) describe the long axis lengths, *a*, of the clasts; (c) and (d) describe the short axis lengths, *c*.

APPENDIX D:

RAW DATA FROM LADAKH

(Italics indicate data not entirely trusted as representative due to high variability around locality or known difficulties in data collection)
(Blanks indicate data not collected)

D1. Field Season 2006 – Basgo Valley

TABLE D1. FIELD DATA FROM BASGO VALLEY

Locality	Longitude (°)	Latitude (°)	Elevation (m) (from GPS)	Slope	Bankfull width (m)	Bankfull depth (m)	Max. gorge height (m)
BG4	34.34039	77.36374	4841	0.182	8.8	0.9	0
BG5	34.33973	77.3606	4834	0.093	45.3	0.4	8
BG6	34.33894	77.35748	4807	0.079	15.4	0.7	7.5
BG7	34.33918	77.35426	4754	0.116	8.5	0.7	15
BG8	34.33861	77.35108	4712	0.123	18.3	0.8	21
BG9	34.33629	77.3493	4658	0.114	8.5	0.8	19.5
BG10	34.33345	77.34682	4600	0.123	24.4	0.6	10
BG3A	34.33119	77.34482	4559	0.200	41.6	0.9	32
BG2A	34.3297	77.34327	4528	0.158	40	1.2	35
BG11	34.32854	77.34196	4511	0.173	24.4	1.5	25
BG12	34.32752	77.34065	4480	0.176	41.9		28
BG13	34.32488	77.33927	4404	0.128	28.5	1.3	37
BG14	34.3225	77.33737	4415	0.155	27.5	1.25	53
BG1A	34.3191	77.33788	4286	0.151	*30*	1.2	53
BG15	34.31644	77.33737	4258	0.149	15.9	1.3	21
BG16	34.31439	77.33547		0.110	11.4	1.1	18.5
BG17	34.31255	77.33302	4178	0.123	12.8	*1.6*	40
BG18	34.31001	77.33189	4142	0.100	27.1	1.4	9
BG19	34.30812	77.32956	4099	0.087	*12.9*	1.2	14
BG20	34.30706	77.32655	4057	0.148	49.3	1.1	25
BG21	34.30495	77.32444	4023	0.072	*12.2*	1.2	18
BG22	34.30289	77.32229	4044	0.107	17	1.5	13.5
BG23	34.30062	77.32039	3942	0.080	23.6	1.4	7
BG24	34.29742	77.31651	3890	0.095	13.9	2	4
BG25	34.29421	77.31277	3863	0.080	18.8	2.1	5.5
BG26	34.29214	77.3079	3798	0.068	20.2	1.3	4.5
BG27	34.28816	77.3054	3733	0.070	15.6	1.8	7.5
BG28	34.28392	77.30354	3705	0.072	36.2	1.3	7.5
BG29	34.27992	77.30219	3675	0.051	39.8	2.2	3
BG30	34.27631	77.2984	3653	0.066	21.7	1.4	7.5
BG31	34.27293	77.29675	*3595*	0.058	*30*	2	1.7
BG32	34.26791	77.29434	3559	0.058	33.8	2.25	1
BG33	34.25845	77.29178	3491	0.063	32	2.1	5
BG34	34.2543	77.28926	3457	0.073	24.3	1.8	0
BG35	34.24918	77.2862	3427	0.045	56		2
BG36	34.24622	77.28434	3397	0.049	82		2
BG37	34.24185	77.28317	3373	0.054	59.5		8.7
BG38	34.23832	77.27981	3355	0.028	14		5
BG39	34.2299	77.27468	3259	0.053	23.1		2
BG40	34.22523	77.27328	3269	0.054	18.6		1.7
BG41	34.21963	77.27656	3234	0.044	11.8		2
BG42	34.21552	77.28109	3213	0.042	19.7		2

D2. Field Season 2006 – Leh Valley

TABLE D2. FIELD DATA FROM LEH VALLEY

Locality	Longitude (°)	Latitude (°)	Elevation (m) (from GPS)	Slope	Bankfull width (m)	Bankfull depth (m)	Max. gorge height (m)
L2	34.27665	77.5764	5164	0.147	34.4	0.6	2
L3	34.2757	77.57951	5148	0.063	61.2	0.6	1
L4	34.27518	77.58269	5104	0.117	160.2	0.25	0
L5	34.27502	77.58594	5080	0.051	110	0.3	0
L6	34.27359	77.58876	5074	0.033	48.3	0.55	0
L1A	34.27315	77.5926	5034	0.198	8	*1*	5
L7	34.27258	77.59579	5015	0.096	110	*1.2*	0
L8	34.27232	77.59916	4995	0.077	82.7		0
L9	34.27075	77.60172	4975	0.037	94.2		0
L10	34.26897	77.60411	4976	0.021	43.9		0
L11	34.26733	77.60664	4963	0.061	35.7	0.8	0
L12	34.26559	77.60955	4903	0.059	36.9	0.9	0
L13	34.26433	77.61238	4864	0.009	64.8	0.6	0
L14	34.26297	77.6153	4825	0.014	34	1.4	0
L15	34.26072	77.61768	4790	0.082	5.7	1.8	3
L16	34.25808	77.6184	4763	0.042	31.8	1.5	2
L17	34.25545	77.61914	4733	0.091	56.6	1.3	1.5
L18	34.25283	77.61942	4690	0.098	19.1	1.5	4
L19	34.25018	77.6189	4664	0.106	15.2	1.6	13.5
L20	34.24758	77.618	4628	0.155	15.2	1.8	16
L21	34.24544	77.61601	4588	0.193	11.7	3	24.5
L22	34.24281	77.61554	4526	0.204	*32.5*	1.7	35
L23	34.24039	77.61409	4476	0.146	50.3	2	62
L24	34.23831	77.61201	4418	0.233	49.3	2.3	65
L25	34.23582	77.61085	4357	0.216	32.5	1.7	52
L26	34.23312	77.61089	4399	0.089	23.6	2.8	60
L27	34.23045	77.61088	4262	0.119	*43.9*	3.1	44
L28	34.22776	77.61135	4234	0.201	46.3	2.7	55
L29	34.22509	77.61157	4196	0.149	46	2.8	45
L30	34.22274	77.60999	4137	0.117	36.8	*2.1*	26
L31	34.22113	77.6088	4112	0.115	51.9	3.4	30
L32	34.21783	77.60676	4062	0.066	89.7	2.4	20
L33	34.21508	77.60651	4018	0.070	35.4	3.1	8.5
L34	34.21365	77.60929	3991	0.070	41.1	2.6	4
L35	34.21215	77.61209	3971	0.058	*52.7*	*1.65*	1
L36	34.20931	77.61225	3966	0.095	26.3	2.1	1
L37	34.20787	77.60949	3906	0.075	*30.5*	2.4	1.9
L38	34.20484	77.60405	3855	0.066	*88*		1.3
L39	34.20262	77.60059	3837	0.058	*80*		3.5
L40	34.19954	77.59773	3802	0.061			2
L41	34.19498	77.59565	3762				

D3. Field Season 2008 – Sobu Valley

TABLE D3. FIELD DATA FROM SOBU VALLEY

Locality	Longitude (°)	Latitude (°)	Elevation (m) (from GPS)	Slope	Bankfull width (m)	Bankfull depth (m)	Max. gorge height (m)
S1	34.21043	77.68285	4894	0.038	7.9	0.44	5.5
S2	34.20848	77.68136	4897	0.099	8.5	0.77	4.8
S3	34.20794	77.67881	4881	0.103	5.7	0.54	10.4
S4	34.20552	77.67809	4851	0.089	10.3	0.42	7
S4B	34.20457	77.67681	4816				13.1
S5	34.20379	77.67642	4806	0.188	7.3	0.53	19.3
S6	34.20180	77.67502	4738	0.155	7.1	0.65	14.8
S7	34.19948	77.67370	4680	0.124	3.2	0.72	13.7
S8	34.19768	77.67299	4656	0.178	5	0.72	14.4
S9	34.19559	77.67264	4611	0.164	8.9	0.58	36.4
S10	34.19398	77.67083	4574	0.171	17.5		58.3
S11	34.19208	77.66906	4519	0.251	25.1		50.1
S12	34.19042	77.66807	4478	0.223	32.8		91.8
S13	34.18820	77.66715	4446	0.171	18		76.2
S14	34.18597	77.66636	4371	0.154	5.7	0.7	81.6
S15	34.18378	77.66616	4356	0.134	15		62.8
S16	34.18182	77.66426	4308	0.169	22.6		60.8
S17	34.18086	77.66183	4273	0.150	7.7	*0.61*	78
S18	34.17835	77.66125	4228	0.140	6.8		77.6
S19	34.17646	77.66355	4195	0.126	3.7	>0.23	46.5
S20	34.17414	77.66400	4134	0.119	3.6	0.56	37.6
S21	34.17173	77.66383	4110	0.117	4.9	0.6	26.1
S22	34.16931	77.66297	4081	0.115	3.6	0.55	40.3
S23	34.16689	77.66233	4058	0.094	4.6	0.72	28.7
S24	34.16430	77.66304	4012	0.133	5.5	0.83	18.9
S25	34.16208	77.66249	3974	0.103	4.4	0.87	19
S26	34.15911	77.66265	3944	0.091	4.5	0.9	24
S27	34.15714	77.66260	3912	0.103	3	0.78	18.4
S28	34.15512	77.66092	3883	0.096	4.9	1.3	
S29	34.15470	77.65891	3863	0.098	5.6	0.58	5.7
S30	34.15208	77.65751	3829	0.087	4.3	0.83	2.9
S31	34.14671	77.65370	3768	0.101	5.7	0.98	*4.8*
S32	34.14416	77.64940	3722	0.080	5.5	0.67	*5.3*
S33	34.13702	77.64069	3630	0.072	7.6	1.34	6.6
S34	34.13411	77.63291	3585	0.079	5.8	0.85	3.1
S35	34.12913	77.62007	3471	0.066	*25.1*	1.08	7.3

D4. Field Season 2008 – Karu Valley

TABLE D4. FIELD DATA FROM KARU VALLEY

Locality	Longitude (°)	Latitude (°)	Elevation (m) (from GPS)	Slope	Bankfull width (m)	Bankfull depth (m)	Max. gorge height (m)
K1	34.01468	77.90000	4784	0.080	3.9	0.5	1.6
K2	34.01653	77.89769	4762	0.073	6	0.66	11
K3	34.01759	77.89591	4728	0.176	*28.3*	*0.43*	16.9
K4	34.01768	77.89350	4664	0.300	20.3	*0.7*	20
KG1	34.01738	77.89142	4598				37.9
KG2	34.01722	77.88830	*4478*				*105.3*
K5	34.01866	77.88461	4405	0.143	10.3	1.17	54
K6	34.01807	77.88149	4386	0.124	7.8	1.33	47.6
K7	34.01812	77.87913	4346	0.166	8.7	1.2	35
K8	34.01724	77.87587	4302	0.115	6.3	1.1	26.1
K9	34.01576	77.87368	4266	0.131	4.6	1.35	29
K10	34.01396	77.87195	4227	0.099	5.4	0.96	27.3
K11	34.01149	77.87042	4184	0.089	12.4	0.67	28.5
K12	34.00984	77.86886	4178	0.061	3.3	0.94	37.1
K13	34.00861	77.86708	4179	0.098	6.6	1.06	25
K14	34.00684	77.86502	4127	0.080	4.1	0.6	14.7
K15	34.00566	77.86326	4131	0.063	4.9	1.5	16.2
K16	34.00533	77.86018	4103	0.073	6	1.09	12.7
K17	34.00363	77.85803	4068	0.084	6.7	1.22	5.2
K18	34.00166	77.85646	4060	0.052	5.8	0.75	6.2
K19	33.99979	77.85551	4042	0.101	15	0.93	7.2
K20	33.99977	77.85278	4029	0.066	9.4	0.78	4.5
K21	33.99913	77.85135	4014	0.061	11	1.1	4.8
K22	33.99854	77.84857	3990	0.072	8.4	1.32	4.6
K23	33.99731	77.84205	3955	0.089	18.5	1.55	1.7
K24	33.99724	77.83099	3871	0.077	7.5	1	
K25	33.99529	77.82620	3854	0.056	8.7	0.83	4.1
K26	33.99344	77.82126	3824	0.077	5.7	1.18	5.8
K27	33.98501	77.80849	3742	0.037	16.5	1.95	6.5
K28	33.98291	77.80698	3739	0.021	*17.4*	*1.8*	*9.1*
K29	33.98111	77.80594	3733	0.031	*13*	*1.8*	*9.3*
K31	33.96018	77.79250	3609	0.030	7	1.3	*3*
K30	33.95887	77.79186	3598	0.044	*18.7*	*1.75*	*5.4*
K32	33.95812	77.79103	3619	0.009	11.6	1.45	*5.3*